

EXPERIMENTAL STUDY ON MITIGATION OF EARTHQUAKE HAZARDS  
USING GEOSYNTHETICS

by

Mustafa Sekman

B.S., Civil Engineering, Middle East Technical University, 2012

Submitted to the Institute for Graduate Studies in  
Science and Engineering in partial fulfillment of  
the requirements for the degree of  
Master of Science

Graduate Program in Civil Engineering

Boğaziçi University

2016

## ACKNOWLEDGEMENTS

I would like to express my deepest gratitude to Assoc. Prof. Ayşe Edinçliler for her invaluable guidance and help during the preparation of the thesis. I would like to acknowledge her patience and her positive approach during the impasse moments of my studies.

I would also like to express my thanks to my friends Burak Horoz, Selahattin Akalp, Simon Karabulut and Barış Göztepe for their help in the preparation of this thesis.

I would like to thank experts and technicians, who helped me during my experiments in KOERI Shaking Table Laboratory.

Most of all, I would like to express my deepest gratitude to my parents for their invaluable support and encouragement. I cannot compensate their self-sacrifice, patience, and love.

## ABSTRACT

### EXPERIMENTAL STUDY ON MITIGATION OF EARTHQUAKE HAZARDS USING GEOSYNTHETICS

In this study, it is aimed to experimentally evaluate the effectiveness and robustness of an applicable, low-cost alternative seismic isolation (SI) system valid for low-rise and mid-rise buildings. This alternative SI system is comprised of a geotextile laid over a geomembrane located within a soil profile beneath the structure with a cylindrical shape. Because of involving geotechnics in contrast to conventional SI, proposed alternative SI system is named as Geotechnical Seismic Isolation (GSI). To obtain results that are more reliable, and to observe soil structure behavior during the excitation, an experimental setup was developed. For this purpose, a laminar box and 1:10 scaled building models were constructed. The effectiveness of the proposed GSI system was assessed by comparing the response of performed shaking table experiments with and without utilizing proposed alternative SI system. Effects of the number of the story of the building, horizontal length to depth ratio of geosynthetics, type of geosynthetics and ground motion characteristic on GSI system were investigated. Due to the curved shaped nature of the geosynthetic layer, permanent slips are diminished by the restoring effect of the gravitational forces of the isolated soil and structure mass. The comparative results of experiments revealed that GSI system can reduce the horizontal accelerations, horizontal drifts, Arias intensity, base shear, and base moment of the building. By using the proposed GSI isolation system, seismic energy transmitted from ground to structure is dissipated through slip displacement between geotextile and geomembrane. Noticeable reductions due to proposed GSI system can improve the resistance capacity of the structures against strong ground motions.

## ÖZET

# GEOSENTETİKLER KULLANILARAK DEPREM ETKİLERİNİN AZALATILMASININ DENEYSEL OLARAK İNCELENMESİ

Mevcut tez çalışmasında, az ve orta katlı binalar için kolay uygulanabilir, düşük maliyetli alternatif sismik izolasyon (SI) sisteminin etkinliği ve geçerliliğinin deneysel olarak incelenmesi amaçlanmıştır. Bu sistemde, yapı temelini altındaki zemin profili içerisine PTFE geomembran üzerine örgüsüz geotekstil kaplama kavisli şekilde yerleştirilmiştir. Önerilen alternatif sismik izolasyon tekniği alışlagelmiş sismik izolasyon tekniklerinden farklı olarak doğrudan geoteknik içerdiği için Geoteknik Sismik İzolasyon (GSI) olarak adlandırılmıştır. Yapı zemin davranışını inceleyebilmek için laminer kutu ve 1:10 ölçekli bina modelleri dizayn edilerek sarsma masası deney düzeneği oluşturulmuştur. Önerilen alternatif SI sisteminin etkinliğini araştırmak için alternatif SI sistemi kullanılarak ve kullanılmadan sarsma masası testleri gerçekleştirilmiştir. Ayrıca izole edilecek yapının kat sayısının, yerleştirilecek geosentetik malzemelerin genişliğinin derinliğe oranının, geosentetik malzemelerin tipinin ve deprem karakteristiğinin önerilen alternatif SI sistemi üzerindeki etkileri incelenmiştir. Geosentetik tabakası kavisli şekilde yerleştirildiğinde yerçekimi kuvvetinin yalıtılmış zemin ve yapı kütlelerinin üzerinde oluşturduğu geri çağırım etkisiyle kalıcı kaymalar azalmaktadır. Deney sonuçları, alternatif SI sistemi kullanıldığında; binadaki yatay ivmelerde, yatay ötelenmelerde, Arias şiddetinde, taban kesme kuvvetinde ve taban momentinde azalma olduğunu göstermektedir. Zeminden yapıya iletilen sismik enerji, geosentetiklerin birbirleri üzerinde yapacağı kayma deplasmanları ile sönmülenecektir. Deney sonuçları değerlendirildiğinde, önerilen GSI sisteminin kuvvetli yer hareketlerine maruz kalan binaların dayanma gücünü arttırdığını göstermiştir.

## TABLE OF CONTENTS

ACKNOWLEDGEMENTS . . . . .	iii
ABSTRACT . . . . .	iv
ÖZET . . . . .	v
LIST OF FIGURES . . . . .	ix
LIST OF TABLES . . . . .	xvii
LIST OF SYMBOLS . . . . .	xxi
LIST OF ACRONYMS/ABBREVIATIONS . . . . .	xxii
1. INTRODUCTION . . . . .	1
1.1. General . . . . .	1
1.2. Problem Statement . . . . .	2
1.3. Objective of the Thesis . . . . .	3
1.4. Organization of the Thesis . . . . .	3
2. LITERATURE REVIEW . . . . .	5
2.1. Seismic Isolation . . . . .	5
2.1.1. Passive Seismic Isolation . . . . .	6
2.1.2. Hybrid Seismic Isolation with Semi-Active /Active Devices . . . . .	8
2.1.3. Hybrid Seismic Isolation with Passive Energy Dissipaters . . . . .	8
2.2. Geotechnical Seismic Isolation . . . . .	10
2.2.1. Rubber-Soil Mixture (RSM) . . . . .	11
2.2.2. GSI with Geosynthetics . . . . .	13
3. EXPERIMENTAL STUDY . . . . .	31
3.1. Materials and Methods . . . . .	31
3.1.1. Shaking Table Facilities . . . . .	31
3.1.2. Measuring Instruments . . . . .	31
3.1.3. Soil Material . . . . .	32
3.1.4. GSI Geosynthetic Materials . . . . .	32
3.1.5. Input Seismic Motions . . . . .	34
3.2. Experimental Setup and Setup Preparation . . . . .	35
3.2.1. Soil Container . . . . .	36

3.2.2.	Scaled Building Models . . . . .	49
3.2.3.	Properties of the Geosynthetics . . . . .	52
3.3.	Shaking Table Experiments . . . . .	58
3.3.1.	Soil Preparation and Instrumentation . . . . .	63
4.	RESULTS OF SHAKING TABLE EXPERIMENTS . . . . .	66
4.1.	Unisolated Ground with the 5-Story Building Model . . . . .	68
4.2.	Soil Response to the Seismic Motions . . . . .	71
4.3.	Case1; GSI 1 Placed 10 cm underneath the 5-Story Building Model . .	72
4.3.1.	Seismic Response of Case 1 under Kocaeli Earthquake Motion .	72
4.3.2.	Seismic Response of Case 1 under El Centro Earthquake Motion	74
4.3.3.	Seismic Seismic Response of Case 1 under Kobe Earthquake Motion	76
4.4.	Case 2; GSI 1 Placed 15 cm underneath the 5-Story Building Model . .	78
4.4.1.	Seismic Response of Case 2 under Kocaeli Earthquake Motion .	78
4.4.2.	Seismic Response of Case 2 under El Centro Earthquake Motion	80
4.4.3.	Seismic Response of Case 2 under Kobe Earthquake Motion . .	82
4.5.	Case 3; GSI 2 Placed 10 cm underneath the 5-Story Building Model . .	84
4.5.1.	Seismic Response of Case 3 under Kocaeli Earthquake Motion .	84
4.5.2.	Seismic Response of Case 3 under El Centro Earthquake Motion	86
4.5.3.	Seismic Response of Case 3 under Kobe Earthquake Motion . .	88
4.6.	Case 4; GSI 2 Placed 15 cm underneath the 5-Story Building Model . .	90
4.6.1.	Seismic Response of Case 4 under Kocaeli Earthquake Motion .	90
4.6.2.	Seismic Response of Case 4 under El Centro Earthquake Motion	92
4.6.3.	Seismic Response of Case 4 under Kobe Earthquake Motion . .	94
4.7.	Case 5; GSI 3 Placed 10 cm underneath the 5-Story Building Model . .	96
4.7.1.	Seismic Response of Case 5 under Kocaeli Earthquake Motion .	96
4.7.2.	Seismic Response of Case 5 under El Centro Earthquake Motion	99
4.7.3.	Seismic Response of Case 5 under Kobe Earthquake Motion . .	101
4.8.	Case 6; GSI 3 Placed 15 underneath the 5-Story Building Model . . . .	103
4.8.1.	Seismic Response of Case 6 under Kocaeli Earthquake Motion .	103
4.8.2.	Seismic Response of Case 6 under El Centro Earthquake Motion	105
4.8.3.	Seismic Response of Case 6 under Kobe Earthquake Motion . .	107
4.9.	CM-3; Unisolated Ground with the 3-Story Building Model . . . . .	109

4.10. Case 7; GSI 2 Placed 10 cm underneath the 3-Story Building Model . .	111
4.10.1. Seismic Response of Case 7 under Kocaeli Earthquake Motion .	112
4.10.2. Seismic Response of Case 7 under El Centro Earthquake Motion	114
4.10.3. Seismic Response of Case 7 under Kobe Earthquake Motion . .	116
4.11. Case 8; GSI 2 Placed 15 cm underneath the 3-Story Building Model . .	118
4.11.1. Seismic Response of Case 8 under Kocaeli Earthquake Motion .	118
4.11.2. Seismic Response of Case 8 under El Centro Earthquake Motion	120
4.11.3. Seismic Response of Case 8 under Kobe Earthquake Motion . .	122
5. PARAMETRIC STUDY . . . . .	125
5.1. Seismic Response of the Cases under Earthquake Motions with Real PGA and Cyclic Sinusoidal Motion with First Mode Frequency of the Building Model . . . . .	125
5.2. Effects of the Proposed GSI System on Performance Indicator Param- eters under Earthquake Motions with Increasing PGA and Cyclic Sinu- soidal Motion with Various Frequencies . . . . .	130
5.2.1. Effects of Proposed GSI System on Top Floor Acceleration . . .	130
5.2.2. Effects of Proposed GSI System on Foundation Acceleration . .	131
5.2.3. Effects of Proposed GSI System on Top Floor Drift . . . . .	132
5.2.4. Effects of Proposed GSI System on First-Floor Drift . . . . .	133
5.2.5. Effects of Proposed GSI System on Base Shear . . . . .	134
5.2.6. Effects of Proposed GSI System on Base Moment . . . . .	136
5.2.7. Effects of Proposed GSI System on Top Floor Arias Intensity .	137
5.2.8. Effects of Proposed GSI System on Foundation Arias Intensity .	138
6. SUMMARY AND CONCLUSIONS . . . . .	140
6.1. Summary . . . . .	140
6.2. Conclusions . . . . .	141
6.3. Recommendations for Future Studies . . . . .	143
APPENDIX A: PROPERTIES OF THE UTILIZED GEOSYNTHETICS . . .	145
REFERENCES . . . . .	148

## LIST OF FIGURES

Figure 2.1.	Branches of Passive Seismic Isolation. . . . .	6
Figure 2.2.	Scheme of Lead-Plug Bearing. . . . .	7
Figure 2.3.	Scheme of Friction Pendulum System. . . . .	7
Figure 2.4.	The Overall Number of Building Applications of SI in the Most Active Countries (Martelli & Forni, 2010). . . . .	8
Figure 2.5.	Sketch of the Del Mare Hospital (Martelli & Forni, 2010). . . . .	9
Figure 2.6.	Left: Carquinez Bridge, California Right: Marquam Bridge, Oregon (Martelli & Forni, 2010). . . . .	9
Figure 2.7.	Seismically Isolated Japanese Private House and Recentering Devices (Martelli & Forni, 2010). . . . .	10
Figure 2.8.	Branches of Geotechnical Seismic Isolation (Tsang et al., 2009). . . . .	11
Figure 2.9.	Finite Element Model of Geotechnical Seismic Isolation System with the Use of RSM (Tsang <i>et al.</i> , 2012). . . . .	13
Figure 2.10.	Sketch of Foundation Isolation (Yegian & Kadakal, 2004). . . . .	14
Figure 2.11.	The Sketch of Soil Isolation (Yegian & Catan, 2004). . . . .	15
Figure 2.12.	The Shaking Table Setup That is used for Their Experiments (Yegian & Lahlaf, 1992.a). . . . .	16

Figure 2.13. Seismic Response of a Typical Building with Geosynthetic Foundation Isolation (Yegian <i>et al.</i> , 1999). . . . .	19
Figure 2.14. Schematic Diagram of the Cyclic Load Test Setup (Yegian <i>et al.</i> , 1999). . . . .	20
Figure 2.15. The Experimental Setup and Measurement Instruments Used in Testing the Building Model on the Shaking Table (Yegian <i>et al.</i> , 1999). . . . .	20
Figure 2.16. Cylindrical-Shaped and Tub-Shaped Soil Isolation Systems Tested Using a Shaking Table (Yegian & Catan, 2004). . . . .	23
Figure 2.17. Schematic of the Shaking Table Setup Using Cylindrical-Shaped Isolation liner (Yegian & Catan, 2004). . . . .	24
Figure 2.18. The ratio of Peak Transmitted Acceleration to Peak Table Acceleration as a Function of Peak Table Acceleration (Yegian & Catan, 2004). . . . .	25
Figure 2.19. Base and Transmitted Acceleration Response Spectra of Cylindrical-Shaped Isolated Soil Using the Santa Cruz Record Scaled to 0.6g (Yegian & Catan, 2004). . . . .	25
Figure 2.20. Transmitted Acceleration as a Function of H/D ratio Computed Analytically Using 2 Hz Cyclic Shaking, with 0.6g Base Acceleration Amplitude (Yegian & Catan, 2004). . . . .	26
Figure 2.21. In-Soil Isolation Systems (a) Cylindrical Liner Geometry, (b) Tub Liner Geometry, (c) Trapezoidal Liner Geometry, (d) Compound Trapezoidal Liner Geometry (Georgarakos <i>et al.</i> , 2005). . . . .	27

Figure 2.22. Schematic Illustration of the in-Soil Isolation System under Consideration (Tsatsis <i>et al.</i> , 2013). . . . .	28
Figure 2.23. A View of the Test Setup for the 3-Storey Model (Kalpakci, 2013). . . . .	29
Figure 3.1. The Grain-Size Distribution of the Silivri Sand. . . . .	32
Figure 3.2. (a) 1 mm Thick Junifol PEHD Geomembrane and (b) 1 mm Thick PTFE Geomembrane Sheets. . . . .	33
Figure 3.3. (a) Typar DuPont SF 56 and (b) Typar DuPont SF 44 Nonwoven Geotextiles. . . . .	34
Figure 3.4. Acceleration Time History of the Original (a) 1940 El Centro, (b) 1995 Kobe and (c) 1999 Kocaeli Earthquake Records. . . . .	35
Figure 3.5. Examples of Rigid Containers. . . . .	37
Figure 3.6. Examples of Equivalent Shear Beam Containers. . . . .	38
Figure 3.7. Examples of Laminar Containers. . . . .	39
Figure 3.8. The Front View of Uni-directional Laminar Box. . . . .	40
Figure 3.9. A View of Roller Bearing House with Rubber Strip Stopper. . . . .	41
Figure 3.10. The Measured Friction Forces from Pullout Test. . . . .	43
Figure 3.11. A View of Thin Rubber Membrane Located Inside the Laminar Box. . . . .	44
Figure 3.12. Instrumentation Layout of the Empty Laminar Box. . . . .	44

Figure 3.13. (a) Acceleration versus Time and (b) Displacement versus Time Graphs under 0.5 Hz Cyclic Sinusoidal Motion. . . . .	45
Figure 3.14. Front View of Instrumentation Layout of the Laminar Box Filled with Soil. . . . .	46
Figure 3.15. (a) Section and (b) Top View of Instrumentation Layout of the Laminar Box Filled with Soil. . . . .	47
Figure 3.16. Acceleration versus Time Graph of the Laminar Box Filled with Soil.	48
Figure 3.17. 1:10 Scaled 5-Story Building Model with St 42 Steel Column. . . . .	51
Figure 3.18. 1:10 Scaled 5-Story Building Model with High Carbon Steel Column.	52
Figure 3.19. (a) A View of Rigid Block Test Setup and (b) Experimental Setup Layout of the Rigid Block Experiment. . . . .	53
Figure 3.20. Free Body Diagram of the Rigid Block Experiment (Yegian & Lahlaf (1992)). . . . .	53
Figure 3.21. % Reduction under Eight Different Shaking Table Motions as 1 Hz, 2 Hz, 3 Hz, 4 Hz, 5 Hz, El Centro Earthquake, Kobe Earthquake and Kocaeli Earthquake, Respectively. . . . .	56
Figure 3.22. Peak Block Accelerations versus Peak Table Accelerations under Eight Different Shaking Table Motions. . . . .	56
Figure 3.23. Slip Displacements of the Block. . . . .	57
Figure 3.24. (a) Time History, (b) Fourier Spectrum, and (c) Response Spectrum of Time Scaled El Centro Earthquake (Array #9 Station). . . . .	61

Figure 3.25.	(a) Time History, (b) Fourier Spectrum, and (c) Response Spectrum of Time Scaled Kobe Earthquake (KJMA Station). . . . .	62
Figure 3.26.	(a) Time History, (b) Fourier Spectrum, and (c) Response Spectrum of Time Scaled Kocaeli Earthquake (Izmit Station). . . . .	62
Figure 3.27.	Soil Filling and Compaction. . . . .	64
Figure 3.28.	Sketch of Proposed GSI System Experiment Setup with 5-story and 3-Story Scaled Building Models. . . . .	64
Figure 3.29.	A View of Experimental Setup. . . . .	65
Figure 4.1.	(a) Foundation, (b) Top Floor Horizontal Acceleration Response and (c) First Floor Drift of the CM-5 under Kocaeli Earthquake. . . . .	69
Figure 4.2.	(a) Foundation, (b) Top Floor Horizontal Acceleration Response and (c) First Floor Drift of the CM-5 under El Centro Earthquake. . . . .	70
Figure 4.3.	Foundation, (b) Top Floor Horizontal Acceleration Response and (c) First Floor Drift of the CM-5 under Kobe Earthquake. . . . .	70
Figure 4.4.	Foundation, Top Floor Horizontal Acceleration Response, First Floor Drift of Case 1 under Kocaeli Earthquake. . . . .	73
Figure 4.5.	Foundation, Top Floor Horizontal Acceleration Response, First Floor Drift of Case 1 under El Centro Earthquake. . . . .	75
Figure 4.6.	Foundation, Top Floor Horizontal Acceleration Response, First Floor Drift of Case 1 under Kobe Earthquake. . . . .	77

Figure 4.7.	Foundation, Top Floor Horizontal Acceleration Response, First Floor Drift of Case 2 under Kocaeli Earthquake. . . . .	79
Figure 4.8.	Foundation, Top Floor Horizontal Acceleration Response, First Floor Drift of Case 2 under El Centro Earthquake. . . . .	81
Figure 4.9.	Foundation, Top Floor Horizontal Acceleration Response, First Floor Drift of Case 2 under Kobe Earthquake. . . . .	83
Figure 4.10.	Foundation, Top Floor Horizontal Acceleration Response, First Floor Drift of Case 3 under Kocaeli Earthquake. . . . .	85
Figure 4.11.	Foundation, Top Floor Horizontal Acceleration Response, First Floor Drift of Case 3 under El Centro Earthquake. . . . .	87
Figure 4.12.	Foundation, Top Floor Horizontal Acceleration Response, First Floor Drift of Case 3 under Kobe Earthquake. . . . .	89
Figure 4.13.	Foundation, Top Floor Horizontal Acceleration Response, First Floor Drift of Case 4 under Kocaeli Earthquake. . . . .	91
Figure 4.14.	Foundation, Top Floor Horizontal Acceleration Response, First Floor Drift of Case 4 under El Centro Earthquake. . . . .	93
Figure 4.15.	Foundation, Top Floor Horizontal Acceleration Response, First Floor Drift of Case 4 under Kobe Earthquake. . . . .	95
Figure 4.16.	Foundation, Top Floor Horizontal Acceleration Response, First Floor Drift of Case 5 under Kocaeli Earthquake. . . . .	98
Figure 4.17.	Foundation, Top Floor Horizontal Acceleration Response, First Floor Drift of Case 5 under El Centro Earthquake. . . . .	100

Figure 4.18. Foundation, Top Floor Horizontal Acceleration Response, First Floor Drift of Case 5 under Kobe Earthquake. . . . .	102
Figure 4.19. Foundation, Top Floor Horizontal Acceleration Response, First Floor Drift of Case 6 under Kocaeli Earthquake. . . . .	104
Figure 4.20. Foundation, Top Floor Horizontal Acceleration Response, First Floor Drift of Case 6 under El Centro Earthquake. . . . .	106
Figure 4.21. Foundation, Top Floor Horizontal Acceleration Response, First Floor Drift of Case 6 under Kobe Earthquake. . . . .	108
Figure 4.22. Foundation, Top Floor Horizontal Acceleration Response, First Floor Drift of CM-3 under Kocaeli Earthquake. . . . .	110
Figure 4.23. Foundation, Top Floor Horizontal Acceleration Response, First Floor Drift of CM-3 under El Centro Earthquake. . . . .	110
Figure 4.24. Foundation, Top Floor Horizontal Acceleration Response, First Floor Drift of CM-3 under Kobe Earthquake. . . . .	111
Figure 4.25. Foundation, Top Floor Horizontal Acceleration Response, First Floor Drift of Case 7 under Kocaeli Earthquake. . . . .	113
Figure 4.26. Foundation, Top Floor Horizontal Acceleration Response, First Floor Drift of Case 7 under El Centro Earthquake. . . . .	115
Figure 4.27. Foundation, Top Floor Horizontal Acceleration Response, First Floor Drift of Case 7 under Kobe Earthquake. . . . .	117
Figure 4.28. Foundation, Top Floor Horizontal Acceleration Response, First Floor Drift of Case 8 under Kocaeli Earthquake. . . . .	119

Figure 4.29.	Foundation, Top Floor Horizontal Acceleration Response, First Floor Drift of Case 8 under El Centro Earthquake. . . . .	121
Figure 4.30.	Foundation, Top Floor Horizontal Acceleration Response, First Floor Drift of Case 8 under Kobe Earthquake. . . . .	123
Figure 4.31.	Typical Slips Occurred After Severe Ground Motions. . . . .	124
Figure 5.1.	% Reduction of Top Floor Acceleration under Kocaeli Earthquake, El Centro Earthquake, Kobe Earthquake Records. . . . .	131
Figure 5.2.	% Reduction of Foundation Acceleration under Kocaeli Earthquake, El Centro Earthquake, Kobe Earthquake Records. . . . .	132
Figure 5.3.	% Reduction of Top Floor Drift under Kocaeli Earthquake, El Centro Earthquake, Kobe Earthquake Records. . . . .	133
Figure 5.4.	% Reduction of First Floor Drift under Kocaeli Earthquake, El Centro Earthquake, Kobe Earthquake Records. . . . .	134
Figure 5.5.	% Reduction of Base Shear under Kocaeli Earthquake, El Centro Earthquake, Kobe Earthquake Records. . . . .	135
Figure 5.6.	% Reduction of Base Moment under Kocaeli Earthquake, El Centro Earthquake, Kobe Earthquake Records. . . . .	136
Figure 5.7.	% Reduction of Top Floor Arias Intensity under Kocaeli Earthquake, El Centro Earthquake, Kobe Earthquake Records. . . . .	138
Figure 5.8.	% Reduction of Foundation Arias Intensity under Kocaeli Earthquake, El Centro Earthquake, Kobe Earthquake Records. . . . .	139

## LIST OF TABLES

Table 2.1.	Measured Dynamic Angles of Friction (Yegian & Lahlaf, 1992.a). . .	16
Table 2.2.	List of Geosynthetic Couples Investigated for Suitability as Foundation Isolators (Yegian & Kadakal, 2004). . . . .	22
Table 3.1.	Information about the Earthquakes (PEER Ground Motion Database). . .	34
Table 3.2.	Examples of Rigid Containers Presented in the Literature (Bhattacharya <i>et al.</i> , 2012). . . . .	36
Table 3.3.	Examples of Equivalent Shear Beam container (Bhattacharya <i>et al.</i> , 2012). . . . .	38
Table 3.4.	Examples of Laminar Containers (Bhattacharya <i>et al.</i> , 2012). . . .	39
Table 3.5.	Scaling Parameter of the Building Model. . . . .	50
Table 3.6.	Block Acceleration ( $a_b$ ) and Dynamic Friction Angles ( $\phi_d$ ) of the Three Geomembrane/Geotextile Configurations at the First Observation of Sliding. . . . .	54
Table 3.7.	Measured Peak Table Accelerations ( $A_t$ ), Peak Block (Residual Acceleration) Accelerations ( $A_b$ ) and Slip Displacements ( $D_s$ ). . . . .	55
Table 4.1.	The Cases Created to Carry Out the Proposed GSI System Experiments. . . . .	66
Table 4.2.	Soil Response to the Seismic Motions. . . . .	71

Table 4.3.	Acceleration Reduction of A3 as a Result of Application of the Proposed GSI System. . . . .	72
Table 4.4.	Comparison of Case 1 with the CM-5 under Kocaeli Earthquake. . .	74
Table 4.5.	Comparison of Case 1 with the CM-5 under El Centro Earthquake.	76
Table 4.6.	Comparison of Case 1 with the CM-5 under Kobe Earthquake. . .	78
Table 4.7.	Comparison of Case 2 with the CM-5 under Kocaeli Earthquake. . .	80
Table 4.8.	Comparison of Case 2 with the CM-5 under El Centro Earthquake.	82
Table 4.9.	Comparison of Case 2 with the CM-5 under Kobe Earthquake. . .	84
Table 4.10.	Comparison of Case 3 with the CM-5 under Kocaeli Earthquake. . .	86
Table 4.11.	Comparison of Case 3 with the CM-5 under El Centro Earthquake.	88
Table 4.12.	Comparison of Case 3 with the CM-5 under Kobe Earthquake. . .	90
Table 4.13.	Comparison of Case 4 with the CM-5 under Kocaeli Earthquake. . .	92
Table 4.14.	Comparison of Case 4 with the CM-5 under El Centro Earthquake.	94
Table 4.15.	Comparison of Case 4 with the CM-5 under Kobe Earthquake. . .	96
Table 4.16.	Comparison of Case 5 with the CM-5 under Kocaeli Earthquake. . .	99
Table 4.17.	Comparison of Case 5 with the CM-5 under El Centro Earthquake.	101
Table 4.18.	Comparison of Case 5 with the CM-5 under Kobe Earthquake. . .	103

Table 4.19.	Comparison of Case 6 with the CM-5 under Kocaeli Earthquake. .	105
Table 4.20.	Comparison of Case 6 with the CM-5 under El Centro Earthquake.	107
Table 4.21.	Comparison of Case 6 with the CM-5 under Kobe Earthquake. . .	109
Table 4.22.	Comparison of Case 7 with the CM-3 under Kocaeli Earthquake. .	114
Table 4.23.	Comparison of Case 7 with the CM-3 under El Centro Earthquake.	116
Table 4.24.	Comparison of Case 7 with the CM-3 under Kobe Earthquake. . .	118
Table 4.25.	Comparison of Case 8 with the CM-3 under Kocaeli Earthquake. .	120
Table 4.26.	Comparison of Case 8 with the CM-3 under El Centro Earthquake.	122
Table 4.27.	Comparison of Case 8 with the CM-3 under Kobe Earthquake. . .	124
Table 5.1.	% Reduction of Selected Performance Indicator Parameters of Case 1. . . . .	126
Table 5.2.	% Reduction of Selected Performance Indicator Parameters of Case 2. . . . .	126
Table 5.3.	% Reduction of Selected Performance Indicator Parameters of Case 3. . . . .	127
Table 5.4.	% Reduction of Selected Performance Indicator Parameters of Case 4. . . . .	127
Table 5.5.	% Reduction of Selected Performance Indicator Parameters of Case 5. . . . .	128

Table 5.6.	% Reduction of Selected Performance Indicator Parameters of Case 6. . . . .	128
Table 5.7.	% Reduction of Selected Performance Indicator Parameters of Case 7. . . . .	129
Table 5.8.	% Reduction of Selected Performance Indicator Parameters of Case 8. . . . .	129
Table A.1.	Properties of the Nonwoven Geotextiles. . . . .	145
Table A.2.	Properties of the Junifol PEHD Geomembrane. . . . .	146
Table A.3.	Properties of the 1 mm Thick PTFE Geomembrane Sheet. . . . .	147

## LIST OF SYMBOLS

$a_b$	Block acceleration at the first observation of sliding
$A_b$	Residual acceleration
$a_{ff,max}$	Maximum acceleration that read at the free field
$A_t$	Measured peak table acceleration
$C_c$	The coefficient of curvature
$C_u$	The coefficient of uniformity
$D_s$	Block slip displacement
$f$	Ricker pulse
$f_o$	Ricker wavelet
$F_d$	Dynamic force
$G_s$	Specific gravity
$\phi$	Internal friction angle
$\phi_d$	Dynamic friction angles at the first observation of sliding

**LIST OF ACRONYMS/ABBREVIATIONS**

CM-5	Control Model of 5-Story Building Model
CM-3	Control Model of 3-Story Building Model
ESB	Equivalent Shear Beam
FPS	Friction Pendulum System
GSI	Geotechnical Seismic Isolation
HDPE	High-Density Polyethylene
ODS	Optical Distance Sensors
PGA	Peak Ground Acceleration
PGD	Peak Ground Displacement
PGV	Peak Ground Velocity
PTFE	Polytetrafluoroethylene
RMS	Root Mean Square
RSM	Rubber-Soil Mixture
SI	Seismic Isolation
UHMWPE	Ultra-High Molecular Weight Polyethylene

# 1. INTRODUCTION

## 1.1. General

Nowadays, construction of new structures has become faster and safer by the help of enhancing technology. During all stages of construction, civil engineers take precautions against almost all disasters such as fire, flood, and earthquake. However, destructive effects of severe earthquakes such as in Japan (1995), Turkey (1999), Taiwan (1999), and Haiti (2010) cannot be prevented just through strengthening of the structure. Some researchers, such as Chang *et al.* (2002), stated that increasing resistance capacity of the structures against to earthquakes via additional shear walls braced frames, and moment resisting frames are concluded with high floor accelerations for stiff buildings, or large interstory drifts for flexible buildings. Besides, the structure contents and nonstructural components may suffer significant damage during a major earthquake, even if the structure itself remains intact. Especially hospital buildings, fire and police stations, and telecommunication centers, that have to be operational right after the earthquake, are not permitted to undergo large drift or any structural or nonstructural damage because these vital buildings contain extremely costly and sensitive equipment. As a result, the concept of Seismic Isolation (SI) concept has been emerged to minimize interstory drifts and floor accelerations.

The main idea of SI is to reduce the earthquake forces that are subjected to horizontal load carrying elements of the structure. To provide this, implemented SI system should shift the natural period of the structure and/or increase the damping ratio of the structure. Conventional SI techniques involve different isolation systems such as elastomeric bearings, and slide bearing. However, these systems are expensive and difficult to implement, especially in developing countries. Recent studies in known literature propose alternative ways using low-cost mechanisms with already available materials including the geosynthetics and scrap tire as an alternative SI. Kavazanjian *et al.* (1991), Yegian & Lahlaf (1992.a), Yegian *et al.* (1995), Yegian & Catan (2004), Yegian & Kadakal (2004), Georgarakos *et al.* (2005) have proposed to use geosynthetics

as seismic isolation material. Researchers used geosynthetic in different configurations such as placing geosynthetics just under the foundation or placing soil beneath the foundation with various geometrical shapes. Likewise, static and dynamic properties of scrap tire mixed with the soil have been investigated by J.H. Lee *et al.* (1999), Tatlısoz *et al.* (1998), Edinçliler *et al.* (2004), and scrap tire has been suggested to utilize an SI material placing around the foundation soil by Tsang *et al.* (2008), Tsang *et al.* (2009).

In this thesis, it is aspired to experimentally evaluate the effectiveness of an applicable, low-cost SI system that is comprised of a geotextile laid over a geomembrane located in the soil beneath the structure with a recommended shape under strong earthquake motions. Pioneer study of this system is one conducted by Yegian & Catan (2004) where the system was named as Soil Isolation. However, the most general concept is described as Geotechnical Seismic Isolation (GSI), which was proposed by Tsang (2009). The other researches related to GSI using geosynthetics were commonly carried out by placing geosynthetics under rigid blocks to get dynamic properties which were evaluated to be the most suitable geosynthetics for different dynamic loading conditions, the details of which are discussed in the following part of the thesis.

Experimental study involves; design, construction, and performance tests of the laminar box, 1:10 scaled 3-story and 5-story building models, determining the dynamic properties of the geosynthetics materials, carrying out shaking table tests with and without proposed GSI with geosynthetics. The effects of two different horizontal length to depth ratio ( $H/D$ ) of GSI material with three set of geosynthetics materials are investigated to evaluate the seismic performance of the tested models. More importantly, the soil-structure behavior is considered in this thesis as distinctively from the literature studies.

## 1.2. Problem Statement

Some numerical and experimental researches have been conducted to seek an alternative SI with geosynthetics. Most of the numerical researches were not verified with

the experimentally and did not consider the superstructure-soil behavior. Moreover, previous experimental researches on the similar subject have not covered the effect of GSI system on both the foundation soil and superstructure in the same experimental model. In other words, research on GSI system with different configurations without considering the building models and oppositely, GSI system without taking into account the ground response are available in the literature. While determining the effectiveness of the proposed GSI system for the structures, it can be important to observe the seismic behavior of the foundation soil and structure together. The more realistic experimental researches are needed to verify the effectiveness and robustness of the proposed GSI system.

### **1.3. Objective of the Thesis**

The aim of this thesis is to determine the effectiveness of GSI system on seismic behavior of low-rise and mid-rise buildings through shaking table experiments. This study is the first experimental study in the literature that makes possible to evaluate the validity of the proposed GSI system together with the soil and structure by considering fundamental base isolation principles. As mentioned, previous experimental researches on the similar subject did not cover the effects of GSI system on the foundation soil and superstructure in the same experimental model. While determining the effectiveness of the GSI system for the structures, it can be important to observe the seismic behavior of the foundation soil and structure altogether. The thesis aims to obtain preliminary results by considering the needs in the literature. By using the experiences from both experimental and numerical studies done in the literature, a new shaking table test set-up was developed to check the validity of proposed GSI system by taking into account the seismic behavior of soil and structure. It is aimed to be a guidance for further detailed investigations.

### **1.4. Organization of the Thesis**

The thesis starts with the general information about the SI system and continues with the literature study about the GSI system. The following section includes the

details about the physical modeling and the experimental setups. The results of the experimental program are given in further sections. Finally, summary and conclusions of the whole study are provided in the last section.

## 2. LITERATURE REVIEW

### 2.1. Seismic Isolation

Seismic isolation simply can be expressed that introduction of flexibility at the base of the structure in the horizontal direction while at the same time introducing damping elements to restrict the amplitude or extent of the motion caused by the earthquake somewhat akin to shock absorbers (Islam *et al.*, 2011).

Moreover, Monfared *et al.*, in 2013, summarized most known benefits of the SI systems. These benefits are given below:

- If the suitable seismic SI system is used, structural damage will be decreased.
- SI prevents the plastic deformation of the structure by providing elastic behavior to the super-structure. Besides, damage to private services and facilities would be of little concern that would normally affect gas, water, or sewage leakage for unfortified structures.
- Evacuation routes and corridors are usually secured in a seismic-isolated building after an earthquake so, horror of an earthquake can be eased, and the psychological burden is alleviated.
- Restriction in earthquake excitation forces could lead to slender structural elements and consequently the considerable reduction in the whole weight of the structure, which gives the noticeable reduction in construction materials and construction costs.

SI can be made with implementing various type SI devices. By the help of enhancing technology SI concepts is improved and divided into three types, which are passive seismic isolation techniques, hybrid seismic isolation with semi-active /active devices, and hybrid seismic isolation with passive energy dissipaters (Patil & Reddy, 2012).

### 2.1.1. Passive Seismic Isolation

The basic logic of the passive SI technique can be described as dissipating the earthquake energy via special devices. Briefly, passive isolation technique is classified according to working mechanism as seen in Figure 2.1.

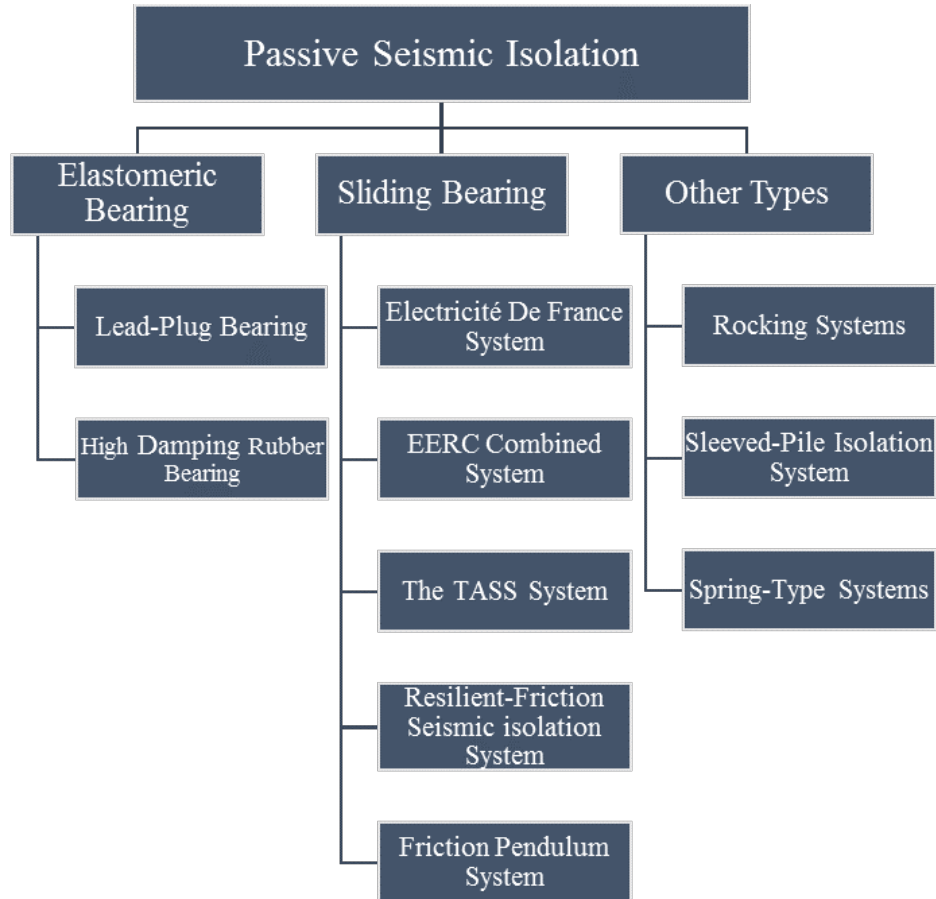


Figure 2.1. Branches of Passive Seismic Isolation.

The most applied passive SI type is the elastomeric bearings also known as the laminated rubber bearings. These isolators consist of multilayered laminated hard rubber bearings with layers of reinforcing steel plates (Figure 2.2). The system can easily sustain the vertical loads with steel plates and it is flexible under horizontal loads with the help of laminated rubber. The transmitted seismic forces from the ground to the superstructure are reduced through transforming the horizontal forces to large relative displacements across the bearings. According to allowable displacement capacity of the structure, displacement can be controlled by adjusting the damping

of the bearing. For instance, the lead plug can be inserted into laminated rubber to reduce displacement.

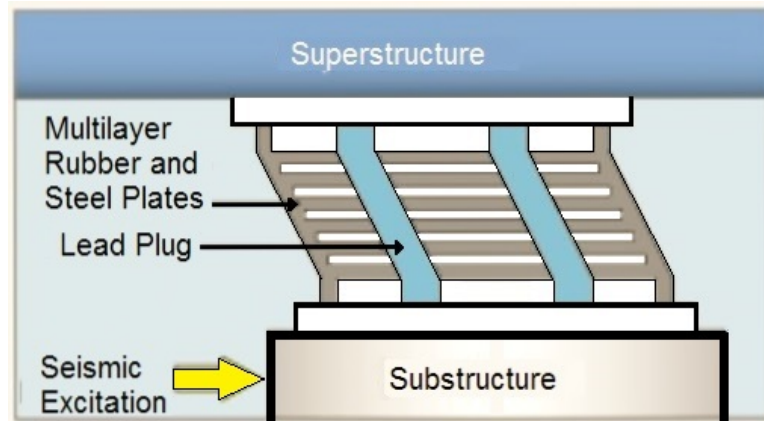


Figure 2.2. Scheme of Lead-Plug Bearing.

The second common type of the SI is sliding bearing type SI systems. This kind of isolation systems are aimed to increase flexibility in a structure is to provide a sliding or friction surface between the foundation and the base of the structure. In other words, the static friction force restricts the shear force transmitted to the superstructure across the isolation interface. This friction force can be computed and controlled by selecting the size, geometry, and material of the isolators (Figure 2.3). A low level of friction will limit the transfer of shear across the isolation interface. Thereby, lower the coefficient friction is transmitted the lower the shear force. However, the friction force across the isolation interface must be sufficiently high to sustain strong winds and small earthquakes without sliding.

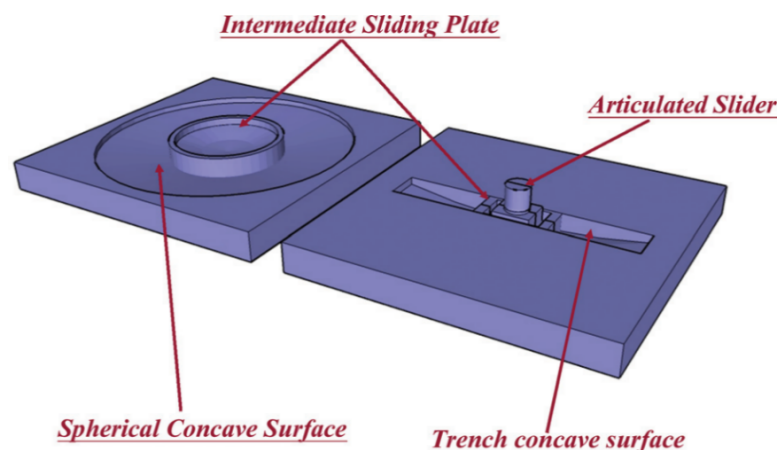


Figure 2.3. Scheme of Friction Pendulum System.

### 2.1.2. Hybrid Seismic Isolation with Semi-Active /Active Devices

As an example, Centre of the Italian Navy at Ancona, Italy, was picked to analyze the behavior of a hybrid SI system with semi-active /active devices composed by low damping rubber bearings acting as passive seismic isolators, and magnetorheological dampers, acting as semi-active controlling devices. The analysis revealed that approximately up to 50% reduction of the building accelerations can be provided via the hybrid SI system with semi-active /active devices.

### 2.1.3. Hybrid Seismic Isolation with Passive Energy Dissipaters

The energy dissipating devices such as a visco-elastic damper, elastoplastic damper, and non-buckling brace mainly dissipate the earthquake energy and reduce the effect of the earthquake on the structure. These energy dissipating devices mainly dampers can be employed in the different appropriate location of the structure. As a result, if they are utilized in couple with passive SI techniques this will be called hybrid SI with passive energy dissipaters.

SI mechanism has been using by countries that are strongly influenced by earthquake experiences such as Japan. Martelli & Forni, 2010 has indicated countries that using SI actively and some seismically isolated building in these countries (Figure 2.4).

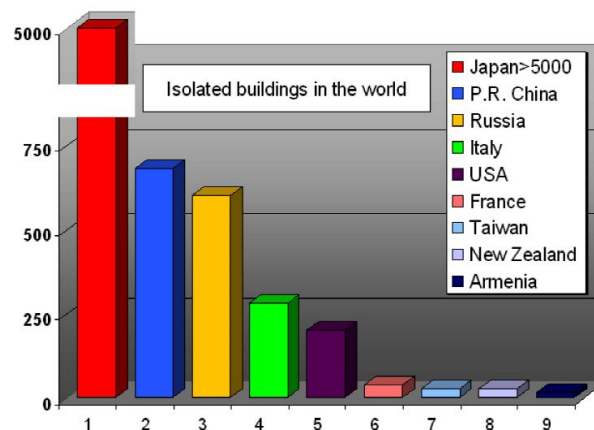


Figure 2.4. The Overall Number of Building Applications of SI in the Most Active Countries (Martelli & Forni, 2010).

However, these figures are going to be increased with the regulation in the obligatory design code that require SI for the buildings are crucial to operating even immediate after earthquake such as a hospital, communications centers. Moreover, applications have been developed for all type of both new and existing structures like bridges, civil and industrial buildings, cultural heritage, and industrial components, including power plants. There are many examples of the SI with different structures that are given by Martelli & Forni in 2010;

Del Mare Hospital was constructed in Naples, Italy. This region is considered as seismic zone 2. Thus, 327 unit high damping rubber bearings that few of them are seen on the right of Figure 2.5 were used its construction to isolate seismically this hospital building.



Figure 2.5. Sketch of the Del Mare Hospital (Martelli & Forni, 2010).

The existing Carquinez Bridge in California has seismically retrofitted by using shock transmitter units as seen on the left of Figure 2.6. Also, as seen on the right of Figure 2.6, Marquam Bridge in Oregon has retrofitted by using rubber bearing and elastic-plastic dampers.

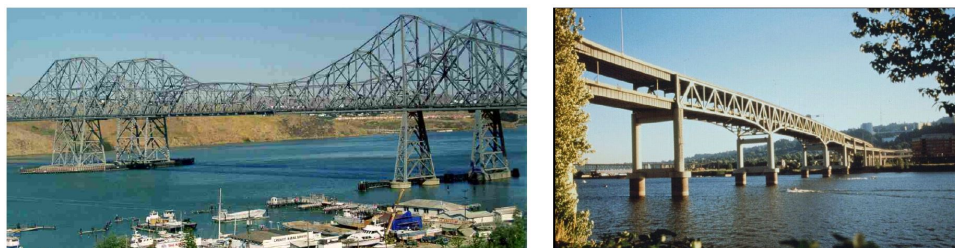


Figure 2.6. Left: Carquinez Bridge, California Right: Marquam Bridge, Oregon (Martelli & Forni, 2010).

SI is not only used in crucially important structure but also, it is used in private houses. Many Japanese private houses protected by SI system that formed by steel sphere recirculation isolators viscous dampers and recentering devices as seen in Figure 2.7.



Figure 2.7. Seismically Isolated Japanese Private House and Recentering Devices (Martelli & Forni, 2010).

## 2.2. Geotechnical Seismic Isolation

Besides all these conventional SI technique, many researchers try to find alternative ways to conventional SI. The reasons to seek for alternative SI techniques are quite convincing because the low-cost alternative seismic isolation could significantly benefit developing countries where resources and technology are not adequate for earthquake mitigation using well-developed, yet expensive, techniques. For this reason, alternative ways that require easiness of application, affordable and available raw materials have been sought out. Some alternative ways have been developed in the known literature considering these aspects.

The aim of SI is to reduce the earthquake energy transmitted to a structure by placing the structural columns on mechanical isolators. If this additional implementation will be executed geotechnically in soil with alternative ways, this is named as Geotechnical Seismic Isolation (GSI). Tsang *et al.*, in 2008, have classified the GSI into two types according to their working mechanism as seen in Figure 2.8. These are Rubber-Soil Mixture (RSM) and GSI with geosynthetics.

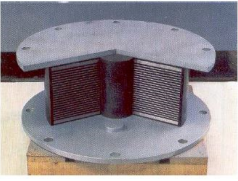
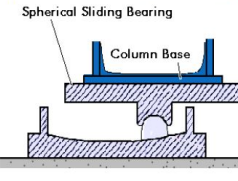
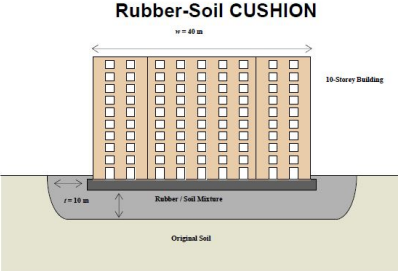
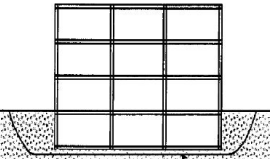
	Stiffness / Damping	Sliding / Friction
Conventional "Structural"	<p><b>Laminated Rubber Bearing</b></p> 	<p><b>Spherical Sliding Bearing</b></p> 
DEFINITION: A flexible or sliding interface positioned between a structure and its foundation for the purpose of decoupling the motions of the ground from that of the structure.		
New "Geotechnical"	<p><b>Rubber-Soil CUSHION</b></p> 	<p><b>Smooth Synthetic Liner</b></p>  <p>Yegian MK, Catnan M. (2004). Soil Isolation for Seismic Protection Using a Smooth Synthetic Liner. <i>JGGE (ASCE)</i>, 130(11):1131-9.</p>
PROPOSED DEFINITION: A flexible or sliding interface is in direct contact with geological sediments and the isolation mechanism primarily involves geotechnics.		

Figure 2.8. Branches of Geotechnical Seismic Isolation (Tsang et al., 2009).

### 2.2.1. Rubber-Soil Mixture (RSM)

The first type of GSI is RSM. It has been employed for various purposes in construction area for the reasons of having low unit weight, low bulk density, high drainage capacity, and high seismic absorption capacity. Lightweight fill, backfill for retaining walls and ground improvement are the common areas of utilization. Many researches about the RSM was conducted on novel infrastructures protection, retaining walls, and other backfill applications.

Lee *et al.* (1999) investigated the effect of shredded tires and the sand mixture as lightweight backfill. In their study, the full-scale wall was modeled, and horizontal pressure acting on the wall due to backfill was determined numerically. According to the result of the numerical analysis, the minimum horizontal pressure was obtained from the RSM. For the at-rest condition, the effect of the RSM reinforcement in reducing the lateral pressure on the wall is minimal. This result was expected, as the displacements required to mobilize the pullout force do not fully develop under this condition. The active case shows large deformations of the tire shred fill near the wall surface; the

deformations are reduced as the distance from the wall increases. In this case, the RSM reinforcement significantly reduces the horizontal pressure on the wall. Furthermore, the results for the RSM fill indicate that this material behaves almost as stiffly as a conventional granular gravel backfill. The deformations on the surface of the backfill are small, and the reinforcement provides a slight reduction in the lateral pressure for the active case.

Edinçliler *et al.* (2004) performed a set of large-scale direct shear test and dynamic triaxial test with tire buffing and tire buffing-sand mixture. Shear strength parameters and strain behavior of the materials were determined. Results of the conducted direct shear tests with the tire buffing and tire buffing-sand mixture revealed stiff behavior at low strains and higher failure displacements rather than pure sand. Dynamic shear modulus and damping characteristics of the tire buffing and tire buffing-sand mixture were determined with the dynamic triaxial tests. The deduction can be easily made that dynamic shear modulus of tire buffing was increased when it was mixed with sand considering the test results. Besides, if the ratio of tire buffing in the sand mixture is increased, there will be a reduction in the shear modulus and a major increase in damping values.

However, new utilization area for RSM has been introduced by Tsang (2008) as a GSI material. Basically, RSM is applied by mixing rubber into the soil beneath the substructure using the seismic absorption capacity of the rubber, the damping ratio of the soil is increased. Working principle is quite similar to the rubber bearings type of seismic isolator. Both rubber bearings and RSM dissipate the earthquake motion by flexibility and damping. Tsang (2008) has proposed to use RSM beneath the structure as a layer. Scrap tire cramps were used as rubber in this mixture. It was proven with numerically that SI method using RSM has the ability to reduce both horizontal and vertical ground motions.

Tsang *et al.* (2012) have conducted the one of the most significant research on this subject. Seismic isolation for low to medium rise building using granulated rubber- soil mixtures were evaluated using numerical analysis. RSM with 75% rubber by volume

selected for finite element modeling. To assess the effectiveness of the GSI-RSM system, different input parameters were investigated like the number of stories, the width of the building, length of piles, and the thickness of RSM layer. Numeric model of the RSM system can be seen in Figure 2.9.

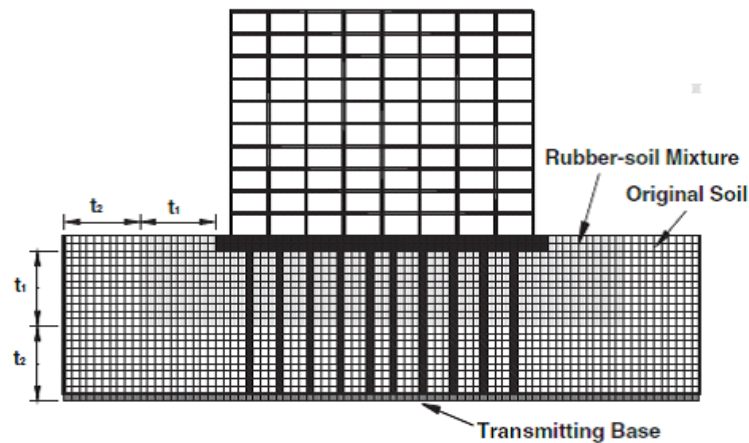


Figure 2.9. Finite Element Model of Geotechnical Seismic Isolation System with the Use of RSM (Tsang *et al.*, 2012).

Numeric analysis performed under El Salvador (2001), Northridge (1994) and Duzce (1999) earthquakes. According to results of this model, on average, the horizontal accelerations of the roof can be reduced by 50-70%, horizontal acceleration of the footing by 40-60% and inter-drift of the first floor by 40-60%.

There were many researches related to the RSM as a GSI material, and still some researches have been maintaining to develop GSI-RSM technique.

### 2.2.2. GSI with Geosynthetics

The second type of GSI technique is GSI with geosynthetics. Geosynthetics have been used in many different construction areas for decades. The main aims of utilization are separation, reinforcement, filtration, drainage, and containment applications. However, in past decades geosynthetics has been started to utilize as a GSI material. Working principal of GSI with geosynthetics was inspired by sliding bearing type of BI

such as Friction Pendulum System (FPS).

FPS is a frictional isolation system that combines a sliding action and a restoring force by geometry. The FPS isolator consists of the articulated slider between two spherical surfaces as seen in Figure 2.3. Slider in contact with the spherical surfaces is coated with a low friction composite material. One side of the slider sits in a spherical cavity. As the slider moves over the spherical surface, it causes the supported mass to rise and provides the restoring force for the system. Friction between the articulated slider and the spherical surface generates damping in the isolators. Considering this system geosynthetics are placed the beneath the substructure as a separative layer. Geosynthetics generate the friction by slipping on each other similar to FPS thereby; transmitted accelerations from the ground to the structure are reduced.

Two alternative systems were explored for the use of geosynthetics (Yegian & Kadakal, 2004; Yegian & Catan, 2004). In the first system, geosynthetics was placed immediately underneath the foundation of a structure. This system is called as foundation isolation and is shown schematically in Figure 2.10.

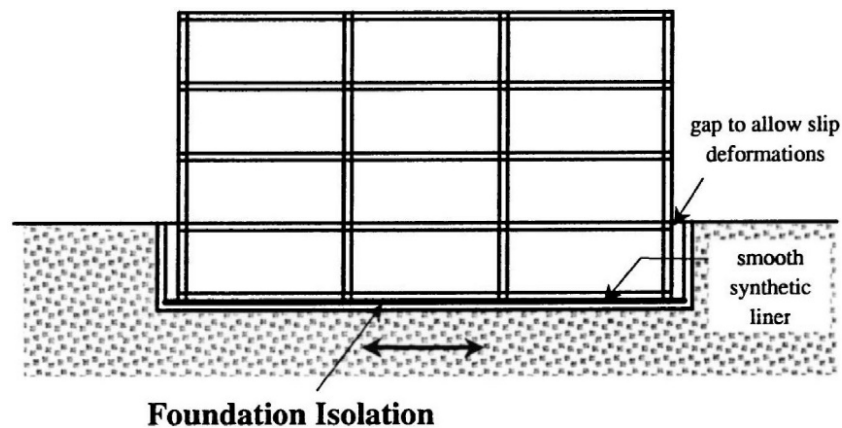


Figure 2.10. Sketch of Foundation Isolation (Yegian & Kadakal, 2004).

The second system is the placement of geosynthetics within the soil profile at some depth below the foundation of a structure as seen in the Figure 2.11. This system is named as soil isolation.

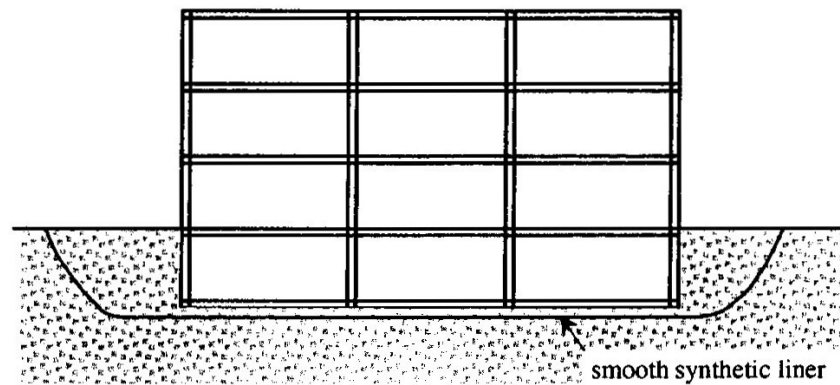


Figure 2.11. The Sketch of Soil Isolation (Yegian & Catan, 2004).

In addition, researchers Yegian & Catan (2004), Georgarakos *et al.* (2005) and Tsatsis *et al.* (2013) have tried the soil isolation approach with different geometries. Several geometries were investigated, such as cylindrical, tube-shaped, trapezoidal, and trapezoidal with wedges.

Geosynthetic materials have studied with different depth, geometry, and geosynthetic type. Most of these studies are investigated and summarized below with the chronological order.

Yegian & Lahlaf (1992.a) conducted shaking table experiments to find dynamic properties of geosynthetic couples that are used as an SI for seismic hazard mitigation. High-density polyethylene (HDPE) geomembrane (Gundle HD60) and non-woven geotextile (Polyfelt TS700) were used as geosynthetic materials. Shaking table setup was consist of concrete block and additional weights that create normal pressure from 3.4 kPa to 34 kPa as seen in Figure 2.12.

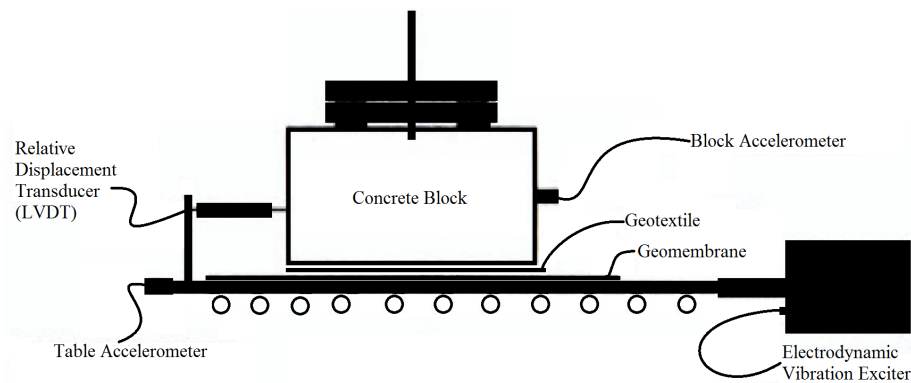


Figure 2.12. The Shaking Table Setup That is used for Their Experiments (Yegian & Lahlaf, 1992.a).

The geomembrane was fixed to shaking table and geotextile under the concrete block was free to move during excitation. According to taken shear stress and shear displacement, dynamic friction angle at the block starting to slide and residual friction angle after sliding initiated were obtained. Obtained dynamic properties of the geosynthetic couple are summarized in Table 2.1. As a result, it was revealed that geomembrane /geotextile couple can be used as an alternative SI.

Table 2.1. Measured Dynamic Angles of Friction (Yegian & Lahlaf, 1992.a).

Interface Condition	Acceleration transmitted to block at first observation of sliding	Peak dynamic friction	Acceleration transmitted to the block after sliding is initiated	Residual dynamic friction angle
Geomembrane <sup>a</sup> /geotextile <sup>b</sup> dry	0.2 g	11.3°	0.19 g <sup>c</sup> -0.24 g <sup>d</sup>	10.7 - 13.5 <sup>0</sup>
Geomembrane <sup>a</sup> /geotextile <sup>b</sup> submerged	0.19 g	10.7 <sup>0</sup>	0.17 g <sup>c</sup> -0.23 g <sup>f</sup>	9.6-13 <sup>0</sup>
<sup>a</sup> Gundle HD60: hard, Smooth HDPE				
<sup>b</sup> Polyfelt TS700: Nonwoven, continuous filament, needlepunched geotextile				
<sup>c</sup> At first observation of sliding				
<sup>d</sup> At table acceleration of 0.4 g				

Yegian & Lahlaf (1992.b) carried out shaking table tests with using the same setup that used previous research (Yegian & Lahlaf, 1992.a). Nonetheless, as distinct from the prior study, the geomembrane, and geotextile were lubricated with the Teflon oil to slide well. Lubrication decreased the transmitted acceleration roughly from 0.2g

to 0.1g.

Yegian & Lahlaf (1993) investigated the factors influencing the dynamic interface friction angle with conducted shaking table experiments. Previous experiments revealed the effect of geomembrane surface conditioning, wetting, normal stress, and effect of shaking table frequency. This reviewed research emphasized the significance of geomembrane orientation on the measured dynamic friction angle. Shaking table tests performed on a geomembrane/geotextile interface where the direction of motion of the shaking table was perpendicular to the cross-machine direction of the geomembrane. HDPE geomembrane (Gundle HD60) and non-woven geotextile (Polyfelt TS700) were employed as geosynthetic materials. The normal stress was 8.5 kPa and frequency of the motion of the shaking table was 2 Hz. According to obtained results, the orientation of the geomembrane on the direction of motion did not have an appreciable effect on dynamic peak and residual friction angles of a geomembrane/ geotextile interface.

Yegian *et al.* (1995.a) performed the shaking table tests to find out the seismic response of geomembrane/geotextile interface. The plexiglass box filled with soil was used as a weight block. The box had no top or bottom plates that allow the placement of soil and leads weights to increase the normal contact stress. HDPE geomembrane (60 MIL) and non-woven geotextile (Polyfelt TS700) were employed as geosynthetic materials. 2, 5 and 10 Hz harmonic frequencies and scaled 1988 Armenian, Saguenay earthquake, Canada earthquake 1990 Manjil and Iran earthquake were applied as a shaking table input. Effects of geosynthetics on the peak ground acceleration (PGA), frequency characteristics of the transmitted motion and slip along geosynthetic interface were investigated. As a result, the geosynthetic interface was limited the transmitted acceleration by creating slip deformations along the interface under harmonic motions. However, under earthquake excitations, limiting acceleration was not constant, and it was changed with the amplitude and frequency content of the earthquake record.

Yegian *et al.* (1995.b) altered the test setup in their companion article that is Yegian *et al.* (1995.a). In addition to their first study, geomembrane/sand interface was

investigated. Shaking table tests performed with both cyclic and earthquake motions. The test results clearly presented the reduction in the transmitted block acceleration. However, considering the amount of reduction, geomembrane/geotextile interface was decreased the acceleration better than geomembrane/Ottawa sand interface. The ratio of transmitted acceleration between geomembrane and sand was almost 2/3.

Yegian & Kadakal (1998) performed shaking table tests. They created the two test configuration to investigate the dynamic properties of geomembrane/geotextile interface. The first setup was for cyclic load tests and the second setup was for rigid block tests. HDPE geomembrane (60 MIL) and heat-bonded non-woven geotextile (Tympar 3601) were employed as geosynthetic materials. Cyclic load tests were performed to get the friction coefficients of the geomembrane/geotextile interface under constant displacement rates. Rigid block tests were carried out to simulate the dynamic loads induced in the geomembrane/geotextile interface during earthquakes. The friction coefficient of the geomembrane/geotextile interface was measured as 0.28 from the harmonic rigid block tests under 0.6g table acceleration. Besides, the coefficient of the geomembrane/geotextile interface was obtained as 0.3 under the 1994 Northridge earthquake records. The geotextile was not placed under the block directly. Instead, it was placed under the compacted soil to simulate geotextile soil effect better. In addition, both capacitive and piezometric accelerometers were used during the tests to increase the accuracy of the measurement.

Yegian *et al.* (1999) introduced the foundation isolation concept for the first time in this reviewed study. The concept was indicated that the use of horizontally placed smooth geosynthetics underneath building foundations would absorb seismic energy as seen in the Figure 2.13. Thus, transmit significantly smaller accelerations to the overlying structure.

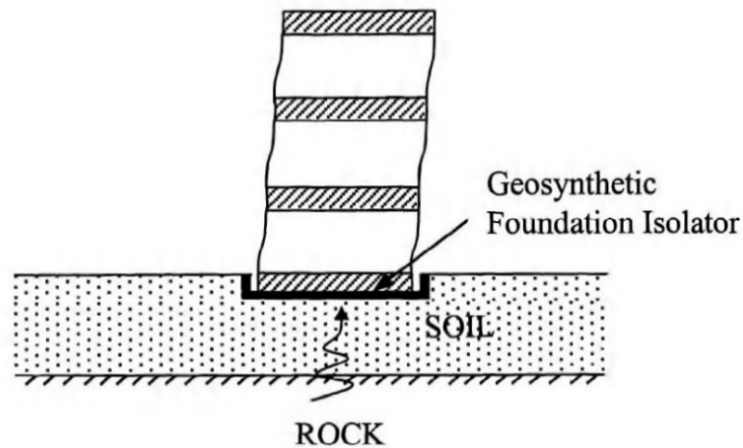


Figure 2.13. Seismic Response of a Typical Building with Geosynthetic Foundation Isolation (Yegian *et al.*, 1999).

Shaking table experiments were conducted with both rigid block and simple single story building model to investigate this concept. Firstly, suitable geosynthetic interfaces for foundation isolation were identified. Four different interfaces that were HDPE/HDPE, Smooth HDPE/Nonwoven spun bonded geotextile, Polytetrafluoroethylene (PTFE)/PTFE and ultra-high molecular weight polyethylene (UHMWPE)/ Nonwoven spun bonded geotextile were subjected to rigid block shaking table experiments.

Figure 2.14 shows the rigid block experiment setup, with these experiments friction coefficients and transmitted accelerations of the interfaces, were acquired and evaluated to continue the building model experiment with the most appropriate geosynthetic couple. UHMWPE/Nonwoven spun bonded geotextile was stated as the most suitable geosynthetic couple according to friction coefficient (0.06) and transmitted accelerations (from 0.1g to 0.07g). Shaking table tests were carried out with the single story building model (Figure 2.15) by employing UHMWPE/Nonwoven spun bonded geotextile couple.

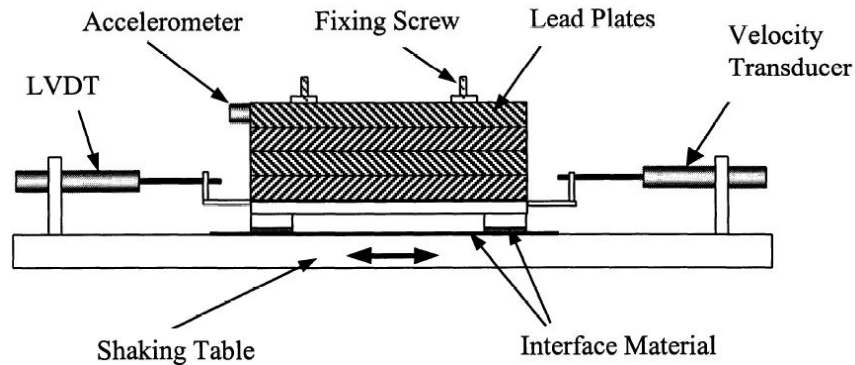


Figure 2.14. Schematic Diagram of the Cyclic Load Test Setup (Yegian *et al.*, 1999).

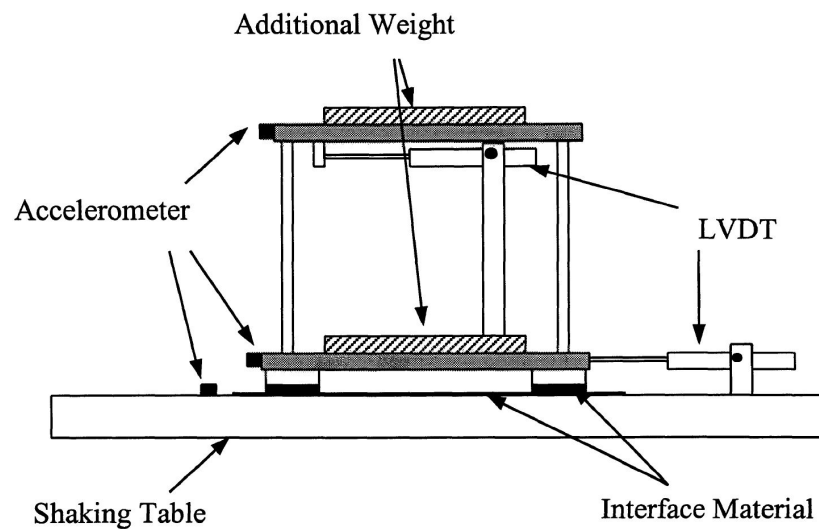


Figure 2.15. The Experimental Setup and Measurement Instruments Used in Testing the Building Model on the Shaking Table (Yegian *et al.*, 1999).

The Santa Cruz, Capitola, and Corralitos station records of the 1989 Loma Prieta earthquake were applied to the single story building model. Single story building model was placed as such free to slide over the UHMWPE/ Nonwoven spun bonded geotextile couple. The experiments results showed that at a base acceleration greater than 0.07g the geosynthetic couple absorbed the earthquake energy, and thus dramatically reduced the column shear forces in the building model. For example, at a base acceleration of 0.4g, the column shear force in the building model on foundation isolation was only 35% of that corresponding to the fixed case. These results demonstrated the excellent energy absorption capacity of UHMWPE/geotextile interface.

Yegian & Kadakal (2004) revised and expanded the study that was Yegian *et al.* (1999). In this reviewed study, the geosynthetic material requirements that should be satisfied to use as a foundation isolation material was listed. These requirements was experienced the prior studies quoted directly as;

- The friction coefficient during sliding should be small to minimize the acceleration transmitted through the interface. In general, friction coefficients between 0.05 and 0.15 would be desirable for the isolation concept to be used worldwide not only in regions of high seismicity, but also where earthquakes pose a moderate threat, and seismic mitigation measures can be cost prohibitive.
- The static friction coefficient should be slightly larger than the dynamic coefficient to prevent sliding under non-seismic loads including the wind.
- To simplify the introduction of foundation isolation in engineering design, the friction coefficient should be insensitive to several factors including sliding velocity, normal stress, sliding distance, moisture, and temperature.
- The interface material should be resistant to chemical and biological attacks, and to long-term creep effects.
- The maximum and permanent slip displacements induced by an earthquake should be small enough to allow the functionality of the structure and its utilities.

In this reviewed study, cycling loading and rigid block shaking table experiments were carried out to evaluate the dynamic response of geosynthetic couple's interface. The tested geosynthetic couples and their friction coefficients regarding cyclic test are listed in Table 2.2.

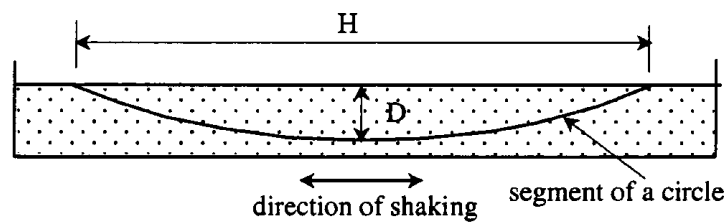
Table 2.2. List of Geosynthetic Couples Investigated for Suitability as Foundation Isolators (Yegian & Kadakal, 2004).

Interface	Description	Friction coefficient <sup>a</sup>
Geotextile/HDPE	A high-strength nonwoven geotextile, "Tyvar 3601" against 1.5 mm smooth HDPE (high density polyethylene)	0.15 - 0.3
PTFE/PTFE	Two sheets of 1.5 mm thickness PTFE (polypropylene)	0.08 - 0.15
UHMWPE/UHMWPE	Two layers of 6.4 mm thick UHMEPE (ultra high molecular weight polyethylene) TIVAR 88-2, Antistatic	0.09 - 0.25
Geotextile/UHMWPE	Tyvar 3601 geotextile against TIVAR 88-2, 6.4 mm thick UHMWPE	0.06 - 0.08
<sup>a</sup> Range depends on number of cycles, normal stress, and sliding velocity.		

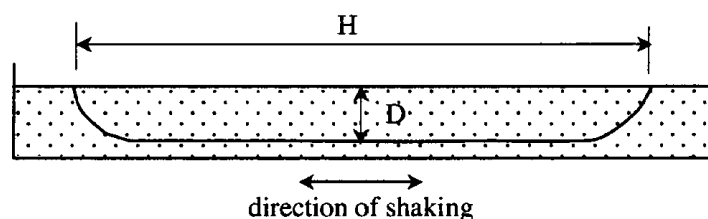
Moreover, the effect of the number of cycles, the effect of normal stress and effect of sliding velocity were investigated during cyclic load tests. According to the cyclic test results beyond ten cycles, the variation in friction coefficient was negligible. The friction coefficient slightly decreased with increasing normal stress of up to about 80 kPa, beyond which the friction coefficient remained constant. Both the friction coefficient of the geotextile/HDPE and PTFE/PTFE interfaces decreased significantly in the friction coefficient with an increase in sliding velocity. The UHMWPE/UHMWPE interface exhibited a significant reduction in sliding velocity. The friction coefficient of the geotextile/UHMWPE interface was small and independent from the sliding velocity. Cyclic test results implied that the best candidate couple was geotextile/UHMWPE. Permanent deformations, transmitted accelerations and effect of excitation frequency and amplitude rigid block and single story building models were tested under harmonic and earthquake motions with the same setup of Yegian *et al.* (1999) to see the dynamic response of the geosynthetic couple. Results of the tests were confirmed to the conclusion of cyclic load tests that was the geotextile/UHMWPE interface was a suitable liner for foundation isolation. Static friction and dynamic coefficient of geotextile/UHMWPE interface was obtained as 0.1 and 0.07, respectively. Furthermore, it was emphasized that the friction coefficient was inappreciably affected by normal stress, the number of cycles, and slip velocity.

Yegian & Catan (2004) evaluated the soil isolation concept both experimentally and analytically also, identified the benefits and limitations of soil isolation in this

study. Briefly, soil isolation concept can be defined as placing smooth geosynthetic liner within a soil deposit that can dissipate earthquake energy through slip deformations along the geosynthetic liner interface. This system was named as soil isolation because the soil layer above the geosynthetic liner is isolated from the underlying soil deposit that is experiencing the seismic excitation. The companion of this reviewed study that was Yegian & Kadakal, 2004 identified the ideal geosynthetic couple as Geotextile/UHMWPE. Typar 3601 geotextile was employed with TIVAR 88-2, 6.4 mm thick UHMWPE. The dynamic frictional properties of geotextile/UHMWPE were investigated extensively using cyclic load and rigid block shaking table tests in the companion study. Thereby, material selection was not the primary concern of this study. The main interest of this study was finding a suitable shape and depth of the geosynthetics with conducting shaking table experiments. The main criteria were specified as possible permanent slip deformation of the structure after an excitation should not exceed the allowable slip deformation limit for the health of the structure. The geometry of the geosynthetics was decided as cylindrical shaped. This geometry helps to bring isolated soil deposit back to its horizontal position after excitation by gravitational force. Cylindrical shaped and tube shaped geosynthetic geometry were proposed in this reviewed study as seen in the Figure 2.16.



(a) Cylindrical-shaped soil isolation liner test,  $H/D = 6.6$



(b) Tub-shaped soil isolation liner test,  $H/D = 9$

Figure 2.16. Cylindrical-Shaped and Tub-Shaped Soil Isolation Systems Tested Using a Shaking Table (Yegian & Catan, 2004).

Shaking table tests were carried out to find out the effect of the geosynthetics shape to the soil isolation. The 179 cm x 46 cm x 46 cm plexiglass rigid sided soil container was used to simulate the soil isolation. Firstly, cylindrical-shaped soil isolation was tested with the shaking table setup as seen in the Figure 2.17.

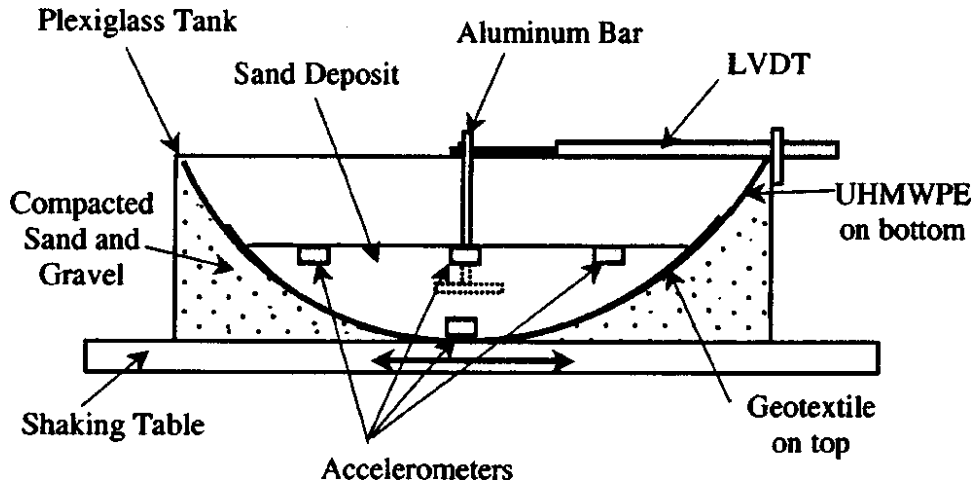


Figure 2.17. Schematic of the Shaking Table Setup Using Cylindrical-Shaped Isolation liner (Yegian & Catan, 2004).

2, 5, and 10 Hz harmonic motions also Santa Cruz and Capitola records of the Loma Prieta earthquake (1989) and Northridge earthquake (1994) motions were applied to the setup. Figure 2.18 shows the transmitted accelerations of the cylindrically shaped soil isolation. Underlying geosynthetics dissipate the accelerations that come from different motions.

Secondly, tube-shaped soil isolation setup was tested on the shaking table. Same inputs were applied to this test setup, and again the acceleration was dissipated. Figure 2.19 shows response spectra of the base and transmitted accelerations under Santa Cruz earthquake motion. Yegian & Catan indicated that the cylindrical and tube shaped soil isolation demonstrated very similar results.

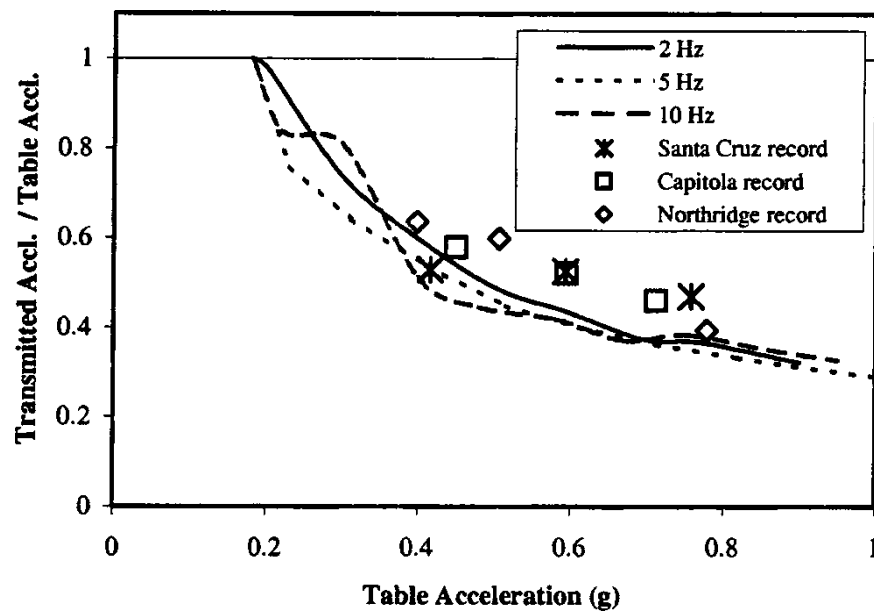


Figure 2.18. The ratio of Peak Transmitted Acceleration to Peak Table Acceleration as a Function of Peak Table Acceleration (Yegian & Catan, 2004).

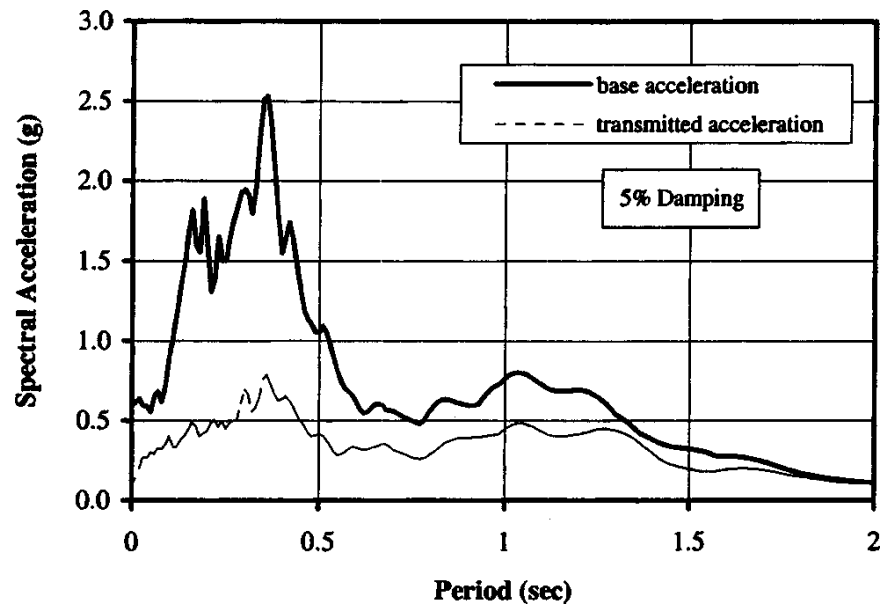


Figure 2.19. Base and Transmitted Acceleration Response Spectra of Cylindrical-Shaped Isolated Soil Using the Santa Cruz Record Scaled to 0.6g (Yegian & Catan, 2004).

After all, the relationship between the horizontal length of the GSI layer towards the direction of excitation (H) and depth of the isolated soil mass (D) was investigated by a simple analytical model that was developed for the evaluation of the dynamic

response of the isolated soil mass. Further sensitivity analysis was performed to determine the effect of liner curvature on the effectiveness of soil isolation analytically. Figure 2.20 shows the measured transmitted horizontal acceleration from the midpoint of the isolated soil region, experienced a 2 Hz harmonic horizontal motion, as a function of the ratio H to D. It was clearly seen that the effect of liner curvature was stabilized after H/D exceeds the roughly six.

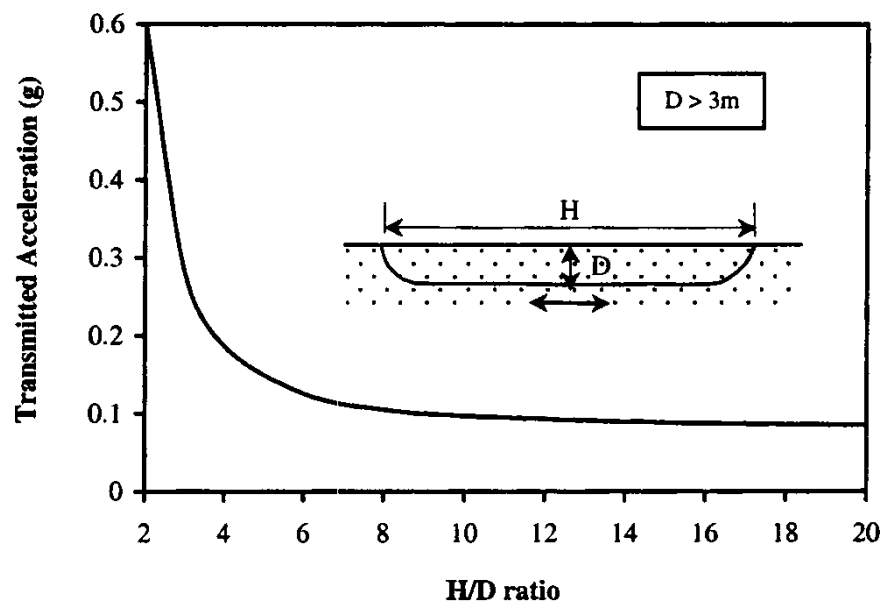


Figure 2.20. Transmitted Acceleration as a Function of H/D ratio Computed Analytically Using 2 Hz Cyclic Shaking, with 0.6g Base Acceleration Amplitude (Yegian & Catan, 2004).

Georgarakos *et al.* (2005) developed a numerical model to investigate the soil isolation concept with different geosynthetic geometries. Cylindrical shaped, tube-shaped, trapezoidal shaped with side angle 30° and 60° and compound trapezoidal shaped that are sketched in Figure 2.21 were modeled with finite element code ABAQUS. Firstly, the analyses were carried out to calibrate the interface properties and dynamic response of the isolated soil with the experimental data taken from Yegian & Catan, 2004.

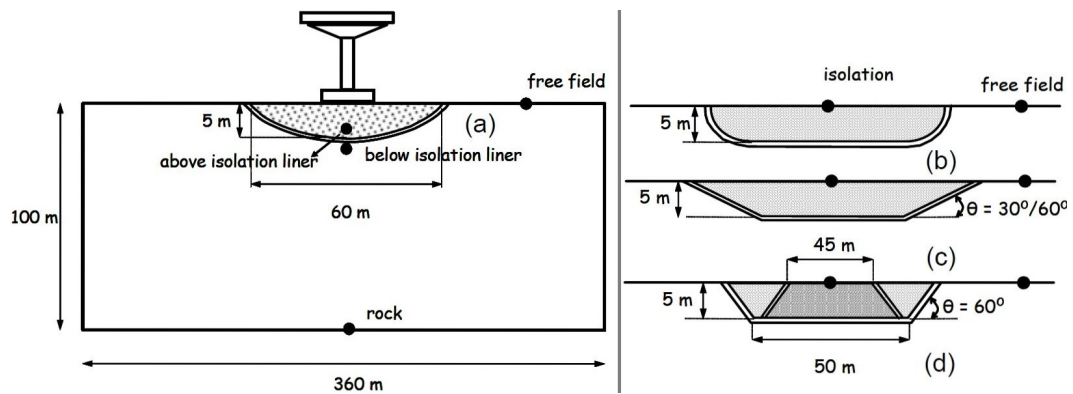


Figure 2.21. In-Soil Isolation Systems (a) Cylindrical Liner Geometry, (b) Tub Liner Geometry, (c) Trapezoidal Liner Geometry, (d) Compound Trapezoidal Liner Geometry (Georgarakos *et al.*, 2005).

The final comparison was made with the measurements taken from the mid-point of the isolated soil surface after applying Ricker Wavelet  $f_0 = 1.0$  Hz, maximum acceleration that was read at the free field as  $(a_{ff,max}) = 0.66g$ . The measured maximum acceleration response from cylindrical geosynthetic geometry was  $0.18g$ , from tube geosynthetic geometry was  $0.26g$  from trapezoidal geosynthetic geometry was not clarified and lastly from compound trapezoidal geosynthetic geometry was  $0.21g$ . As a conclusion, cylindrical shaped was determined as the most effective GSI geometry according to this reviewed research.

Arab & Kavazanjian (2010) introduced non-linear time domain model of the isolated block on a horizontal plane with geosynthetics using a Mohr-Coulomb elastic-perfectly plastic interface model. The model was capable of reproducing shaking table tests under harmonic and earthquake motions with good accuracy. The results taken from the numerical model were compared with the shaking table experiment results of Yegian *et al.* (1998) and Yegian, and Kadakal (2004). Performed analyses and comparisons showed that the frequency domain model under predicted the maximum transient displacement of the block relative to the plane, the permanent residual displacement of the block, and the spectral accelerations of the block at periods less than 0.5 seconds. Therefore, while frequency domain analyses were an efficient and convenient way to model seismic response, the Yegian *et al.* (1998) recommendations for frequency do-

main modeling under predict key elements of the response of a GSI system. Additional analyses were required to develop recommendations for use of frequency domain analysis in the design of GSI systems.

Tsatsis *et al.* (2013) performed a numerical study about soil isolation inspired by Yegian (2004) and Georgarakos *et al.*, studies. Compound trapezoidal shape (Figure 2.22) was selected to investigate the soil isolation concept.

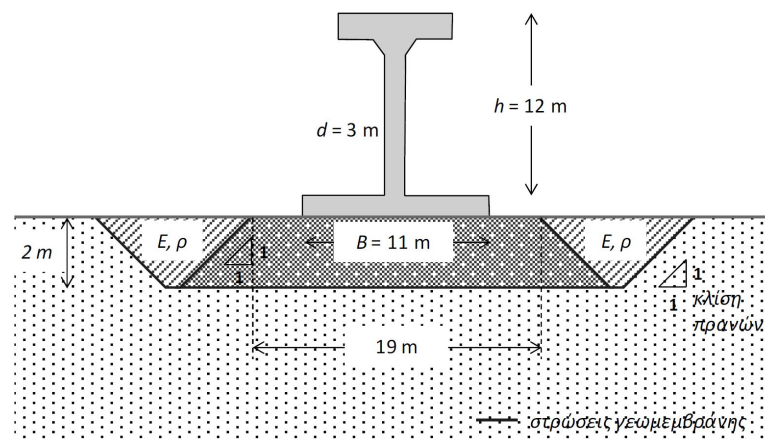


Figure 2.22. Schematic Illustration of the in-Soil Isolation System under Consideration (Tsatsis *et al.*, 2013).

The system was analyzed employing the finite element code ABAQUS by taking account of the soil, bridge pier as a superstructure, footing uplift, sliding, and P- $\delta$  effects. Model parameters were calibrated against moment-curvature relations of the reinforced concrete pier, computed through section analysis utilizing the XTRACT software. First Ricker pulses with  $f = 2\text{Hz}$  and gradually increasing maximum acceleration (0.1g to 0.5g) were subjected and then the Takatori record of Kobe (Japan 1995) earthquake was subjected to numerical model to evaluate dynamic response of the system. Measured 1.0g maximum acceleration under Kobe earthquake, was decreased to 0.35g with employing soil isolation system. To sum up, soil isolation system proved to have a rather beneficial effect on the seismic performance of the bridge piers in this reviewed study. Even though the decrease of the peak acceleration that was transmitted to the bridge pier was not sufficient to allow the design for reduced seismic loads, it proved to quite effective in ensuring its survivability. The sliding surface of the

geosynthetics was curved due to the pier imposed additional stresses. In other words, trapezoidal shaped geometry of geosynthetics was turned into cylindrical shaped owing to a load of the superstructure. Therefore, it should be reconsidered that if the geosynthetic orientation will be cylindrical shaped.

Kalpakci (2013) conducted shaking table experiments to evaluate foundation isolation system with 3-story and 5-story scaled building models. Foundation isolation system emerged and developed by Yegian *et al.* (1999) and Yegian & Kadakal (2004). In addition to these researches, Kalpakci added 3-story and 5-story scaled building models. The scaled building models were made of fiberglass and aluminum materials. UHMWPE geomembrane (TIVAR 88-2 6.4 mm thick) and non-woven geotextile (Tytar- 3601) was employed as isolation materials. For the fixed base experiments, the model was mounted directly to the table. For the isolated base cases, geomembrane was fixed to the shaking table from the four corners, and a fiberglass block beneath the models (the foundation of the model) was covered with the geotextile. Figure 2.23 shows the fixed base and isolated base 3-story scaled building model of the shaking table experiments.

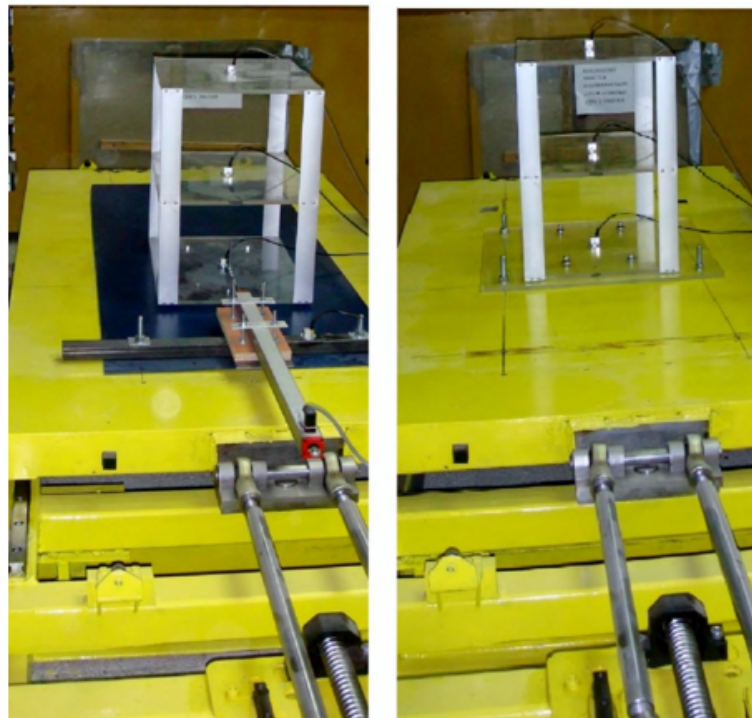


Figure 2.23. A View of the Test Setup for the 3-Storey Model (Kalpakci, 2013).

1, 2, 3, 4 Hz harmonic motions and Landers (1992), Chalfant Valley (1986), Loma Prieta (1989), Coalinga (1983), Northridge (1994) and San Fernando (1971) modified earthquakes were applied to test setups. To sum up, if the input motion exceeds the threshold acceleration system would be functioned, however; transmitted accelerations were dependent to input motion frequency and natural frequency of the structure. Moreover, the maximum reductions in the accelerations were obtained for the cases where the input motion frequency was in the close vicinity of the natural frequency of the superstructure.

### 3. EXPERIMENTAL STUDY

Experimental study section covers materials and methods, experimental setup and setup preparation and shaking table experiments.

#### 3.1. Materials and Methods

The materials and methods part contains detailed information about shaking table facilities, measuring instruments, soil material, GSI geosynthetic materials, and input seismic motions.

##### 3.1.1. Shaking Table Facilities

Shaking table test facilities at Boğaziçi University Kandilli Observatory and Earthquake Research Institute was utilized for this research. Shaking table is specified as uniaxial hydraulic shaking table. It can apply uni-axial horizontal vibration driven by a servo-hydraulic actuator. The dimension of shaking table is 3 m x 3 m. Also, it is capable of carrying and shaking a maximum 10-ton payload with 2g acceleration (i.e. two times the acceleration of gravity in the horizontal direction). The shaking table is ideally suited for seismic applications because the hydraulic actuator can produce a stroke of +/- 12 cm (24 cm total stroke). The actuator has a 3-stage servo-valve controlled by an analog inner-loop control system (displacement based), and a digital outer-loop control system (acceleration feedback based). It is controlled by the newly modified computer-based software system.

##### 3.1.2. Measuring Instruments

$\pm 3g$  capacity accelerometers and  $\pm 20g$  capacity accelerometers were used in the experiments to measure the acceleration. Leuze ODSL 96B M/V6.XL-1200-S12 optical distance sensors (ODS) with 150 - 1200 mm measurement range and  $\pm 2\%$  absolute measurement accuracy were utilized for measuring displacements. 16 - Channel dy-

nanic data logger was used for data acquisition. The sample rate for cyclic sinusoidal motions was taken as 1000 sample/sec and for earthquake motions, the sample rate was taken as 500 sample/sec.

### 3.1.3. Soil Material

The soil material used in the experiments is named as “Silivri Sand” which is locally found around Istanbul region. The grain-size distribution of the sand was determined according to the American Standard Test Method of D422 as shown in Figure 3.1. According to the Unified Soil Classification System, the sand material is classified as poorly graded sand (SP) with the coefficient of curvature as  $C_u = 2.29$  and the coefficient of uniformity as  $C_c = 1.1$ . The quick triaxial test conducted by Cagatay (2008) gives the internal friction angle as  $\phi = 41.48^\circ$ . Specific gravity of sand was obtained as  $G_s = 2.67$  and bulk unit weight as  $\gamma_{bulk} = 16.5 \text{ kN/m}^3$ . The maximum and minimum void ratios of the sand were obtained as 0.73 and 0.37, respectively.

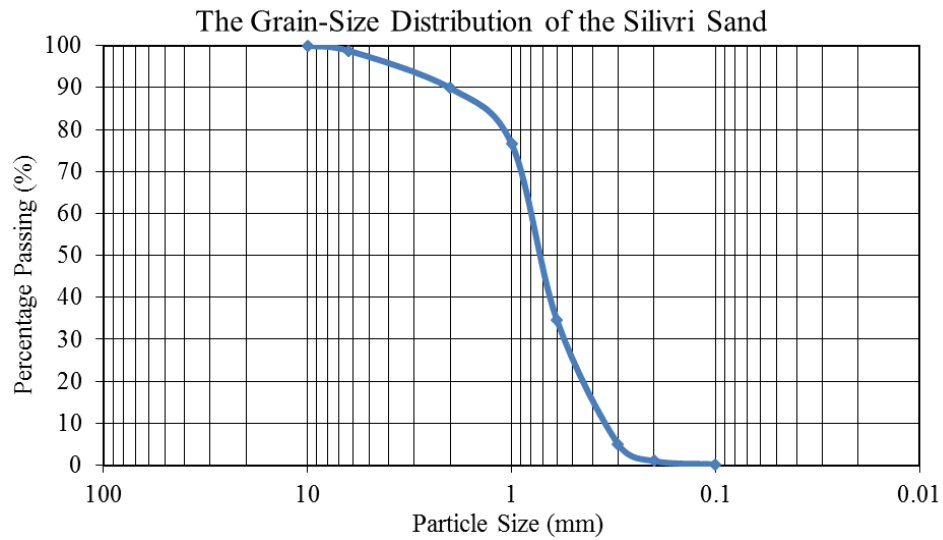


Figure 3.1. The Grain-Size Distribution of the Silivri Sand.

### 3.1.4. GSI Geosynthetic Materials

The simple idea of the proposed GSI system is transforming ground motion to slip displacement via creating an additional geosynthetic layer beneath the structure. This

geosynthetics layer consists of two geosynthetics in the way that one on the top of the other. Moreover, Yegian & Kadakal, in 2004 summarized the requirements, which is given in Section 2.2.2 to select geosynthetics for an alternative SI. Considering all given requirements and reviewing the literature, commercially available two geomembranes and two geotextiles were decided to utilize. Geomembranes were 1.0 mm thick PTFE sheet and 1.0 mm thick HDPE (junifol PEHD) that are illustrated in Figure 3.2a and Figure 3.2b, respectively.

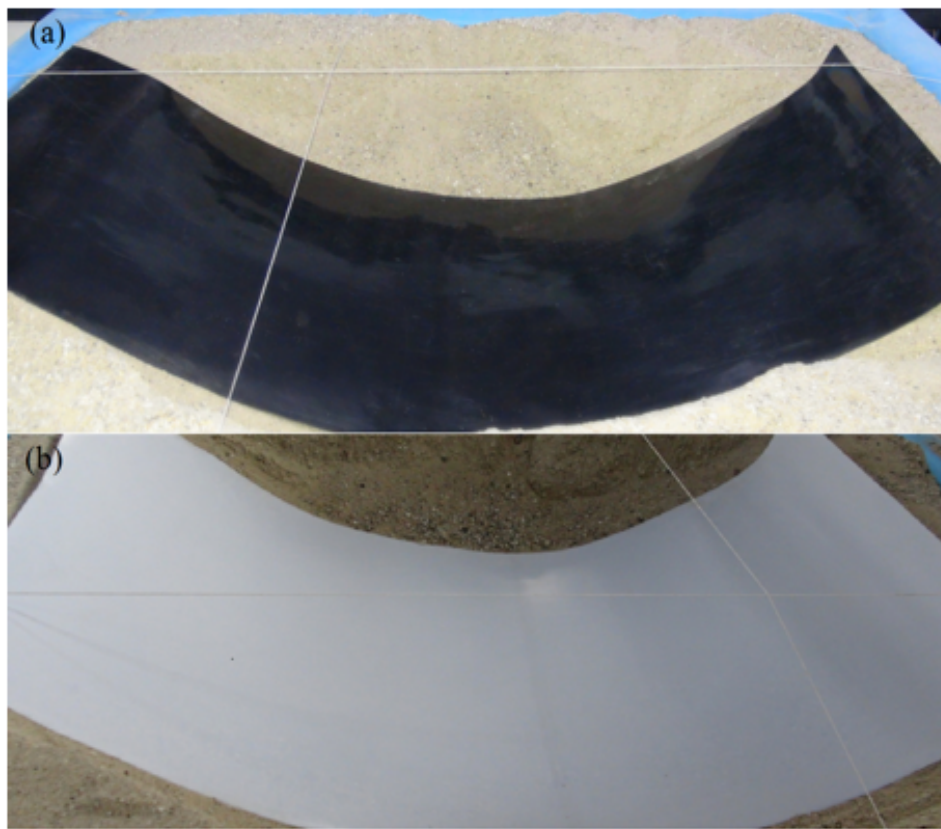


Figure 3.2. (a) 1 mm Thick Junifol PEHD Geomembrane and (b) 1 mm Thick PTFE Geomembrane Sheets.

Geotextiles were 150 and 190 gr/m<sup>2</sup> nonwoven geotextile (Typar DuPont SF 44 and SF 56) as seen in Figure 3.1. Properties of geosynthetics were given in the Table A.1, Table A.2, and Table A.3 in Appendix A.

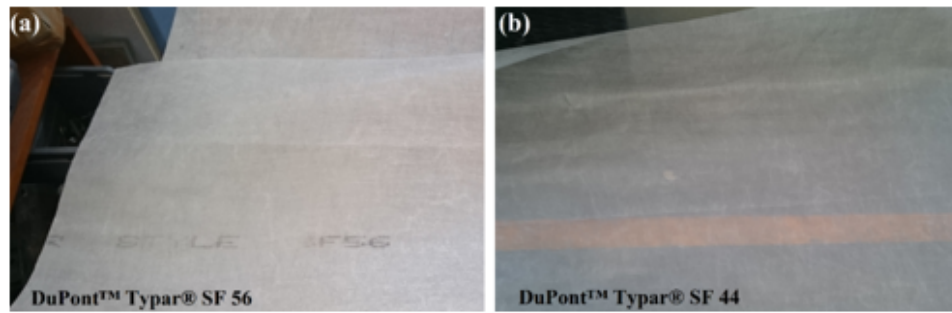


Figure 3.3. (a) Typar DuPont SF 56 and (b) Typar DuPont SF 44 Nonwoven Geotextiles.

### 3.1.5. Input Seismic Motions

From all different severe earthquakes, three different earthquake motions have been selected for the shaking table tests as input motion. These are the 1940 El Centro (Array #9 station), 1995 Kobe (KJMA station), and 1999 Kocaeli (Izmit station) earthquakes as seen in Figure 3.4. Because of having the uniaxial shaking table in the laboratory, the horizontal component of the earthquakes were selected. During the selection of earthquakes, frequency content, and applicability to the shaking table were considered. The basic specifications of the earthquakes were tabulated in Table 3.1. The earthquake data were obtained from the PEER Ground Motion Database - PEER Center.

Table 3.1. Information about the Earthquakes (PEER Ground Motion Database).

Earthquake Name	Date	Station Name	Earthquake Magnitude	Component	High Pass Filter (Hz)	Low Pass Filter (Hz)	PGA (g)	PGV (cm/sec)	PGD (cm)
Imperial Valley-02	19.08.1940 4:37:00	El Centro Array #9	6.95	N-S	0.20	15	0.32	31.74	18.01
Kobe, Japan	16.01.1995 20:46:00	KJMA	6.90	N-S	0.05		0.82	77.83	18.87
Kocaeli, Turkey	17/8/1999	Izmit	7.51	E-W	0.10	30	0.22	27.02	14.61

In addition to earthquake motions, cyclic sinusoidal motions were used with different frequencies. Frequencies of the cyclic sinusoidal motions were determined to each shaking table model.

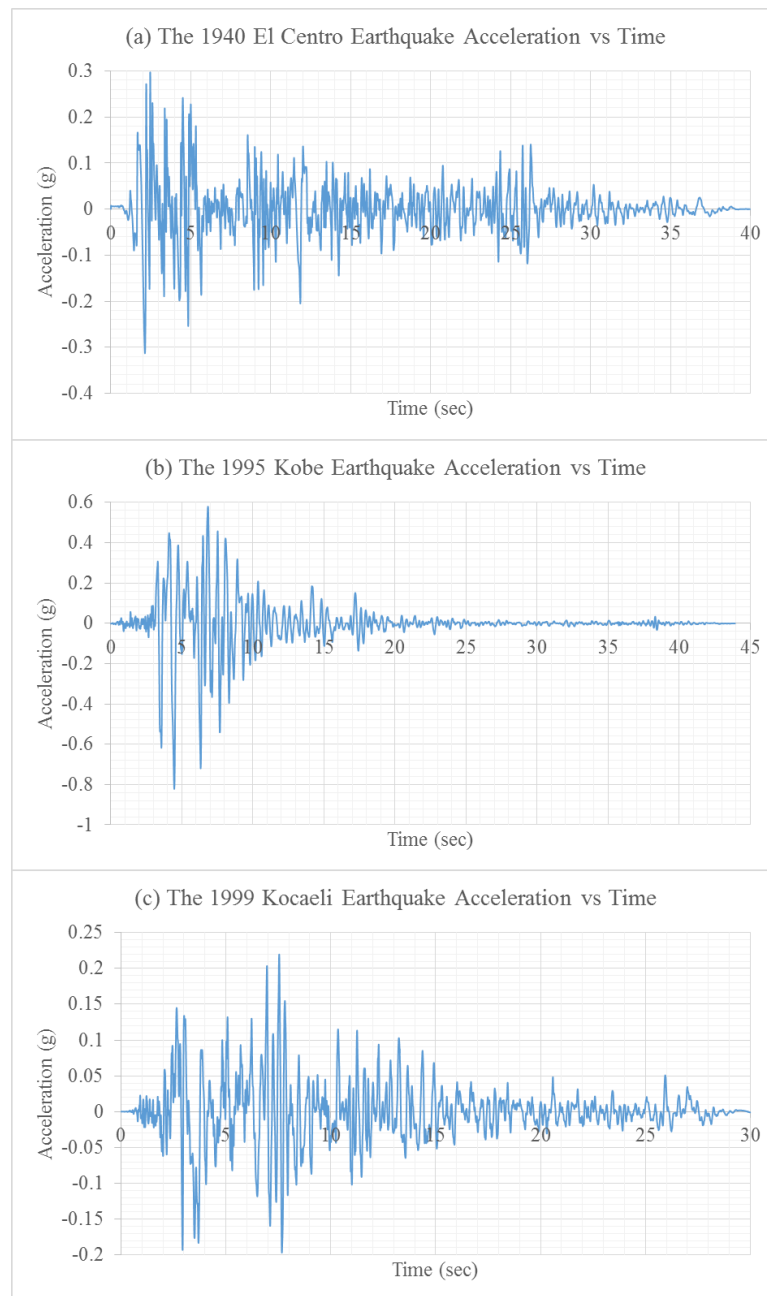


Figure 3.4. Acceleration Time History of the Original (a) 1940 El Centro, (b) 1995 Kobe and (c) 1999 Kocaeli Earthquake Records.

### 3.2. Experimental Setup and Setup Preparation

Experimental setup and setup preparation chapter is mainly comprised of three parts that were the design, construction and performance test of the laminar box, design, and construction of the scaled buildings model and obtaining the dynamic

properties of the geosynthetic materials. The establishment of the setup is described in detail in this chapter.

### 3.2.1. Soil Container

The geotechnical model cannot be directly mounted on shaking table because of the requirement of confinement. Soil should be placed in a container. In literature, there are two kinds of soil container to make geotechnical experiments in it. These are rigid sided and flexible sided soil container. Rigid sided soil container has higher end wall shear stiffness than the stiffness of the contained soil. Figure 3.5 shows the utilized rigid sided soil containers in different studies. The artificial rigid boundaries create the stress and strain similarity problems, and P-waves generation and reflection problems. These problems play a crucial role in reflecting soil behavior in the geotechnical experiments. The several examples of the rigid soil container that were used for shaking table and centrifuge experiments in literature are listed in Table 3.2.

Table 3.2. Examples of Rigid Containers Presented in the Literature (Bhattacharya *et al.*, 2012).

Shape	Shaking direction	L - B - H (mm)	L/H	Side - walls	Base & end - walls	Reference
Rectangular	1 - D	597-270-150	4	Teflon	Rough sand paper	Adalier and Elgamal (2002)
Rectangular	1 - D	500-565-190	2.6	No-details	No-details	Whitman and Lambe (1986)
Rectangular	2 - D	712-432-440	1.6	Smooth plastic membrane	Base covered by sand-glue mixture	Ng <i>et al.</i> (2004)
Rectangular	1 - D	1500-400-1000	1.5	Perspex and wood plates	Terram geotextile membrane	Norton (2008)
Rectangular	1 - D	450-240-400	1.1	Perpex	PTFE (poly tetra fluoro ethylene) sheets	Dash (2010)

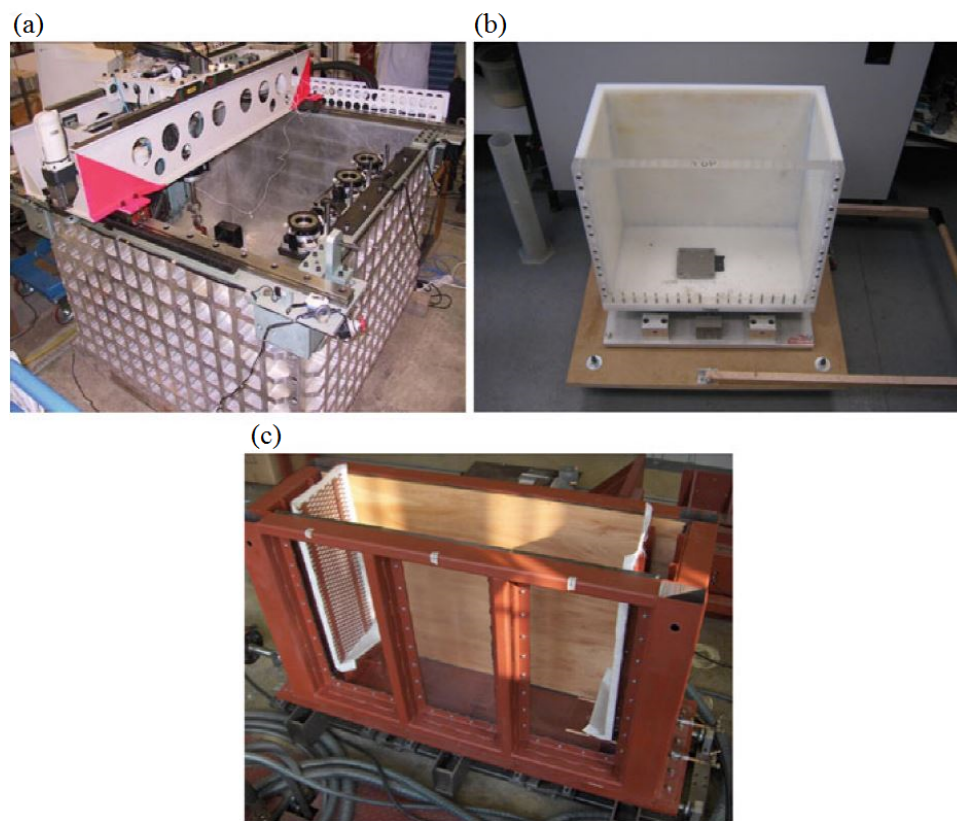


Figure 3.5. Examples of Rigid Containers: (a) Rigid Container used in Centrifuge at the Hong Kong University of Science and Technology. (b) Rigid Box used in the Small Shaking Table at the University of Bristol. (c) Rigid Box used in the Shaking Table at the University of Oxford (Bhattacharya *et al.*, 2012).

Unlike rigid sided soil container, flexible sided soil containers permit the soil to deform freely as in natural ground when subjected to seismic excitations. Basically, there are two types of the flexible sided soil container in the literature. These are the equivalent shear beam (ESB) box and laminar box. The ESB boxes consist of successive rubber and metal layers. The stiffness of the end walls of the ESB box that is directly related to the stiffness of the rubber used as layers is designed to match the shear stiffness of the contained soil. In other words, natural frequencies of both box and contained soil have to be coupled. It is expected that soil and box behave like an equivalent shear beam. However, the shear stiffness of the soil could show variation during the shaking depending on the strain level. Thereby, coupling the stiffness of the contained soil and box is possible only at a particular strain level. The examples of the ESB box are listed in Table 3.3 and are shown in Figure 3.6.

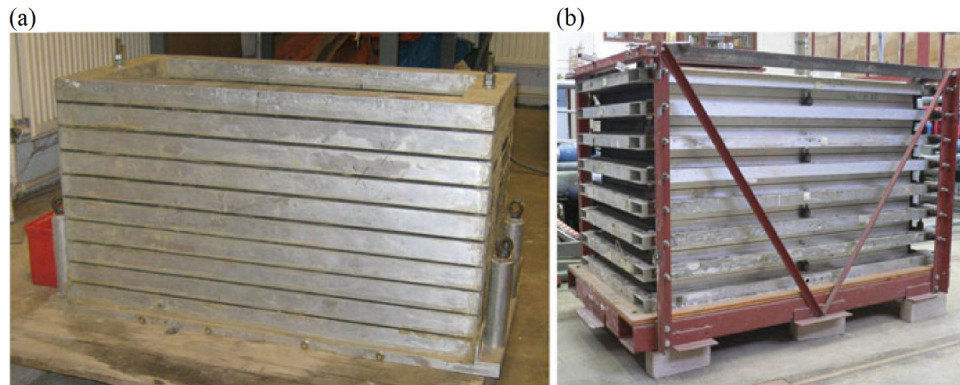


Figure 3.6. Examples of Equivalent Shear Beam Containers: (a) ESB Used in Centrifuge Testing, University of Cambridge (b) Shear Stack Used in 1-g Testing, University of Bristol (Bhattacharya *et al.*, 2012).

Table 3.3. Examples of Equivalent Shear Beam container (Bhattacharya *et al.*, 2012).

Shape	Shaking direction	L - B - H (mm)	L/H	1-g/ N-g	Reference
Rectangular	1 - D	2000-750-1750	1.1	1 - g	Carvalho <i>et al.</i> (2010)
Rectangular	1 - D	1200-550-800	1.5	1 - g	Dar (1993)
Rectangular	1 - D	4270-910-1220	3.5	1 - g	Fishman <i>et al.</i> (1995)
Rectangular	1 - D	4800-1000-1200	4	1 - g	Crewe <i>et al.</i> (1995)
Rectangular	1 - D	560-250-226	2.5	N - g	Zeng and Schofield (1996)
Rectangular	1 - D	800-350-600	1.3	N - g	Madabhushi <i>et al.</i> (1998)

Laminar boxes generally consist of a stack of laminates supported individually by bearings and a steel guide connected to an external frame. Table 3.4 provides the list of different types of laminar boxes presented in the literature. The most common shape of the laminar box is rectangular. However, for two-dimensional shaking table tests, the shape of the box can be square, circular, or 12-sided polygon. Figure 3.7 shows the two different laminar boxes.

Table 3.4. Examples of Laminar Containers (Bhattacharya *et al.*, 2012).

Shape	Shaking direction	L - B - H (mm)	L/H	1-g/ N-g	Design	Reference
Rectangular	1 - D	900-350-470	1.9	1 - g	Stack of laminae seperated by bearing	Gibson (1997)
Rectangular	1 - D	1000-500-1000	1	1 - g	Stack of laminae seperated by bearing	Prasad <i>et al.</i> (2004)
Circular	2 - D	2280-2130 (D-H)	1.1	1 - g	Container hanging on the top lamina supported by frame	Meymand (1998)
Rectangular	2 - D	1888-1888-1520	1.2	1 - g	Laminae supported by a frame and move independently	Ueng and Chen (2010)
Rectangular	1 - D	457-254-254	1.8	N - g	Stack of laminae seperated by bearing	Van Laak <i>et al.</i> (1994)
Rectangular	1 - D	710-355-355	2	N - g	Stack of laminae seperated by bearing	Pamuk <i>et al.</i> (2007)
12-sided polygon	2 - D	584-500 (D-H)	1.2	N - g	Stack of laminae seperated by bearing	Shen <i>et al.</i> (1998)
Rectangular	1 - D	900-450-807	1.1	1 - g	Laminae supported individually by bearings and steel guide conneted to an external frame	Turan <i>et al.</i> (2009)
Square	2 - D	1000-1000-1000	1	1 - g	Laminae supported individually by bearings	Jafarzadeh (2004)

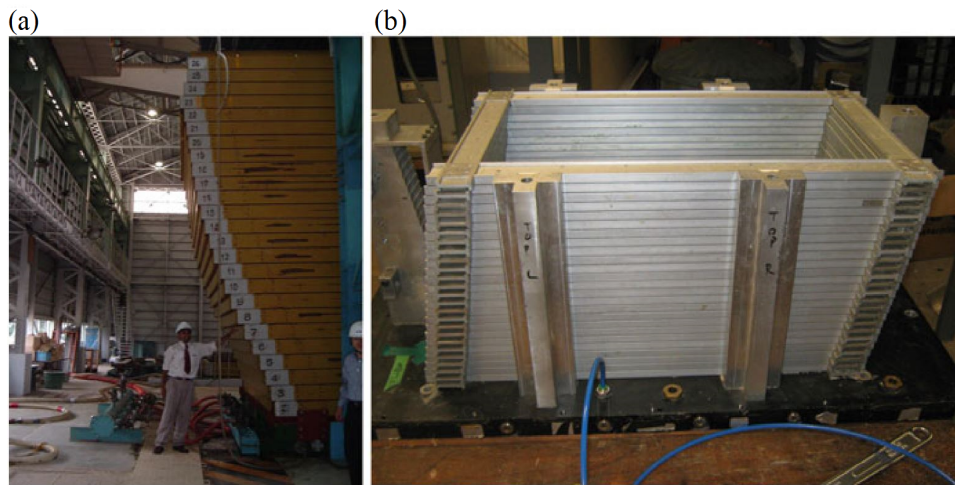


Figure 3.7. Examples of Laminar Containers: (a) Large Laminar Container Used In 1-G Testing In Tsukuba, Japan (b) Laminar Container Used In Centrifuge, University of Cambridge (Bhattacharya *et al.*, 2012).

The basic design principle of a laminar box is to minimize the lateral stiffness of the container to ensure that the soil governs the response of the soil box system. To achieve this, the friction between laminates should converge to zero. If the resistance between two laminates becomes smaller than the resistance of the contained soil in the box, soil can deform freely as in the natural ground without artificial boundary

restriction. For reaching this goal, it is strictly required that the container should be a flexible one having the deformation capacity in the horizontal plane.

In this study, by the help of experiences, guidance and knowledge taken from the literature, the laminar box was designed, constructed, and verified the performance criteria to simulate the field conditions in the laboratory. The laminar box that was utilized in this research was designed as 1.5 meters towards the direction of shaking by 1.3 meters with 1-meter depth as seen in Figure 3.8. Dimensions of the laminar box were determined by considering the maximum loading capacity of the shaking table. Also considering possible torsion problem during one directional shaking, the geometry of laminar box was decided as rectangular instead of a square geometry.



Figure 3.8. The Front View of Uni-directional Laminar Box.

The laminar box consists of layers, roller bearings, base plate, side guides and internal membrane components. Eighteen sliding layers that were made by steel I-beam were composed of the walls of the laminar box. While designing the laminar box, one of the most important issues was sliding and stopping the mechanism of the laminates that were provided with roller bearings and rubber stoppers in this case. Friction forces between laminates were minimized by using six sets roller bearings per laminate. Each set includes three roller bearings placed side by side. In total, 324 roller bearings provide the sliding to the laminates. Rubber strips were placed at both ends of bearing houses that were constructed from stainless steel as seen in Figure 3.9.



Figure 3.9. A View of Roller Bearing House with Rubber Strip Stopper.

Additional inertial effects that could be caused by stroking the roller bearings to rubber strips at the end of the bearing houses were restricted by using shock absorption feature of rubber. The lowest layer was fixed on a steel base that was fixed to shaking table. The side guides were made of steel tube sections to take precaution against unexpected accident. The membrane was attached to inner surface of the laminar box to prevent soil leakage that occurs in the box towards the gaps between two laminates. Additionally, between membrane and sidewalls of the box was greased to avoid additional friction forces.

After designing and manufacturing of the laminar box, it was subjected to some performance tests. Prasad *et al.* (2004), Jafarzadeh (2004), Whitman & Lambe (1986), and Ecemis & Kahraman (2012) performed tests on the laminar box. These performance tests investigate the effect of inertia, friction, membrane, and boundary on laminar box performance.

- Inertia effect

Inertia effect is contributed by the mass of the box itself. The measured acceleration ( $a$ ) in where the soil would be less than the actual because of the inertia of the box itself. Accounting for this effect, a simple correction factor can be used for measured acceleration. Considering  $m_1$  and  $m_2$  to be the mass of soil within a layer

and the layer of box, respectively then, total dynamic force is given as,

$$F_d = (m_1 + m_2) \times a \quad (3.1)$$

However, it is desired that the entire force is transferred onto the soil. Therefore, if  $a'$  be the desired acceleration in soil without the influence of box, then,

$$F_d = m_1 \times a' \quad (3.2)$$

Equating the above two equations, actual acceleration in soil is given by,

$$a' = \left( \frac{m_1 + m_2}{m_1} \right) \times a \quad (3.3)$$

where  $a'$  is the acceleration of the soil without the influence of the container,  $a$  is the measured acceleration,  $m_1$  is the weight of soil in the container,  $m_2$  is the weight of total laminates

$$a' = (1.3) \times a \quad (3.4)$$

The influence coefficient is computed as approximately 1.3, and this coefficient is normal up to 1.5.

- Friction effect

Static pullout tests were performed to determine friction forces of the roller bearings that are required to initiate motion of the laminate. By performing these tests, the friction effect on the performance of the box was demonstrated clearly. Measurements were done with the load cell that has 50 kg load measurement capacity by attaching the laminates and applying the static forces for each layer. The measured friction forces were the function of both the coefficient of friction between the laminates and the laminate weight. Cumulative laminate weight increases from top to bottom because of joining weights of the upper laminate together. The measured friction forces are

plotted in Figure 3.10.

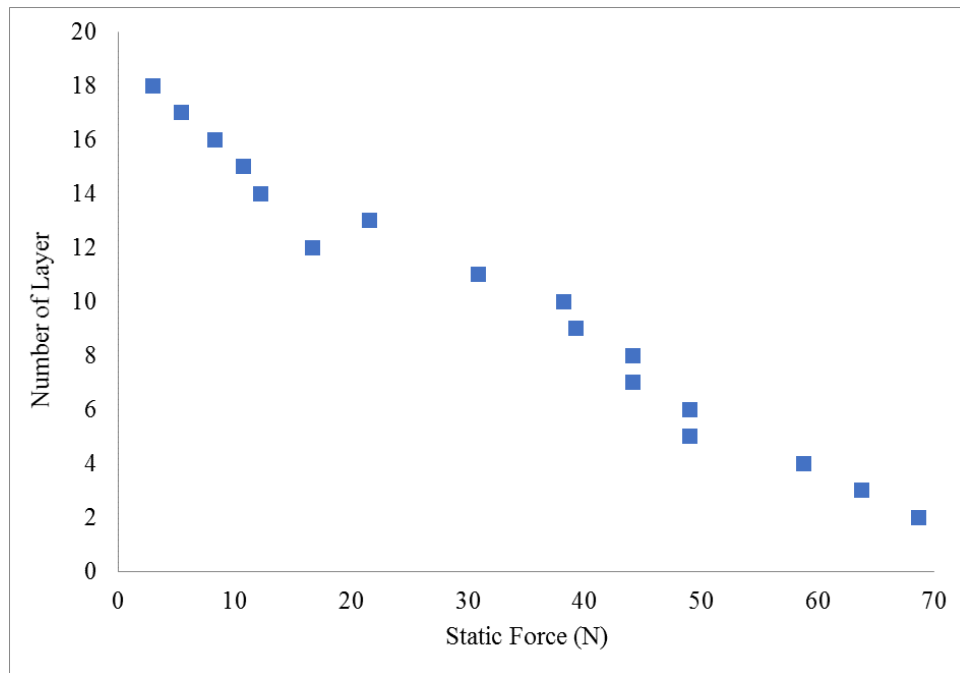


Figure 3.10. The Measured Friction Forces from Pullout Test.

The required maximum force to initiate the laminate motion was measured as 69 N from the bottom layer. The average friction force was about 33 N. In addition, the average coefficient of friction was computed as 0.07. After filling the laminar box with the soil whose unit weight is assumed as  $16.5 \text{ kN/m}^3$  and friction angle is  $\phi = 41.48^\circ$ , soil resistance near the bottom would be 20.9 kN of which almost 0.003 of this resistance was equal to static friction. Thereby, static friction force can be neglected.

- Membrane effect

1.0 mm thick rubber membrane was employed in the present research as seen the Figure 3.11. The stiffness of the membrane was sufficiently small compared to contained soil. Hence, the membrane would not influence the performance of contained soil. In addition, the effect of the membrane was localized near the edge of the laminar box. At the center of the soil, effect of the membrane was negligible.

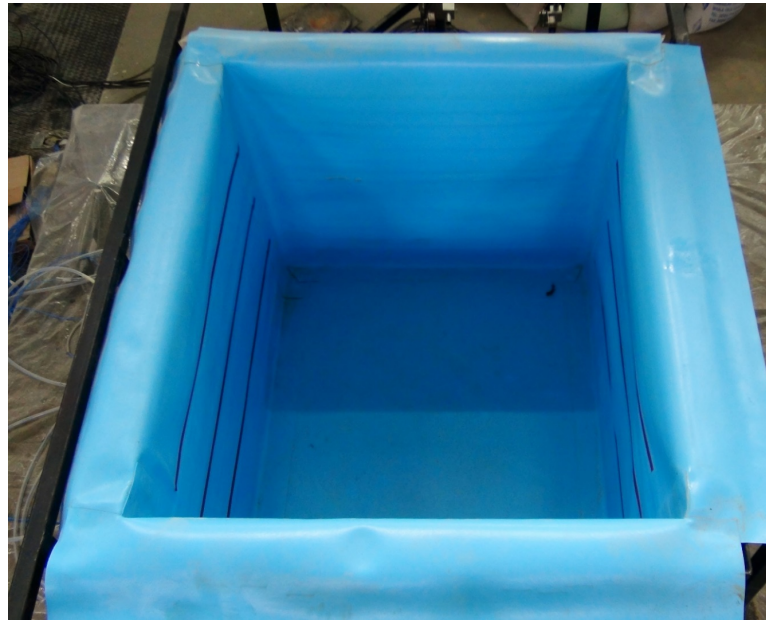


Figure 3.11. A View of Thin Rubber Membrane Located Inside the Laminar Box.

- Boundary effect

The performance of the laminar box boundaries was investigated by carrying out series of shaking table tests. The empty laminar box was inspected to identify the natural behavior of the laminar box. Instrumentation layout of the empty laminar box was sketched in Figure 3.12.

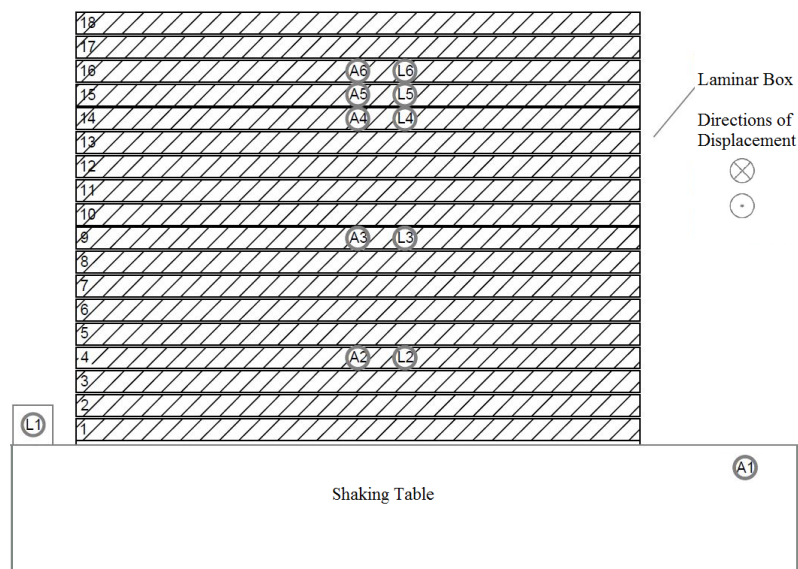


Figure 3.12. Instrumentation Layout of the Empty Laminar Box.

Five accelerometers and five optical distance sensors (ODS) were mounted as pairs on the front side of the laminar box. Accelerometers tagged as “A” and ODSs tagged as “L.” A1 and L1 collected the data from the shaking table for verifying the given input motion. The rest of instruments were placed from bottom to top as seen in the Figure 3.12. The cyclic sinusoidal motion of 0.5 Hz with 0.05g, 1 Hz with 0.25g, 2 Hz with 0.75g, 3 Hz with 0.75g, 4 Hz with 0.8g, and 5 Hz with 1.0g were applied to the laminar box via shaking table.

The Figure 3.13a and Figure 3.13b show the measured accelerations and displacements under the cyclic sinusoidal motion with 0.5 Hz. As expected, both acceleration and displacement decreased from bottom to top which means acceleration and displacement were diminished when moving upward.

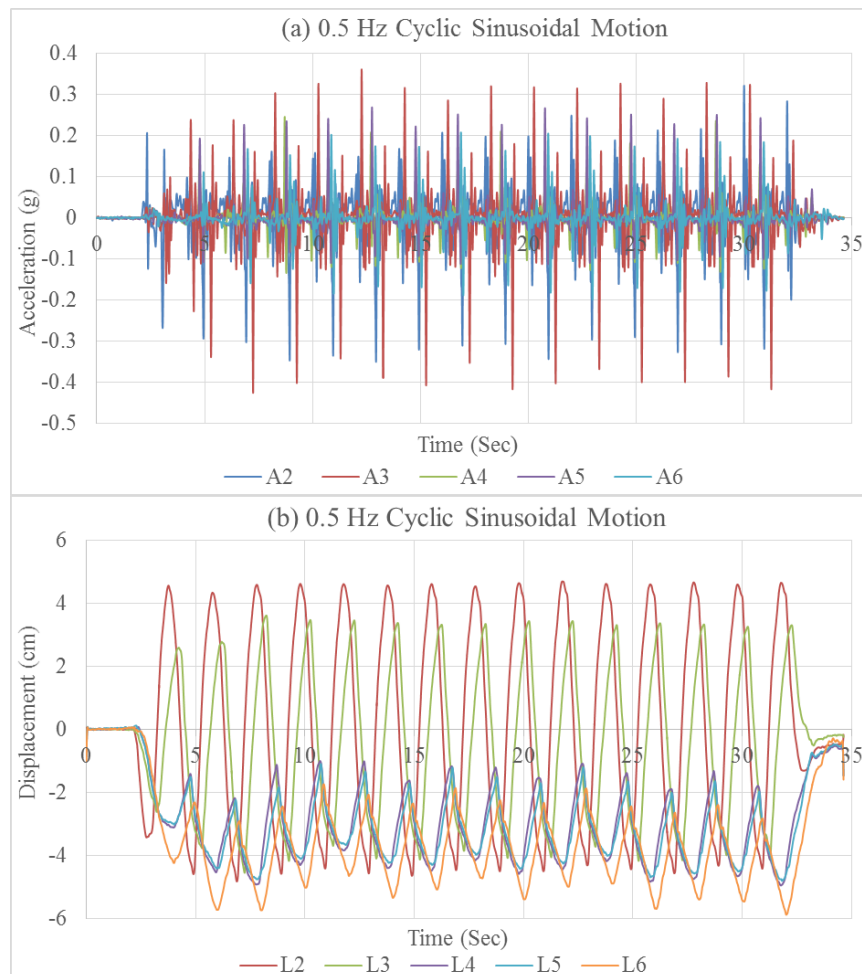


Figure 3.13. (a) Acceleration versus Time and (b) Displacement versus Time Graphs under 0.5 Hz Cyclic Sinusoidal Motion.

The soil was filled through compaction of four equal subsequent layers. Then, shaking table tests were proceeded with filled box to estimate the impact of the laminar box boundary on the soil behavior. Figure 3.14 shows the instrumentation layout of the laminar box filled with soil.

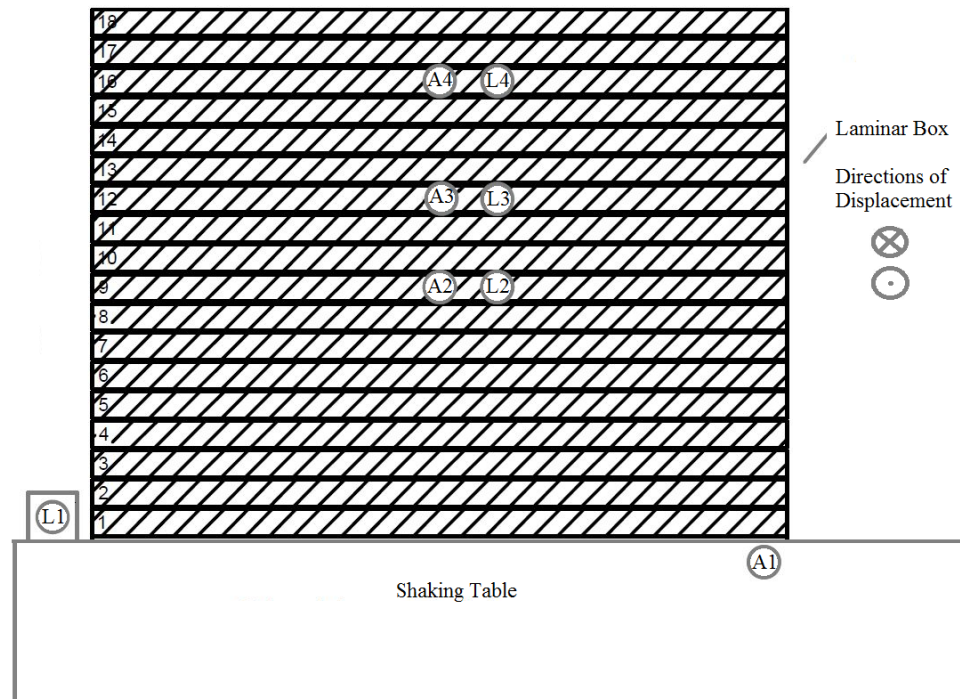


Figure 3.14. Front View of Instrumentation Layout of the Laminar Box Filled with Soil.

In total, three ODS and eleven accelerometers were placed to monitor the behavior of the filled soil. Three ODS and three accelerometers A2, L2, A3, L3 and A4, L4 were mounted on three different layers from bottom to top. Eight accelerometers were situated in the soil. Four accelerometers A7, A8, A9, and A10, were placed on a same horizontal plane whose height was  $1/2$  of the total height of the laminar box at the four corners 15 cm away from the sides as seen in the Figure 3.15b. The rest of the four accelerometers A5, A6, A11, and A12 were located at a vertical axis that passes through the midpoint of the box with the height of respectively  $1/4$ ,  $2/4$ ,  $3/4$  and  $4/4$  of the total height from the bottom as seen in the Figure 3.15a.

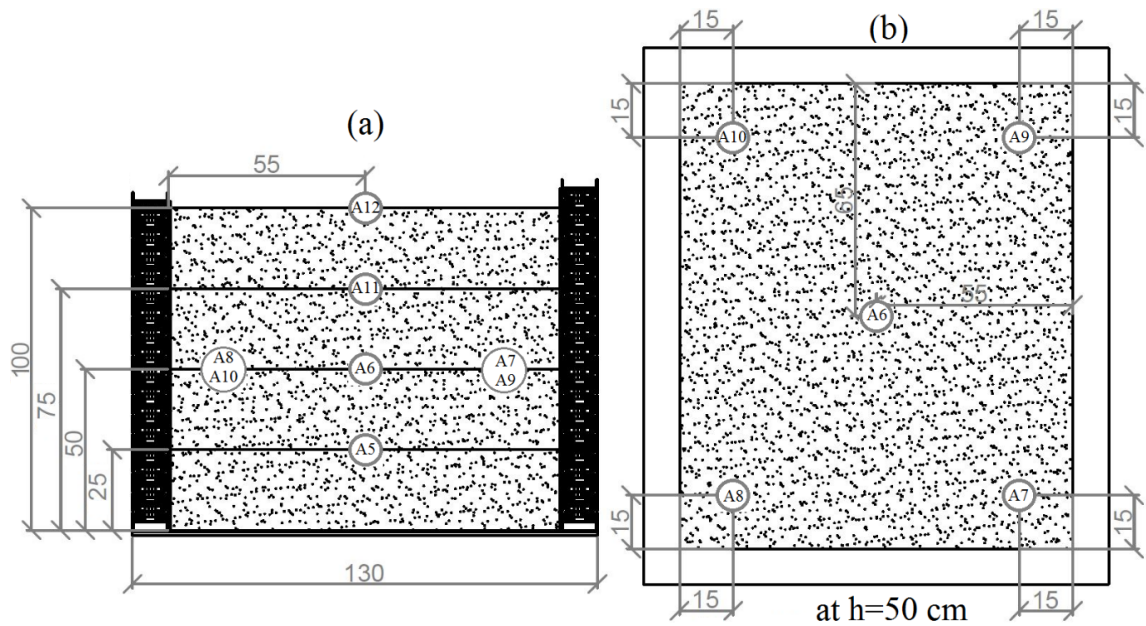


Figure 3.15. (a) Section and (b) Top View of Instrumentation Layout of the Laminar Box Filled with Soil.

Cyclic sinusoidal motions that have 0.5 Hz with 0.1g, 1 Hz with 0.3g, 2 Hz with 0.7g, 3 Hz with 0.4g, 4 Hz with 0.5g and 5 Hz with 0.5g were applied to the laminar box. In addition to cyclic sinusoidal motion, real El Centro earthquake, Kobe earthquake, and Kocaeli earthquake records were applied to the laminar box to ensure linear soil behavior. The measurements of accelerometers were compared to examine the influence of the box boundaries on soil behavior (Figure 3.16a, Figure 3.16b, and Figure 3.16c). The comparison was done with the accelerometers A6, A7, A8, A9, and A10 that were at the same horizontal plane. Since, they are located nearby at the same horizontal plane in a relatively homogenous soil, it is expected that the measured acceleration values are almost identical. Figure 3.16a shows the acceleration values of A6, A7, A8, A9, and A10 under 0.5 Hz cyclic sinusoidal motion. Measured accelerations from A6, A7, A8, A9, and A10 under 1 Hz sinusoidal motion and Kobe earthquake are monitored in Figure 3.16b and Figure 3.16c. Like expected, there is no significant difference among A6, A7, A8, A9, and A10 under different shaking table motions.

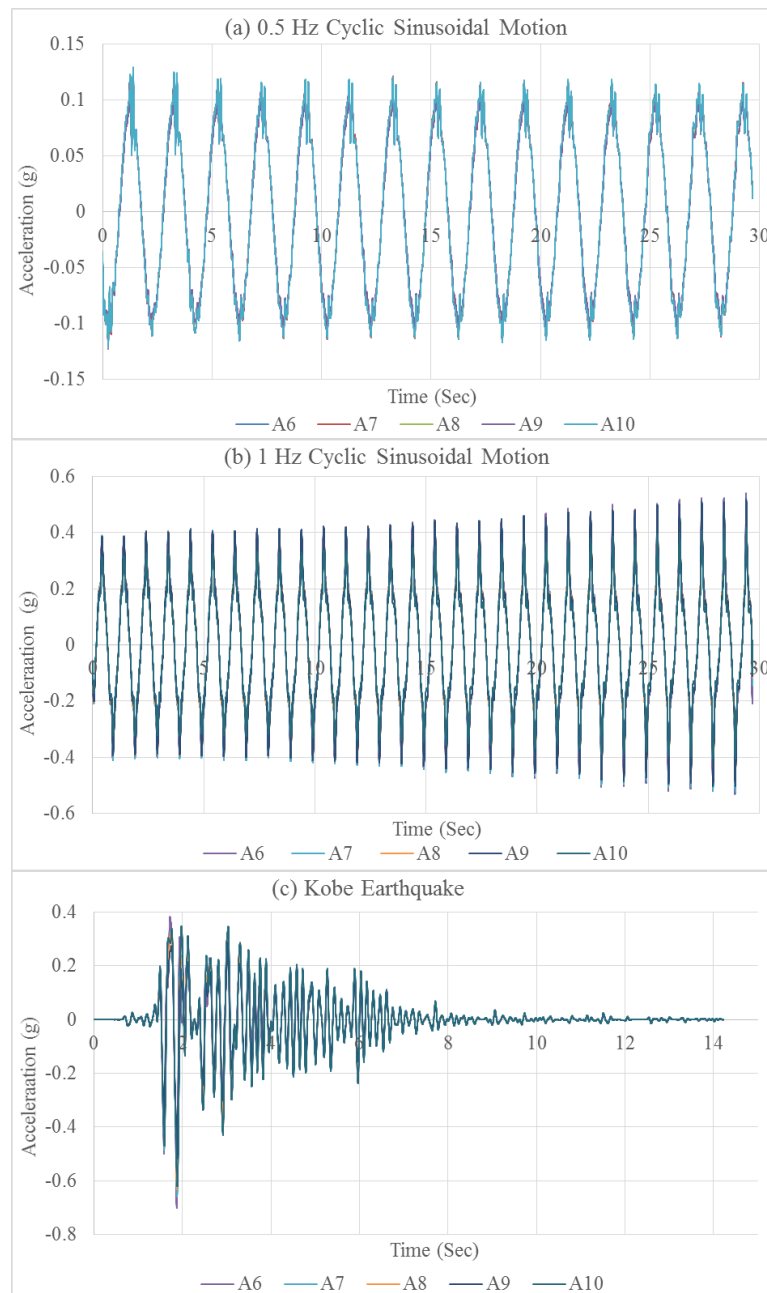


Figure 3.16. (a) Acceleration versus Time Graphs under 0.5 Hz Cyclic Sinusoidal Motion, (b) Acceleration versus Time Graph under 1 Hz Cyclic Sinusoidal Motion and (c) Acceleration versus Time Graph of the Laminar Box Filled with Soil under the Real Kobe Earthquake Records.

Four different performance tests related to the inertia of the laminar box, friction between the laminates, stiffness of the membrane, and restriction of the boundary were performed for the constructed laminar box to analyze the reliability of the box. The

findings from four distinct performance tests demonstrated that the laminar box and flexible boundaries of the laminar box functioned appropriately.

### **3.2.2. Scaled Building Models**

The proposed GSI system is applicable for low-rise and mid-rise buildings hence, the model prototypes were selected 5-story and 3-story buildings for this research. The dimensions of the laminar box and influences of the horizontal stress distribution toward the boundary of the laminar box due to the foundation, were restricted the scaling factor of the building models. The dimensions of laminar box do not allow the full-scale buildings thereby, considering maximum allowable dimensions for the building model 1:10 scale factor was determined. Besides, in known literature 1:10 scale factor has been typically used due to ease of manufacturing and reliability. Similitude requirements that taken from Harris & Sabnis (1999) Section 2.5 was considered in the model designing process. In consequence of using the currently available material to manufacture the building, material properties were not scaled. The most important issue during the design and scaling of the building was soil structure behavior that occurs during the experiments because, this research directly interests the GSI and its effectiveness. By taking into consideration this, the prototype was scaled oriented with base pressure and soil structure behavior. The scale factors for required parameter given in Table 3.5. Some physical quantities, such as acceleration and strain, remain the same even after scaling.

Table 3.5. Scaling Parameter of the Building Model.

Parameter	1:10 Scale Model/ Prototype	
Length	L	1/10
Time	$\sqrt{L}$	$1/\sqrt{10}$
Mass	$L^2$	1/ 100
Displacement	L	1/10
Acceleration	1	1/1
Stress	1	1/1
Strain	1	1/1
Force	$L^2$	1/100

First, columns of the scaled 5-story building model were manufactured with steel grade St 42 as seen in the left of Figure 3.17. At the end of the performance tests, the highest displacement value was measured from the top floor of the building approximately 3 mm. It was decided that this values may not be sufficient to see the effect of proposed GSI system on the displacement of the building clearly. Besides, measured displacement values are nearly in the same range of the tolerable reading error of the ODS, which is stated in the device catalog as 2%. Displacements of the building models were amplified by replacing the St 42 steel columns with relatively slim high carbon steel columns to increase the reliability of the measurement and to observe the response of the buildings expressly. As shown in the Figure 3.18 two identical column was placed side by side not to suffer from additional the torsion and local buckling problem arising out of the slim column geometry. The scaled buildings models were modeled with the computer software program SAP 2000 to verify the behavior of the building models. Furthermore, the modal information that obtained from the SAP 2000 analyses were compared with the free vibration test results. Results of the comparison were acquired as a quite similar. As mentioned before the main interest of this research was evaluating the effectiveness and robustness of the proposed GSI system thence, structural characteristics of the building model were created and scaled simply.



Figure 3.17. 1:10 Scaled 5-Story Building Model with St 42 Steel Column.

The specifications of the buildings are summarized as such: High carbon steel columns whose dimension was 26.5 cm x 5 cm x 0.5 cm were tied with metric eight bolts to floors. Floors of the building models were made of St 42 steel with a dimension of 30 cm x 30 cm x 1 cm also, the weight blocks of the floors were made of St 42 with a dimension of 30 cm x 30 cm x 2 cm. Four flanges were welded on every floor as connection apparatus for attaching the columns. Foundation was made of St 42 steel with a dimension of 35 cm x 35 cm x 2 cm. The story weight blocks and foundation blocks were manufactured as piecewise for the ease of carrying and reconstruction. The final height of the 5-story building was 135 cm without foundation, and the final height 3-story building was 81 cm without foundation.

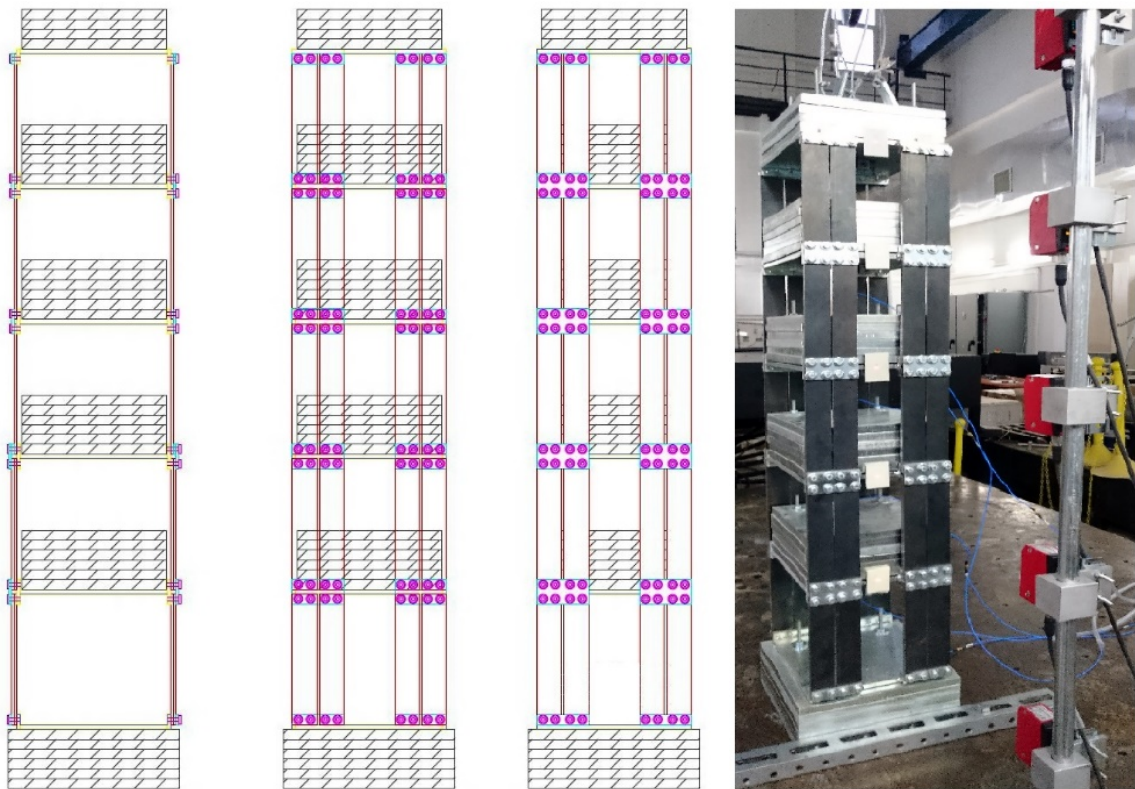


Figure 3.18. 1:10 Scaled 5-Story Building Model with High Carbon Steel Column.

### 3.2.3. Properties of the Geosynthetics

In order to get dynamic properties of the geosynthetic couples, shaking table tests were carried out. The shaking table test setup was prepared as like in the literature. The geomembrane was directly fixed on the shaking table surface and the geotextile was attached to the bottom of the solid block that created 9.6 kPa normal stress. Figure 3.19a shows a view of the rigid block experiment setup and Figure 3.19b displays the sketch of the setup. Displacement data were gathered from three ODS, one of them collect the relative displacement directly to improve the certainty of the experiment. 1 Hz with 0.32g, 2 Hz with 0.63g, 3 Hz with 0.77g 4 Hz with 0.67g and 5 Hz with 0.8g of cyclic sinusoidal motions and the real El Centro, Kobe and Kocaeli earthquakes records were applied to rigid block experiments.

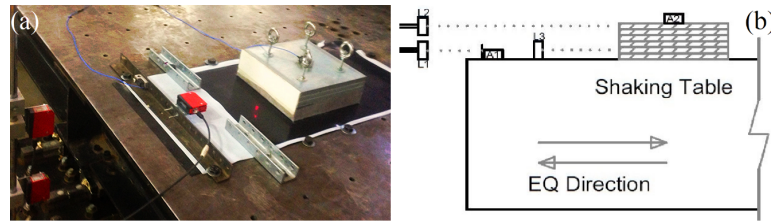


Figure 3.19. (a) A View of Rigid Block Test Setup and (b) Experimental Setup Layout of the Rigid Block Experiment.

The shaking table motions are transferred to the block by means of the shearing resistance of the geomembrane/geotextile interface that forms the contact. As the amplitude of base acceleration is increased, eventually a level is reached when the shearing resistance of the interface is not sufficient to transfer the impulse, and relative movement between the two geosynthetics is observed. The magnitude of the acceleration at which this slip initiates provides the coefficient of dynamic friction of the interface. Yegian & Lahlaf (1992) expressed in detail how dynamic interface properties could be found with shaking table test. Free body diagram of the shake table setup was sketched in the Figure 3.20.

The following formulation is presented to relate the measured acceleration of the block ( $a_b$ ) with the shear stress transmitted through the geomembrane/geotextile system.

$$\phi_d = \tan^{-1} \left( \frac{a_b}{g} \right) \quad (3.5)$$

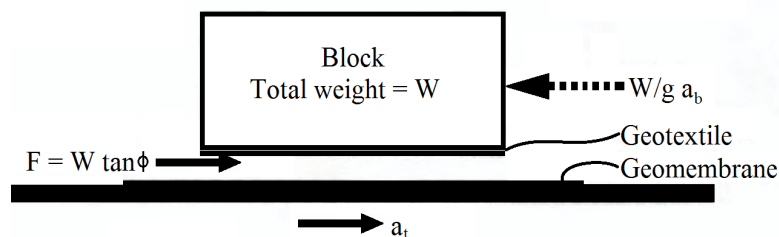


Figure 3.20. Free Body Diagram of the Rigid Block Experiment (Yegian & Lahlaf (1992)).

Three different geomembrane/geotextile configurations were assessed with the shaking table to determine their dynamic properties. With the given formula above, dynamic friction angles of the three geomembrane/geotextile configurations were calculated at the first observation of sliding as listed in Table 3.6. Average of the friction angles was computed to see the difference among the three geomembrane/geotextile couples clearly. PTFE/SF 44 couple has minimum dynamic friction angle ( $\phi_d$ ) at the first observation of sliding.

Table 3.6. Block Acceleration ( $a_b$ ) and Dynamic Friction Angles ( $\phi_d$ ) of the Three Geomembrane/Geotextile Configurations at the First Observation of Sliding.

Shaking Table Motions	PTFE/SF 44		PTFE/SF 56		HDPE/SF 44	
	$a_b$ (g)	$\phi_d$ ( $^\circ$ )	$a_b$ (g)	$\phi_d$ ( $^\circ$ )	$a_b$ (g)	$\phi_d$ ( $^\circ$ )
1 Hz	0.132	7.510	0.127	7.260	0.261	14.630
2 Hz	0.111	6.320	0.123	7.030	0.244	13.700
3 Hz	0.098	5.600	0.128	7.290	0.219	12.350
4 Hz	0.108	6.180	0.111	6.360	0.223	12.580
5 Hz	0.086	4.890	0.126	7.150	0.214	12.090
El Centro Eq.	0.132	7.530	0.139	7.910	— <sup>1</sup>	— <sup>1</sup>
Kobe Eq.	0.119	6.760	0.115	6.550	0.299	16.640
Kocaeli Eq.	0.115	6.550	0.142	8.090	— <sup>1</sup>	— <sup>1</sup>
Avg.	0.112	6.418	0.126	7.205	0.243	13.665

The other specified property for geomembrane/geotextile couple is limitations of acceleration that transmitted to the block after sliding initiated which is called as residual acceleration. Table 3.7 involves both measured peak table ( $A_t$ ) and peak block ( $A_b$ , residual acceleration) accelerations under different shaking table motions for three geosynthetic couples. Roughly, threshold acceleration values that are required to initiate the working of the GSI system were 0.11g for PTFE/SF44, 0.13g for PTFE/SF56 and 0.24g for HDPE/SF44. The percentage (%) reduction parameter was utilized to compare the effectiveness of geosynthetic couples clearly. % reduction was computed with 100% minus the ratio between the peak block acceleration and peak table accel-

<sup>1</sup>Any activity was not observed.

ation as a percentage. According to experiments results (Table 3.7), if the acceleration amplitude was increased % reduction will increase. In other words, proposed GSI system performed a better response at higher acceleration values according to rigid block experiments. Figure 3.21 shows the % reduction parameter under selected eight input motions as 1 Hz, 2 Hz, 3 Hz, 4 Hz, 5 Hz, real El Centro, Kobe and Kocaeli earthquake motions, respectively. In addition to acceleration values, Table 3.7 includes the peak slip displacements ( $D_s$ ) regarding given shaking table motions.

Table 3.7. Measured Peak Table Accelerations ( $A_t$ ), Peak Block (Residual Acceleration) Accelerations ( $A_b$ ) and Slip Displacements ( $D_s$ ).

PTFE/SF44								
	1 Hz	2 Hz	3 Hz	4 Hz	5 Hz	El Centro Eq.	Kobe Eq.	Kocaeli Eq.
$A_t$ (g)	0.34	0.63	0.76	0.67	0.79	0.34	0.69	0.21
$A_b$ (g)	0.19	0.20	0.19	0.20	0.21	0.15	0.18	0.14
% Reduction	45	69	74	70	74	57	74	36
$D_s$ (cm)	6.99	3.81	7.29	2.57	3.82	0.47	2.98	0.50
PTFE/SF56								
	1 Hz	2 Hz	3 Hz	4 Hz	5 Hz	El Centro Eq.	Kobe Eq.	Kocaeli Eq.
$A_t$ (g)	0.32	0.62	0.77	0.68	0.82	0.33	0.74	0.24
$A_b$ (g)	0.20	0.21	0.21	0.21	0.22	0.17	0.19	0.16
% Reduction	38	67	73	69	73	50	74	34
$D_s$ (cm)	4.08	6.08	7.76	5.08	4.69	0.45	2.83	0.31
HDPE/SF44								
	1 Hz	2 Hz	3 Hz	4 Hz	5 Hz	El Centro Eq.	Kobe Eq.	Kocaeli Eq.
$A_t$ (g)	0.35	0.63	0.77	0.67	0.81	0.32	0.78	0.24
$A_b$ (g)	0.30	0.33	0.33	0.35	0.35	0.28	0.33	0.24
% Reduction	12	48	57	48	56	13	58	0
$D_s$ (cm)	1.14	3.77	3.99	5.45	9.87	0.15	1.36	0.16

Figure 3.22 shows the plots of peak block acceleration versus peak table acceleration under eight selected motions. Note that during these tests, the block acceleration was almost identical to the shaking table acceleration until sliding observed. Slip Displacements of the block with PTFE/ SF44 under cyclic sinusoidal motion with 1 Hz and 5 Hz and real Kobe Earthquake motion are monitored in Figure 3.23a, Figure 3.23b, and Figure 3.23c.

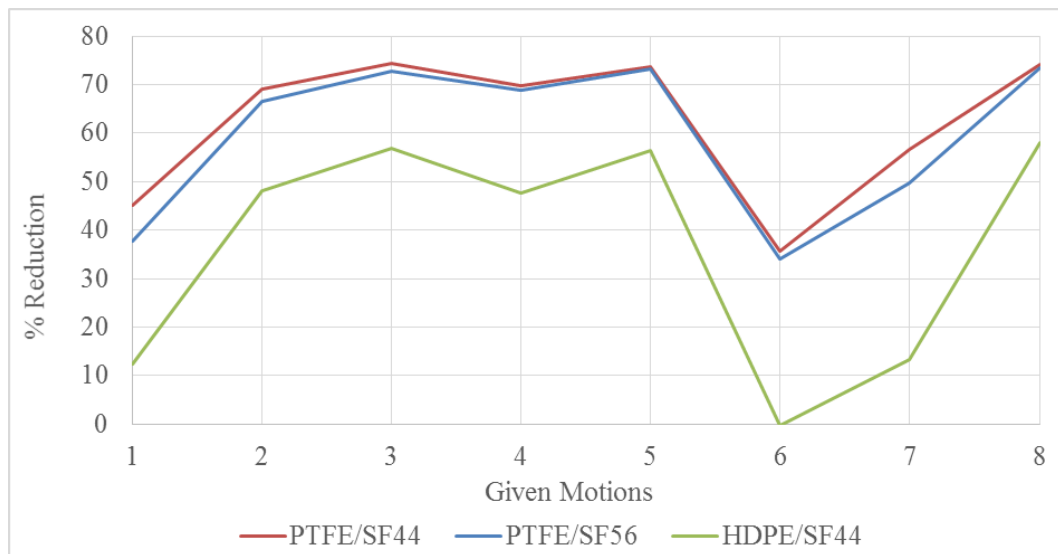


Figure 3.21. % Reduction under Eight Different Shaking Table Motions as 1 Hz, 2 Hz, 3 Hz, 4 Hz, 5 Hz, El Centro Earthquake, Kobe Earthquake and Kocaeli Earthquake, Respectively.

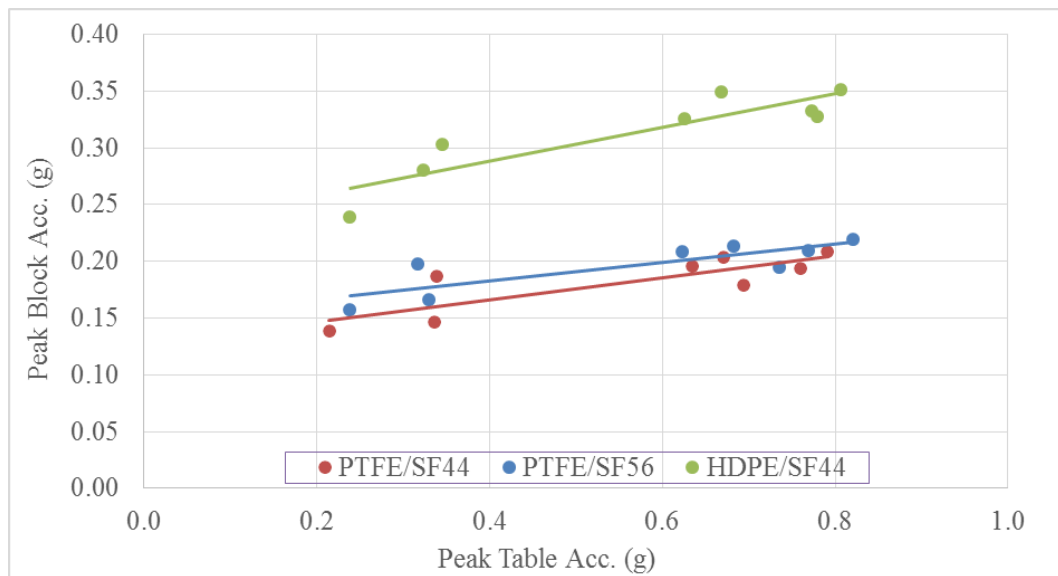


Figure 3.22. Peak Block Accelerations versus Peak Table Accelerations under Eight Different Shaking Table Motions as 1 Hz, 2 Hz, 3 Hz, 4 Hz, 5 Hz, El Centro Earthquake, Kobe Earthquake and Kocaeli Earthquake, Respectively.

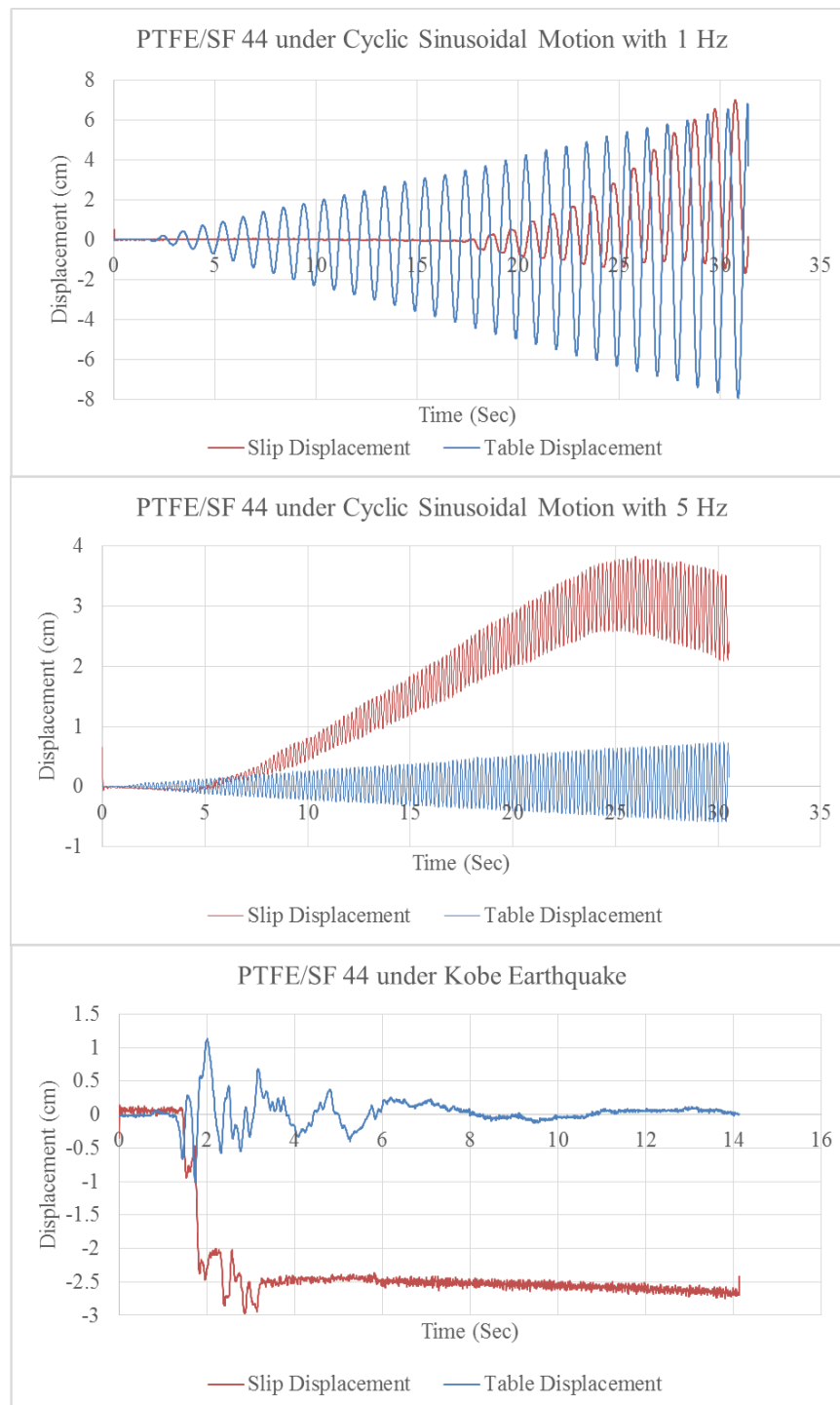


Figure 3.23. (a) Slip Displacements of the Block under 1 Hz Cyclic Sinusoidal Motion, (b) Slip Displacements of the Block under 5 Hz Cyclic Sinusoidal Motion, and (c) Slip Displacements of the Block under Kobe Earthquake record.

Geomembrane/geotextile couple limits the acceleration that transmitted to block after sliding initiated. PTFE/SF 44 has minimum residual dynamic friction angle that

means this couple reduces the transmitted acceleration more than others do.

All these results would provide the information during the input selection and material selection for the following GSI experiments. Besides the friction between the geomembrane and geotextile were verified with the related prior studies. The results of the shaking table tests, which were performed on a geomembrane/geotextile system, clearly showed that there was a certain limiting value for the shearing resistance. Thus, any structure, or a soil deposit that is resting on the geotextile, can experience only a limiting acceleration, beyond which relative displacement will be initiated along the geomembrane/geotextile interface.

### 3.3. Shaking Table Experiments

After interpreting the literature studies, the cylindrical shape was selected as the geometry of the geosynthetics to proceed with the experiments of GSI with geosynthetics. Three research were investigated for the geometry of the GSI in known literature. These are Yegian & Catan (2004), Georgarakos *et al.* (2005), and Tsatsis *et al.* (2013) chronologically. Yegian & Catan (2004) performed experimental research on cylindrical and tube shaped geosynthetics geometry. It was known that cylindrically shaped geosynthetics geometry generates the restoring gravitational force that would bring the isolated sand deposit back to its horizontal position. Thus, cylindrical shaped would be decreased the permanent slip of the both structure and isolated soil region after experiencing seismic excitations. Their experimental results confirmed the effectiveness of the restoring gravitational force after their shaking table tests. However, the tub-shaped geometry was proposed in their research because of the ease of construction. Then, Georgarakos *et al.* (2005) analyzed the cylindrical shaped, tube-shaped, trapezoidal shaped with side angle  $30^\circ$  and  $60^\circ$  and compound trapezoidal shaped geosynthetic geometry numerically. In contradiction to Yegian's findings, cylindrical and compound trapezoidal shaped geosynthetics geometry was proposed. For the sake of ease of construction, trapezoidal shaped geosynthetics geometry was recommended, but tube-shaped geosynthetic geometry was eliminated. As a final study about this topic, Tsatsis *et al.* (2013) analyzed the compound trapezoidal shaped geosynthetic ge-

ometry numerically. At the end of the research, it was revealed that trapezoidal shape was turned into a cylindrical shape geosynthetic geometry after being subjected to the seismic excitation. This means almost all geometrical shape of geosynthetics including the trapezoidal shape tends to transform into cylindrical shape after seismic motions. Considering gravity restoring effect and the results of the mentioned studies, it can be deduced that cylindrically shaped geosynthetics geometry is the most efficient one among the others. As the stroke of the shaking table is uniaxial horizontal direction, geosynthetics were curved only in the direction of shaking. By determining geometric shape of the geosynthetics, one experimental parameter that was the geometric shape of the geosynthetics was removed based on prior research.

The experimental parameters of the shaking table experiments involve geosynthetic types, GSI depths (H/D ratio), and the number of building story. Even though the ideal geosynthetic couple was procured as PTFE/ SF44, to enhance the reliability of this research, PTFE/SF56, and HDPE/SF44, geosynthetic couples would be added to the experimental program of the proposed GSI system. Yegian & Catan (2004) plotted the graph displaying the transmitted acceleration versus H/D ratio. This chart helped to decide ideal GSI depth (H/D ratio) according to the width of the covered geosynthetics as seen in the Figure 3.20. In the current research, GSI width toward the shaking direction was established as constant 1 meter due to the dimensions of the laminar box. Thereby, depth of the GSI became directly proportional to transmitted acceleration. This means that if the GSI depth is increased, transmitted acceleration to the building increases for this condition. Transmitted acceleration becomes quite stable after H/D ratio exceeds 6.0. Therefore, depth of the GSI was distinguished as 10 cm (H/D = 10) and 15 cm (H/D = 6.7). The final experimental parameter was the number of building story. This proposed GSI system with geosynthetics is valid for low to medium rise structures. Hence, 3-story and 5-story building models were used in proposed GSI system experiments.

Input motions of the shaking table that were applied for proposed GSI system experiments were divided into two categories that were cyclic sinusoidal and earthquake motions. According to Kalpakci (2013), geosynthetics reduced the transmitted

acceleration of the building when the input motion frequency is in close vicinity of the natural frequency of the structure. Hence, frequencies of the cyclic sinusoidal motions were decided regarding dominant frequencies of the building that were devised from the free vibration test. According to free vibration tests, cyclic sinusoidal motion frequencies of the 5-story building model were obtained 28 Hz, 24.5 Hz, 18.68 Hz, 11.7 Hz, 3.25 Hz. Cyclic sinusoidal motion frequencies of the 3-story building model were measured 26 Hz, 18.68 Hz, and 5Hz. Earthquake motions were specified as in Section 3.1.4 according to their characteristics. These were the 1940 El Centro (Array #9 station), 1995 Kobe (KJMA station), and 1999 Kocaeli (Izmit station) Earthquake records. As can be clearly observed from the response spectra and Fourier amplitude spectra in Figure 3.24-Figure 3.26 that the 1995 Kobe earthquake record has the longest duration, and it has quite high spectral values rather than the 1940 El Centro and the 1999 Kocaeli earthquake records. Moreover, Kobe earthquake record has its peak values in the acceleration response spectrum in longer periods than other given earthquake records. The 1999 Kocaeli earthquake record has the shortest duration, and it has relatively high-frequency content, unlike the 1995 Kobe and the 1940 El Centro earthquake records. The 1940 El Centro earthquake record does not have high-frequency content like the 1999 Kocaeli earthquake record, but it has higher duration than the 1999 Kocaeli earthquake record.

To apply the earthquake records to proposed GSI system and building models, duration of the earthquake input data were scaled 1:10 by multiplying duration with a scaling factor of  $\sqrt{10}$  in the light of similitude rules taken from Harris & Sabnis (1999). In other words, to maintain dynamic similitude, each record was compressed in time by a factor of  $\sqrt{10}$ . Time history, Fourier amplitude spectrum, and response spectrum graphs of the scaled earthquake motions are shown in the Figure 3.24, Figure 3.25, and Figure 3.26, respectively.

Due to the fact that the risk of hazard level in the soil or structure is directly proportional to the amplitude of the earthquake. The amplitude of the motions can be examined simply by the response quantities. In addition to time scaling, the acceleration amplitudes of the earthquake records were scaled to evaluate effectiveness

and robustness of the proposed GSI system under various amplitudes. Peak ground acceleration (PGA) of El Centro earthquake was scaled by 1.0, 1.42, 1.72, 2.25, 2.53, and 2.78. Peak ground acceleration of Kobe earthquake was scaled by 0.91, 1.0, and 1.08. Peak ground acceleration of Kocaeli earthquake was scaled by 1.0, 1.54, and 2.27. After scaling PGA of the earthquakes, 12 earthquake motions with various peak accelerations ranging from 0.22g to 0.89g were obtained. On the other side, the acceleration amplitudes of the cyclic sinusoidal motions were determined according to the response of the building models. Acceleration amplitudes of the cyclic sinusoidal motions of the 5-story building model were 0.3g for 28 Hz, 0.5g for 24.5 Hz, 0.3g for 18.68 Hz, 0.35g for 11.7 Hz and 0.25g for 3.25 Hz. Acceleration amplitudes of the cyclic sinusoidal motions of the 3-story building model were 0.5g for 26 Hz, 0.5g for 18.68 Hz and 0.3g for 5 Hz.

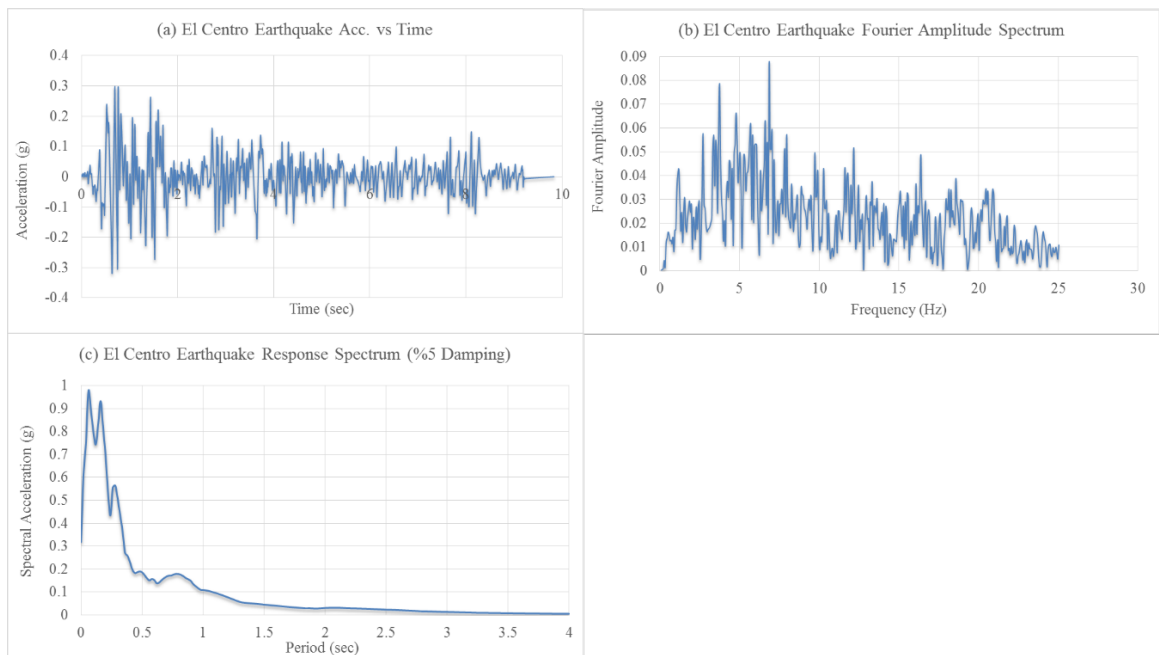


Figure 3.24. (a) Time History, (b) Fourier Spectrum, and (c) Response Spectrum of Time Scaled El Centro Earthquake (Array #9 Station).

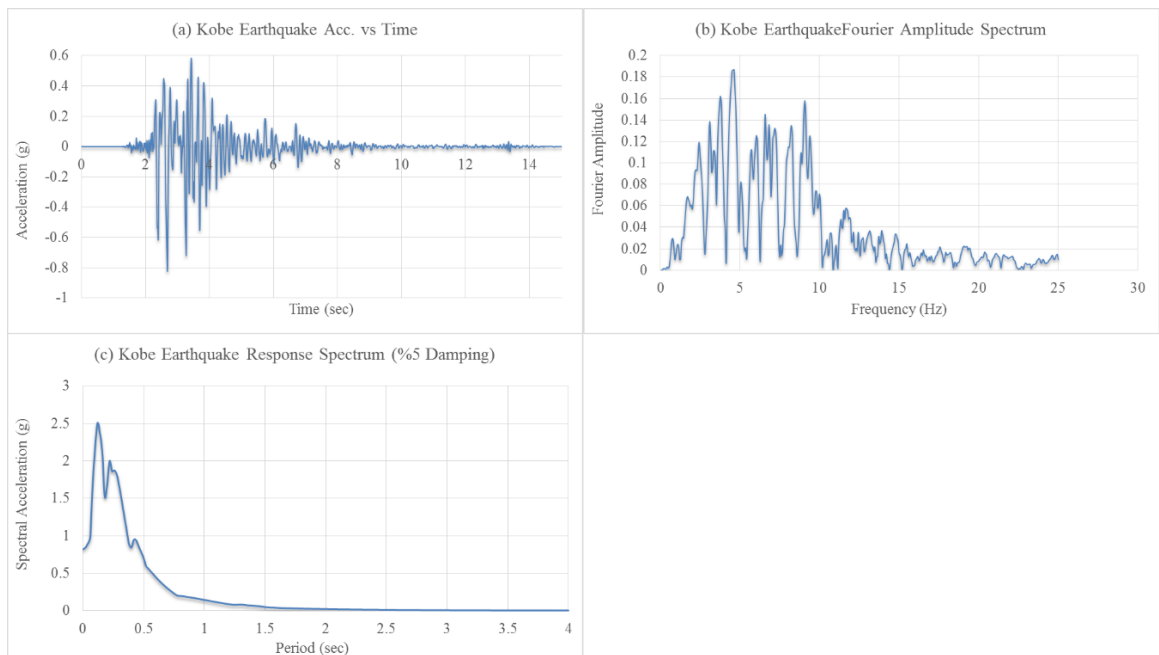


Figure 3.25. (a) Time History, (b) Fourier Spectrum, and (c) Response Spectrum of Time Scaled Kobe Earthquake (KJMA Station).

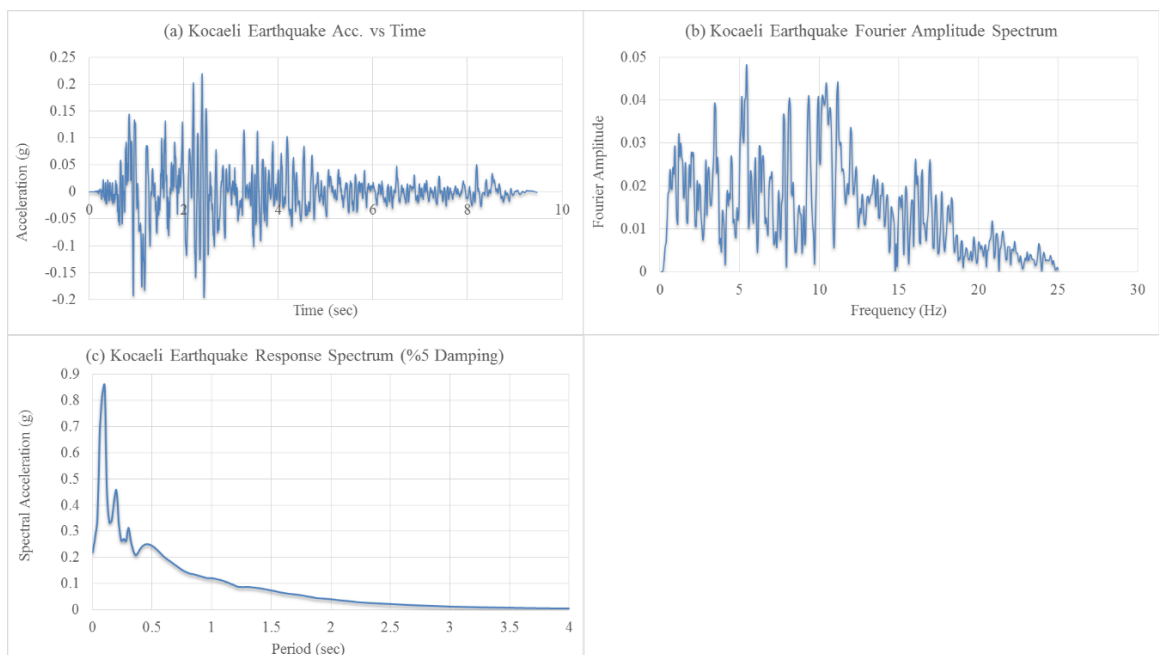


Figure 3.26. (a) Time History, (b) Fourier Spectrum, and (c) Response Spectrum of Time Scaled Kocaeli Earthquake (Izmit Station).

### 3.3.1. Soil Preparation and Instrumentation

Locations of the in-soil accelerometers were carefully selected to understand the influence of the GSI. Three in-soil accelerometers having  $\pm 3g$  capacity were installed. The first in-soil accelerometer was located at the center of the laminar box under the GSI layer. The second one was installed in between the foundation of building model and GSI layer. The last accelerometer was placed outside of the isolated soil region, near the surface.

In total, an approximately 2.7 tons of Silivri sand were used. The unit weight of the compacted Silivri sand is  $18.4 \text{ kN/m}^3$  ( $D_r = 85\%$ ). The soil preparation and instrumentation process was done as follows. The dry sand was placed through compaction of four equal layers as given in the Figure 3.27. Each equal subsequent level was filled with roughly 0.7 tons of Silivri sand. Once the sand was installed in the layers, compaction process begun. Sand was compacted manually with the identical procedure for each subsequent layers. After compacting the second layer, the first accelerometer, tagged as “A2”, was installed at the midpoint of the layer. At the end of the compaction of the third layer, according to the specified H/D ratio, the curved shape was acquired by adding sand mildly. Then, geotextile was placed over the geomembrane. Sand was filled over the geosynthetics up to half of the GSI depth (H/D ratio) and compacted lightly not to disturb the accelerometer. Later, the second accelerometer that was tagged as “A3” was placed at the midpoint of the compacted soil. The placement of sand was carried on until reaching the foundation depth. When the foundation depth was reached, sand was compacted gently and building model was installed. Finally, the laminar box was filled with sand completely and the sand was again compacted manually. The third accelerometer was installed at free field, outside of the isolated region.



Figure 3.27. Soil Filling and Compaction.

After soil preparation and in-soil instrumentation, six accelerometers for 5-story building model and four accelerometers for 3-story building model with  $\pm 20g$  capacity were mounted on the building model to record accelerations. Six ODS's were utilized for measuring story displacements. Sketches of experiment setup with 5-story and 3-story building models are shown in Figure 3.28, and Figure 3.29. Almost identical instrumentation scheme was used for two models. ODS's were projected at the midpoint of the front side of each floor. Likewise,  $\pm 20g$  capacity accelerometers were mounted on the midpoint of every floor under the slab.

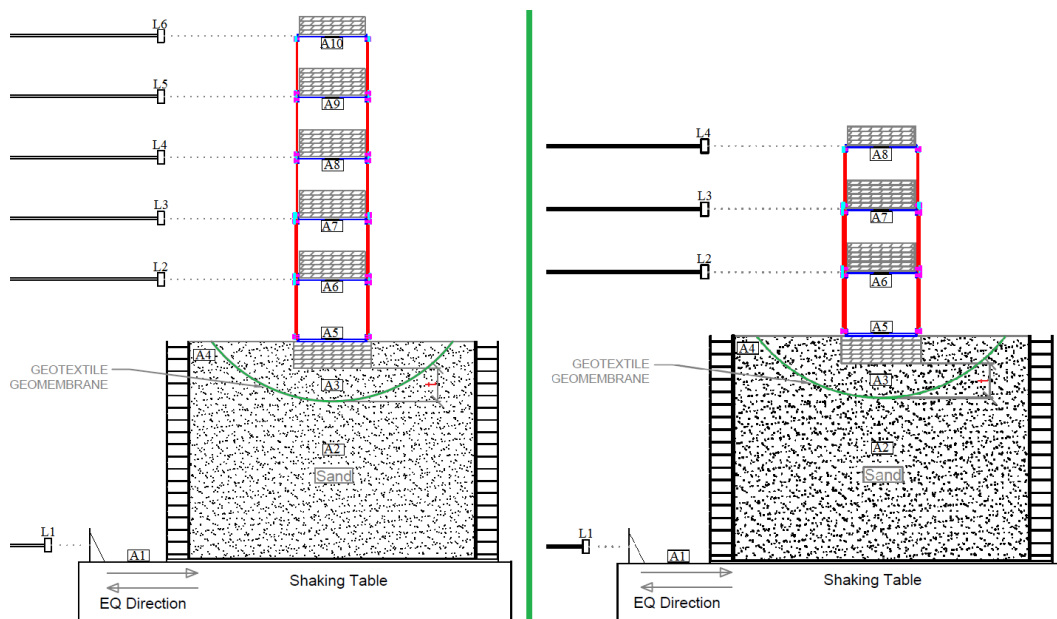


Figure 3.28. Sketch of Proposed GSI System Experiment Setup with 5-story and 3-Story Scaled Building Models.



Figure 3.29. A View of Experimental Setup.

## 4. RESULTS OF SHAKING TABLE EXPERIMENTS

In order to investigate the effectiveness and robustness of the proposed GSI system, series of shaking table experiments that covered performance tests of the laminar box, rigid block tests for geosynthetic selection and experiments of the GSI system have been conducted in all stages of this research. Cases were established to evaluate the effects of the number of building story, depth of GSI (H/D ratio), type of GSI material and ground motion characteristics for proposed GSI system as seen in Table 4.1. Cases would exemplify the illustrating and comparing the test results better. Some cases were repeated at least three times to verify and improve the reliability of the experiments. Control models (CM) were created to observe the behavior of the unisolated system including 5-story and 3-story building models under same input motions with the cases. The results of the experiments would be presented as comparisons that were made based on control model.

Table 4.1. The Cases Created to Carry Out the Proposed GSI System Experiments.

Case No	Number of Story	Depth of the GSI <sup>1</sup>	Type of the GSI Material	Cyclic Sinusoidal Motions	El Centro Eq. (PGA)	Kobe Eq. (PGA)	Kocaeli Eq. (PGA)
CM-5	5	-	-				
Case 1	5	10 cm	GSI 1				
Case 2	5	15 cm	GSI 1	28 Hz			
Case 3	5	10 cm	GSI 2	24.5 Hz	0.35 g		
Case 4	5	15 cm	GSI 2	18.68 Hz	0.46 g	0.74 g	0.22 g
Case 5	5	10 cm	GSI 3	11.7 Hz	0.55 g	0.80 g	0.34 g
Case 6	5	15 cm	GSI 3	3.25 Hz	0.72 g	0.89 g	0.50 g
CM-3	3	-	-	26 Hz	0.81 g		
Case 7	3	10 cm	GSI 2	18.68 Hz	0.89 g		
Case 8	3	15 cm	GSI 2	5 Hz			

Type of the GSI Material:

<sup>1</sup>Depth of the GSI: depth from the foundation of the building model.

- GSI 1: Junifol HDPE 1mm geomembrane with Typar DuPont SF44 nonwoven geotextile
- GSI 2: PTFE 1mm geomembrane with Typar DuPont SF44 nonwoven geotextile
- GSI 3: PTFE 1mm geomembrane with Typar DuPont SF56 nonwoven geotextile
- 10 cm ( $H/D = 10$ ), 15 cm ( $H/D = 6.7$ )

Coherent with the literature (Tsang *et al.*, 2012 and Adir, 2013), three main performance indicators that were foundation horizontal acceleration response, top floor horizontal acceleration response and first-floor drift and their peak and root-mean-square (RMS) parameters were selected. The mid-point of the top floor was chosen since it typically represents the maximum horizontal acceleration response of the structure. The mid-point of the foundation was chosen as it is commonly considered as the location where earthquake input ground motion is applied in an ordinary structural analysis. Because the soft-story mechanism is the major cause of the collapse of many buildings in earthquakes, first-floor drift has been chosen as the third parameter. Furthermore, the “percentage (%) reduction” parameter was computed to exemplify better the effectiveness of the proposed GSI system regarding its ability to reduce the acceleration and drift demand in a structure. This parameter was computed as 100% minus the response quantity gathered from the proposed GSI system expressed as a percentage (%) of the respective response quantity as obtained from the control model.

Beside of these performance indicator parameters used in the literature, five additional performance indicator parameters were chosen. Arias intensity parameter was selected to observe the earthquake energy dissipation and strength of earthquake as a comparison between isolated and unisolated systems. Both Arias intensity and % reduction of Arias intensity were computed for each floor. Peak spectral acceleration was chosen as performance indicator parameter. Peak spectral acceleration values for each floor and % reduction of them are illustrated to clarify the reduction in the spectral acceleration. The shifting of the natural period of the structure is a feature of the conventional seismic isolation system. To determine whether this feature was valid or not for proposed GSI system, natural period and period shifting ratio were presented. Base shear and base moment were chosen as performance indicator parameters to see effects

of proposed GSI system on total lateral seismic forces and its relevance to building height.

In total 164 experiments selected to create the cases and 32 of them belonged to the control models. The most reasonable results regarding % reduction were chosen from the 132 experiments. The test results under Kocaeli earthquake, El Centro earthquake, and Kobe earthquake were decided to illustrate both graphical and tabular. Cyclic sinusoidal motions with natural frequencies of the buildings that were obtained from the free-vibration tests would be investigated in parametric study part of the thesis in detail.

#### **4.1. Unisolated Ground with the 5-Story Building Model**

CM-5 was established to observe the behavior of the unisolated system including 5-story building model under chosen earthquake motions. Figure 4.1, Figure 4.2, and Figure 4.3 illustrate the foundation horizontal acceleration response, top floor horizontal acceleration response and first-floor drift of CM-5 under Kocaeli, El Centro, and Kobe earthquakes, respectively. In order to clarify the effectiveness of the proposed GSI system, the experiment results of the cases are presented as a comparison that was made based on control model.

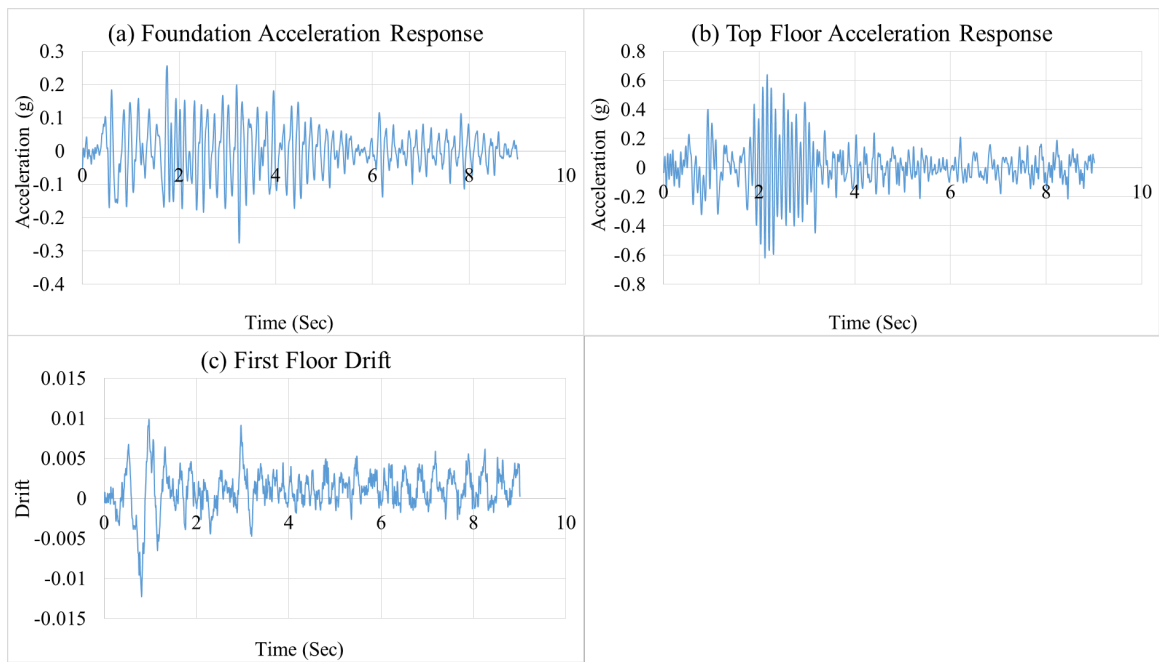


Figure 4.1. (a) Foundation, (b) Top Floor Horizontal Acceleration Response and (c) First Floor Drift of the CM-5 under Kocaeli Earthquake.

It can be observed from Figure 4.1, Figure 4.2, and Figure 4.3 that the measured maximum foundation accelerations are 0.27g, 0.44g, and 1.2g for Kocaeli, El Centro, and Kobe earthquakes, respectively. The measured maximum top floor accelerations for the Kocaeli, El Centro, and Kobe earthquakes are as 0.64g, 0.55g, and 1.48g, respectively. The first-floor drifts values belong the Kocaeli, El Centro, and Kobe earthquakes are 0.012, 0.011, and 0.029.

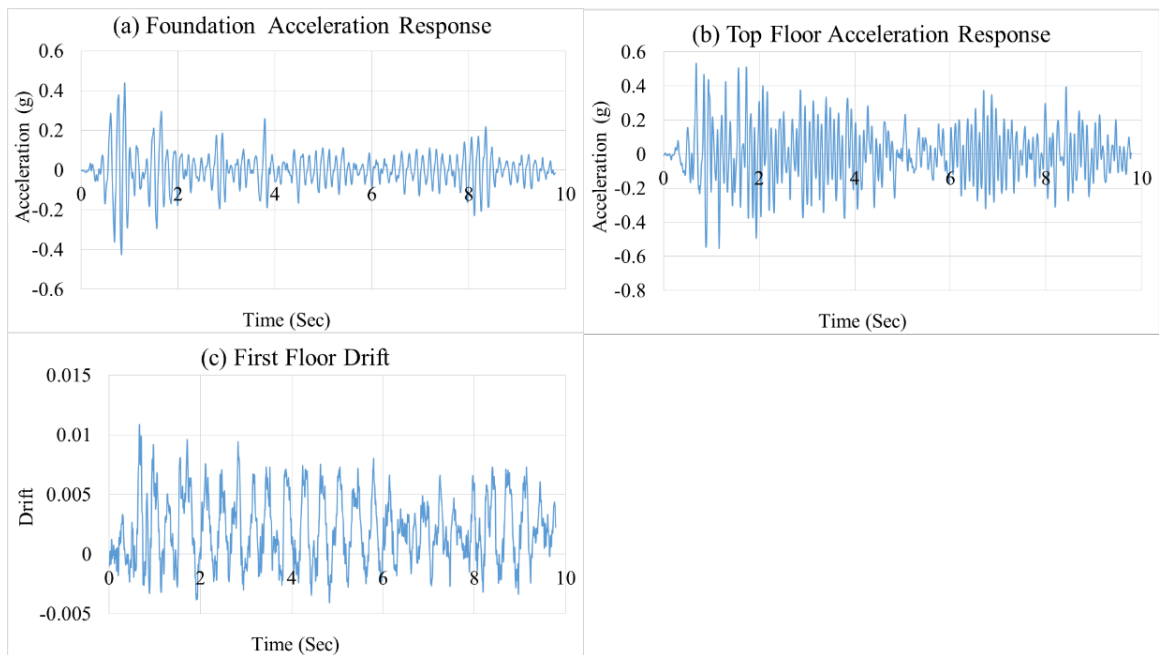


Figure 4.2. (a) Foundation, (b) Top Floor Horizontal Acceleration Response and (c) First Floor Drift of the CM-5 under El Centro Earthquake.

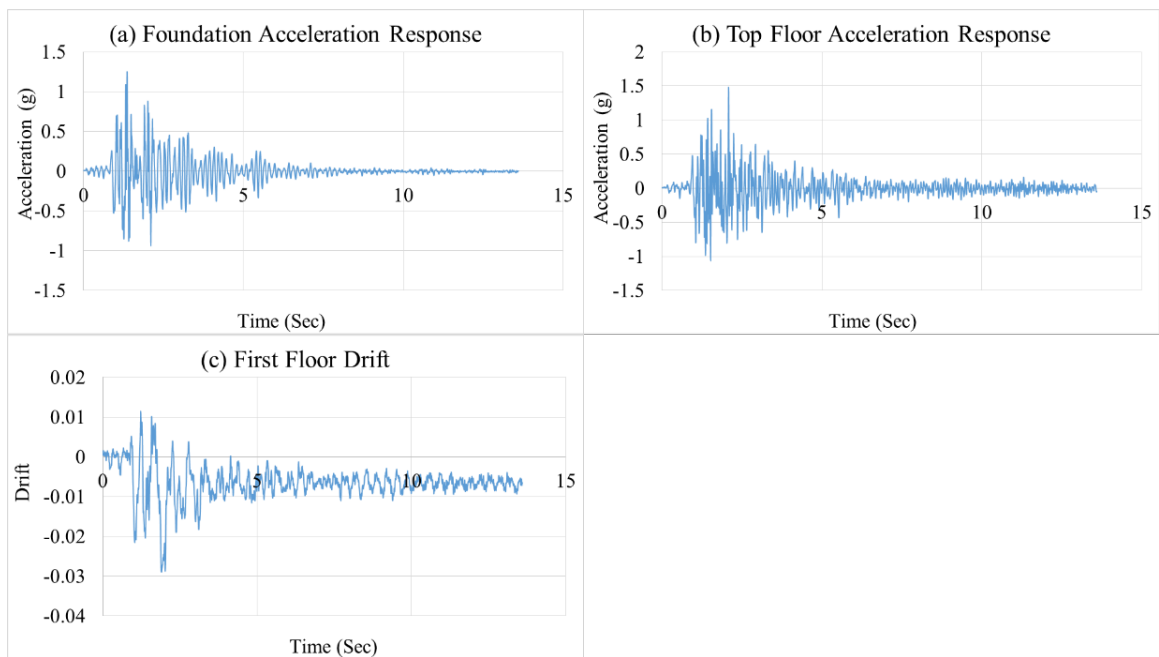


Figure 4.3. Foundation, (b) Top Floor Horizontal Acceleration Response and (c) First Floor Drift of the CM-5 under Kobe Earthquake.

## 4.2. Soil Response to the Seismic Motions

Soil seismic response may show variety under different seismic motions according to soil characteristic. For different types of soil, acceleration could be amplified or diminished while passing through the soil. In this study, Silivri sand was used as mentioned. The peak accelerations were measured from the shaking table (A1 as a base acceleration, the center of the laminar box (A2) and almost at three-quarters height of the laminar box (A3) for the unisolated case under Kocaeli, El Centro, Kobe earthquakes with real PGA, and Cyclic sinusoidal motion with 11.7 Hz are summarized in Table 4.2. Besides, acceleration variations of the Silivri sand from A1 to A2 and from A2 to A3 are also listed in Table 4.2 as a percentage. As can be observed in Table 4.2, Silivri sand has a tendency to amplify the acceleration while passing through. The variations in the in-soil acceleration due to the characteristic of the applied seismic motions are relatively slight. Because of higher traveling distances between A1 and A2, acceleration amplification is relatively high compared to those obtained from A2 to A3. However, under the Kobe earthquake motion, an unexpected reduction in the acceleration response was observed while traveling from A2 to A3. Moreover, the acceleration reductions of A3 due to the application of proposed GSI system are tabulated in Table 4.3. As specified, A3 was placed in between GSI layer and foundation of the building model. This means that in-soil effects of the applied GSI system on acceleration obtained from the A3. Additionally, in-soil acceleration reductions due to the application of proposed GSI system are presented together with the acceleration reductions of building models in following tables to observe the relationship between acceleration response of in-soil and building models.

Table 4.2. Soil Response to the Seismic Motions.

Soil Response to the Seismic Motions					
Seismic Motions	Measured Peak Acceleration (g)			Variation of Acceleration (%)	
	A1	A2	A3	From A1 to A2	From A2 to A3
Kocaeli Earthquake	0.21	0.24	0.27	14	11
El Centro Earthquake	0.33	0.38	0.42	13	9
Kobe Earthquake	0.83	0.99	0.95	16	-5
Cyclic Sinusoidal Motion	0.39	0.45	0.50	12	11

Table 4.3. Acceleration Reduction of A3 as a Result of Application of the Proposed GSI System.

In-Soil Acceleration Reduction								
Cases	Input Motions							
	Kocaeli Earthquake		El Centro Earthquake		Kobe Earthquake		Cyclic Sinusoidal Motion	
	% Reduction of A3 (%)							
	RMS	Peak	RMS	Peak	RMS	Peak	RMS	Peak
Case 1	9	16	-14	-16	2	-4	31	-13
Case 2	4	0	18	11	6	-28	11	12
Case 3	5	1	8	3	7	-40	37	-13
Case 4	9	4	-6	-20	0	-49	30	-14
Case 5	19	13	10	-8	11	-6	32	-1
Case 6	-3	-9	6	-4	4	-27	21	-10
Case 7	-3	-1	3	-4	-2	3	-8	-8
Case 8	2	2	-1	-2	-5	0	3	-1

#### 4.3. Case1; GSI 1 Placed 10 cm underneath the 5-Story Building Model

For the Case 1, Junifol HDPE 1 mm geomembrane with Typar DuPont SF44 nonwoven geotextile, which were tagged together as GSI 1, were placed with cylindrical shaped 10 cm ( $H/D = 10$ ) under the foundation. 5-story building model excited with selected earthquake motions. Moreover, given results below related to the comparison between Case 1 and CM-5 under Kocaeli earthquake, El Centro earthquake, and Kobe earthquake, respectively.

##### 4.3.1. Seismic Response of Case 1 under Kocaeli Earthquake Motion

Figure 4.4a, Figure 4.4b, and Figure 4.4c illustrate the reduced foundation acceleration, reduced top floor acceleration, and the first-floor drift comparing CM-5. The reduction of foundation acceleration is roughly 12% in RMS and 28% in peak values as seen in Figure 4.4c. Similarly, the acceleration reduction in the midpoint of the isolated soil region is 9% in RMS and 16% in peak values (Table 4.4). However, acceleration reduction values become up to 39% in RMS and 32% in peak values at the upper stories. The first-floor drift is reduced approximately 17% in RMS, and there is no reduction for the top floor. Figure 4.4e represents the % reduction of base shear

and correspondingly base moment that are diminished roughly 30% and 35% in RMS, respectively. It can be observed from Figure 4.4f, Arias intensity values computed for the floors are reduced up to 60%. In brief, all performance indicator parameters are indicated that proposed GSI system reduces the seismic effects in general. Detailed information about the performance indicator parameters is provided in Table 4.4 in such sequence; horizontal acceleration response, horizontal story drift, Arias intensity, peak spectral acceleration, period lengthening ratio of the floors and base shear and base moment of the 5-story building model. On the other side, the natural period of the 5-story building did not alter, but peak spectral acceleration was decreased up to 35% as seen in Table 4.4.

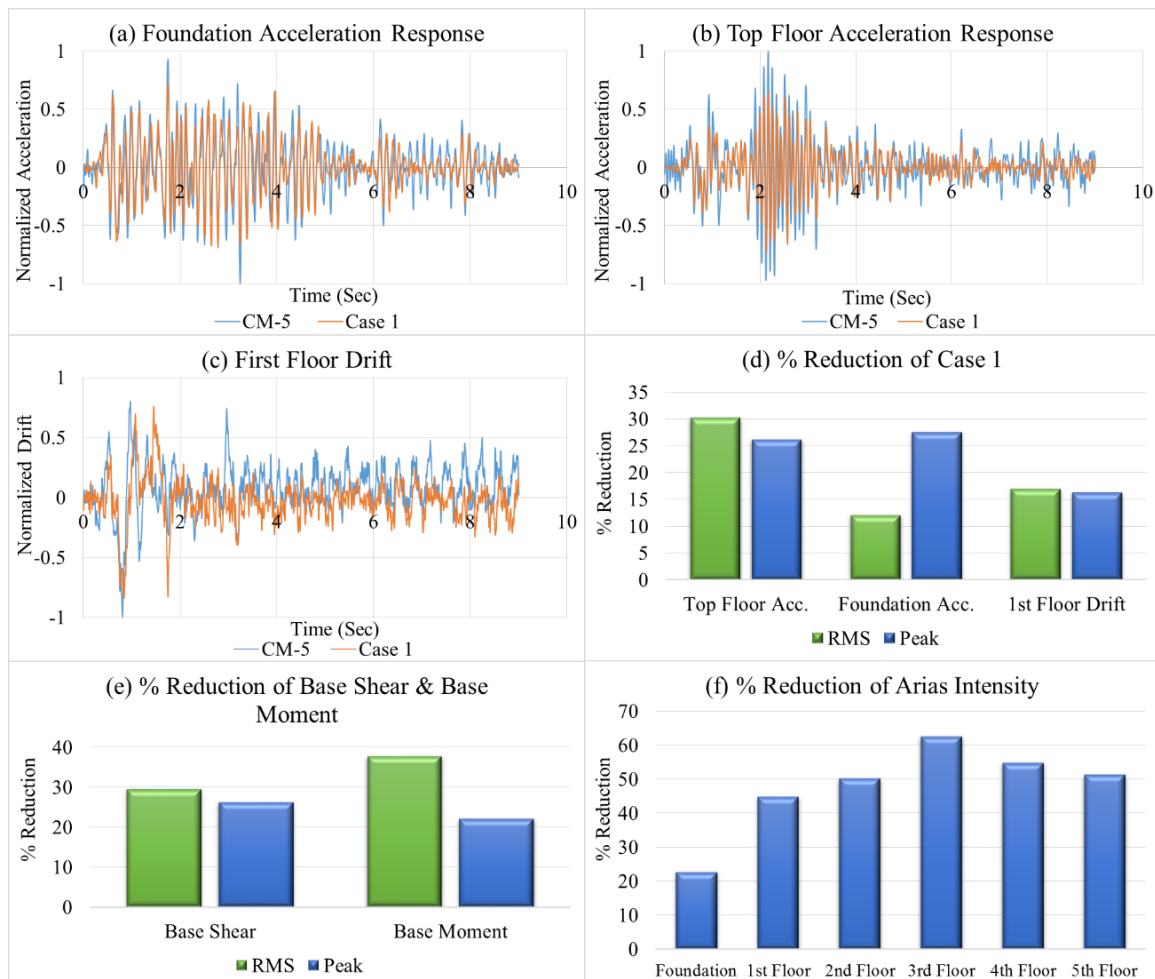


Figure 4.4. (a) Foundation, (b) Top Floor Horizontal Acceleration Response, (c) First Floor Drift, (d) % Reduction of Case 1, (e) % Reduction of Base Shear & Base Moment and (f) % Reduction of Arias Intensity of Case 1 Comparing CM-5 under Kocaeli Earthquake.

Table 4.4. Comparison of Case 1 with the CM-5 under Kocaeli Earthquake.

Results of Case 1 Comparing CM-5 under Kocaeli Earthquake																
	In-soil		Foundation		1st Floor		2nd Floor		3rd Floor		4th Floor		5th Floor			
	RMS	Peak	RMS	Peak	RMS	Peak	RMS	Peak	RMS	Peak	RMS	Peak	RMS	Peak		
Horizontal Acceleration (g)																
CM-5	0.07	0.27	0.07	0.28	0.12	0.57	0.12	0.56	0.07	0.29	0.09	0.33	0.14	0.64		
Case 1	0.06	0.23	0.06	0.20	0.09	0.39	0.08	0.41	0.04	0.20	0.06	0.23	0.10	0.47		
% Reduction	9	16	12	28	26	32	29	27	39	31	33	31	30	26		
Horizontal Story Drift																
CM-5	-	-	-	-	0.07	0.34	0.07	0.27	0.05	0.24	0.08	0.41	0.06	0.20		
Case 1	-	-	-	-	0.06	0.28	0.06	0.33	0.07	0.32	0.06	0.35	0.06	0.25		
% Reduction	-	-	-	-	17	16	11	-20	-52	-37	27	13	-2	-28		
Arias Intensity (m/sec)																
CM-5	0.68		0.69		1.93		1.93		0.69		1.01		2.88			
Case 1	0.56		0.54		1.07		0.96		0.26		0.46		1.40			
% Reduction	17		23		45		50		63		55		51			
Peak Spectral Acceleration (g)																
CM-5	-		1.25		3.73		3.98		1.77		2.23		4.43			
Case 1	-		1.18		2.54		2.61		1.13		1.42		2.85			
% Reduction	-		6		32		34		36		36		36			
Period Lengthening Ratio																
Fundamental Period (sec)																
CM-5	-		0.15		0.09		0.09		0.09		0.09		0.09			
Case 1	-		0.15		0.09		0.09		0.09		0.09		0.09			
Period Length. Ratio	-		1.00		1.00		1.00		1.00		1.00		1.00			
Base Shear (kN)																
	RMS				Peak				RMS				Peak			
CM-5	0.86				3.97				0.36				1.23			
Case 1	0.61				2.93				0.22				0.96			
% Reduction	29				26				38				22			

#### 4.3.2. Seismic Response of Case 1 under El Centro Earthquake Motion

It can be seen in Figure 4.5a, d, and f that there is no reduction in the foundation level regarding acceleration and Arias intensity. Likewise, the measured acceleration from the midpoint of the isolated soil region is magnified (Table 4.5). However, reduction of the acceleration and Arias intensity parameters exist at the upper story levels up to 28% in RMS and 33% in peak regarding the acceleration and up to 48% regarding Arias intensity. Figure 4.5b illustrates top floor horizontal acceleration response and the reduction can be seen when comparing the control model. Almost all floor drifts are reduced for this particular case. First-floor drift is decreased approximately 30% in RMS as seen in Table 4.5 and top floor drift is magnified. Figure 4.5e represents the % reduction of base shear and base moment that are diminished roughly 25% and 28% in RMS correspondingly. The information about the other performance indicator

parameters is listed in such order; horizontal acceleration response, horizontal story drift, Arias intensity, peak spectral acceleration, period lengthening ratio of the floors and base shear and base moment of the 5-story building model (Table 4.5). On the other side, shifting of the natural period is not observed integrally but period lengthening ratio of the first floor and fourth floor computed as 1.7. Besides, peak spectral accelerations are reduced up to 32% as seen in Table 4.5.

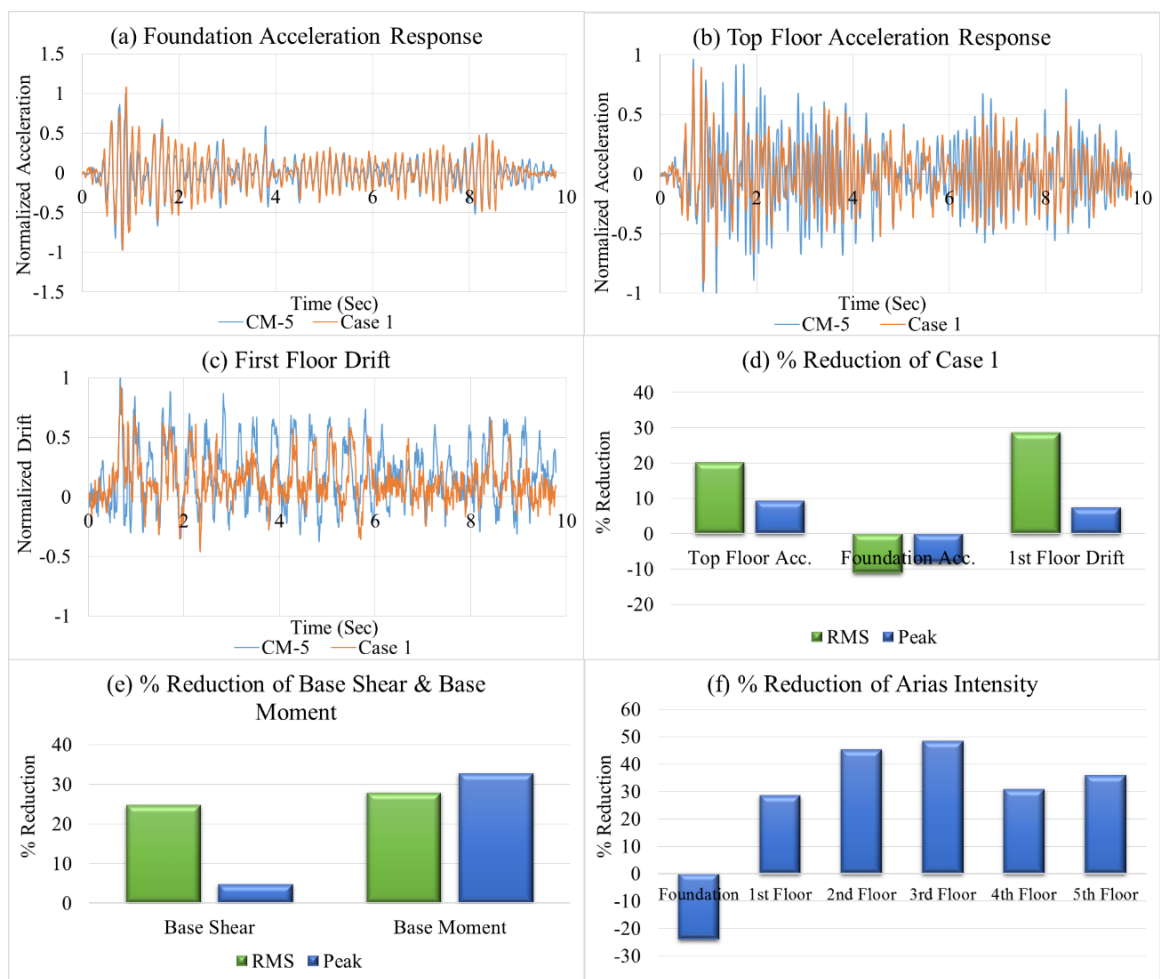


Figure 4.5. (a) Foundation, (b) Top Floor Horizontal Acceleration Response, (c) First Floor Drift, (d) % Reduction of Case 1, (e) % Reduction of Base Shear & Base Moment and (f) % Reduction of Arias Intensity of Case 1 Comparing CM-5 under El Centro Earthquake.

Table 4.5. Comparison of Case 1 with the CM-5 under El Centro Earthquake.

Results of Case 1 Comparing CM-5 under El Centro Earthquake																
	In-soil		Foundation		1st Floor		2nd Floor		3rd Floor		4th Floor		5th Floor			
	RMS	Peak	RMS	Peak	RMS	Peak	RMS	Peak	RMS	Peak	RMS	Peak	RMS	Peak		
Horizontal Acceleration (g)																
CM-5	0.09	0.42	0.09	0.44	0.13	0.55	0.13	0.47	0.08	0.33	0.09	0.36	0.16	0.55		
Case 1	0.10	0.49	0.10	0.48	0.11	0.56	0.09	0.46	0.05	0.22	0.08	0.36	0.13	0.50		
% Reduction	-14	-16	-11	-8	16	-1	26	3	28	34	17	-2	20	9		
Horizontal Story Drift																
CM-5	-	-	-	-	0.09	0.30	0.11	0.27	0.05	0.26	0.11	0.39	0.05	0.17		
Case 1	-	-	-	-	0.07	0.28	0.06	0.27	0.06	0.28	0.12	0.34	0.05	0.18		
% Reduction	-	-	-	-	29	7	41	2	-18	-7	-9	12	0	-6		
Arias Intensity (m/sec)																
CM-5	1.20		1.21		2.50		2.40		0.89		1.32		3.75			
Case 1	1.57		1.50		1.79		1.31		0.46		0.91		2.40			
% Reduction	-30		-24		29		45		48		31		36			
Peak Spectral Acceleration (g)																
CM-5	-		2.03		2.24		2.56		1.28		1.29		2.76			
Case 1	-		2.23		1.88		1.75		0.84		1.18		1.99			
% Reduction	-		-10		16		32		34		9		28			
Period Lengthening Ratio																
CM-5	-		0.14		0.09		0.09		0.09		0.09		0.09			
Case 1	-		0.15		0.15		0.09		0.09		0.15		0.09			
Period Length. Ratio	-		1.07		1.71		1.00		1.00		1.76		1.00			
Base Shear (kN)																
	RMS				Peak				RMS				Peak			
CM-5	0.93				3.35				0.38				1.39			
Case 1	0.70				3.19				0.28				0.94			
% Reduction	25				5				28				33			

#### 4.3.3. Seismic Response of Case 1 under Kobe Earthquake Motion

Figure 4.6a, Figure 4.6b, Figure 4.6c, and d illustrate the decrease of foundation acceleration, top floor acceleration, and first-floor drift of the 5-story building model. The reduction of the foundation acceleration is roughly 5% in RMS and 4% in peak. Variation of acceleration in the midpoint of the isolated soil region can be ignored (Table 4.6). Moreover, these ratios ascend at the upstairs up to 10% in RMS and 15% in peak. Both % reduction of third and fifth-floor drifts are negative, but the other floors have some drift reduction. Figure 4.6e represents the % reduction of base shear and correspondingly base moment that are both diminished roughly 10% in RMS. As can be observed in Figure 4.6f Arias intensity values calculated for the floors are reduced up to 20%. The detailed performance indicator parameters that are horizontal acceleration response, horizontal story drift, Arias intensity, peak spectral acceleration, period lengthening ratio of the floors and base shear and base moment of the 5-story

building model are summarized in Table 4.6, respectively. On the other side, shifting of the natural period is not detected entirely but period lengthening ratio of the first floor and fifth floor are computed as 1.4 and 1.1, respectively. Moreover, peak spectral accelerations are reduced up to 15% as shown in Table 4.6.

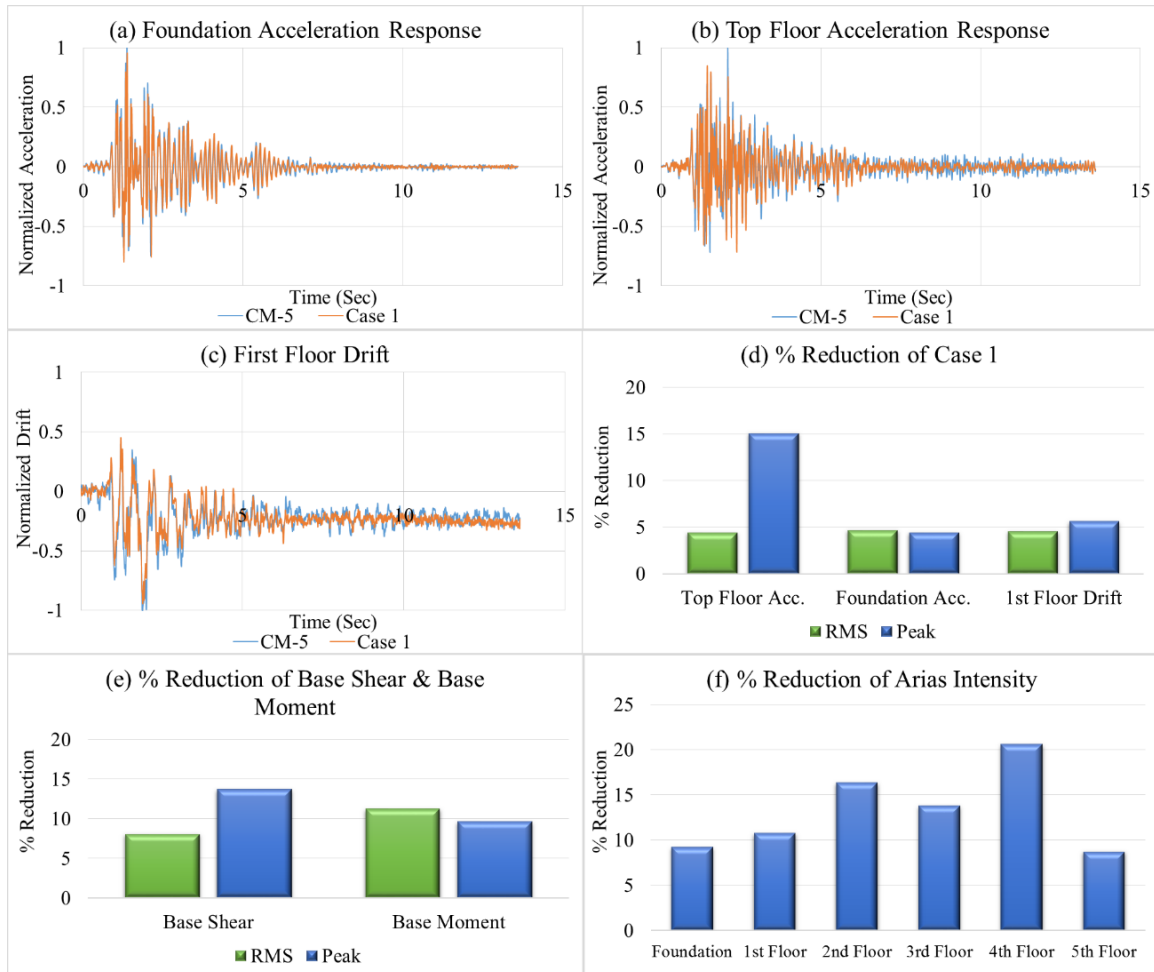


Figure 4.6. (a) Foundation, (b) Top Floor Horizontal Acceleration Response, (c) First Floor Drift, (d) % Reduction of Case 1, (e) % Reduction of Base Shear & Base Moment and (f) % Reduction of Arias Intensity of Case 1 Comparing CM-5 under Kobe Earthquake.

Table 4.6. Comparison of Case 1 with the CM-5 under Kobe Earthquake.

Results of Case 1 Comparing CM-5 under Kobe Earthquake															
	In-soil		Foundation		1st Floor		2nd Floor		3rd Floor		4th Floor		5th Floor		
	RMS	Peak	RMS	Peak	RMS	Peak	RMS	Peak	RMS	Peak	RMS	Peak	RMS	Peak	
Horizontal Acceleration (g)															
CM-5	0.16	0.95	0.17	1.25	0.19	1.61	0.15	1.25	0.14	1.04	0.15	1.01	0.19	1.48	
Case 1	0.16	0.98	0.16	1.19	0.18	1.37	0.14	1.32	0.13	1.07	0.13	0.86	0.18	1.26	
% Reduction	2	-4	5	4	5	15	8	-6	7	-3	11	14	4	15	
Horizontal Story Drift															
CM-5	-	-	-	-	0.21	0.80	0.20	0.80	0.18	0.75	0.16	0.78	0.15	0.67	
Case 1	-	-	-	-	0.20	0.75	0.17	0.69	0.19	0.81	0.16	0.67	0.15	0.77	
% Reduction	-	-	-	-	5	6	15	14	-7	-7	-2	15	-1	-15	
Arias Intensity (m/sec)															
CM-5	5.67		5.91		7.49		4.92		4.13		4.54		7.49		
Case 1	5.44		5.37		6.68		4.11		3.56		3.61		6.84		
% Reduction	4		9		11		16		14		21		9		
Peak Spectral Acceleration (g)															
CM-5	-		3.99		4.56		3.96		4.58		4.52		4.83		
Case 1	-		3.69		4.64		3.93		5.28		3.74		4.44		
% Reduction	-		8		-2		1		-15		17		8		
Period Lengthening Ratio															
CM-5	-		0.16		0.04		0.04		0.06		0.04		0.04		
Case 1	-		0.16		0.06		0.04		0.06		0.04		0.05		
Period Length. Ratio	-		1.00		1.38		1.00		1.00		1.00		1.13		
Base Shear (kN)															
	RMS				Peak				RMS				Peak		
CM-5	1.02				7.42				0.41				2.80		
Case 1	0.94				6.40				0.37				2.53		
% Reduction	8				14				11				10		

#### 4.4. Case 2; GSI 1 Placed 15 cm underneath the 5-Story Building Model

For the Case 2, GSI 1 was placed with cylindrical shaped 15 cm ( $H/D = 6.7$ ) under the foundation. 5-story building model was tested under chosen earthquake motions. Additionally, results of the experiments that are illustrated below as comparison with the unisolated model belong to Kocaeli earthquake, El Centro earthquake, and Kobe earthquake, respectively.

##### 4.4.1. Seismic Response of Case 2 under Kocaeli Earthquake Motion

Figure 4.7a, Figure 4.7b, and Figure 4.7c present the reduced foundation acceleration, reduced first-floor drift, and amplified top floor acceleration comparing CM-5. The reduction of foundation acceleration is roughly 5% both in RMS and in peak as seen in Figure 4.7d. There is nearly no acceleration variation observed in the midpoint

of the isolated soil region (Table 4.7). However, these values become negative at the upper stories. This means there is no acceleration reduction in the building except foundation level. The first-floor drift is reduced approximately 20% in RMS. Figure 4.7e represents there is no decrease in the base shear and correspondingly base moment. It can be observed from Figure 4.7f, Arias intensity values are magnified except foundation comparing the CM-5. Detailed information about the other performance indicator parameters is provided in Table 4.7. On the other side, any significant alteration of the natural period of the 5-story building is not detected, and peak spectral accelerations are not changed remarkably as seen in Table 4.7.

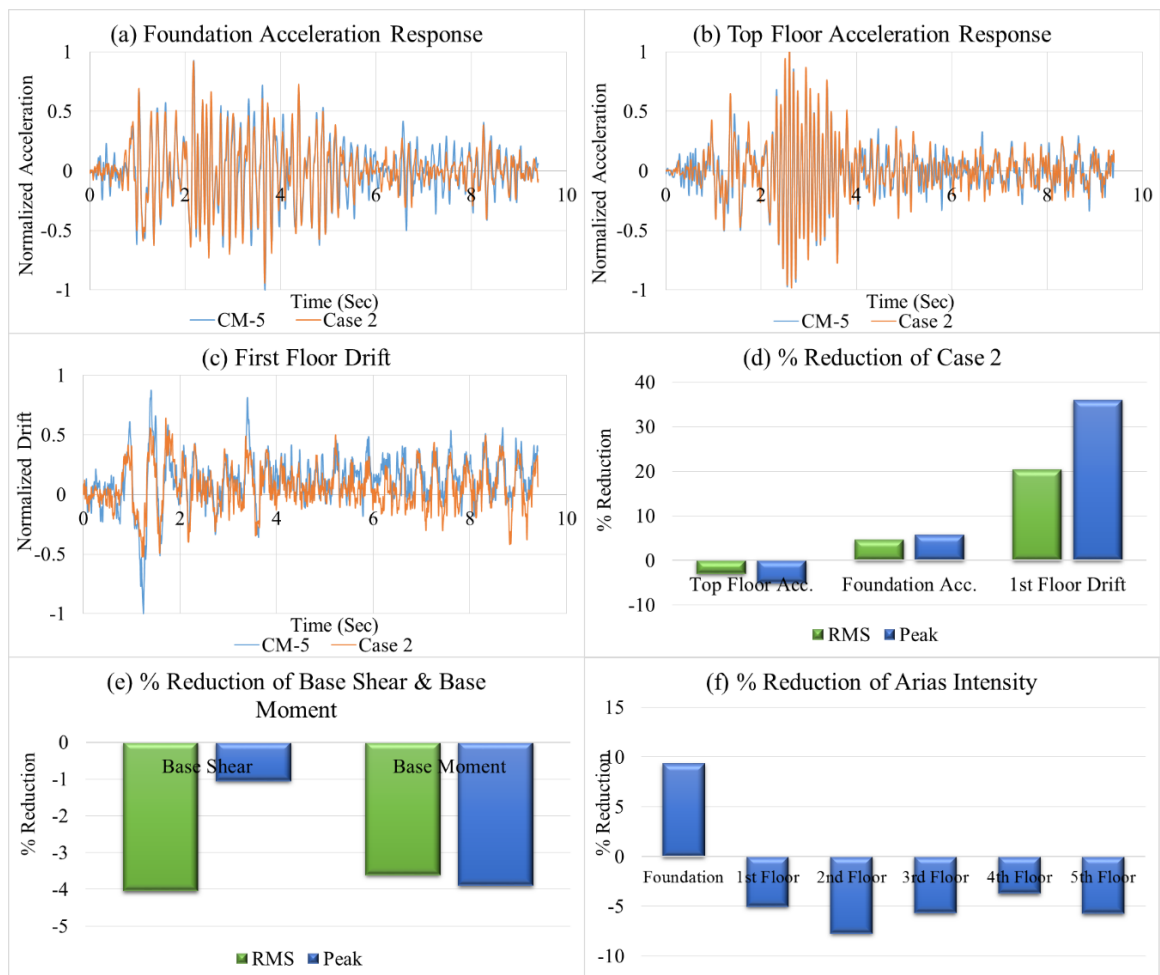


Figure 4.7. (a) Foundation, (b) Top Floor Horizontal Acceleration Response, (c) First Floor Drift, (d) % Reduction of Case 2, (e) % Reduction of Base Shear & Base Moment and (f) % Reduction of Arias Intensity of Case 2 Comparing CM-5 under Kocaeli Earthquake.

Table 4.7. Comparison of Case 2 with the CM-5 under Kocaeli Earthquake.

Results of Case 2 Comparing CM-5 under Kocaeli Earthquake																
	In-soil		Foundation		1st Floor		2nd Floor		3rd Floor		4th Floor		5th Floor			
	RMS	Peak	RMS	Peak	RMS	Peak	RMS	Peak	RMS	Peak	RMS	Peak	RMS	Peak		
Horizontal Acceleration (g)																
CM-5	0.07	0.27	0.07	0.28	0.12	0.57	0.12	0.56	0.07	0.29	0.08	0.33	0.14	0.64		
Case 2	0.07	0.27	0.07	0.26	0.12	0.60	0.12	0.59	0.07	0.30	0.09	0.36	0.15	0.67		
% Reduction	4	0	5	6	-3	-4	-4	-6	-3	-5	-2	-7	-3	-5		
Horizontal Story Drift																
CM-5	-	-	-	-	0.08	0.32	0.07	0.26	0.05	0.23	0.09	0.41	0.06	0.21		
Case 2	-	-	-	-	0.06	0.21	0.06	0.19	0.05	0.16	0.06	0.23	0.05	0.17		
% Reduction	-	-	-	-	20	36	15	28	-18	30	26	46	17	19		
Arias Intensity (m/sec)																
CM-5	0.68		0.70		1.94		1.93		0.69		1.02		2.89			
Case 2	0.63		0.63		2.03		2.08		0.73		1.05		3.05			
% Reduction	8		9		-5		-8		-6		-4		-6			
Peak Spectral Acceleration (g)																
CM-5	-		1.25		3.73		3.98		1.77		2.23		4.43			
Case 2	-		1.24		3.77		4.02		1.76		2.26		4.46			
% Reduction	-		1		-1		-1		0		-1		-1			
Period Lengthening Ratio																
CM-5	-		0.15		0.09		0.09		0.09		0.09		0.09			
Case 2	-		0.10		0.09		0.09		0.09		0.09		0.09			
Period Length. Ratio	-		0.66		1.00		1.00		1.00		1.00		1.00			
Base Shear (kN)																
	RMS				Peak				RMS				Peak			
CM-5	0.84				3.97				0.35				1.23			
Case 2	0.88				4.01				0.36				1.27			
% Reduction	-4				-1				-4				-4			

#### 4.4.2. Seismic Response of Case 2 under El Centro Earthquake Motion

The reduction of the foundation acceleration, top floor horizontal acceleration, and first-floor drift are shown in Figure 4.8a, Figure 4.8b, and Figure 4.8c comparing CM-5. The reduction of foundation acceleration is roughly 19% in RMS and 16% in peak as seen in Figure 4.8c. Like foundation, the acceleration reduction in the midpoint of the isolated soil region is 18% in RMS and 11% in peak values (Table 4.8). However, these values become up to 36% in RMS and 22% in peak at the upper stories. The first-floor drift is reduced approximately 48% in RMS, and there is no top floor reduction observed. Figure 4.8e shows the % reduction of base shear and base moment that are diminished roughly 30% and 20% in RMS, respectively. As can be observed in Figure 4.8f, Arias intensity values computed for the floors are reduced up to 60%. In brief, all indicator parameters indicate that proposed GSI system reduces the seismic effects, in general, such as transmitted acceleration and story drifts. Detailed information

about performance indicator parameters is summarized in Table 4.8 as respectively; horizontal acceleration response, horizontal story drift, Arias intensity, peak spectral acceleration, period lengthening ratio of the floors and base shear and base moment of the 5-story building model. The period lengthening ratio of the first-floor third and fourth floor are computed as 1.7, 0.6, and 1.7, respectively. On the other side, peak spectral accelerations are diminished up to 40% as seen in Table 4.8.

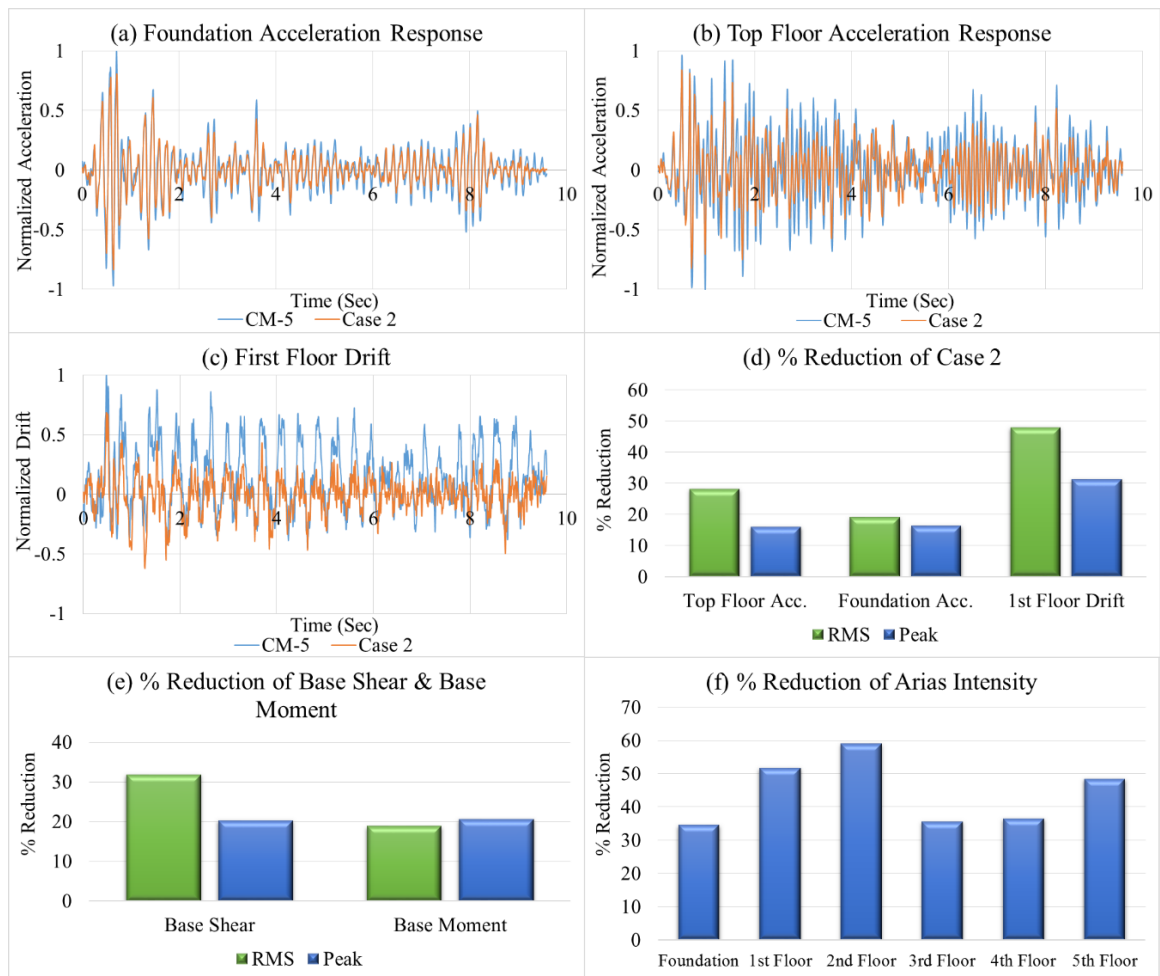


Figure 4.8. (a) Foundation, (b) Top Floor Horizontal Acceleration Response, (c) First Floor Drift, (d) % Reduction of Case 2, (e) % Reduction of Base Shear and Base Moment and (f) % Reduction of Arias Intensity of Case 2 Comparing CM-5 under El Centro Earthquake.



side, shifting of the natural period of the 5-story building is not changed totally but period lengthening ratio of the second floor and top floor computed as 2.1. Besides, peak spectral accelerations are decreased up to 20% as seen in Table 4.9.

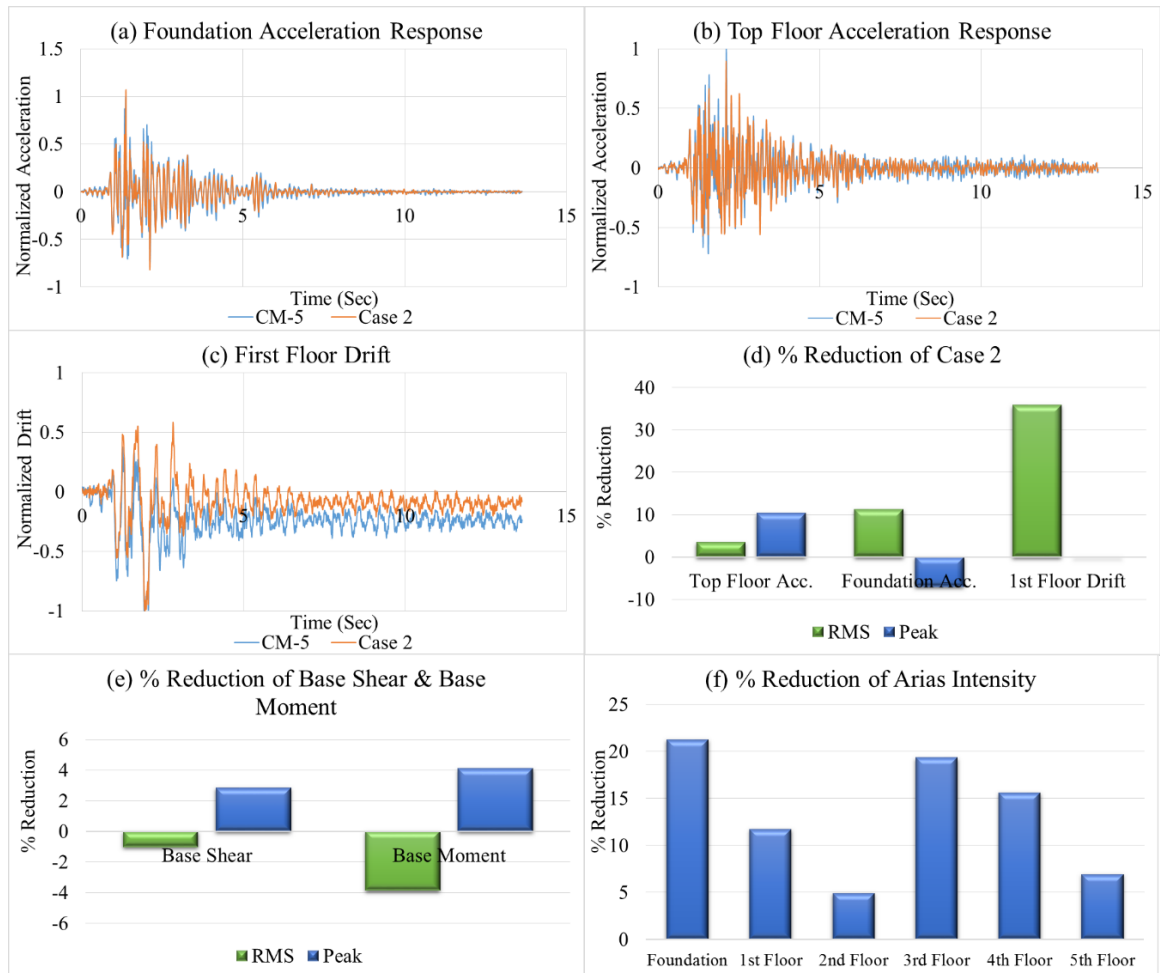


Figure 4.9. (a) Foundation, (b) Top Floor Horizontal Acceleration Response, (c) First Floor Drift, (d) % Reduction of Case 2, (e) % Reduction of Base Shear & Base Moment and (f) % Reduction of Arias Intensity of Case 2 Comparing CM-5 under Kobe Earthquake.



of the isolated soil region is decreased 5% in RMS, but there is no reduction obtained in peak value (Table 4.10). However, RMS values of acceleration reduction become negative at the upper stories. This means there is no acceleration reduction at the building except foundation level. First and fourth-floor drifts are reduced up to 38% in RMS, but other story drifts are magnified. Almost no reduction of the base shear and base moment is shown in Figure 4.10e. It can be observed from Figure 4.10f that Arias intensity values calculated for the floors are magnified except foundation comparing the CM-5. Detailed information about the performance indicator parameters is provided in Table 4.10. On the other hand, any significant alteration in the natural period of the 5-story building is not observed. Moreover, peak spectral accelerations are decreased up to 13% (Table 4.10).

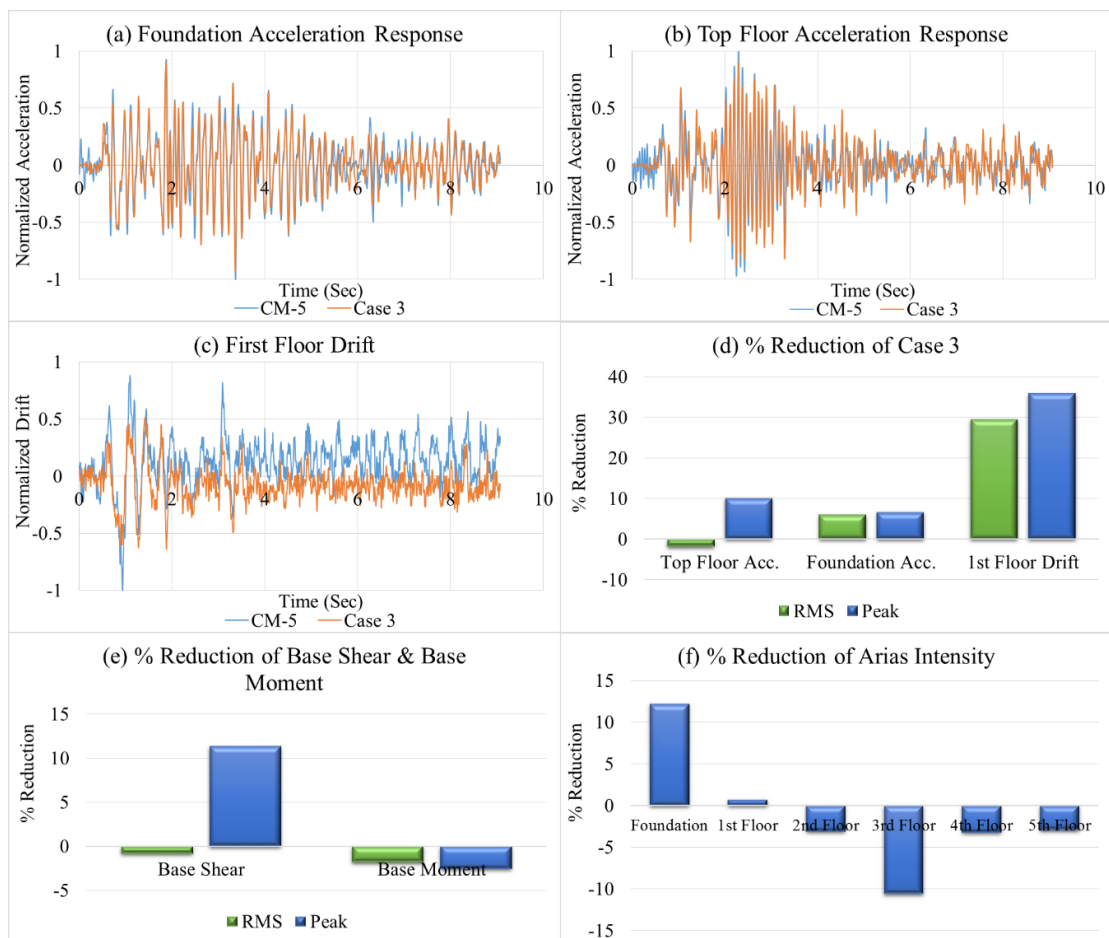


Figure 4.10. (a) Foundation, (b) Top Floor Horizontal Acceleration Response, (c) First Floor Drift, (d) % Reduction of Case 3, (e) % Reduction of Base Shear & Base Moment and (f) % Reduction of Arias Intensity of Case 3 Comparing the CM-5 under Kocaeli Earthquake.



the CM-5. Detailed information about the horizontal acceleration response, horizontal story drift, Arias intensity, peak spectral acceleration, period lengthening ratio of the floors and base shear and base moment is summarized in Table 4.11. On the other side, changing in the natural period of the 5-story building is not observed except the third floor. Peak spectral acceleration of foundation is decreased roughly 13%. Nevertheless, the peak spectral accelerations of the upper floors are magnified (Table 4.11).

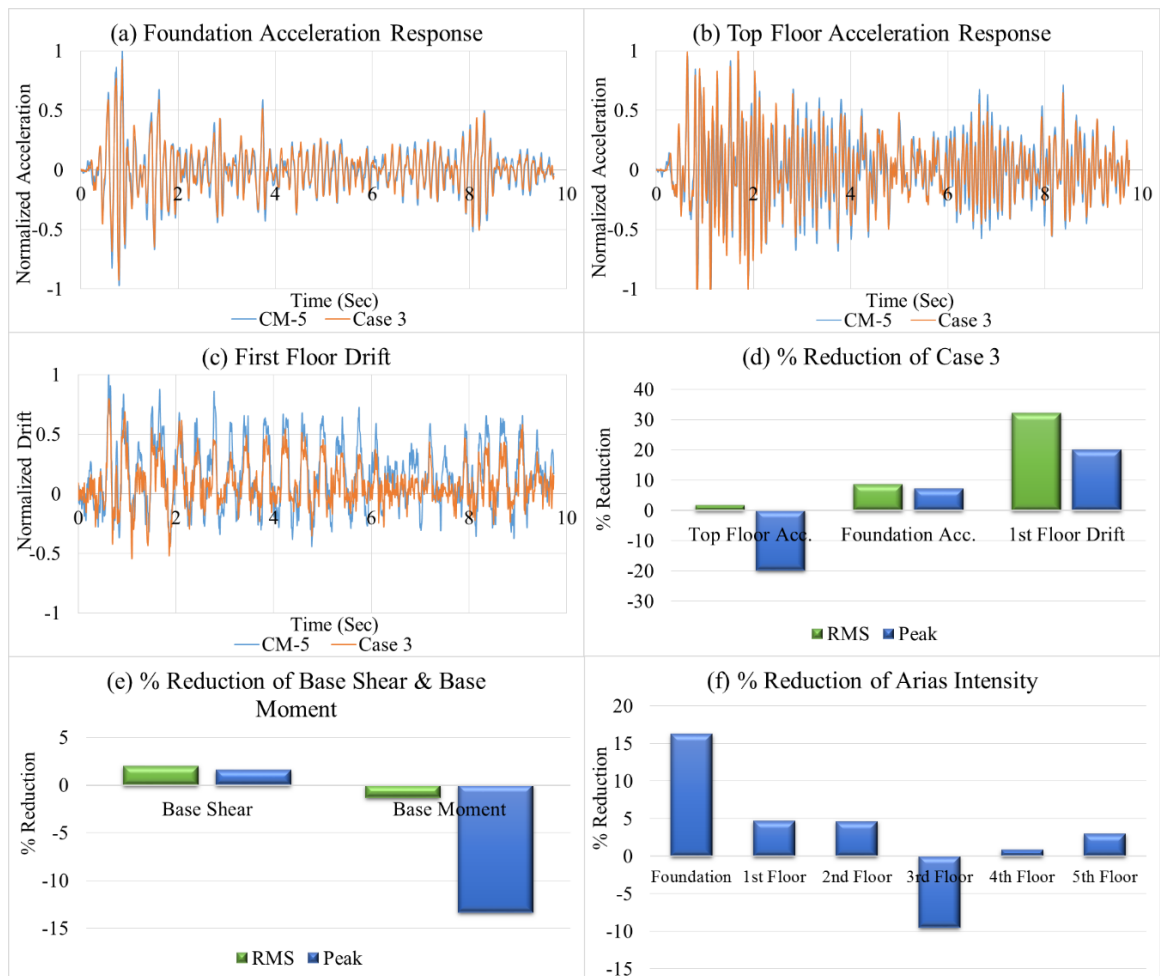


Figure 4.11. (a) Foundation, (b) Top Floor Horizontal Acceleration Response, (c) First Floor Drift, (d) % Reduction of Case 3, (e) % Reduction of Base Shear & Base Moment and (f) % Reduction of Arias Intensity of Case 3 Comparing the CM-5 under El Centro Earthquake.

Table 4.11. Comparison of Case 3 with the CM-5 under El Centro Earthquake.

Results of Case 3 Comparing CM-5 under El Centro Earthquake																
	In-soil		Foundation		1st Floor		2nd Floor		3rd Floor		4th Floor		5th Floor			
	RMS	Peak	RMS	Peak	RMS	Peak	RMS	Peak	RMS	Peak	RMS	Peak	RMS	Peak		
Horizontal Acceleration (g)																
CM-5	0.09	0.42	0.09	0.44	0.13	0.55	0.13	0.47	0.08	0.33	0.09	0.36	0.16	0.55		
Case 3	0.08	0.41	0.08	0.41	0.13	0.52	0.12	0.49	0.08	0.41	0.09	0.36	0.16	0.66		
% Reduction	8	3	9	7	3	5	2	-5	-4	-24	1	0	2	-20		
Horizontal Story Drift																
CM-5	-	-	-	-	0.09	0.28	0.10	0.27	0.05	0.26	0.10	0.38	0.06	0.17		
Case 3	-	-	-	-	0.06	0.23	0.08	0.24	0.05	0.25	0.05	0.23	0.07	0.24		
% Reduction	-	-	-	-	32	20	19	11	0	5	46	40	-20	-38		
Arias Intensity (m/sec)																
CM-5	1.20		1.21		2.50		2.40		0.89		1.32		3.75			
Case 3	1.02		1.01		2.39		2.29		0.97		1.31		3.63			
% Reduction	15		16		5		5		-9		1		3			
Peak Spectral Acceleration (g)																
CM-5	-		2.03		2.24		2.56		1.28		1.29		2.76			
Case 3	-		1.75		2.53		2.83		1.62		1.43		3.03			
% Reduction	-		14		-13		-10		-26		-10		-9			
Period Lengthening Ratio																
CM-5	-		0.14		0.09		0.09		0.09		0.09		0.09			
Case 3	-		0.15		0.09		0.09		0.06		0.09		0.09			
Period Length. Ratio	-		1.07		1.00		1.00		0.65		1.00		1.00			
Base Shear (kN)																
	RMS				Peak				RMS				Peak			
CM-5	0.93				3.35				0.39				1.39			
Case 3	0.91				3.29				0.39				1.58			
% Reduction	2				2				-1				-13			

#### 4.5.3. Seismic Response of Case 3 under Kobe Earthquake Motion

As can be observed in Figure 4.12a, Figure 4.12b, Figure 4.12c, and Figure 4.12d there is no noticeable reduction in foundation acceleration, top floor acceleration, and first-floor drift of the 5-story building model. The reduction of foundation acceleration is roughly 11% in RMS, and there is no decrease in the peak value of it. Similarly, the measured acceleration from the midpoint of the isolated soil region is decreased 7% in RMS but magnified in peak value (Table 4.12). Besides, acceleration reductions become up to 9% in RMS and 19% in peak at the upper stories. The first-floor drift is magnified. Figure 4.12e represents the % reduction of base shear and correspondingly base moment that are both nearly the same with the CM-5. As can be observed in Figure 4.12f Arias intensity values calculated for the floors are reduced up to 20%. The detailed parameters that are horizontal acceleration response, horizontal story drift, Arias intensity, peak spectral acceleration, period lengthening ratio of the floors

and base shear and base moment of 5-story building model are listed in Table 4.12, respectively. On the hand, the variation of the natural period is observed at the first, second floor and top floor. Besides, peak spectral accelerations are reduced up to 13% as seen in Table 4.12.

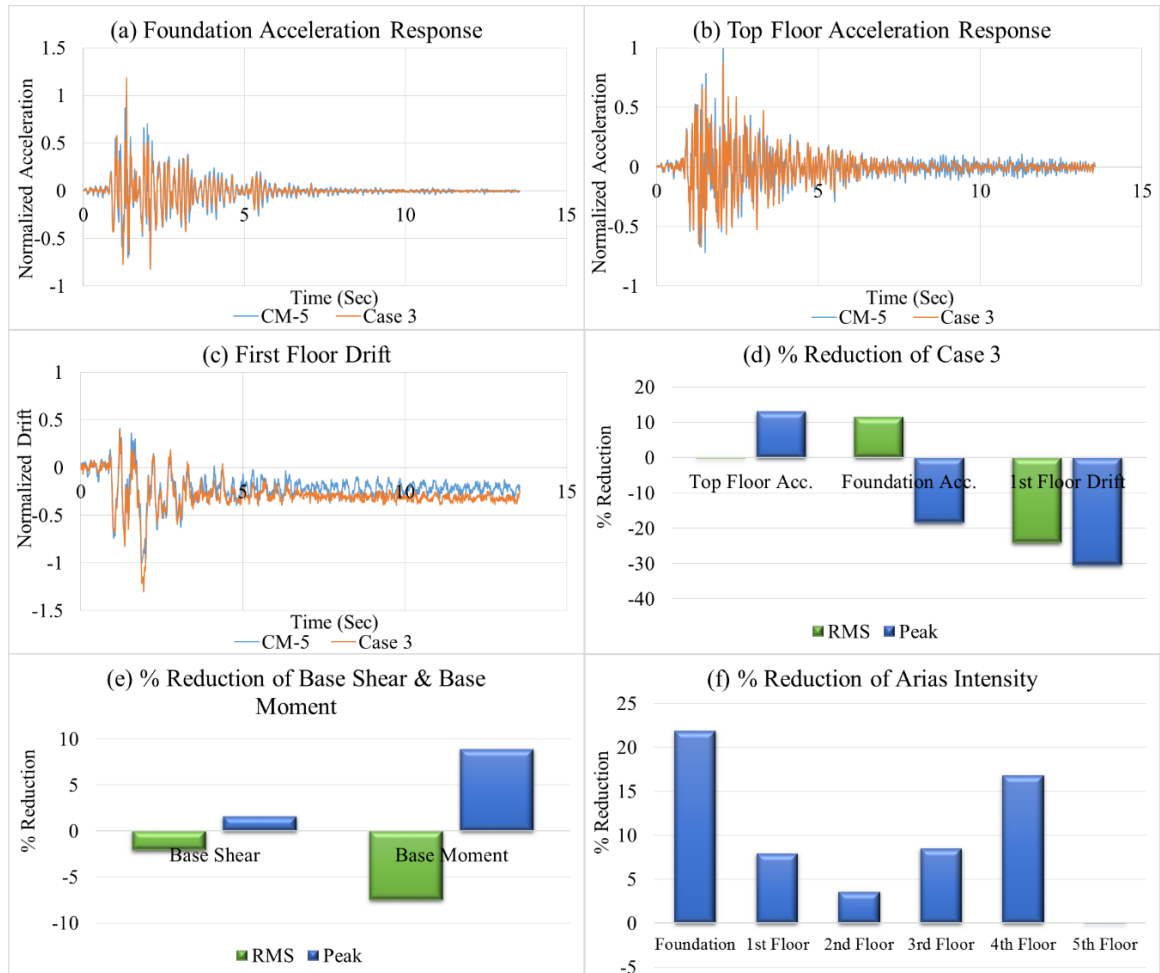


Figure 4.12. (a) Foundation, (b) Top Floor Horizontal Acceleration Response, (c) First Floor Drift, (d) % Reduction of Case 3, (e) % Reduction of Base Shear & Base Moment and (f) % Reduction of Arias Intensity of Case 3 Comparing the CM-5 under Kobe Earthquake.



of the isolated soil region is 9% in RMS and 4% in peak values (Table 4.13). However, acceleration reduction values become up to 21% in RMS and 25% in peak at the upper stories. Even though the first-floor drift is decreased approximately 32% in RMS, the top floor drift is enlarged. Figure 4.13e represents the % reduction of base shear and base moment that are diminished both roughly 20% in RMS. It can be observed from Figure 4.13f that Arias intensity values calculated for the floors are reduced up to 38%. In brief, almost all indicator parameters indicate that proposed GSI system reduces the seismic effects for this particular case. Detailed information about the performance indicator parameters is provided in Table 4.13. On the other side, the natural period of the 5-story building is not shifted, but peak spectral accelerations are reduced up to 26% as seen in Table 4.13.

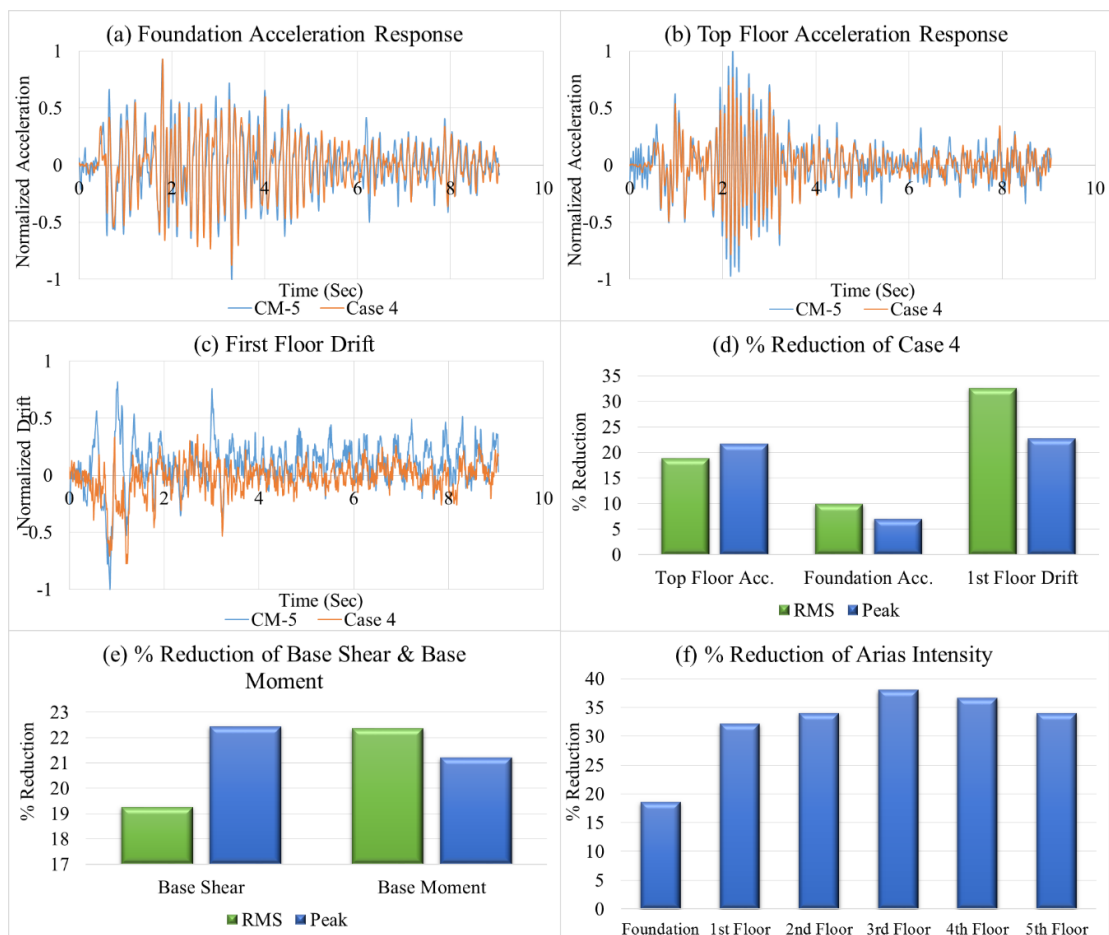


Figure 4.13. (a) Foundation, (b) Top Floor Horizontal Acceleration Response, (c) First Floor Drift, (d) % Reduction of Case 4, (e) % Reduction of Base Shear & Base Moment and (f) % Reduction of Arias Intensity of Case 4 Comparing the CM-5 under Kocaeli Earthquake.

Table 4.13. Comparison of Case 4 with the CM-5 under Kocaeli Earthquake.

Results of Case 4 Comparing CM-5 under Kocaeli Earthquake															
	In-soil		Foundation		1st Floor		2nd Floor		3rd Floor		4th Floor		5th Floor		
	RMS	Peak	RMS	Peak	RMS	Peak	RMS	Peak	RMS	Peak	RMS	Peak	RMS	Peak	
Horizontal Acceleration (g)															
CM-5	0.07	0.27	0.07	0.28	0.12	0.57	0.12	0.56	0.07	0.29	0.09	0.33	0.14	0.64	
Case 4	0.06	0.26	0.06	0.26	0.10	0.45	0.10	0.44	0.06	0.20	0.07	0.25	0.12	0.50	
% Reduction	9	4	10	7	18	22	19	21	21	29	21	25	19	22	
Horizontal Story Drift															
CM-5	-	-	-	-	0.07	0.33	0.07	0.27	0.05	0.24	0.08	0.41	0.06	0.20	
Case 4	-	-	-	-	0.05	0.26	0.06	0.27	0.05	0.21	0.06	0.22	0.08	0.35	
% Reduction	-	-	-	-	33	23	11	1	-8	10	30	47	-42	-77	
Arias Intensity (m/sec)															
CM-5	0.68		0.69		1.93		1.93		0.69		1.01		2.88		
Case 4	0.57		0.57		1.31		1.27		0.43		0.64		1.90		
% Reduction	17		19		32		34		38		37		34		
Peak Spectral Acceleration (g)															
CM-5	-		1.25		3.73		3.98		1.77		2.23		4.43		
Case 4	-		1.25		2.85		3.02		1.30		1.67		3.34		
% Reduction	-		0		23		24		26		25		24		
Period Lengthening Ratio															
CM-5	-		0.15		0.09		0.09		0.09		0.09		0.09		
Case 4	-		0.15		0.09		0.09		0.09		0.09		0.09		
Period Length. Ratio	-		1.00		1.00		1.00		1.00		1.00		1.00		
Base Shear (kN)															
	RMS				Peak				RMS				Peak		
CM-5	0.86				3.97				0.35				1.23		
Case 4	0.69				3.08				0.28				0.97		
% Reduction	19				22				22				21		

#### 4.6.2. Seismic Response of Case 4 under El Centro Earthquake Motion

It can be observed from Figure 4.14a, Figure 4.14d, and Figure 4.14f that there is no reduction of acceleration and Arias intensity in the foundation of the 5-story building model. Same as the foundation, there is no acceleration decrease observed in the midpoint of the isolated soil region (Table 4.14). However, both reduction of the acceleration and Arias intensity parameters exist at the upper story levels up to 11% in RMS and peak for acceleration and up to 21% for Arias intensity. Figure 4.14b illustrates the reduction of top floor acceleration comparing the control model. Although the first-floor drift is decreased approximately 40% in RMS, the top floor drift is magnified in RMS as seen in Table 4.14. Base shear and base moment that are diminished both approximately 10% in RMS are presented in Figure 4.14e. The information about the other parameters that are horizontal acceleration response, horizontal story drift, Arias intensity, peak spectral acceleration, period lengthening ratio of the floors and

base shear and base moment of 5-story building model is summarized in Table 4.14, respectively. On the other side, there is no alteration in the natural period of the 5-story building, but peak spectral accelerations are reduced up to 16% as seen in Table 4.14.

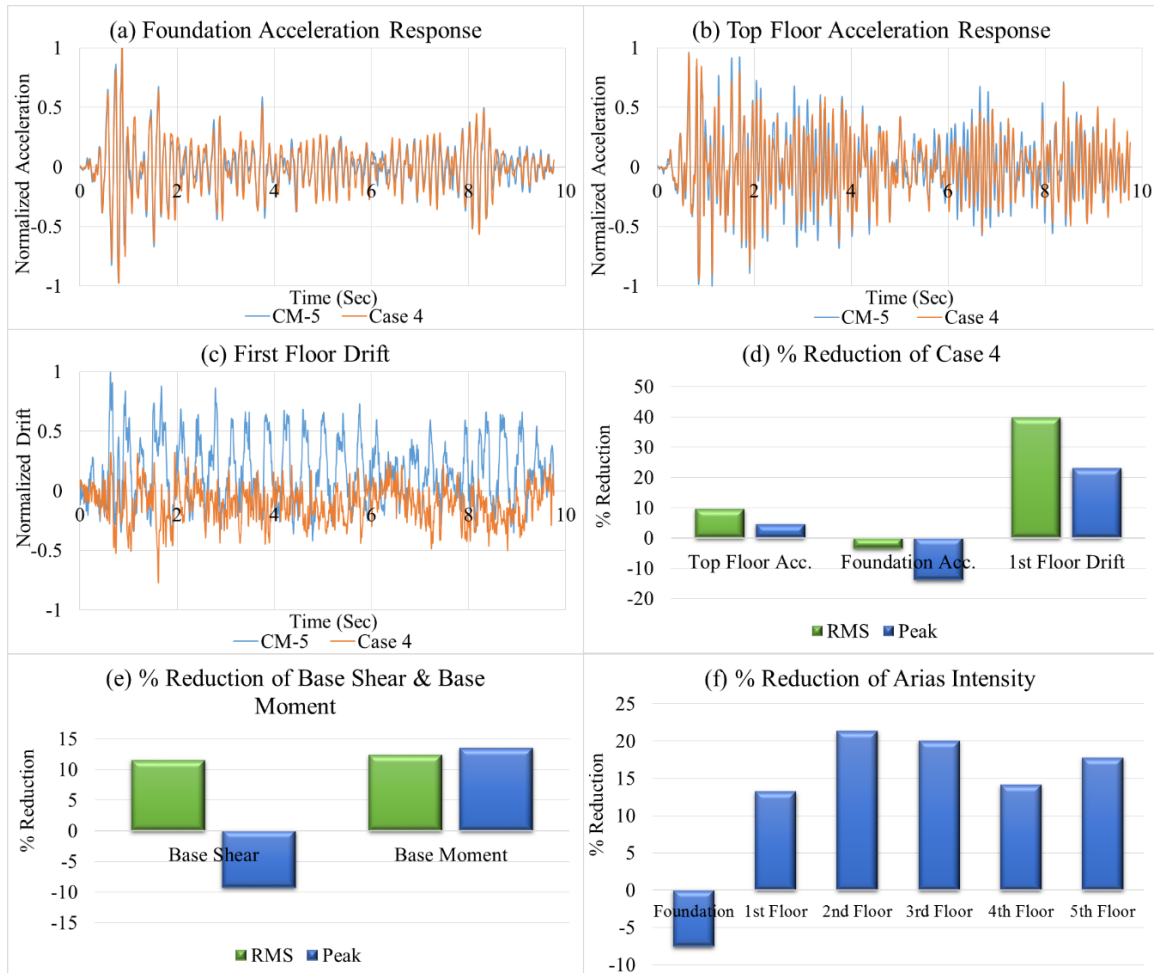


Figure 4.14. (a) Foundation, (b) Top Floor Horizontal Acceleration Response, (c) First Floor Drift, (d) % Reduction of Case 4, (e) % Reduction of Base Shear & Base Moment and (f) % Reduction of Arias Intensity of Case 4 under Comparing CM-5 El Centro Earthquake.

Table 4.14. Comparison of Case 4 with the CM-5 under El Centro Earthquake.

Results of Case 4 Comparing CM-5 under El Centro Earthquake																
	In-soil		Foundation		1st Floor		2nd Floor		3rd Floor		4th Floor		5th Floor			
	RMS	Peak	RMS	Peak	RMS	Peak	RMS	Peak	RMS	Peak	RMS	Peak	RMS	Peak		
Horizontal Acceleration (g)																
CM-5	0.09	0.42	0.09	0.44	0.13	0.55	0.13	0.47	0.08	0.33	0.09	0.36	0.16	0.55		
Case 4	0.09	0.51	0.09	0.50	0.12	0.59	0.11	0.51	0.07	0.29	0.09	0.37	0.14	0.53		
% Reduction	-6	-20	-4	-14	7	-8	11	-10	11	11	7	-5	9	4		
Horizontal Story Drift																
CM-5	-	-	-	-	0.09	0.29	0.10	0.27	0.05	0.26	0.10	0.38	0.05	0.17		
Case 4	-	-	-	-	0.05	0.22	0.05	0.19	0.06	0.23	0.08	0.26	0.15	0.43		
% Reduction	-	-	-	-	40	23	47	31	-3	12	24	32	-187	-153		
Arias Intensity (m/sec)																
CM-5	1.20		1.21		2.50		2.40		0.89		1.32		3.75			
Case 4	1.34		1.30		2.17		1.89		0.71		1.13		3.08			
% Reduction	-12		-8		13		21		20		14		18			
Peak Spectral Acceleration (g)																
CM-5	-		2.03		2.24		2.56		1.28		1.29		2.76			
Case 4	-		2.04		2.02		2.22		1.08		1.19		2.43			
% Reduction	-		-1		10		13		16		8		12			
Period Lengthening Ratio																
CM-5	-		0.14		0.09		0.09		0.09		0.09		0.09			
Case 4	-		0.14		0.09		0.09		0.09		0.09		0.09			
Period Length. Ratio	-		1.00		1.00		1.00		1.00		1.00		1.00			
Base Shear (kN)																
	RMS				Peak				RMS				Peak			
CM-5	0.93				3.35				0.38				1.39			
Case 4	0.82				3.66				0.34				1.20			
% Reduction	12				-9				12				13			

#### 4.6.3. Seismic Response of Case 4 under Kobe Earthquake Motion

Figure 4.15a, Figure 4.15b, and Figure 4.15d indicate the reduction of top floor acceleration, amplification of both foundation acceleration, and first-floor drift of the 5-story building model. There is no acceleration reduction observed in the midpoint of the isolated soil region (Table 4.15). Although the reduction of foundation acceleration is roughly 7% in RMS, there is no reduction in peak values. Besides, acceleration reduction rises at the upstairs up to 18% in RMS and 33% in peak values. The first-floor drift is enlarged in RMS. Due to slight permanent displacement that can be shown in the Figure 4.15c, drift values may become larger than the unisolated condition. Figure 4.15e represents the % reduction of base shear and base moment that are decreased up to 5% and 9% in RMS, respectively. Figure 4.15f shows that Arias intensity values computed for the floors are reduced up to 25%. As additional information, horizontal acceleration response, horizontal story drift, Arias intensity,

peak spectral acceleration, period lengthening ratio of the floors and base shear and base moment of 5-story building model are provided in Table 4.15. On the other side, the natural period of the 5-story building is not changed significantly, but peak spectral accelerations are reduced up to 25% as seen in Table 4.15.

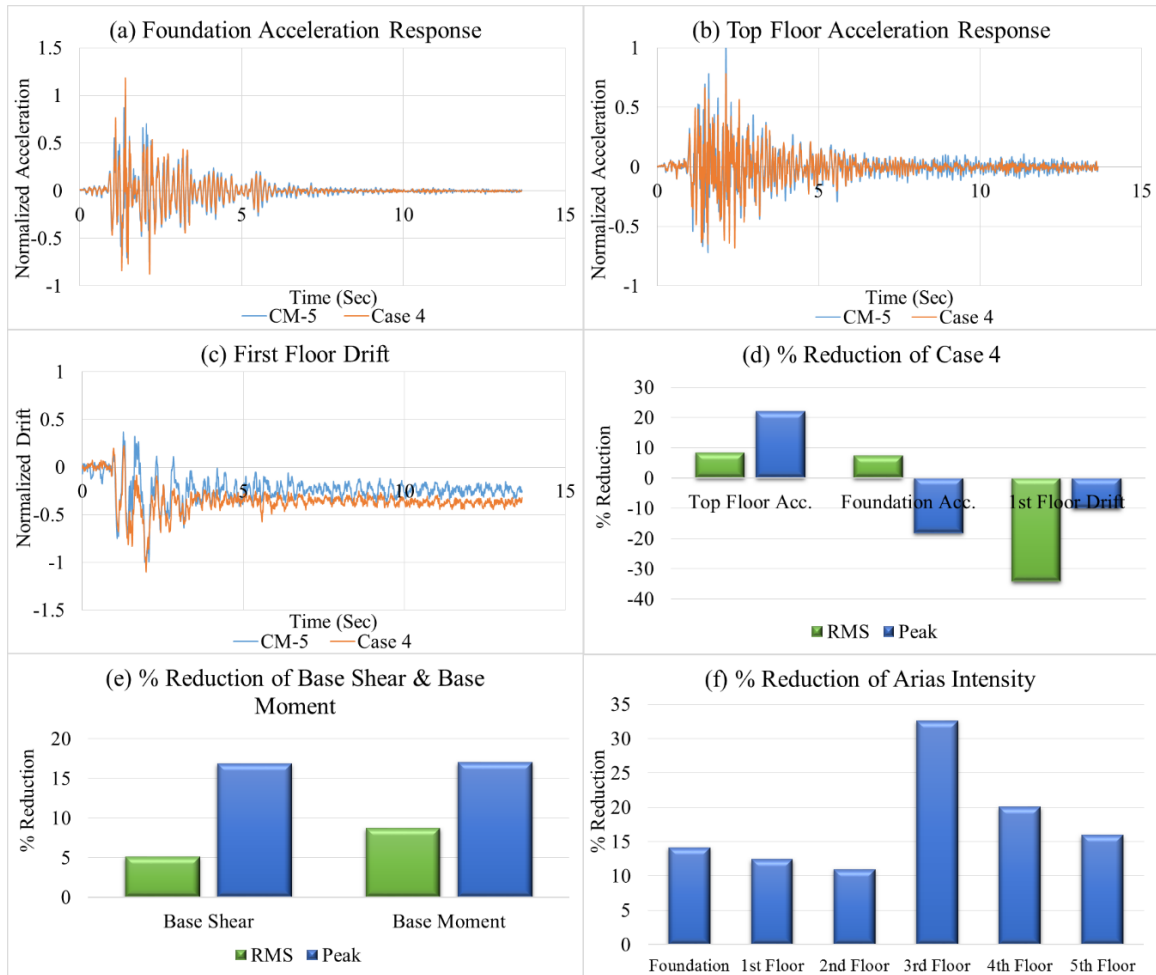


Figure 4.15. (a) Foundation, (b) Top Floor Horizontal Acceleration Response, (c) First Floor Drift, (d) % Reduction of Case 4, (e) % Reduction of Base Shear & Base Moment and (f) % Reduction of Arias Intensity of Case 4 Comparing CM-5 under Kobe Earthquake.

Table 4.15. Comparison of Case 4 with the CM-5 under Kobe Earthquake.

Results of Case 4 Comparing CM-5 under Kobe Earthquake															
	In-soil		Foundation		1st Floor		2nd Floor		3rd Floor		4th Floor		5th Floor		
	RMS	Peak	RMS	Peak	RMS	Peak	RMS	Peak	RMS	Peak	RMS	Peak	RMS	Peak	
Horizontal Acceleration (g)															
CM-5	0.16	0.95	0.17	1.25	0.19	1.61	0.15	1.25	0.14	1.04	0.15	1.01	0.19	1.48	
Case 4	0.16	1.41	0.16	1.48	0.18	1.14	0.14	1.14	0.11	0.70	0.13	0.85	0.17	1.15	
% Reduction	0	-49	7	-18	6	29	6	9	18	33	11	16	8	22	
Horizontal Story Drift															
CM-5	-	-	-	-	0.23	0.81	0.22	0.81	0.18	0.75	0.17	0.80	0.15	0.66	
Case 4	-	-	-	-	0.30	0.89	0.28	0.81	0.20	0.73	0.33	0.95	0.14	0.63	
% Reduction	-	-	-	-	-34	-10	-31	0	-10	3	-93	-18	8	5	
Arias Intensity (m/sec)															
CM-5	5.67		5.91		7.49		4.92		4.13		4.54		7.49		
Case 4	5.69		5.07		6.56		4.38		2.78		3.63		6.30		
% Reduction	0		14		12		11		33		20		16		
Peak Spectral Acceleration (g)															
CM-5	-		3.99		4.56		3.96		4.58		4.52		4.83		
Case 4	-		3.84		3.75		3.37		3.42		4.05		4.24		
% Reduction	-		4		18		15		25		10		12		
Period Lengthening Ratio															
CM-5	-		0.16		0.04		0.04		0.06		0.04		0.04		
Case 4	-		0.16		0.04		0.04		0.06		0.04		0.04		
Period Length. Ratio	-		1.00		1.00		1.00		0.92		1.00		1.00		
Base Shear (kN)															
	RMS				Peak				RMS				Peak		
CM-5	1.02				7.42				0.41				2.80		
Case 4	0.97				6.17				0.38				2.33		
% Reduction	5				17				9				17		

#### 4.7. Case 5; GSI 3 Placed 10 cm underneath the 5-Story Building Model

For the Case 5, PTFE 1 mm geomembrane with Typar DuPont SF56 nonwoven geotextile, which were tagged together as GSI 3, were placed with cylindrical shaped 10 cm ( $H/D = 10$ ) under the foundation. 5-story building model excited with the selected earthquake motions. Besides, the results of Case 5 comparing with a unisolated case that are given below, belong to Kocaeli earthquake, El Centro earthquake, and Kobe earthquake, respectively.

##### 4.7.1. Seismic Response of Case 5 under Kocaeli Earthquake Motion

The reduction of the foundation acceleration, top floor acceleration, and first-floor drift comparing CM-5 are presented in Figure 4.16a, Figure 4.16b, and Figure 4.16c. The foundation acceleration is decreased approximately 23% in both RMS and

peak as seen in Figure 4.16c. Similarly, the measured acceleration from the midpoint of the isolated soil region is reduced 19% in RMS and 13% in peak value (Table 4.16). Nonetheless, acceleration reduction becomes up to 24% in RMS and 32% in peak at the upper stories. Even though the first-floor drift is decreased approximately 35% in RMS, the top floor drift is magnified. Figure 4.16e shows the % reduction of base shear and base moment that are diminished roughly 23% and 15% in RMS, respectively. As can be observed in Figure 4.16f, Arias intensity values calculated for the floors are reduced up to 37%. In brief, almost all indicator parameters indicate that proposed GSI system decreases the seismic effects. Detailed information about the performance indicator parameters is provided in such sequence; horizontal acceleration response, horizontal story drift, Arias intensity, peak spectral acceleration, period lengthening ratio of the floors and base shear and base moment of 5-story building model( Table 4.16. On the other side, there is no changing in the natural period of the 5-story building, but peak spectral accelerations are reduced up to 37% as seen in Table 4.16.

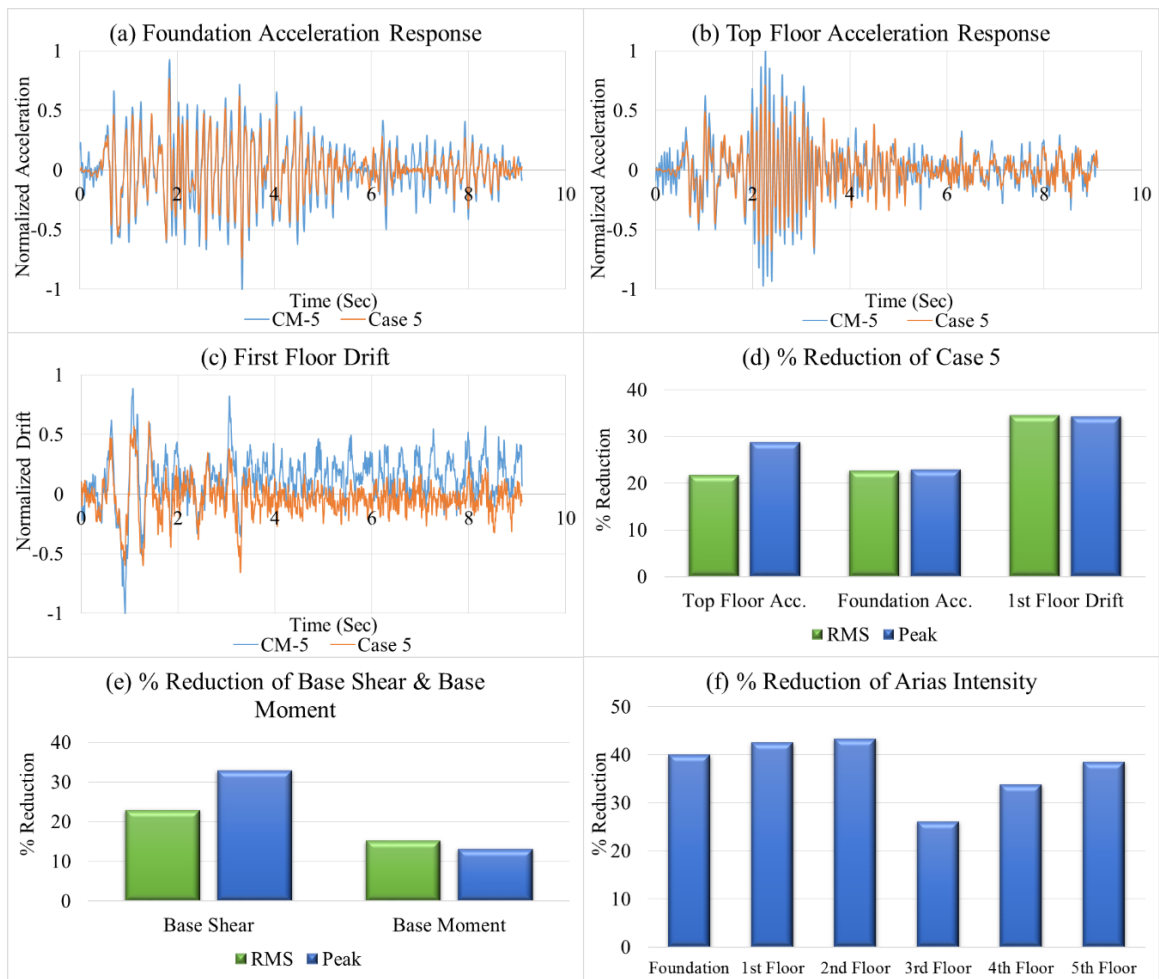


Figure 4.16. (a) Foundation, (b) Top Floor Horizontal Acceleration Response, (c) First Floor Drift, (d) % Reduction of Case 5, (e) % Reduction of Base Shear & Base Moment and (f) % Reduction of Arias Intensity of Case 5 Comparing CM-5 under Kocaeli Earthquake.

Table 4.16. Comparison of Case 5 with the CM-5 under Kocaeli Earthquake.

Results of Case 5 Comparing CM-5 under Kocaeli Earthquake																
	In-soil		Foundation		1st Floor		2nd Floor		3rd Floor		4th Floor		5th Floor			
	RMS	Peak	RMS	Peak	RMS	Peak	RMS	Peak	RMS	Peak	RMS	Peak	RMS	Peak		
Horizontal Acceleration (g)																
CM-5	0.07	0.27	0.07	0.28	0.12	0.57	0.12	0.56	0.07	0.29	0.08	0.33	0.14	0.64		
Case 5	0.06	0.23	0.05	0.21	0.09	0.39	0.09	0.37	0.06	0.22	0.07	0.25	0.11	0.46		
% Reduction	19	13	23	23	24	33	25	34	14	24	19	26	22	29		
Horizontal Story Drift																
CM-5	-	-	-	-	0.08	0.32	0.07	0.27	0.04	0.22	0.08	0.41	0.06	0.20		
Case 5	-	-	-	-	0.05	0.21	0.08	0.35	0.06	0.19	0.06	0.27	0.07	0.25		
% Reduction	-	-	-	-	35	34	-12	-28	-36	14	32	33	-8	-21		
Arias Intensity (m/sec)																
CM-5	0.68		0.70		1.93		1.93		0.69		1.01		2.88			
Case 5	0.45		0.42		1.11		1.09		0.51		0.67		1.77			
% Reduction	34		40		42		43		26		34		38			
Peak Spectral Acceleration (g)																
CM-5	-		1.25		3.73		3.98		1.77		2.23		4.43			
Case 5	-		1.02		2.36		2.55		1.20		1.43		2.87			
% Reduction	-		18		37		36		32		36		35			
Period Lengthening Ratio																
CM-5	-		0.15		0.09		0.09		0.09		0.09		0.09			
Case 5	-		0.15		0.09		0.09		0.09		0.09		0.09			
Period Length. Ratio	-		1.00		1.00		1.00		1.00		1.00		1.00			
Base Shear (kN)																
	RMS				Peak				RMS				Peak			
CM-5	0.86				3.97				0.35				1.23			
Case 5	0.66				2.66				0.30				1.07			
% Reduction	23				33				15				13			

#### 4.7.2. Seismic Response of Case 5 under El Centro Earthquake Motion

Figure 4.17a, Figure 4.17b, and Figure 4.17c represent the reduction of foundation acceleration, top floor acceleration, and the first-floor drift comparing CM-5. The foundation acceleration is decreased approximately 14% in RMS and 7% in peak as seen in Figure 4.17c. Also, the measured acceleration from the midpoint of the isolated soil region is reduced 10% in RMS but magnified in peak value (Table 4.17). Nevertheless, acceleration reduction becomes up to 27% in RMS and 12% in peak at the upper stories. The first-floor drift is decreased roughly 14% in RMS. On the contrary, the top floor drift is enlarged. Figure 4.17e shows the base shear that are diminished roughly 9% in RMS but, base moment are nearly same with the unisolated case. As can be observed in Figure 4.17f, Arias intensity values computed for the floors are reduced up to 27%. Detailed information about the performance indicator parameters that are horizontal acceleration response, horizontal story drift, Arias intensity, peak spectral

acceleration, period lengthening ratio of the floors and base shear and base moment of 5-story building model is summarized in Table 4.17. On the other hand, a significant shift in the natural period of the 5-story building is not recognized, but peak spectral accelerations are reduced up to 24% (Table 4.17).

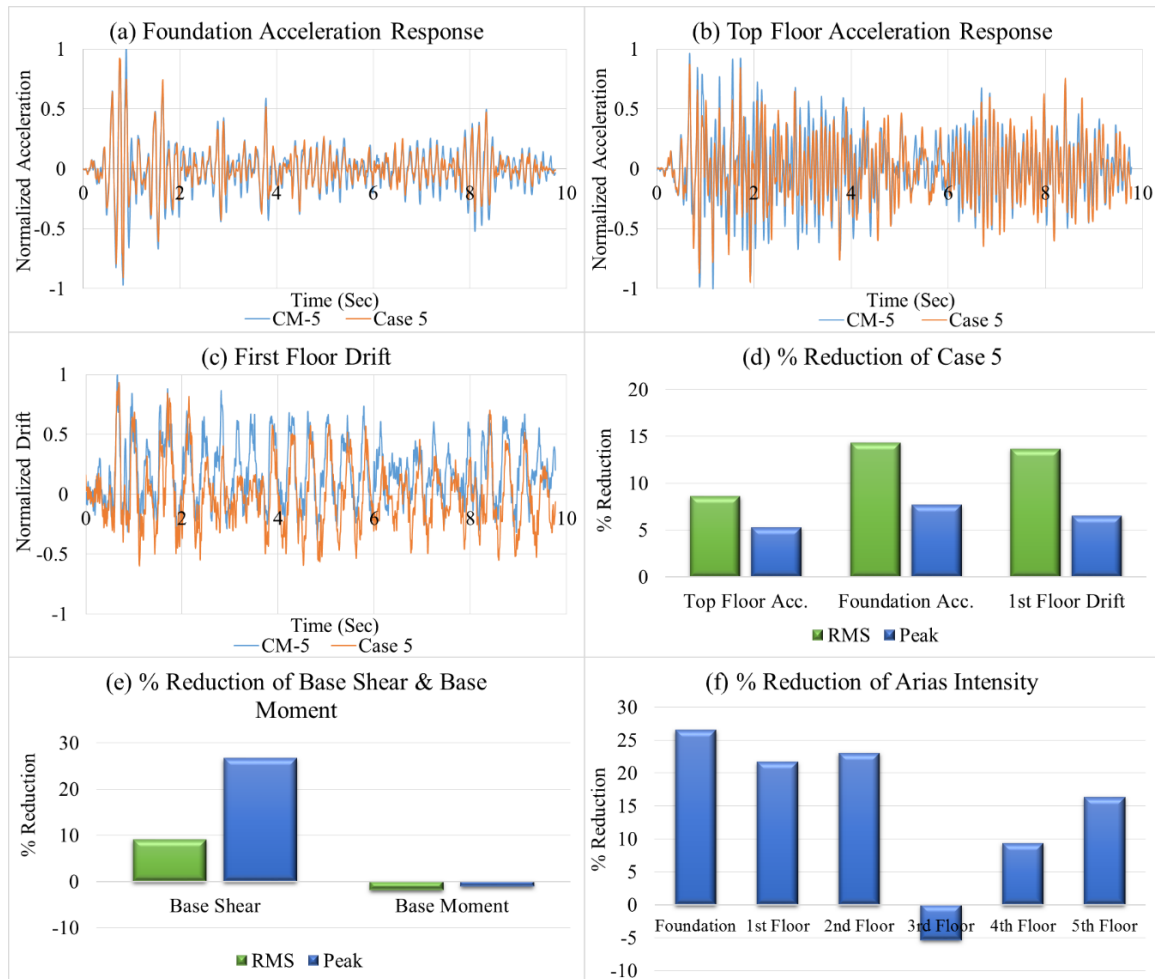


Figure 4.17. (a) Foundation, (b) Top Floor Horizontal Acceleration Response, (c) First Floor Drift, (d) % Reduction of Case 5, (e) % Reduction of Base Shear & Base Moment and (f) % Reduction of Arias Intensity of Case 5 Comparing CM-5 under El Centro Earthquake.

Table 4.17. Comparison of Case 5 with the CM-5 under El Centro Earthquake.

Results of Case 5 Comparing CM-5 under El Centro Earthquake																
	In-soil		Foundation		1st Floor		2nd Floor		3rd Floor		4th Floor		5th Floor			
	RMS	Peak	RMS	Peak	RMS	Peak	RMS	Peak	RMS	Peak	RMS	Peak	RMS	Peak		
Horizontal Acceleration (g)																
CM-5	0.09	0.42	0.09	0.44	0.13	0.55	0.13	0.47	0.08	0.33	0.09	0.36	0.16	0.55		
Case 5	0.08	0.45	0.08	0.41	0.11	0.47	0.11	0.34	0.08	0.34	0.09	0.28	0.14	0.52		
% Reduction	10	-8	14	8	12	15	12	27	-3	-4	5	22	9	5		
Horizontal Story Drift																
CM-5	-	-	-	-	0.09	0.30	0.11	0.27	0.05	0.26	0.11	0.39	0.05	0.16		
Case 5	-	-	-	-	0.08	0.28	0.09	0.30	0.06	0.29	0.06	0.24	0.06	0.24		
% Reduction	-	-	-	-	14	7	16	-11	-19	-12	39	38	-18	-49		
Arias Intensity (m/sec)																
CM-5	1.20		1.21		2.50		2.40		0.89		1.32		3.75			
Case 5	0.98		0.89		1.96		1.85		0.93		1.19		3.13			
% Reduction	18		27		22		23		-5		9		16			
Peak Spectral Acceleration (g)																
CM-5	-		2.03		2.24		2.56		1.28		1.29		2.76			
Case 5	-		1.79		1.70		2.09		1.38		1.09		2.30			
% Reduction	-		11		24		18		-8		16		17			
Period Lengthening Ratio																
CM-5	-		0.14		0.09		0.09		0.09		0.09		0.09			
Case 5	-		0.15		0.09		0.09		0.06		0.09		0.09			
Period Length. Ratio	-		1.04		1.00		1.00		0.65		1.00		1.00			
Base Shear (kN)																
	RMS				Peak				RMS				Peak			
CM-5	0.93				3.35				0.38				1.39			
Case 5	0.84				2.46				0.39				1.41			
% Reduction	9				27				-2				-1			

#### 4.7.3. Seismic Response of Case 5 under Kobe Earthquake Motion

The reduction of foundation acceleration, top floor acceleration, and first-floor drift comparing CM-5 are shown in Figure 4.18a, Figure 4.18b, and Figure 4.18c. The foundation acceleration is reduced approximately 18% in RMS and 16% in peak as seen in Figure 4.18c. The acceleration values are taken from the accelerometer that was placed midpoint of the isolated soil region is decreased 11% in RMS but magnified in peak value (Table 4.18). However, reduction of acceleration values become up to 18% in RMS and 28% in peak at the upper stories. The first-floor drift is decreased approximately 10% in RMS. There is no the top floor drift reduction in contrast with first-floor drift. Figure 4.18e illustrates the base shear and base moment that are diminished roughly 11% and 5% in RMS, respectively. It can be observed from Figure 4.18f that Arias intensity values computed for the floors are decreased up to 33%. In brief, nearly all performance indicator parameters indicate that proposed GSI system

decreases performance indicator parameters like the transmitted acceleration and story drifts generally. Detailed information relative to the performance indicator parameters as respectively; horizontal acceleration response, horizontal story drift, Arias intensity, peak spectral acceleration, period lengthening ratio of the floors and base shear and base moment of 5-story building model is summarized in Table 4.18. On the other side, period lengthening ratio of the first floor, third floor, and top floor are altered. Moreover, peak spectral accelerations are reduced up to 25% as seen in Table 4.18.

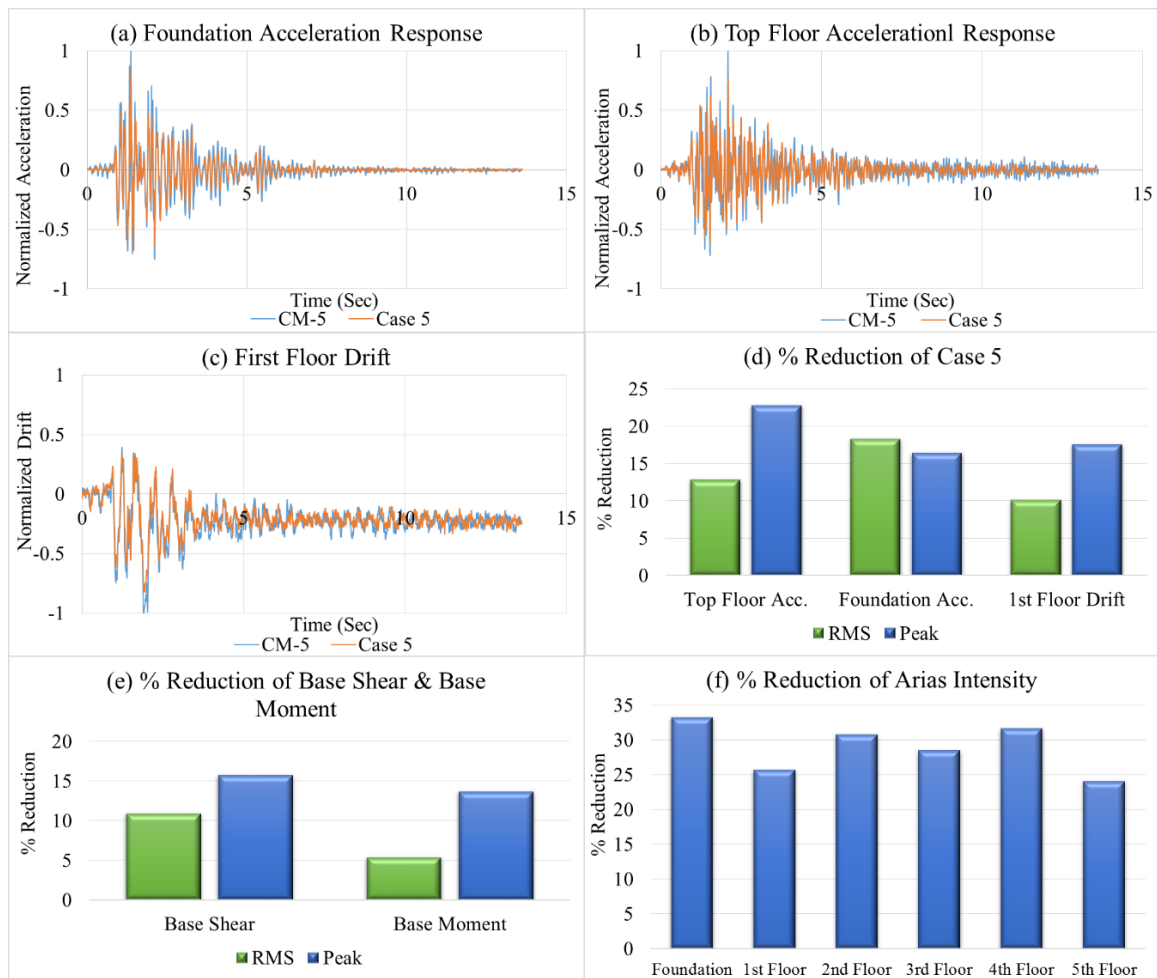


Figure 4.18. (a) Foundation, (b) Top Floor Horizontal Acceleration Response, (c) First Floor Drift, (d) % Reduction of Case 5, (e) % Reduction of Base Shear & Base Moment and (f) % Reduction of Arias Intensity of Case 5 Comparing CM-5 under Kobe Earthquake.

Table 4.18. Comparison of Case 5 with the CM-5 under Kobe Earthquake.

Results of Case 5 Comparing CM-5 under Kobe Earthquake															
	In-soil		Foundation		1st Floor		2nd Floor		3rd Floor		4th Floor		5th Floor		
	RMS	Peak	RMS	Peak	RMS	Peak	RMS	Peak	RMS	Peak	RMS	Peak	RMS	Peak	
Horizontal Acceleration (g)															
CM-5	0.16	0.95	0.17	1.25	0.19	1.61	0.15	1.25	0.14	1.04	0.15	1.01	0.19	1.48	
Case 5	0.15	1.00	0.14	1.04	0.16	1.26	0.13	0.95	0.12	0.89	0.12	0.73	0.16	1.14	
% Reduction	11	-6	18	16	14	22	17	24	15	14	17	28	13	23	
Horizontal Story Drift															
CM-5	-	-	-	-	0.22	0.80	0.20	0.80	0.18	0.75	0.16	0.79	0.15	0.67	
Case 5	-	-	-	-	0.19	0.66	0.34	0.92	0.09	0.55	0.13	0.76	0.21	0.83	
% Reduction	-	-	-	-	10	18	-66	-15	50	28	18	3	-36	-25	
Arias Intensity (m/sec)															
CM-5	5.67		5.91		7.49		4.92		4.13		4.54		7.49		
Case 5	4.54		3.95		5.56		3.40		2.95		3.11		5.69		
% Reduction	20		33		26		31		28		32		24		
Peak Spectral Acceleration (g)															
CM-5	-		3.99		4.56		3.96		4.58		4.52		4.83		
Case 5	-		3.55		4.55		2.96		4.64		3.43		3.91		
% Reduction	-		11		0		25		-1		24		19		
Period Lengthening Ratio															
CM-5			0.16		0.04		0.04		0.06		0.04		0.04		
Case 5			0.16		0.06		0.04		0.06		0.04		0.06		
Period Length. Ratio			1.00		1.38		1.00		0.92		1.00		1.38		
Base Shear (kN)															
	RMS				Peak				RMS				Peak		
CM-5	1.02				7.42				0.41				2.80		
Case 5	0.91				6.25				0.39				2.42		
% Reduction	11				16				5				14		

#### 4.8. Case 6; GSI 3 Placed 15 underneath the 5-Story Building Model

For the Case 6, GSI 3 were placed with cylindrical shaped 15 cm ( $H/D = 6.7$ ) under the foundation of the building model. 5-story building model tested under Kocaeli earthquake, El Centro earthquake, and Kobe earthquake and the results of these experiments are presented below as comparison with the CM-5.

##### 4.8.1. Seismic Response of Case 6 under Kocaeli Earthquake Motion

Figure 4.19a, Figure 4.19b, and Figure 4.19c represent amplification in both foundation acceleration, top floor acceleration, and reduction in the first-floor drift comparing CM-5. There is no significant acceleration decrease in the 5-story building model for this particular condition as seen in the Table 4.19. Only first floor and fourth-floor drifts are reduced up to 20% in RMS. Similarly, the acceleration decrease is not

obtained from the accelerometer located at the midpoint of the isolated soil region (Table 4.19). Moreover, Figure 4.19e indicates that there is no base shear and base moment reduction. It can be observed from Figure 4.19f, calculated Arias intensity values for the floors are magnified except foundation comparing the CM-5. Detailed information about the performance indicator parameters is provided as the given order horizontal acceleration response, horizontal story drift, Arias intensity, peak spectral acceleration, period lengthening ratio of the floors and base shear and base moment of 5-story building model in Table 4.19. On the other side, the natural period of the 5-story building is not changed. The slight increase of the peak spectral accelerations could be neglected as seen in Table 4.19.

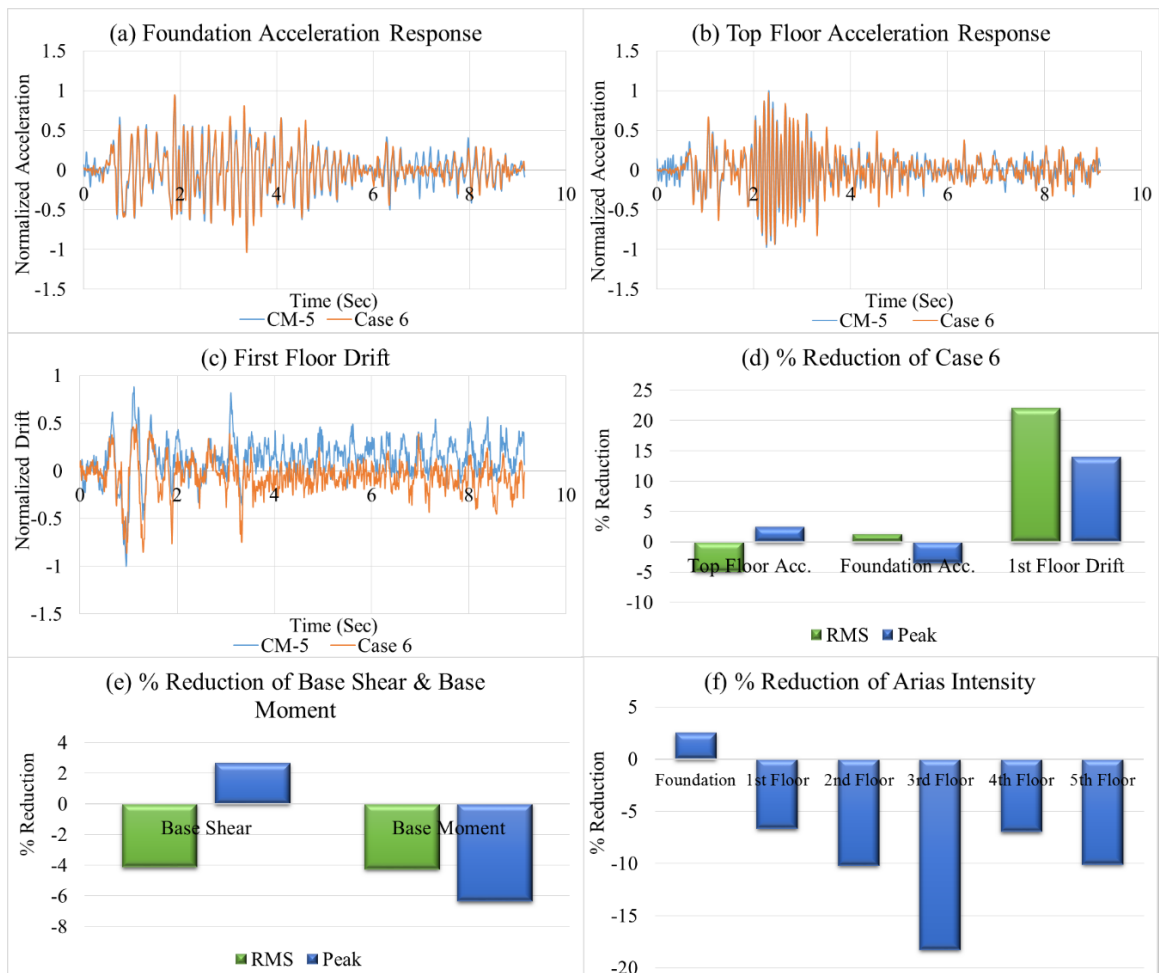


Figure 4.19. (a) Foundation, (b) Top Floor Horizontal Acceleration Response, (c) First Floor Drift, (d) % Reduction of Case 6, (e) % Reduction of Base Shear & Base Moment and (f) % Reduction of Arias Intensity of Case 6 Comparing CM-5 under Kocaeli Earthquake.

Table 4.19. Comparison of Case 6 with the CM-5 under Kocaeli Earthquake.

Results of Case 6 Comparing CM-5 under Kocaeli Earthquake																
	In-soil		Foundation		1st Floor		2nd Floor		3rd Floor		4th Floor		5th Floor			
	RMS	Peak	RMS	Peak	RMS	Peak	RMS	Peak	RMS	Peak	RMS	Peak	RMS	Peak		
Horizontal Acceleration (g)																
CM-5	0.07	0.27	0.07	0.28	0.12	0.57	0.12	0.56	0.07	0.29	0.08	0.33	0.14	0.64		
Case 6	0.07	0.29	0.07	0.29	0.12	0.53	0.12	0.55	0.08	0.28	0.09	0.33	0.15	0.62		
% Reduction	-3	-9	1	-4	-3	7	-5	2	-9	4	-3	1	-5	2		
Horizontal Story Drift																
CM-5	-	-	-	-	0.08	0.32	0.07	0.27	0.04	0.23	0.08	0.41	0.06	0.20		
Case 6	-	-	-	-	0.06	0.28	0.08	0.25	0.08	0.33	0.07	0.29	0.06	0.20		
% Reduction	-	-	-	-	22	14	-9	8	-81	-48	19	27	-5	0		
Arias Intensity (m/sec)																
CM-5	0.68		0.70		1.94		1.93		0.69		1.01		2.88			
Case 6	0.72		0.68		2.06		2.13		0.82		1.08		3.18			
% Reduction	-5		2		-7		-10		-18		-7		-10			
Peak Spectral Acceleration (g)																
CM-5	-		1.25		3.73		3.98		1.77		2.23		4.43			
Case 6	-		1.35		3.51		3.79		1.71		2.10		4.23			
% Reduction	-		-8		6		5		3		6		5			
Period Lengthening Ratio																
CM-5	-		0.15		0.09		0.09		0.09		0.09		0.09			
Case 6	-		0.15		0.09		0.09		0.09		0.09		0.09			
Period Length. Ratio	-		1.00		1.00		1.00		1.00		1.00		1.00			
Base Shear (kN)																
	RMS				Peak				RMS				Peak			
CM-5	0.86				3.97				0.35				1.23			
Case 6	0.89				3.86				0.37				1.30			
% Reduction	-4				3				-4				-6			

#### 4.8.2. Seismic Response of Case 6 under El Centro Earthquake Motion

Figure 4.20a, Figure 4.20b, and Figure 4.20c show the variation due to proposed GSI system such as reduced foundation acceleration, reduced first-floor drift and enlarged top floor acceleration comparing CM-5. The reduction of foundation acceleration is roughly 10% in RMS and 7% in peak values as seen in Figure 4.20d. Unlikely, the obtained acceleration from the midpoint of the isolated soil region is reduced 6% in RMS but magnified in peak value (Table 4.20). Nevertheless, acceleration reduction of the other floors can be ignored. This means there is no acceleration decrease in the 5-story building model except foundation level. Even though the first-floor drift is decreased approximately 30% in RMS, the top floor drift is magnified. Figure 4.20e represents there is almost no reduction in the base shear and correspondingly base moment as RMS. It can be observed from Figure 4.20f, Arias intensity values are not reduced significantly except foundation comparing the CM-5. Detailed information about per-

formance indicator parameters that are horizontal acceleration response, horizontal story drift, Arias intensity, peak spectral acceleration, period lengthening ratio of the floors and base shear and base moment of 5-story building model is provided in Table 4.20. On the other hand, the slight changing in the period lengthening ratios can be underestimated, but peak spectral accelerations are decreased up to 12% (Table 4.20).

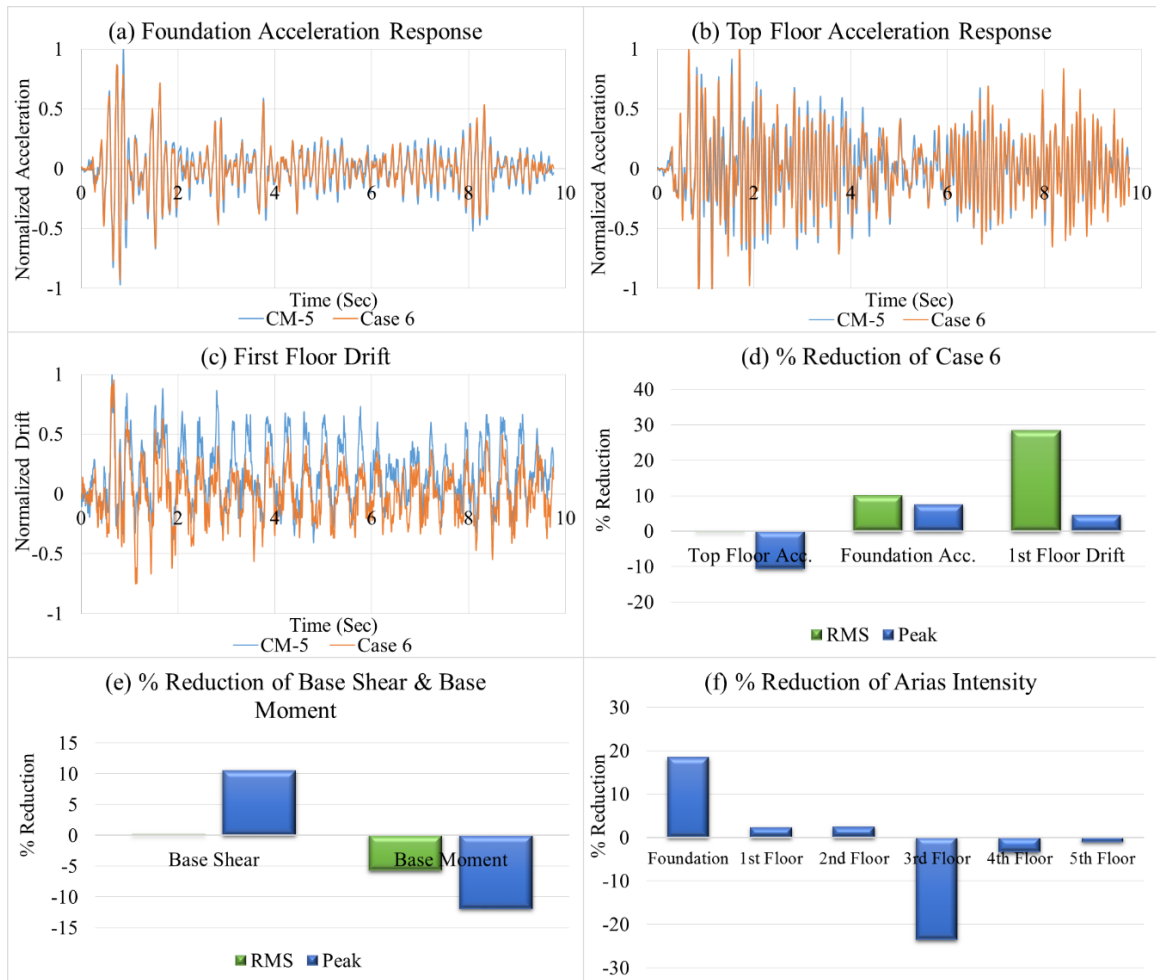


Figure 4.20. (a) Foundation, (b) Top Floor Horizontal Acceleration Response, (c) First Floor Drift, (d) % Reduction of Case 6, (e) % Reduction of Base Shear & Base Moment and (f) % Reduction of Arias Intensity of Case 6 Comparing CM-5 under El Centro Earthquake.

Table 4.20. Comparison of Case 6 with the CM-5 under El Centro Earthquake.

Results of Case 6 Comparing CM-5 under El Centro Earthquake															
	In-soil		Foundation		1st Floor		2nd Floor		3rd Floor		4th Floor		5th Floor		
	RMS	Peak	RMS	Peak	RMS	Peak	RMS	Peak	RMS	Peak	RMS	Peak	RMS	Peak	
Horizontal Acceleration (g)															
CM-5	0.09	0.42	0.09	0.44	0.13	0.55	0.13	0.47	0.08	0.33	0.09	0.36	0.16	0.55	
Case 6	0.08	0.44	0.08	0.41	0.13	0.49	0.12	0.42	0.09	0.39	0.09	0.33	0.16	0.61	
% Reduction	6	-4	10	7	1	11	2	11	-11	-18	-1	8	0	-11	
Horizontal Story Drift															
CM-5	-	-	-	-	0.09	0.29	0.10	0.27	0.05	0.26	0.10	0.38	0.05	0.17	
Case 6	-	-	-	-	0.07	0.28	0.07	0.24	0.07	0.24	0.07	0.25	0.08	0.23	
% Reduction	-	-	-	-	28	5	33	12	-23	8	31	34	-47	-38	
Arias Intensity (m/sec)															
CM-5	1.20		1.21		2.50		2.40		0.89		1.32		3.75		
Case 6	1.07		0.98		2.44		2.34		1.10		1.36		3.79		
% Reduction	11		19		2		2		-24		-3		-1		
Peak Spectral Acceleration (g)															
CM-5	-		2.03		2.24		2.56		1.28		1.29		2.76		
Case 6	-		1.80		2.03		2.26		1.55		1.16		2.43		
% Reduction	-		11		9		12		-21		10		12		
Period Lengthening Ratio															
CM-5	-		0.14		0.09		0.09		0.09		0.09		0.09		
Case 6	-		0.15		0.09		0.09		0.06		0.09		0.09		
Period Length. Ratio	-		1.07		1.06		1.00		0.65		1.06		1.06		
Base Shear (kN)															
	RMS				Peak				RMS				Peak		
CM-5	0.93				3.35				0.38				1.39		
Case 6	0.92				2.99				0.41				1.56		
% Reduction	0				11				-6				-12		

#### 4.8.3. Seismic Response of Case 6 under Kobe Earthquake Motion

Figure 4.21a, Figure 4.21b, and Figure 4.21d indicate that there are decreases in foundation acceleration, top floor acceleration, and amplification in first-floor drift of the 5-story building model. The reduction of foundation acceleration is roughly 13% in RMS and 5% in peak. Oppositely, the obtained acceleration from the midpoint of the isolated soil region is not decreased remarkably (Table 4.21). However, reduction of acceleration ascends at the upstairs up to 13% in RMS and 19% in peak. Unlike expected, almost all the story drifts are enlarged. Obvious permanent displacement that is shown in the Figure 4.21c could be the reason of the amplification of the drifts. Figure 4.21e represents the base shear and base moment are decreased up to 7% and 3% in RMS, respectively. Figure 4.21f shows that computed Arias intensity values for the floors are reduced up to 24%. Horizontal acceleration response, horizontal story drift, Arias intensity, peak spectral acceleration, period lengthening ratio of the floors and

base shear and base moment of 5-story building model are summarized in Table 4.21. On the other side, there is no variation in the natural period of the 5-story building but peak spectral accelerations are decreased up to 18% as seen in Table 4.21.

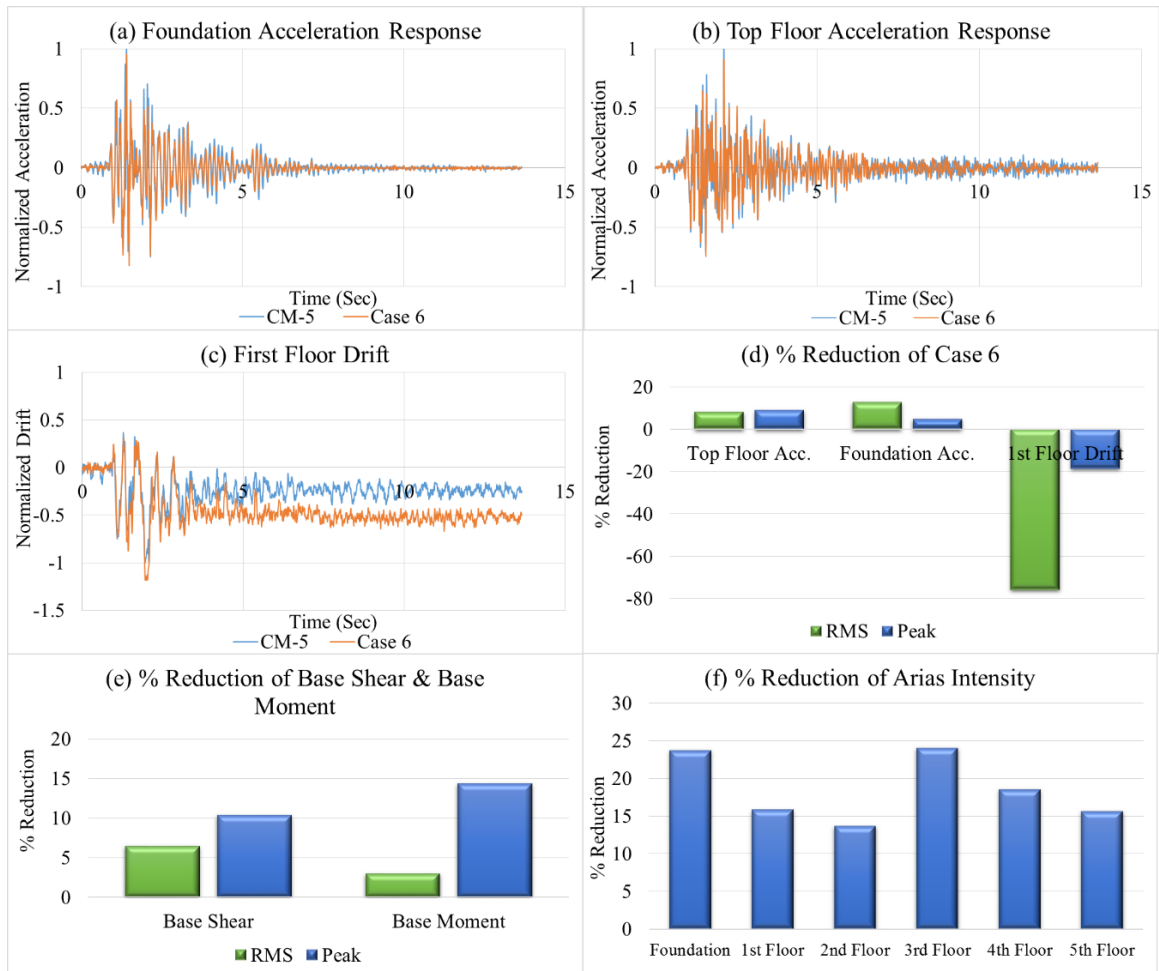


Figure 4.21. (a) Foundation, (b) Top Floor Horizontal Acceleration Response, (c) First Floor Drift, (d) % Reduction of Case 6, (e) % Reduction of Base Shear & Base Moment and (f) % Reduction of Arias Intensity of Case 6 Comparing CM-5 under Kobe Earthquake.



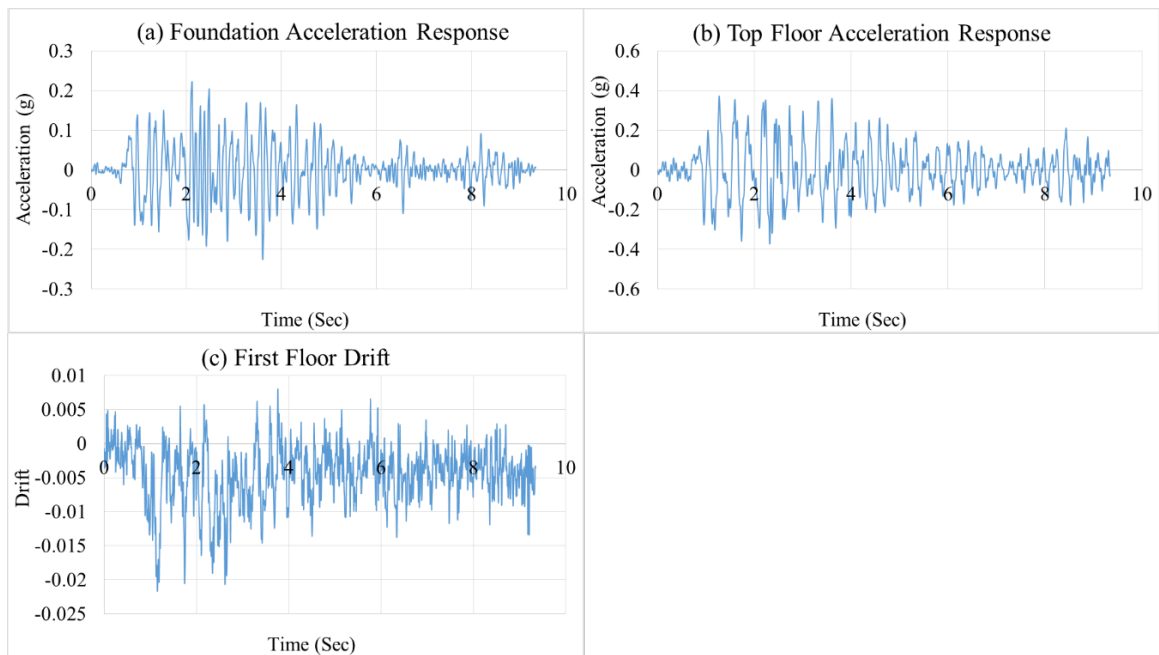


Figure 4.22. (a) Foundation, (b) Top Floor Horizontal Acceleration Response and (c) First Floor Drift of the CM-3 under Kocaeli Earthquake.

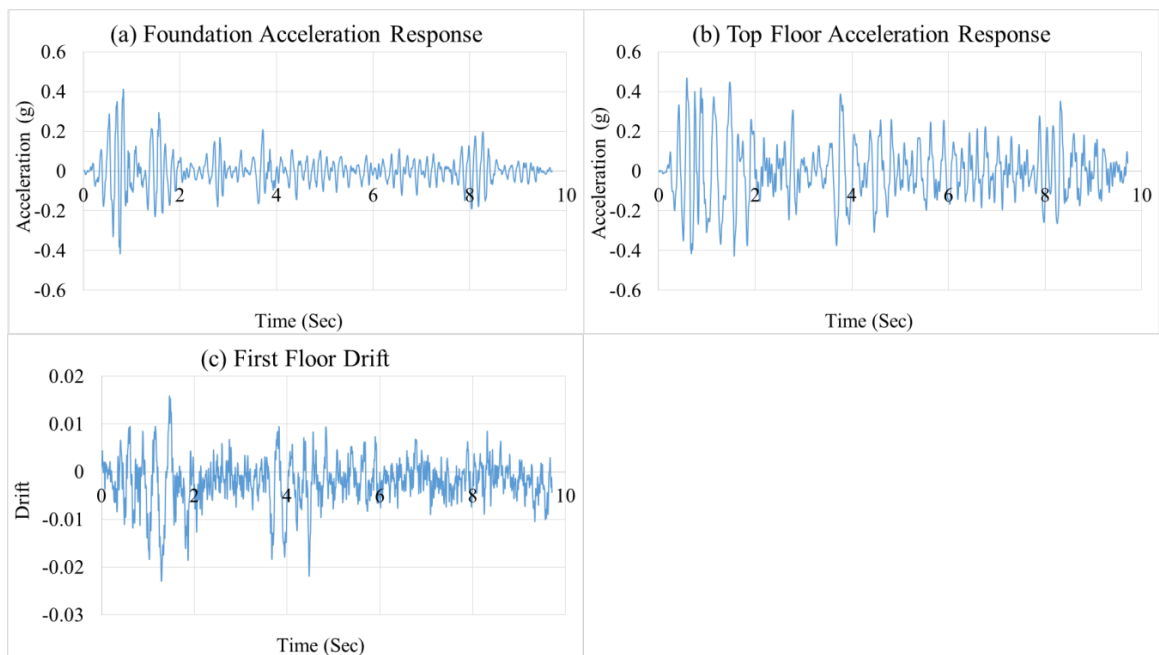


Figure 4.23. (a) Foundation, (b) Top Floor Horizontal Acceleration Response and (c) First Floor Drift of the CM-3 under El Centro Earthquake.

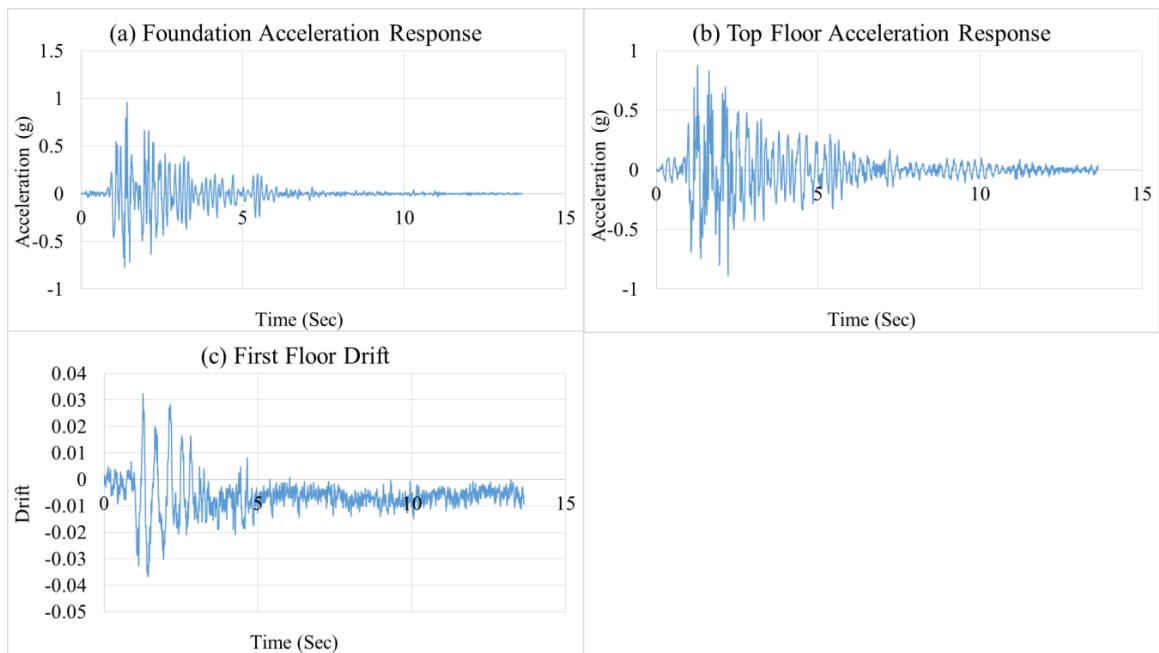


Figure 4.24. (a) Foundation, (b) Top Floor Horizontal Acceleration Response and (c) First Floor Drift of the CM-3 under Kobe Earthquake.

It can be observed from Figure 4.22, Figure 4.23 and Figure 4.24 that the measured maximum foundation accelerations are 0.23g, 0.42g, and 0.96g for Kocaeli, El Centro, and Kobe earthquakes, respectively. The measured maximum top floor accelerations for the Kocaeli, El Centro, and Kobe earthquakes are as 0.37g, 0.47g, and 0.89g, respectively. The first-floor drifts values belong to the Kocaeli, El Centro, and Kobe earthquakes are 0.022, 0.023, and 0.036.

#### 4.10. Case 7; GSI 2 Placed 10 cm underneath the 3-Story Building Model

The Case 7 was constituted with GSI 2 were placed with cylindrical shaped 10 cm ( $H/D = 10$ ) under the foundation. 3-story building model excited with the selected earthquake motions. Moreover, given results of the Case 7 below as a comparison with the unisolated case belong to Kocaeli earthquake, El Centro earthquake, and Kobe earthquake, respectively.

#### 4.10.1. Seismic Response of Case 7 under Kocaeli Earthquake Motion

Figure 4.25a, Figure 4.25b, and Figure 4.25c represent the variation due to proposed GSI system in terms of the foundation acceleration, top floor acceleration, and the first-floor drift comparing CM-3. Changing of acceleration in the midpoint of the isolated soil region can be underestimated (Table 4.22). Likewise, there is no acceleration reduction in the 3-story building model as seen in the Table 4.22. The first-floor drift is reduced by approximately 7% in RMS. Figure 4.25e represents that there is no reductions in the base shear and correspondingly base moment. It can be observed from Figure 4.25f that Arias intensity values of the floors are magnified comparing the CM-3. Detailed information about the performance indicator parameters is provided in such sequence; horizontal acceleration response, horizontal story drift, Arias intensity, peak spectral acceleration, period lengthening ratio of the floors and base shear and base moment of 3-story building model (Table 4.22). The period shifting ratios show variations among the floors. On the other side, although peak spectral acceleration of the foundation is reduced 13%, the other spectral accelerations are not reduced as seen in Table 4.22.

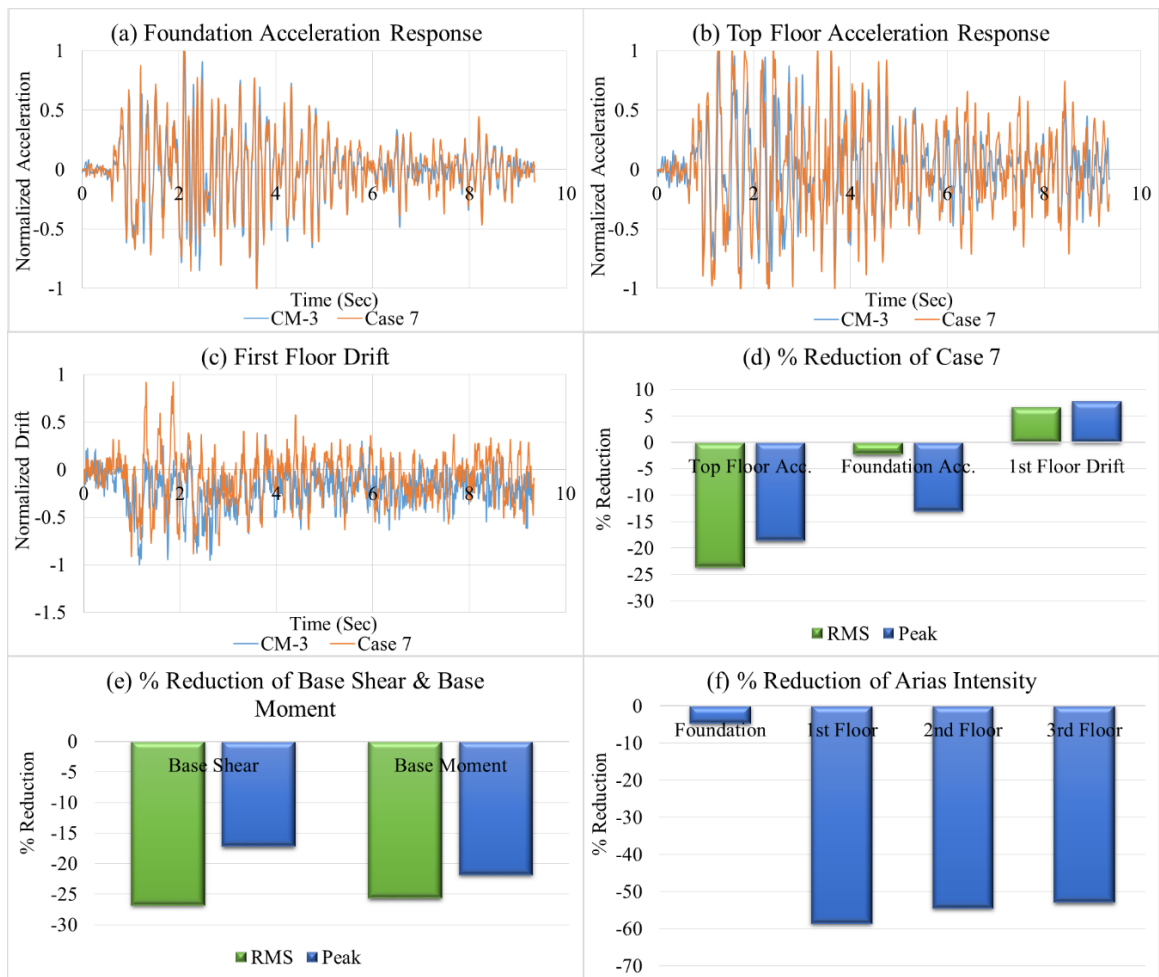


Figure 4.25. (a) Foundation, (b) Top Floor Horizontal Acceleration Response, (c) First Floor Drift, (d) % Reduction of Case 7, (e) % Reduction of Base Shear & Base Moment and (f) % Reduction of Arias Intensity of Case 7 Comparing CM-3 under Kocaeli Earthquake.

Table 4.22. Comparison of Case 7 with the CM-3 under Kocaeli Earthquake.

Results of Case 7 Comparing CM-3 under Kocaeli Earthquake										
	In-soil		Foundation		1st Floor		2nd Floor		3rd Floor	
	RMS	Peak	RMS	Peak	RMS	Peak	RMS	Peak	RMS	Peak
Horizontal Acceleration (g)										
CM-3	0.07	0.27	0.06	0.23	0.06	0.23	0.08	0.27	0.12	0.37
Case 7	0.07	0.27	0.06	0.25	0.07	0.28	0.10	0.30	0.15	0.44
% Reduction	-3	-1	-2	-13	-26	-19	-24	-12	-24	-19
Horizontal Story Drift										
CM-3	-	-	-	-	0.17	0.60	0.07	0.30	0.10	0.38
Case 7	-	-	-	-	0.16	0.55	0.09	0.33	0.05	0.21
% Reduction	-	-	-	-	7	8	-14	-11	52	46
Arias Intensity (m/sec)										
CM-3	0.65		0.53		0.50		0.89		2.05	
Case 7	0.69		0.55		0.79		1.37		3.14	
% Reduction	-5		-5		-59		-55		-53	
Peak Spectral Acceleration (g)										
CM-3	-		1.26		0.91		1.38		1.92	
Case 7	-		1.10		1.21		1.53		2.14	
% Reduction	-		13		-34		-11		-12	
Period Lengthening Ratio										
Fundamental Period (sec)										
CM-3	-		0.09		0.29		0.29		0.29	
Case 7	-		0.09		0.06		0.27		0.27	
Period Length. Ratio	-		1.00		0.19		0.91		0.91	
Base Shear (kN)      Base Moment (kN.m)										
	RMS		Peak		RMS		Peak			
CM-3	0.29		1.04		0.15		0.47			
Case 7	0.37		1.22		0.19		0.58			
% Reduction	-27		-17		-26		-22			

#### 4.10.2. Seismic Response of Case 7 under El Centro Earthquake Motion

According to Figure 4.26a, Figure 4.26b, and Figure 4.26c, there is no significant alteration in 3-story building model regarding foundation acceleration, top floor acceleration, and first-floor drift after applying proposed GSI system. Acceleration reduction is not observed both in the midpoint of the isolated soil region also in the 3-story building model as seen in the Table 4.23. Even though the top floor drift is reduced approximately 28% in RMS, other floor drifts of the 3-story building model are not reduced. Figure 4.26e illustrates the amplification of the base shear and base moment. As can be observed in Figure 4.26f, computed Arias intensity values for the floors are magnified except foundation level comparing the CM-3. Detailed information about the performance indicator parameters that are horizontal acceleration response, horizontal story drift, Arias intensity, peak spectral acceleration, period lengthening

ratio of the floors and base shear and base moment of 3-story building model is provided in Table 4.23. The period shifting ratios show variations among the floors. On the other side, peak spectral acceleration of the foundation is reduced 13%, but the rest of the spectral accelerations are not reduced as seen in Table 4.23.

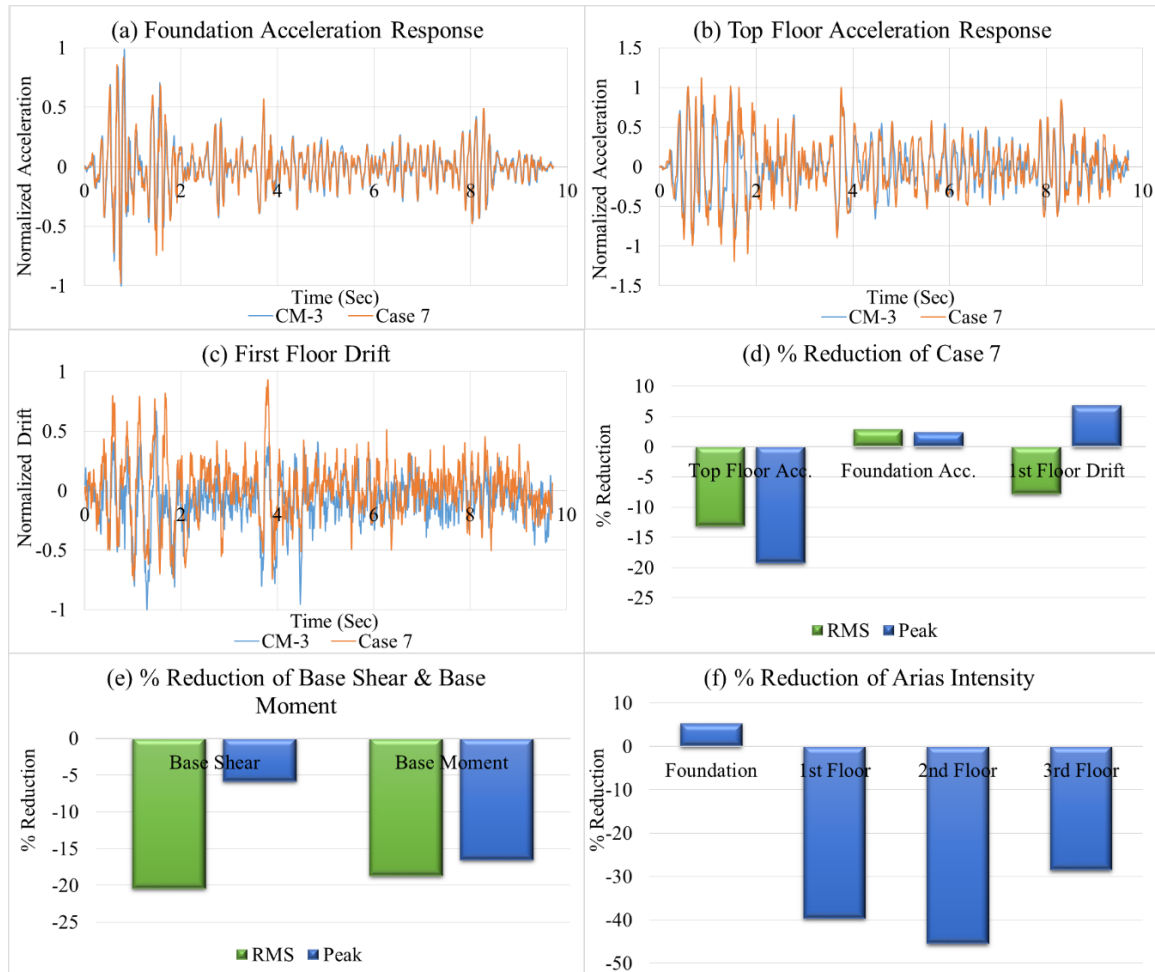


Figure 4.26. (a) Foundation, (b) Top Floor Horizontal Acceleration Response, (c) First Floor Drift, (d) % Reduction of Case 7, (e) % Reduction of Base Shear & Base Moment and (f) % Reduction of Arias Intensity of Case 7 Comparing CM-3 under El Centro Earthquake.

Table 4.23. Comparison of Case 7 with the CM-3 under El Centro Earthquake.

Results of Case 7 Comparing CM-3 under El Centro Earthquake										
	In-soil		Foundation		1st Floor		2nd Floor		3rd Floor	
	RMS	Peak	RMS	Peak	RMS	Peak	RMS	Peak	RMS	Peak
Horizontal Acceleration (g)										
CM-3	0.09	0.46	0.08	0.42	0.07	0.29	0.09	0.31	0.15	0.47
Case 7	0.09	0.48	0.08	0.41	0.08	0.34	0.11	0.46	0.16	0.56
% Reduction	3	-4	3	2	-18	-17	-20	-50	-13	-19
Horizontal Story Drift										
CM-3	-	-	-	-	0.14	0.63	0.09	0.35	0.08	0.33
Case 7	-	-	-	-	0.16	0.59	0.09	0.36	0.06	0.24
% Reduction	-	-	-	-	-8	7	-2	-1	28	27
Arias Intensity (m/sec)										
CM-3	1.31		1.00		0.67		1.27		3.18	
Case 7	1.24		0.94		0.94		1.85		4.09	
% Reduction	5		5		-40		-46		-29	
Peak Spectral Acceleration (g)										
CM-3	-		1.90		0.91		1.35		2.07	
Case 7	-		1.65		1.20		1.94		2.73	
% Reduction	-		13		-32		-44		-32	
Period Lengthening Ratio										
CM-3	-		0.15		0.28		0.28		0.16	
Case 7	-		0.15		0.27		0.27		0.27	
Period Length. Ratio	-		1.00		0.98		0.96		1.74	
Base Shear (kN)      Base Moment (kN.m)										
	RMS		Peak		RMS		Peak			
CM-3	0.34		1.31		0.18		0.58			
Case 7	0.41		1.39		0.21		0.67			
% Reduction	-20		-6		-19		-17			

#### 4.10.3. Seismic Response of Case 7 under Kobe Earthquake Motion

It can be observed from Figure 4.27a, Figure 4.27b, and Figure 4.27c that there is no remarkable reduction in foundation acceleration, top floor acceleration, and first-floor drift comparing CM-3. Moreover, there is no contribution regarding acceleration reduction as seen in the Table 4.24. All drifts of the 3-story building model are magnified. Figure 4.27e illustrates there is no decrease in the base shear and correspondingly base moment. Detailed data regarding the horizontal acceleration response, horizontal story drift, Arias intensity, peak spectral acceleration, period lengthening ratio of the floors and base shear and base moment of 3-story building model are summarized in Table 4.24. It can be easily deduced that proposed GSI system did not enhance the 3-story building model seismically for this particular case.

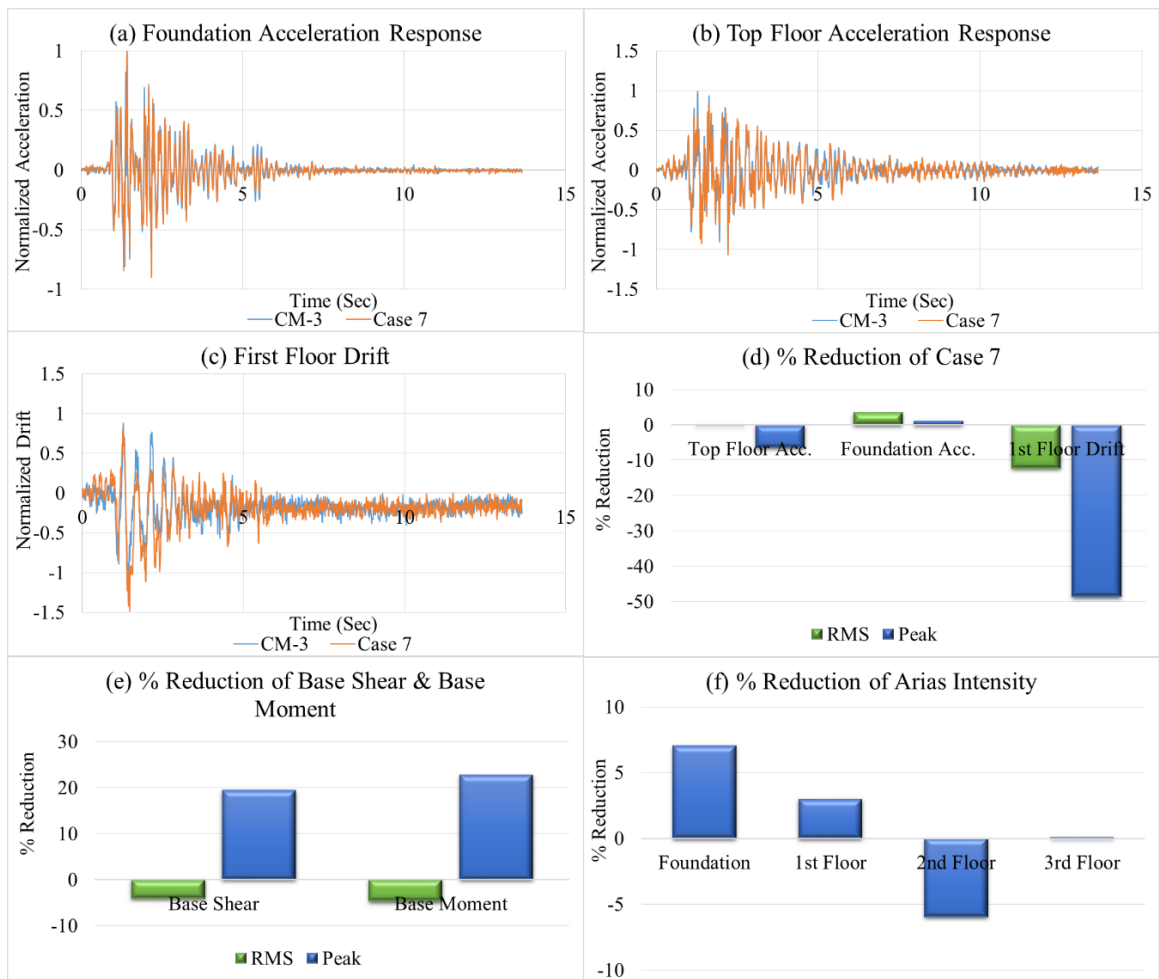


Figure 4.27. (a) Foundation, (b) Top Floor Horizontal Acceleration Response, (c) First Floor Drift, (d) % Reduction of Case 7, (e) % Reduction of Base Shear & Base Moment and (f) % Reduction of Arias Intensity of Case 7 Comparing CM-3 under Kobe Earthquake.

Table 4.24. Comparison of Case 7 with the CM-3 under Kobe Earthquake.

Results of Case 7 Comparing CM-3 under Kobe Earthquake										
	In-soil		Foundation		1st Floor		2nd Floor		3rd Floor	
	RMS	Peak	RMS	Peak	RMS	Peak	RMS	Peak	RMS	Peak
Horizontal Acceleration (g)										
CM-3	0.14	0.93	0.13	0.96	0.11	0.87	0.12	1.19	0.16	0.89
Case 7	0.15	0.90	0.13	0.95	0.11	0.73	0.12	0.98	0.16	0.94
% Reduction	-2	3	4	1	1	16	-3	18	0	-6
Horizontal Story Drift										
CM-3	-	-	-	-	0.25	1.01	0.17	0.93	0.14	0.87
Case 7	-	-	-	-	0.29	1.50	0.25	1.15	0.24	0.94
% Reduction	-	-	-	-	-12	-49	-46	-24	-72	-8
Arias Intensity (m/sec)										
CM-3	4.31		3.58		2.71		2.98		5.29	
Case 7	4.48		3.32		2.63		3.16		5.29	
% Reduction	-4		7		3		-6		0	
Peak Spectral Acceleration (g)										
CM-3	-		3.10		2.83		4.37		2.64	
Case 7	-		3.14		2.74		4.77		2.78	
% Reduction	-		-1		3		-9		-5	
Period Lengthening Ratio										
CM-3	-		0.16		0.06		0.05		0.04	
Case 7	-		0.16		0.05		0.04		0.05	
Period Length. Ratio	-		1.00		0.83		0.89		1.43	
Base Shear (kN)      Base Moment (kN.m)										
	RMS		Peak		RMS		Peak			
CM-3	0.39		3.66		0.18		1.60			
Case 7	0.41		2.95		0.19		1.23			
% Reduction	-4		19		-5		23			

#### 4.11. Case 8; GSI 2 Placed 15 cm underneath the 3-Story Building Model

The Case 8 was constituted with GSI 2 were placed with cylindrical shaped 15 cm ( $H/D = 6.7$ ) under the foundation. 3-story building model agitated under chosen earthquake motions. Furthermore, results of the experiments regarding Case 8 comparing with CM-3 that are provided below belong to Kocaeli earthquake, El Centro earthquake, and Kobe earthquake, respectively.

##### 4.11.1. Seismic Response of Case 8 under Kocaeli Earthquake Motion

Figure 4.28a, Figure 4.28b, and Figure 4.28c illustrate the slight reduction of foundation acceleration and magnification of top floor acceleration and first floor drift comparing CM-3. The obtained acceleration from the midpoint of the isolated soil

region is not reduced remarkably (Table 4.25). The reduction of foundation acceleration is roughly 6% in RMS, and there is no reduction regarding peak values. Although the top floor drift is reduced approximately 30% in RMS, the rest of the drifts of the 3-story building model are not reduced. Figure 4.28e shows there is no reduction in the base shear and correspondingly base moment. As can be observed in Figure 4.28f, except Arias intensity of foundation, any improvement is not observed from the isolated building model comparing the CM-3. Detailed information about the performance indicator parameters of 3-story building model is listed in Table 4.25. The period shifting ratios show variations among the floors. On the other side, peak spectral acceleration of the foundation is reduced 21%, but the rest of the spectral acceleration are nearly same with the CM-3 as seen in Table 4.25.

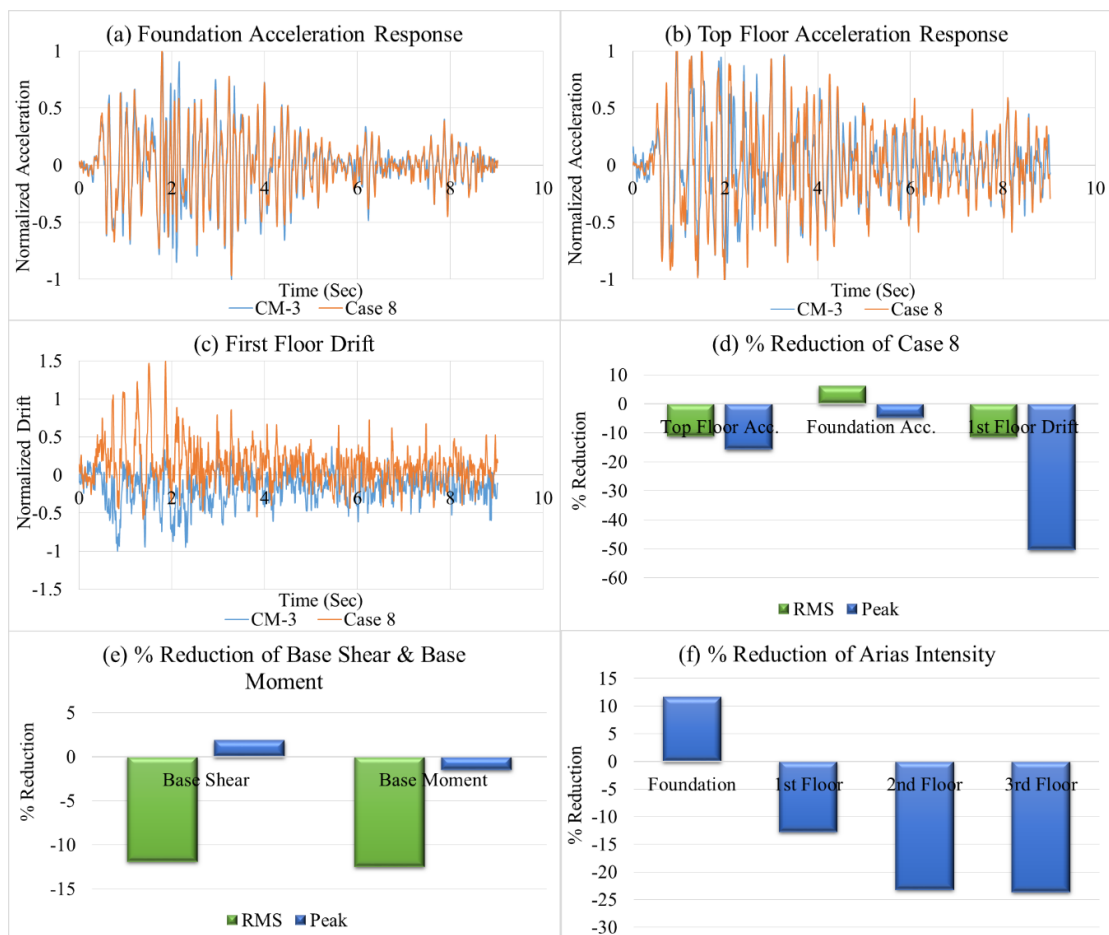


Figure 4.28. (a) Foundation, (b) Top Floor Horizontal Acceleration Response, (c) First Floor Drift, (d) % Reduction of Case 8, (e) % Reduction of Base Shear & Base Moment and (f) % Reduction of Arias Intensity of Case 8 Comparing CM-3 under Kocaeli Earthquake.

Table 4.25. Comparison of Case 8 with the CM-3 under Kocaeli Earthquake.

Results of Case 8 Comparing CM-3 under Kocaeli Earthquake										
	In-soil		Foundation		1st Floor		2nd Floor		3rd Floor	
	RMS	Peak	RMS	Peak	RMS	Peak	RMS	Peak	RMS	Peak
Horizontal Acceleration (g)										
CM-3	0.07	0.27	0.06	0.23	0.06	0.23	0.08	0.27	0.12	0.37
Case 8	0.07	0.26	0.06	0.24	0.06	0.21	0.09	0.27	0.13	0.43
% Reduction	2	2	6	-5	-6	9	-11	-1	-11	-16
Horizontal Story Drift										
CM-3	-	-	-	-	0.15	0.57	0.08	0.30	0.10	0.38
Case 8	-	-	-	-	0.17	0.85	0.08	0.41	0.07	0.23
% Reduction	-	-	-	-	-11	-50	-3	-37	30	39
Arias Intensity (m/sec)										
CM-3	0.65		0.53		0.50		0.88		2.05	
Case 8	0.63		0.47		0.56		1.09		2.53	
% Reduction	3		12		-13		-23		-24	
Peak Spectral Acceleration (g)										
CM-3	-		1.26		0.91		1.38		1.92	
Case 8	-		1.00		0.93		1.39		1.93	
% Reduction	-		21		-3		0		0	
Period Lengthening Ratio										
CM-3	-		0.09		0.29		0.29		0.29	
Case 8	-		0.15		0.06		0.26		0.26	
Period Length. Ratio	-		1.61		0.19		0.90		0.90	
Base Shear (kN)										
	RMS		Peak		RMS		Peak			
CM-3	0.30		1.04		0.15		0.47			
Case 8	0.33		1.02		0.17		0.48			
% Reduction	-12		2		-12		-1			

#### 4.11.2. Seismic Response of Case 8 under El Centro Earthquake Motion

As can be observed in Figure 4.29a, Figure 4.29b, and Figure 4.29c, there is no improvement regarding foundation acceleration, top floor acceleration, and first-floor drift comparing CM-3. There is nearly no acceleration variation observed in the midpoint of the isolated soil region (Table 4.26). The reduction of the foundation acceleration is roughly 3% in RMS and 6% in peak values. The top floor drift is reduced approximately 35% in RMS. On the contrary, other drifts of the 3-story building model are not decreased. Figure 4.29e shows there is no reduction in the base shear and relatively base moment. Figure 4.29f demonstrates that Arias intensity values calculated for the floors are magnified except from the foundation level comparing the CM-3. Detailed information about the performance indicator parameters that are horizontal acceleration response, horizontal story drift, Arias intensity, peak spectral acceleration, period

lengthening ratio of the floors and base shear and base moment of 3-story building model is listed in Table 4.26. The period shifting ratios vary among the floors. On the other hand, peak spectral acceleration of the foundation is reduced 7%, but the rest of the spectral accelerations are magnified compared to CM-3 as seen in Table 4.26.

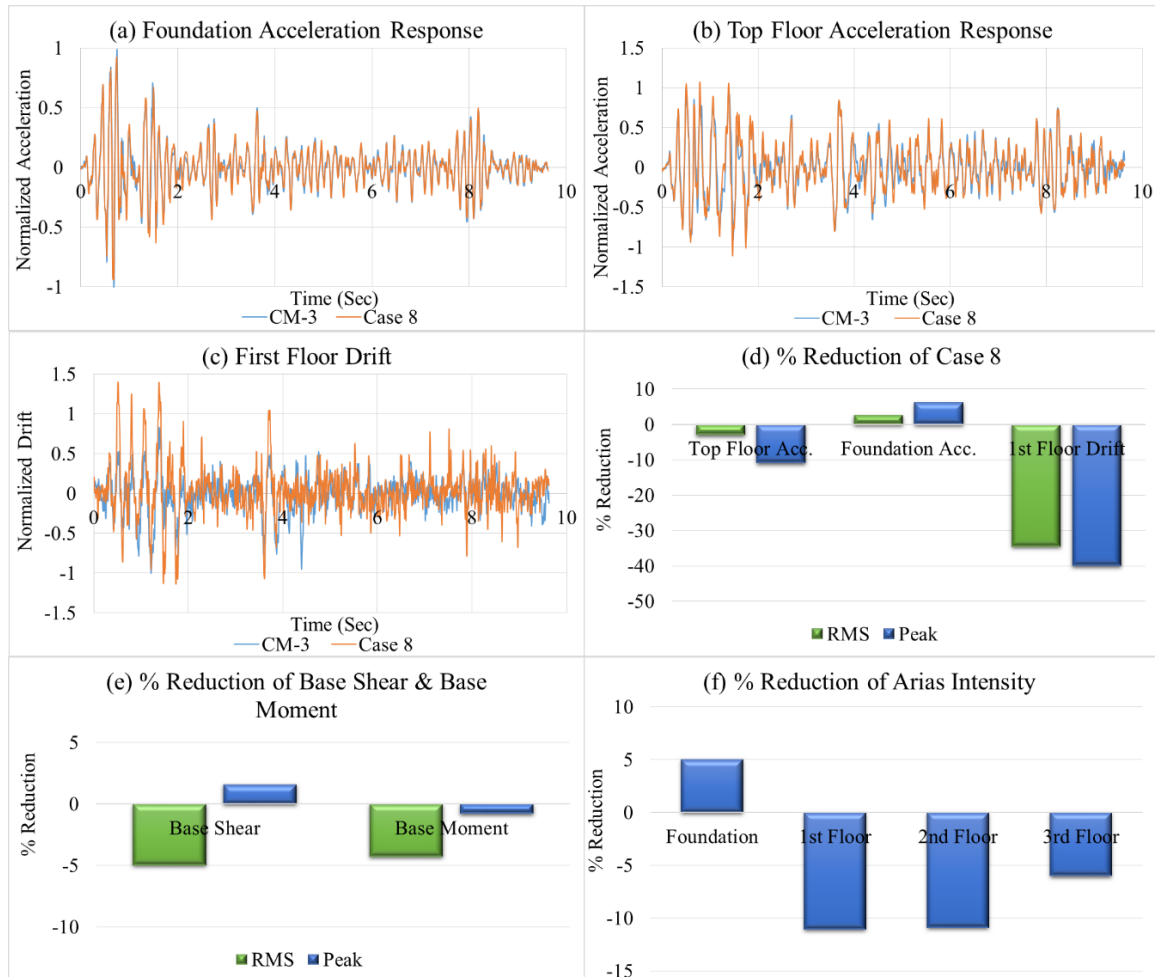


Figure 4.29. (a) Foundation, (b) Top Floor Horizontal Acceleration Response, (c) First Floor Drift, (d) % Reduction of Case 8, (e) % Reduction of Base Shear & Base Moment and (f) % Reduction of Arias Intensity of Case 8 Comparing CM-3 under El Centro Earthquake.

Table 4.26. Comparison of Case 8 with the CM-3 under El Centro Earthquake.

Results of Case 8 Comparing CM-3 under El Centro Earthquake										
	In-soil		Foundation		1st Floor		2nd Floor		3rd Floor	
	RMS	Peak	RMS	Peak	RMS	Peak	RMS	Peak	RMS	Peak
Horizontal Acceleration (g)										
CM-3	0.09	0.46	0.08	0.42	0.07	0.29	0.09	0.31	0.15	0.47
Case 8	0.09	0.47	0.08	0.39	0.07	0.34	0.10	0.33	0.15	0.52
% Reduction	-1	-2	3	6	-5	-17	-5	-8	-3	-11
Horizontal Story Drift										
CM-3	-	-	-	-	0.13	0.58	0.09	0.38	0.08	0.34
Case 8	-	-	-	-	0.18	0.81	0.10	0.44	0.05	0.18
% Reduction	-	-	-	-	-35	-40	-4	-14	35	49
Arias Intensity (m/sec)										
CM-3	1.31		1.00		0.67		1.27		3.18	
Case 8	1.32		0.95		0.75		1.41		3.37	
% Reduction	-1		5		-11		-11		-6	
Peak Spectral Acceleration (g)										
CM-3	-		1.90		0.91		1.35		2.07	
Case 8	-		1.77		1.08		1.66		2.33	
% Reduction (%)	-		7		-19		-23		-13	
Period Lengthening Ratio										
CM-3	-		0.15		0.28		0.28		0.16	
Case 8	-		0.15		0.06		0.27		0.27	
Period Length. Ratio	-		1.00		0.20		0.96		1.74	
Base Shear (kN)										
	RMS		Peak		RMS		Peak			
CM-3	0.34		1.31		0.18		0.58			
Case 8	0.36		1.29		0.18		0.58			
% Reduction	-5		2		-4		-1			

#### 4.11.3. Seismic Response of Case 8 under Kobe Earthquake Motion

Figure 4.30a, Figure 4.30b, and Figure 4.30c represent the variation of foundation acceleration, top floor acceleration, and first-floor drift due to the application of the proposed GSI system. Any significant improvement is not observed in terms of reduction of acceleration. Even though the top floor drift is reduced approximately 13% in RMS, the rest of the drifts of the 3-story building model are not decreased. Figure 4.30e illustrates there is no remarkable reduction in the base shear and base moment. It can be seen in Figure 4.30f that Arias intensity values of the floors are reduced up to 20%. Detailed information about the performance indicator parameters is summarized in such order; horizontal acceleration response, horizontal story drift, Arias intensity, peak spectral acceleration, period lengthening ratio of the floors and base shear and base moment of 3-story building model (Table 4.27). On the other side, peak spectral

acceleration of the second floor is reduced 12%, but the other spectral accelerations do not show any improvement compared to CM-3 as seen in Table 4.27.

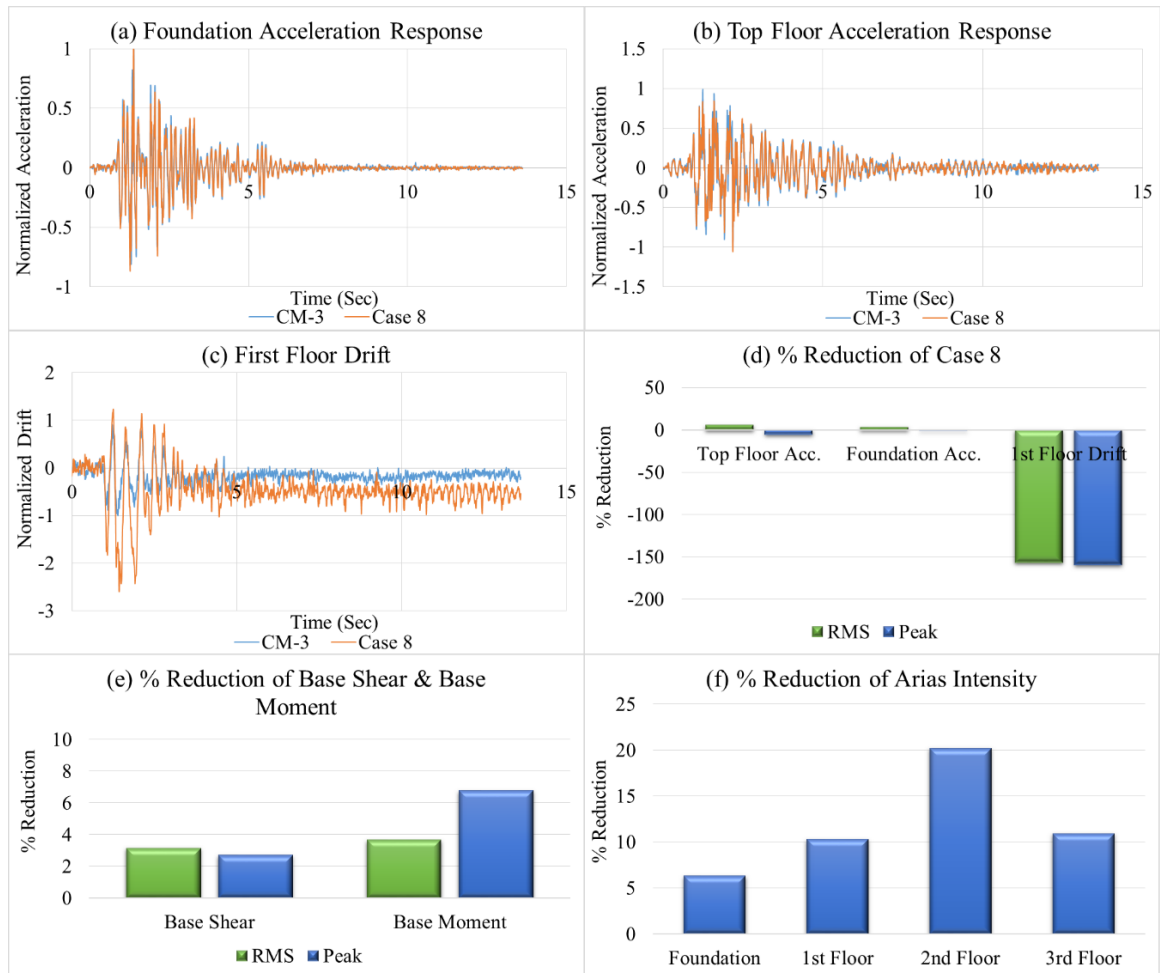


Figure 4.30. (a) Foundation, (b) Top Floor Horizontal Acceleration Response, (c) First Floor Drift, (d) % Reduction of Case 8, (e) % Reduction of Base Shear & Base Moment and (f) % Reduction of Arias Intensity of Case 8 Comparing CM-3 under Kobe Earthquake.

Table 4.27. Comparison of Case 8 with the CM-3 under Kobe Earthquake.

Results of Case 8 Comparing CM-3 under Kobe Earthquake										
	In-soil		Foundation		1st Floor		2nd Floor		3rd Floor	
	RMS	Peak	RMS	Peak	RMS	Peak	RMS	Peak	RMS	Peak
Horizontal Acceleration (g)										
CM-3	0.14	0.93	0.13	0.96	0.11	0.87	0.12	1.19	0.16	0.89
Case 8	0.15	0.94	0.13	0.97	0.11	0.79	0.11	1.00	0.15	0.93
% Reduction	-5	0	3	-1	5	8	11	16	6	-5
Horizontal Story Drift										
CM-3	-	-	-	-	0.24	1.00	0.17	0.92	0.14	0.87
Case 8	-	-	-	-	0.63	2.59	0.30	1.39	0.12	1.05
% Reduction	-	-	-	-	-157	-160	-79	-51	13	-21
Arias Intensity (m/sec)										
CM-3	4.31		3.58		2.71		2.98		5.29	
Case 8	4.72		3.35		2.43		2.38		4.71	
% Reduction	-9		6		10		20		11	
Peak Spectral Acceleration (g)										
CM-3	-		3.10		2.83		4.37		2.64	
Case 8	-		3.20		3.04		3.83		2.57	
% Reduction	-		-3		-7		13		2	
Period Lengthening Ratio										
CM-3	-		0.16		0.06		0.05		0.04	
Case 8	-		0.16		0.06		0.05		0.05	
Period Length. Ratio	-		1.00		0.92		1.00		1.43	
Base Shear (kN)      Base Moment (kN.m)										
	RMS		Peak		RMS		Peak			
CM-3	0.39		3.66		0.18		1.60			
Case 8	0.38		3.56		0.17		1.49			
% Reduction	3		3		4		7			

The typical slips that occurred near the edges of GSI materials appearing at ground level after the severe ground motions are shown in Figure 4.31.



Figure 4.31. Typical Slips Occurred After Severe Ground Motions.

## 5. PARAMETRIC STUDY

Effects of the number of the story, GSI material type, GSI depth (H/D ratio), and ground motion characteristic on effectiveness and robustness of the proposed GSI system were investigated with shaking table experiments. The % reduction of RMS and peak values of the top floor acceleration, foundation acceleration, top floor drift, first-floor drift, base shear, base moment, top floor Arias intensity, and foundation Arias intensity were selected as the eight main performance indicator parameters to evaluate the experiments results. % reduction parameters computed based on unisolated condition. The created eight different cases agitated and results of the cases examined under the % reduction of eight main performance indicator parameters. To achieve optimal condition, in which proposed GSI system performs better among the cases, the obtained results under earthquake records with original PGA and cyclic sinusoidal motion with first mode frequency of the building model were tabulated. Then, earthquake motions with scaled peak accelerations and cyclic sinusoidal motions with various frequencies versus eight different performance indicator parameters were graphed to evaluate the effect of different dynamic motion characteristic (both peak acceleration and frequency content) on the effectiveness of proposed GSI system.

### 5.1. Seismic Response of the Cases under Earthquake Motions with Real PGA and Cyclic Sinusoidal Motion with First Mode Frequency of the Building Model

It can be seen in Table 5.1 that Case 1 show better seismic performance under Kocaeli earthquake rather than El Centro and Kobe earthquake motions. Furthermore, cyclic sinusoidal motion with 11.7 Hz frequency, which coincides with the first mode frequency of the 5-story building model, was more effective than the earthquake motions.

Table 5.1. % Reduction of Selected Performance Indicator Parameters of Case 1.

Case 1								
Performance Indicator Parameters	Ground Motions							
	Kocaeli		El Centro		Kobe		Cyclic Sinusoidal	
	Earthquake		Earthquake		Earthquake		Motion 11.7 Hz	
% Reduction (%)								
	RMS	Peak	RMS	Peak	RMS	Peak	RMS	Peak
Top Floor Acceleration	30	26	20	9	4	15	11	18
Foundation Acceleration	12	28	-11	-8	5	4	22	4
Top Floor Drift	-2	-28	0	-6	-1	-15	20	34
First Floor Drift	17	16	29	7	5	6	35	43
Base Shear	29	26	25	5	8	14	11	16
Base Moment	38	22	28	33	11	10	12	17
Top Floor Arias Intensity	51		36		9		21	
Foundation Arias Intensity	23		-24		9		39	

Table 5.2 indicates that Case 2 made better mitigation of seismic effects under El Centro earthquake among the other earthquake motions. Cyclic sinusoidal motion with 11.7 Hz gave better reductions comparing the given earthquake motions. On the other hand, if Case 1 is compared to Case 2 regarding the mitigation of seismic effects, Case 2 seems better according to these results. This means 15 cm ( $H/D = 6.7$ ) GSI depth is preferable rather than 10 cm ( $H/D = 10$ ) GSI depth under given earthquakes and 11.7 Hz cyclic sinusoidal motion.

Table 5.2. % Reduction of Selected Performance Indicator Parameters of Case 2.

Case 2								
Performance Indicator Parameters	Ground Motions							
	Kocaeli		El Centro		Kobe		Cyclic Sinusoidal	
	Earthquake		Earthquake		Earthquake		Motion 11.7 Hz	
% Reduction (%)								
	RMS	Peak	RMS	Peak	RMS	Peak	RMS	Peak
Top Floor Acceleration	-3	-5	28	16	3	10	-2	0
Foundation Acceleration	5	6	19	16	11	-7	10	11
Top Floor Drift	17	19	0	-3	36	-5	15	25
First Floor Drift	20	36	48	31	36	0	49	54
Base Shear	-4	-1	32	20	-1	3	-2	1
Base Moment	-4	-4	19	21	-4	4	-1	2
Top Floor Arias Intensity	-6		48		7		-4	
Foundation Arias Intensity	9		35		21		18	

It can be observed from Table 5.3 that Case 3 showed better performance under El Centro earthquake motion. Cyclic sinusoidal motion with 11.7 Hz was much better than the earthquake motions in terms of the mitigation of seismic effects. GSI 1 seems more feasible than GSI 2 comparing the results of Case 1 and Case 3 under given

earthquakes and cyclic sinusoidal motion (11.7 Hz).

Table 5.3. % Reduction of Selected Performance Indicator Parameters of Case 3.

Case 3								
Performance Indicator Parameters	Ground Motions							
	Kocaeli		El Centro		Kobe		Cyclic Sinusoidal	
	Earthquake		Earthquake		Earthquake		Motion 11.7 Hz	
% Reduction (%)								
	RMS	Peak	RMS	Peak	RMS	Peak	RMS	Peak
Top Floor Acceleration	-2	10	2	-20	0	13	31	34
Foundation Acceleration	6	7	9	7	11	-18	27	18
Top Floor Drift	-46	-24	-20	-38	11	-6	48	52
First Floor Drift	29	36	32	20	-24	-30	57	57
Base Shear	-1	11	2	2	-2	2	29	30
Base Moment	-2	-3	-1	-13	-7	9	27	27
Top Floor Arias Intensity	-3		3		0		52	
Foundation Arias Intensity	12		16		22		47	

As can be observed in Table 5.4, Kocaeli earthquake motion gave better results for Case 4 rather than other earthquake motions in terms of mitigation of seismic effects. However, greater reductions were obtained under Cyclic sinusoidal motion with 11.7 Hz comparing the given earthquake motions. Case 3 that has 10 cm GSI depth ( $H/D = 10$ ) seemed more attainable than Case 4 that has 15 cm GSI depth ( $H/D = 6.7$ ) after comparing experiment results of Case 4 with Case 3. Moreover, Case 2 that is comprised with GSI 1 was more practicable than the Case 4 that is comprised with GSI 2. In brief, 10 cm GSI depth ( $H/D = 10$ ) was more auspicious than 15 cm GSI depth ( $H/D = 6.7$ ) in terms of  $H/D$  ratio and considering GSI material type GSI 1 was more beneficial than the GSI 2.

Table 5.4. % Reduction of Selected Performance Indicator Parameters of Case 4.

Case 4								
Performance Indicator Parameters	Ground Motions							
	Kocaeli		El Centro		Kobe		Cyclic Sinusoidal	
	Earthquake		Earthquake		Earthquake		Motion 11.7 Hz	
% Reduction (%)								
	RMS	Peak	RMS	Peak	RMS	Peak	RMS	Peak
Top Floor Acceleration	19	22	9	4	8	22	18	26
Foundation Acceleration	10	7	-4	-14	7	-18	19	16
Top Floor Drift	-42	-77	-192	-157	8	5	14	24
First Floor Drift	33	23	41	24	-34	-10	47	45
Base Shear	19	22	12	-9	5	17	16	21
Base Moment	22	21	12	13	9	17	13	16
Top Floor Arias Intensity	34		18		16		32	
Foundation Arias Intensity	19		-8		14		34	

Table 5.5 indicates that Kocaeli earthquake motion showed better reduction among the other earthquakes regarding seismic effects. Cyclic sinusoidal motions with 11.7 Hz was beneficial as much as the Kocaeli earthquake motion. GSI 3 was the most felicitous GSI material type among the other materials in compliance with the seismic effects mitigation of the Case 1, Case 3, and Case 5.

Table 5.5. % Reduction of Selected Performance Indicator Parameters of Case 5.

Case 5								
Performance Indicator Parameters	Ground Motions							
	Kocaeli		El Centro		Kobe		Cyclic Sinusoidal	
	Earthquake		Earthquake		Earthquake		Motion 11.7 Hz	
% Reduction (%)								
	RMS	Peak	RMS	Peak	RMS	Peak	RMS	Peak
Top Floor Acceleration	22	29	9	5	13	23	29	34
Foundation Acceleration	23	23	14	8	18	16	26	11
Top Floor Drift	-8	-21	-18	-49	-36	-25	43	42
First Floor Drift	35	34	14	7	10	18	13	29
Base Shear	23	33	9	27	11	16	28	32
Base Moment	15	13	-2	-1	5	14	27	30
Top Floor Arias Intensity	38		16		24		50	
Foundation Arias Intensity	40		27		33		45	

It can be seen in Table 5.6 that Case 6 showed better mitigation of the seismic effects under Kobe earthquake motion compare to other given earthquakes but, cyclic sinusoidal motion with 11.7 Hz was relatively practicable than the earthquake motions. 10 cm GSI depth ( $H/D = 10$ ) was more feasible when comparing the Case 5 which has 10 GSI depth cm ( $H/D = 10$ ) with Case 6 which has 15 cm ( $H/D = 6.7$ ) GSI depth. Moreover, GSI 1 seemed the most viable GSI material among the other GSI materials comparing the seismic effects mitigation amount of the Case 2, Case 4, and Case 6.

Table 5.6. % Reduction of Selected Performance Indicator Parameters of Case 6.

Case 6								
Performance Indicator Parameters	Ground Motions							
	Kocaeli		El Centro		Kobe		Cyclic Sinusoidal	
	Earthquake		Earthquake		Earthquake		Motion 11.7 Hz	
% Reduction (%)								
	RMS	Peak	RMS	Peak	RMS	Peak	RMS	Peak
Top Floor Acceleration	-5	2	0	-11	8	9	9	17
Foundation Acceleration	1	-4	10	7	13	5	10	8
Top Floor Drift	-5	0	-47	-38	19	-5	12	19
First Floor Drift	22	14	28	5	-76	-19	30	37
Base Shear	-4	3	0	11	6	10	8	14
Base Moment	-4	-6	-6	-12	3	14	6	12
Top Floor Arias Intensity	-10		-1		16		18	
Foundation Arias Intensity	2		19		24		20	

Figure 5.7 represents that Case 7 made better mitigation of seismic effects under Kocaeli earthquake motion compare to other given earthquake motions. Comparing the Case 3, which has same experimental parameters except story number of the building model, with Case 7, 5-story building model seems more feasible to proposed GSI system.

Table 5.7. % Reduction of Selected Performance Indicator Parameters of Case 7.

Case 7								
Performance Indicator Parameters	Ground Motions							
	Kocaeli		El Centro		Kobe		Cyclic Sinusoidal	
	Earthquake		Earthquake		Earthquake		Motion 11.7 Hz	
% Reduction (%)								
	RMS	Peak	RMS	Peak	RMS	Peak	RMS	Peak
Top Floor Acceleration	-24	-19	-13	-19	0	-6	-3	3
Foundation Acceleration	-2	-13	3	2	4	1	-1	-10
Top Floor Drift	68	82	28	27	-72	-8	17	16
First Floor Drift	45	83	-8	7	-12	-49	29	0
Base Shear	-27	-17	-20	-6	-4	19	-3	3
Base Moment	-26	-22	-19	-17	-5	23	-3	5
Top Floor Arias Intensity	-53		-29		0		-8	
Foundation Arias Intensity	-5		5		7		-4	

As can be observed in Table 5.8, Kocaeli earthquake was more effective than other earthquake records for Case 8 considering mitigation of seismic effects. 5-story building model was feasible than the 3-story building model considering the comparison that was made between the Case 4 and Case 8. Furthermore, 10 cm GSI depth ( $H/D = 10$ ) that was used in Case 7 was more beneficial for the proposed GSI system when comparing Case 8 which has 15 cm GSI depth ( $H/D = 6.7$ ).

Table 5.8. % Reduction of Selected Performance Indicator Parameters of Case 8.

Case 8								
Performance Indicator Parameters	Ground Motions							
	Kocaeli		El Centro		Kobe		Cyclic Sinusoidal	
	Earthquake		Earthquake		Earthquake		Motion 11.7 Hz	
% Reduction (%)								
	RMS	Peak	RMS	Peak	RMS	Peak	RMS	Peak
Top Floor Acceleration	-11	-16	-3	-11	6	-5	6	4
Foundation Acceleration	6	-5	3	6	3	-1	6	10
Top Floor Drift	39	81	35	49	13	-21	8	5
First Floor Drift	17	75	-35	-40	-157	-160	11	-46
Base Shear	-12	2	-5	2	3	3	6	6
Base Moment	-12	-1	-4	-1	4	7	5	7
Top Floor Arias Intensity	-24		-6		11		12	
Foundation Arias Intensity	12		5		6		11	

## 5.2. Effects of the Proposed GSI System on Performance Indicator Parameters under Earthquake Motions with Increasing PGA and Cyclic Sinusoidal Motion with Various Frequencies

In order to notice the effectiveness of proposed GSI system, eight performance indicator parameters were investigated one by one under different dynamic input characteristic including different peak accelerations of earthquake records and different frequencies of the cyclic sinusoidal motion. The % reduction values of the performance indicator parameters were graphed with using different scaled peak acceleration for earthquakes and varying frequencies for cyclic sinusoidal motion. By this way, effects of amplitude and frequency of the seismic input motions on the effectiveness of the proposed GSI system were evaluated.

### 5.2.1. Effects of Proposed GSI System on Top Floor Acceleration

Figure 5.1 illustrates the variations of the top floor acceleration due to the application of proposed GSI system. It can be observed from Figure 5.1a that except from Case 1, Case 4, and Case 5 proposed GSI system behaved better under the higher acceleration amplitude of Kocaeli earthquake motion. Especially Case 7 and Case 8 that have 3-story building model were not beneficial under lower acceleration amplitude of Kocaeli earthquake motion. Case 5 is the most efficient case among the other cases under different acceleration amplitudes of Kocaeli earthquake motion. Figure 5.1b illustrates that almost all cases reacted better in the amplitude range between 0.7g and 0.8g of El Centro earthquake motion. Case 2 and Case 3 functioned better under the higher acceleration amplitude, but the other cases functioned better under the lower acceleration amplitude of Kobe earthquake motion as seen in the Figure 5.1c. During the experiments, any top floor acceleration reduction was not observed regarding Case 7 under Kobe earthquake motion. Between 10-15 Hz that are the close vicinity of the natural frequency of the 5-story building model, proposed system served well under cyclic sinusoidal motion comparing the other frequencies as shown in the Figure 5.1d. Case 5 was the most beneficial case under seismic motions.

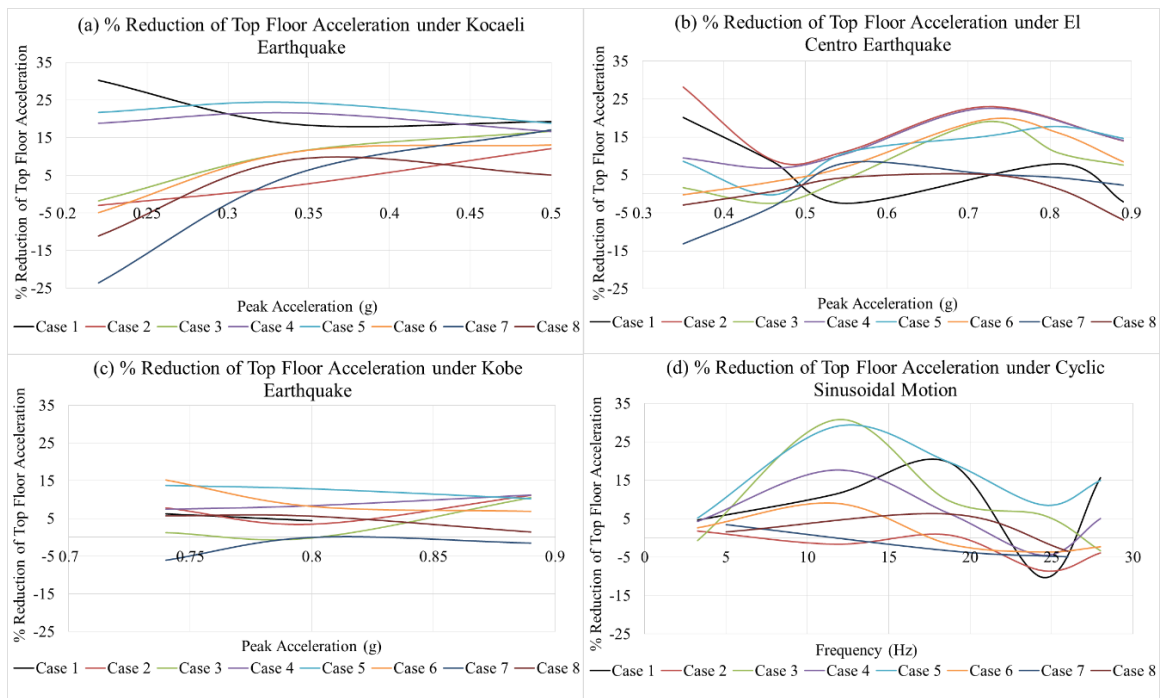


Figure 5.1. % Reduction of Top Floor Acceleration under (a) Kocaeli Earthquake, (b) El Centro Earthquake, (c) Kobe Earthquake Records with the Increasing Peak Acceleration, and (d) Cyclic Sinusoidal Motion with the Increasing Frequency.

### 5.2.2. Effects of Proposed GSI System on Foundation Acceleration

Figure 5.2 represents the changings of foundation acceleration as a result of the application proposed GSI system. Especially Case 7 and Case 8 that have 3-story building model performed better under the higher acceleration amplitude of Kocaeli earthquake motion as seen in the Figure 5.2a. The other cases that have 5-story building model were ineffective under higher acceleration amplitude of Kocaeli earthquake motion. Case 5 was the most efficient case among the other cases under different acceleration amplitudes of Kocaeli earthquake motion. Case 1 was ineffective under low acceleration amplitude of El Centro earthquake motion. Figure 5.2b represents that after 0.8g, the % reduction of proposed GSI system decreased for El Centro earthquake motion. There was downtrend with the increasing acceleration amplitude of Kobe earthquake motion that is clearly seen in Figure 5.2c. It can be observed from Figure 5.2d that between 10-15 Hz that are close to the natural frequency of the 5-story building model, proposed system acted well under cyclic sinusoidal motion comparing

the other frequencies. Case 1 and Case 5 were the most felicitous cases under cyclic sinusoidal motion. Case 7 and Case 8 that have 3-story building model with the 18.68 Hz natural frequency behaved better under higher frequencies of cyclic sinusoidal motion.

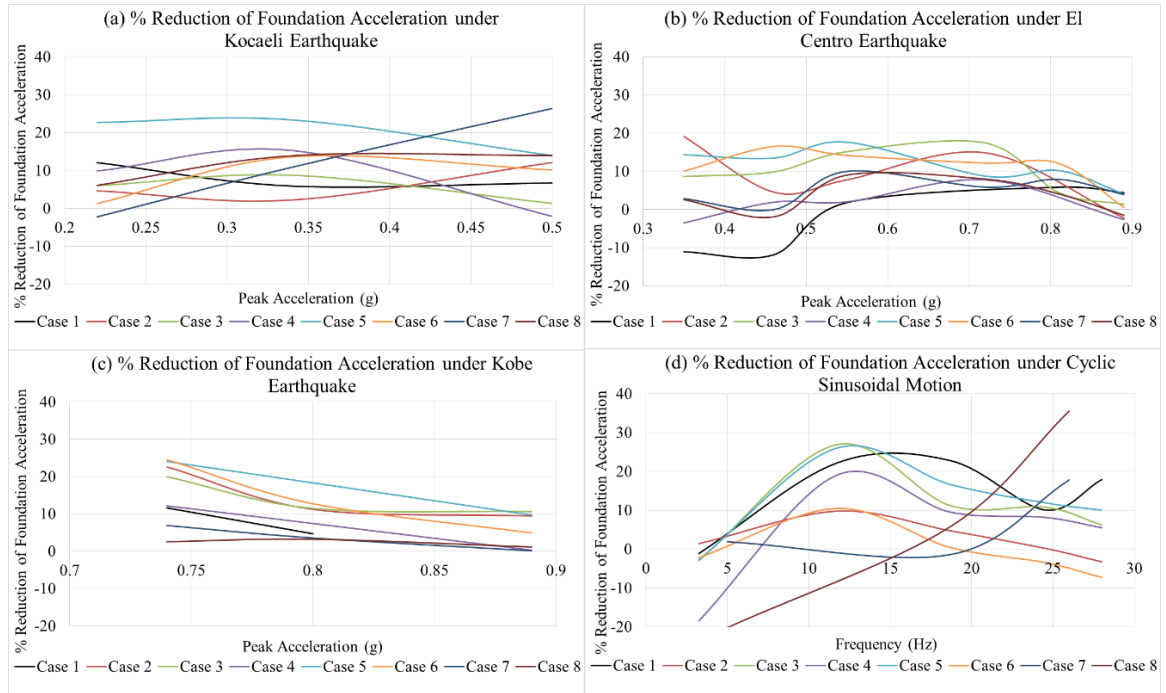


Figure 5.2. % Reduction of Foundation Acceleration under (a) Kocaeli Earthquake, (b) El Centro Earthquake, (c) Kobe Earthquake Records with the Increasing Peak Acceleration, and (d) Cyclic Sinusoidal Motion with the Increasing Frequency.

### 5.2.3. Effects of Proposed GSI System on Top Floor Drift

Variations of top floor drift owing to application of proposed GSI system are shown in Figure 5.3. As can be observed in Figure 5.3a, especially Case 7 and Case 8 that have 3-story building model functioned better under the higher acceleration amplitude of Kocaeli earthquake motion. Case 5 was completely ineffective under all acceleration amplitudes of Kocaeli earthquake motion. Additional slip displacements can be the reason of this. Especially, the cases having lower friction coefficient between geosynthetic couples may be subjected to more story drift at the top floor. Like Case 5, Case 4 and Case 3 were ineffective under lower acceleration amplitude of Kocaeli earthquake motion. Case 8 was the most viable case under El Centro earthquake motion. Figure 5.3b illustrates that after 0.8g the % reduction values were decreased

under El Centro earthquake motion. Case 1 and Case 4 were ineffective under El Centro earthquake motion. There was downtrend with the increasing acceleration amplitude of Kobe earthquake motion that is presented in Figure 5.3c. Case 4, Case 5, and Case 6 did not react under higher acceleration amplitude of the Kobe earthquake motion. Between 10-15 Hz, proposed GSI system was performed well under cyclic sinusoidal motion comparing the other frequencies as seen in Figure 5.3d. Case 3 and Case 5 were the most beneficial cases under cyclic sinusoidal motion.

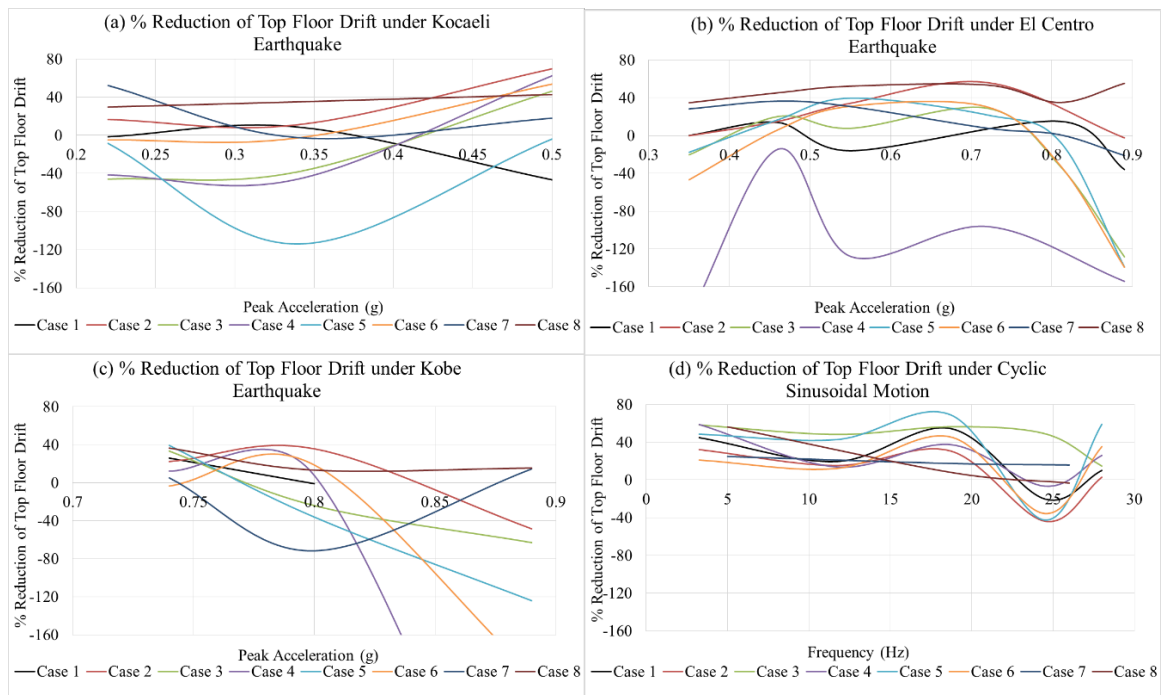


Figure 5.3. % Reduction of Top Floor Drift under (a) Kocaeli Earthquake, (b) El Centro Earthquake, (c) Kobe Earthquake Records with the Increasing Peak Acceleration, and (d) Cyclic Sinusoidal Motion with the Increasing Frequency.

#### 5.2.4. Effects of Proposed GSI System on First-Floor Drift

Figure 5.4 indicates the variations of the first-floor drift because of the application of proposed GSI system. Case 2 and Case 4 served slightly better under the higher acceleration amplitude of Kocaeli earthquake motion as seen in the Figure 5.4a. Case 3, Case 6 and Case 8 did not function around the 0.35g of the Kocaeli earthquake motion. In contrast to other cases, Effectiveness of the Case 1 was reduced with the increasing acceleration amplitude of Kocaeli earthquake motion. Figure 5.4b shows

that Case 4, Case 7, and Case 8 were ineffective under El Centro earthquake motion. Except Case 7 and Case 8, there was a slight increase in reduction of first-floor drifts with the increasing acceleration amplitude of El Centro earthquake motion. Case 2 and Case 3 reacted better when comparing with the other cases under El Centro earthquake motion. It can be observed from Figure 5.4c that except from Case 2 and Case 5, proposed GSI system had no beneficial effect into the reduction of the first-floor drift under Kobe earthquake motion. The most suitable case was Case 5 under Kobe earthquake motion. Figure 5.4d represents that until 15 Hz, proposed system mostly performed well under cyclic sinusoidal motion comparing the other frequencies.

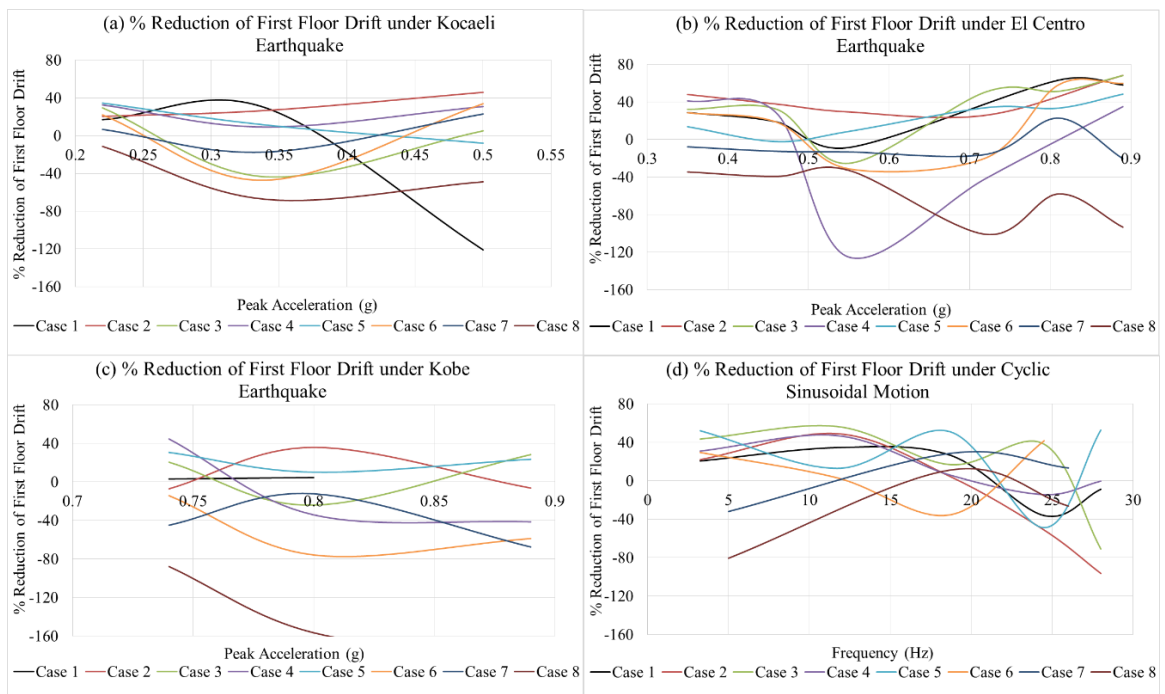


Figure 5.4. % Reduction of First Floor Drift under (a) Kocaeli Earthquake, (b) El Centro Earthquake, (c) Kobe Earthquake Records with the Increasing Peak Acceleration, and (d) Cyclic Sinusoidal Motion with the Increasing Frequency.

### 5.2.5. Effects of Proposed GSI System on Base Shear

Variations of base shear as a result of the application of proposed GSI system are presented in Figure 5.5. Proposed GSI system functioned better at the higher acceleration amplitude of Kocaeli earthquake motion as seen in the Figure 5.5a. Case 7 and

Case 8 that have 3-story building model did not work proper under lower acceleration amplitudes of Kocaeli earthquake motion. Case 1, Case 4, and Case 5 were the most feasible cases among the other cases under different acceleration amplitudes of Kocaeli earthquake motion. Figure 5.5b illustrates that Case 2 was the most appropriate case among the other cases under El Centro earthquake motion. Case 1, Case 7, and Case 8 had low performance when comparing with the other cases under El Centro earthquake motion. It can be observed from Figure 5.5c that Case 5 performed better than the other cases. In addition, Case 7 did not function under Kobe earthquake motion. Case 2 and Case 3 were beneficial under higher acceleration amplitude of the Kobe earthquake motion. Between 10-15 Hz, Case 3, Case 4, and Case 5 were felicitous under cyclic sinusoidal motion comparing the other frequencies (Figure 5.5d). Case 5 was the most suitable cases under cyclic sinusoidal motion.

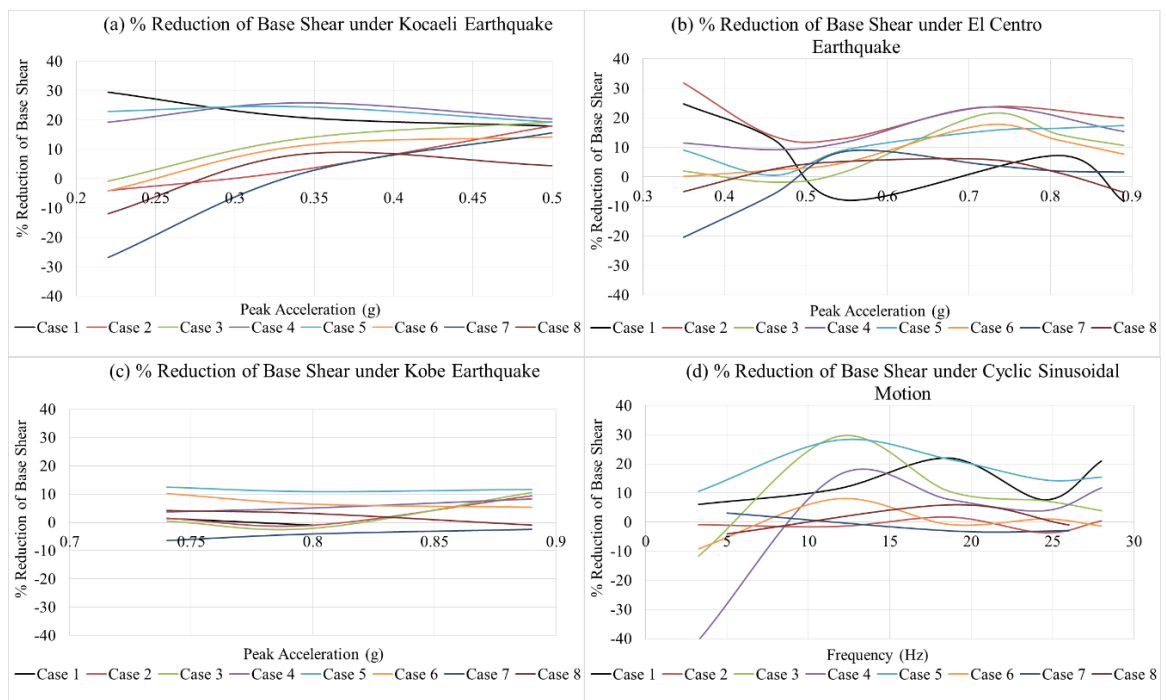


Figure 5.5. % Reduction of Base Shear under (a) Kocaeli Earthquake, (b) El Centro Earthquake, (c) Kobe Earthquake Records with the Increasing Peak Acceleration, and (d) Cyclic Sinusoidal Motion with the Increasing Frequency.

### 5.2.6. Effects of Proposed GSI System on Base Moment

Figure 5.6 illustrates the changings of the base moment due to the application of proposed GSI system. Case 7 and Case 8 that are created with 3-story building model, functioned better at the higher acceleration amplitude of Kocaeli earthquake motion as seen in Figure 5.6a. On the contrary, Case 7 and Case 8 were not viable under lower acceleration amplitudes of Kocaeli earthquake motion. Case 1 and Case 4 were the most beneficial cases among the other cases under different acceleration amplitudes of Kocaeli earthquake motion. Figure 5.6b shows that Case 4 was the most suitable case among the other cases under El Centro and Kobe earthquake motions. Case 1, Case 2, Case 3, and Case 7 did not perform well under lower acceleration amplitude of the Kobe earthquake motion as seen in Figure 5.6c. Between 10-15 Hz, Case 3, Case 4, and Case 5 behaved better under cyclic sinusoidal motion compare to other frequencies (Figure 5.6d). Case 5 were the most beneficial case under cyclic sinusoidal motion. Case 7 became ineffective to effective after 20 Hz that is the close vicinity of the natural frequency of the 3-story building model.

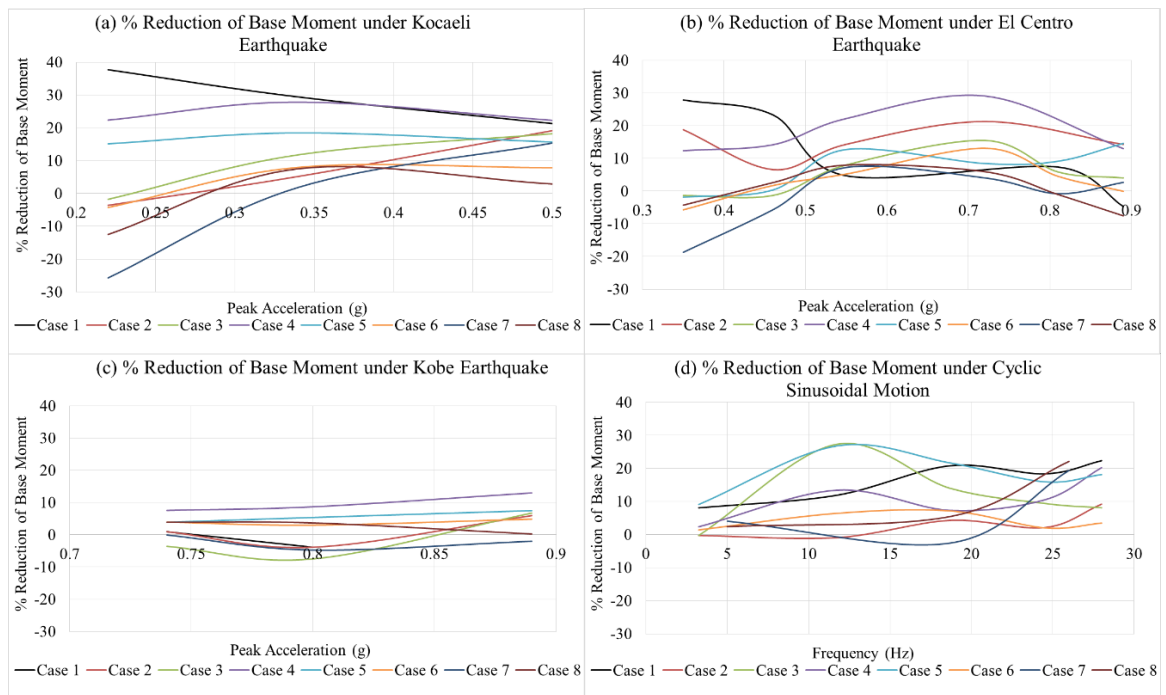


Figure 5.6. % Reduction of Base Moment under (a) Kocaeli Earthquake, (b) El Centro Earthquake, (c) Kobe Earthquake Records with the Increasing Peak Acceleration, and (d) Cyclic Sinusoidal Motion with the Increasing Frequency.

### 5.2.7. Effects of Proposed GSI System on Top Floor Arias Intensity

Variations of the top floor Arias intensity because of application of proposed GSI system are shown in Figure 5.7. As can be observed in Figure 5.7a, except from Case 1, Case 4, and Case 5, proposed GSI system acted better under the higher acceleration amplitude of Kocaeli earthquake motion. Especially Case 7 and Case 8 that have 3-story building model were ineffective under lower acceleration amplitude of Kocaeli earthquake motion. Case 5 was the most efficient case among the other cases under different acceleration amplitudes of Kocaeli earthquake motion. Almost all cases performed better near the 0.7g amplitude of El Centro earthquake motion (Figure 5.7b). Case 2 and Case 3 behaved better under the higher acceleration amplitude of Kobe earthquake motion, but the other cases performed better under the lower acceleration amplitude of Kobe earthquake motion as seen in the Figure 5.7c. According to the experiments results, any top floor acceleration reduction of Case 7 was not observed under Kobe earthquake motion. It can be observed from Figure 5.7d that between 10-15 Hz that are the close vicinity of the natural frequency of the 5-story building model proposed system acted well under cyclic sinusoidal motion comparing with the other frequencies. Case 5 was the most suitable option under almost all seismic motions.

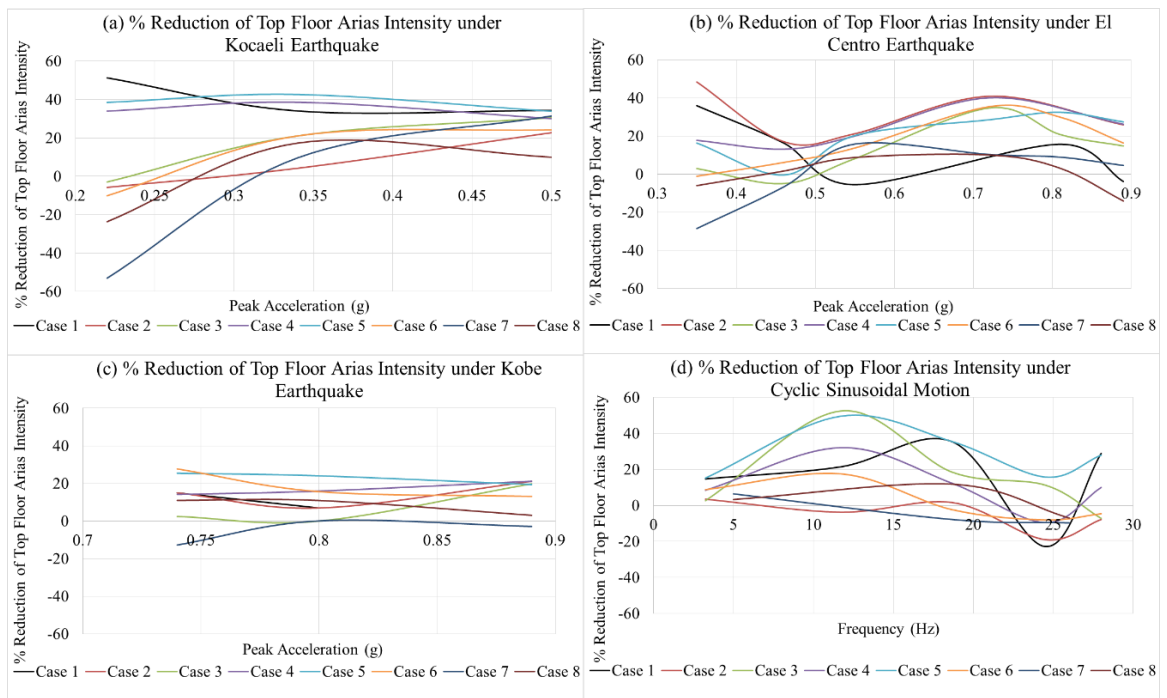


Figure 5.7. % Reduction of Top Floor Arias Intensity under (a) Kocaeli Earthquake, (b) El Centro Earthquake, (c) Kobe Earthquake Records with the Increasing Peak Acceleration, and (d) Cyclic Sinusoidal Motion with the Increasing Frequency.

### 5.2.8. Effects of Proposed GSI System on Foundation Arias Intensity

Figure 5.8 shows the changings of foundation Arias intensity owing to application of proposed GSI system. Especially Case 7 and Case 8 that have 3-story building model functioned better under the higher acceleration amplitude of Kocaeli earthquake motion as seen in the Figure 5.8a. The other cases that have 3-story building model were less feasible under higher acceleration amplitude of Kocaeli earthquake motion. Case 5 was the most efficient case among the other cases under different acceleration amplitudes of Kocaeli earthquake motion. Figure 5.8b illustrates that Case 1 was ineffective under low acceleration amplitude of El Centro earthquake motion. According to experimental data, after 0.8g, reduction of foundation Arias intensity values were decreased under El Centro earthquake motion. There was downtrend, which is presented in Figure 5.8c, with the increasing acceleration amplitude of Kobe earthquake motion. The most beneficial case was Case 5 under Kobe earthquake motion. Between 10-15 Hz, proposed GSI system performed well under cyclic sinusoidal motion comparing the

other frequencies as seen in Figure 5.8d. Case 3 and Case 5 were the most viable cases under cyclic sinusoidal motion. Case 7 and Case 8 that have 3-story building model reacted better under higher frequencies after 15 Hz.

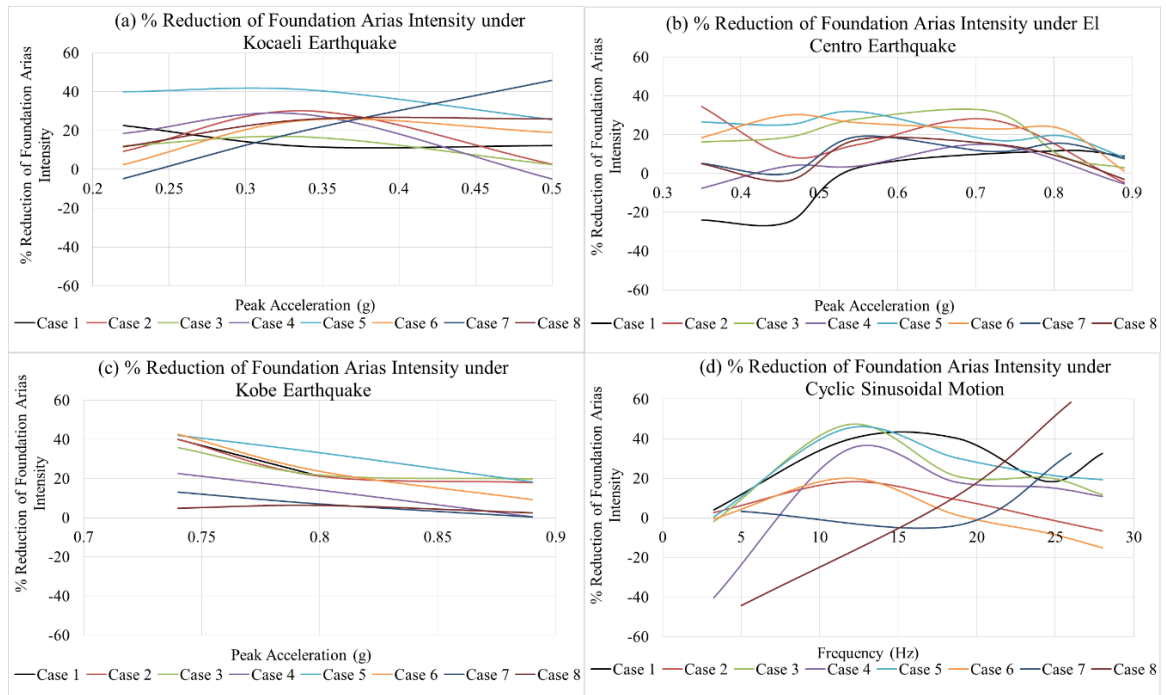


Figure 5.8. % Reduction of Foundation Arias Intensity under (a) Kocaeli Earthquake, (b) El Centro Earthquake, (c) Kobe Earthquake Records with the Increasing Peak Acceleration, and (d) Cyclic Sinusoidal Motion with the Increasing Frequency.

## 6. SUMMARY AND CONCLUSIONS

### 6.1. Summary

In this study, it was aimed to evaluate the behavior and effectiveness of an easily applicable, low-cost alternative seismic isolation system that is called as a geotechnical seismic isolation (GSI) with geosynthetics. The concept of the GSI with geosynthetics can be described as; the geosynthetics placed in a cylindrical shape penetrating the soil profile will dissipate seismic energy through slip displacements, thus transmitting significantly reduced seismic motions to the overlying isolated soil layer and any structure founded on. A nonwoven geotextile over a polytetrafluorethylene geomembrane sheet (geotextile/ PTFE) was found to be well suited for this purpose of GSI from rigid block experiments. The effect of this alternative seismic isolation system on model structures was investigated through shaking table tests both under cyclic sinusoidal and earthquake motions. For this purpose, the flexible sided laminar soil container suitable for the shaking table at Boğaziçi University was designed, manufactured, and tested to verify performance criteria, to simulate the field conditions in the laboratory environment. Then, two models representing 3-storey and 5-story buildings were constructed to measure the dynamic response of the low-rise and mid-rise buildings with proposed GSI system. Accelerations and displacements at each story level were measured during the shaking table experiments. Series of shaking table experiments that covered performance tests of the laminar box, rigid block tests to obtain dynamic properties of the geosynthetics and experiments of proposed GSI system were performed during this research. The 164 of them were used to create the cases and evaluate the proposed GSI system. The eight cases have been established by using both earthquake and cyclic sinusoidal motions. Three different earthquake motions as El Centro (Array #9 station), Kobe (KJMA station), and Kocaeli (Izmit station) with the varying amplitudes ranging from 0.22g to 0.89g were applied to the proposed GSI system. Moreover, cyclic sinusoidal motions with the different frequencies that were obtained from the free vibration test of the building models applied to the proposed GSI system. The effects of the number of the story of the building, GSI depth (H/D ratio), GSI type and ground

motion characteristic on the proposed GSI system were investigated. The conclusions based on the results of conducted experiments are presented in the following part of this section.

## 6.2. Conclusions

The main findings of this study based on the performed experiments can be summarized as follows:

- The application of the proposed GSI system had a rather beneficial effect on the seismic performance of the 3-story and especially 5-story scaled building models. Compared to the 3-story building model, 5-story building model would be more beneficial for the proposed GSI system regarding the experimental results. Lower base shear and base moment values of 3-story building model triggered by the slip displacement could be the reason for not performing well.
- According to performed rigid block experiments, GSI 2 was determined as the most suitable GSI material because of having a lower friction coefficient that leads to larger slip displacement. Yet, the friction coefficient of the GSI 3 was very close to that of GSI 2. On the other hand, results of the proposed GSI system experiments revealed that GSI 3 was the most effective GSI material in terms of acceleration reduction among the other geosynthetic couples that were located 10 cm ( $H/D = 10$ ) underneath the foundation. Moreover, this situation was not acceptable for the cases that had 15 cm GSI depth ( $H/D = 6.7$ ) underneath the foundation. For the cases with 15 cm GSI depth ( $H/D = 6.7$ ), GSI 2 was generally the most suitable type. The distinction relating the GSI depth ( $H/D$  ratio) and GSI type could be associated with the friction coefficient of the GSI material. As the GSI layer is placed deeper with the increasing curvature, the activated soil mass becomes bigger. Due to the bigger isolated soil mass with higher curvature, GSI materials with lower friction coefficients generated less friction forces during the slip. That is why, the GSI materials with lower friction coefficients are prone to transmit less acceleration to the structure through slip displacements under higher GSI depth with higher curvature. In addition to these

findings, the comparisons between the results of rigid block tests and the shaking table experiments with the proposed GSI system revealed that rigid block tests could not reflect the behavior of the GSI system as located in the soil. That is why soil structure behavior should not be underestimated.

- The frequency content of seismic motions strongly affects the seismic response characteristics of a structure. When the frequency content of the ground motion and the natural frequencies of the structure coincide with each other or are close to each other, ground motion is amplified more significantly in a structure. On the other hand, reduction in transmitted accelerations for an isolated structure with the proposed GSI system is highly dependent on the frequency of the ground motion and the natural frequency of the structure. As can be observed from the given results above, the proposed GSI system was the most efficient under cyclic sinusoidal motions with frequencies close to the natural frequency of the structure. In other words, the maximum reductions in measured accelerations were obtained when the ground motion frequency is in the close vicinity of the natural frequency of the structure. This indicates that the proposed GSI system is vitally beneficial when the most destructive damage was expected for the structure.
- It can be observed that when the ground motion frequency exceeds approximately twice of the natural frequency of the structure, proposed GSI system did not provide any improvement.
- Unlike the situation in the cyclic sinusoidal motions, under the earthquake motions, the proposed GSI system was triggered regardless of the seismic motion frequency. Seismic improvement of the proposed GSI system was rather slight under Kobe earthquake motion because of having a long duration and quite high spectral values. In general, proposed GSI system was not beneficial under higher acceleration amplitudes of earthquake motions, such as after 0.8g, because permanent slip displacements may occur exceeding those acceleration amplitudes.
- Proposed GSI system did not change the mode of vibration or the displacement profile of the isolated structure but successfully decreased the magnitudes of acceleration amplitude and displacement for low-rise and mid-rise buildings.
- The spectral accelerations were reduced in general when the proposed GSI system was utilized. In other words, damping of the system was increased. Unlike for the

conventional seismic isolation systems, the spectral accelerations obtained using the proposed GSI system drop significantly at the natural period of the 5-story building model whereas the natural periods of the same building model was not shifted.

- The transmitted top, foundation and in-soil accelerations of the building models can be substantially decreased up to 30%, 36%, and 32%, respectively, and the top and first-floor story drifts can be significantly reduced up to 70% and 68% with the help of proposed GSI system. Similar to the acceleration reduction, the proposed GSI system increased the effectiveness through decreasing inter-story drifts when the ground motion frequencies come close to the natural frequency of the structure. The rest of the performance indicator parameters that are base shear, base moment, top floor Arias intensity, and foundation Arias intensity were reduced up to 32%, 38%, 52%, and 58%, respectively.
- In general, the seismic response improvement in the midpoint of the isolated soil region showed consistency with the foundation response.

As a conclusion, overall experimental studies showed that the proposed GSI system works efficiently under the considered seismic motions. Mitigation of seismic effects can be obtained on low-rise and mid-rise buildings for developing countries by using the GSI with geosynthetics.

### **6.3. Recommendations for Future Studies**

- For the proposed GSI system to be implemented in practice, further research is required in the manufacturing and installation of the geosynthetics, the effects of multidirectional shaking, the impact of environmental conditions on the geosynthetics, the long-term performance of the geosynthetics under creep and geosynthetics deformations induced by soil settlement, soil type, compaction level of soil, and development of an analytical tool for the evaluation of a 3-dimensional GSI system under seismic excitations.
- Experiments with the 3-story building model were performed in order to see whether the number of stories affects the proposed GSI system behavior or not.

The detailed investigations on proposed GSI system should be conducted for different sizes of the buildings such as 2, 4 and 6-story buildings to better understand the effect of the proposed GSI system on low-rise and mid-rise buildings.

- The proposed GSI system exhibited the effectiveness against applied earthquakes but its dependence on earthquake type needs to be addressed.
- Considering the size of the isolated soil region, slips observed near the edges of GSI materials forming at ground level can influence the safety of a structure founded near the isolated region. Nevertheless, in the design phase, the effects of slip deformations near the edges of the isolated region should be included.

## APPENDIX A: PROPERTIES OF THE UTILIZED GEOSYNTHETICS

Table A.1. Properties of the Nonwoven Geotextiles.

Dupont Typar				
Property	Standard	Unit	SF44	SF56
Descriptive properties				
Area weight	EN ISO 9864	g/m <sup>2</sup>	150	190
Thickness under 2 kN/m <sup>2</sup>	EN ISO 9863-1	mm	0.48	0.57
Thickness under 200 kN/m <sup>2</sup>	EN ISO 9863-1	mm	0.4	0.48
Mechanical properties				
Energy Absorbtion	EN ISO 10319	kJ/m <sup>2</sup>	4.5	5.8
Tensile Strength	EN ISO 10319	KN/m	10.3	13.1
Elongation	EN ISO 10319	%	52	52
Tensile Strength at %5	EN ISO 10319	kN/m	4.5	5.7
Puncture CBR	EN ISO 12236	N	1575	1850
Dynamic Cone Puncture	EN ISO 13433	mm	27	22
Grab Strength	ASTM D4632	N	900	1100
Tear Strength	ASTM D4533	N	385	460
Hydraulic properties				
opening Size O <sub>90</sub>	EN ISO 12956	μm	100	80
Permeability V <sub>IH50</sub>	EN ISO11058	10 <sup>-3</sup> m/s	40	35
Flow Rate at 10 cm WH	BS 6906-3	I/(m <sup>2</sup> .s)	70	60
Permeability at 20 kN/m <sup>2</sup>	DIN 60500-4	10 <sup>-4</sup> m/s	2.6	1.9
Permeability at 200 kN/m <sup>2</sup>	DIN 60500-4	10 <sup>-4</sup> m/s	1.8	1.4

Table A.2. Properties of the Junifol PEHD Geomembrane.

Properties	Test method	Unit	Junifol PEHD
Surface			textured
Thickness (min. ave.)	ASTM D 5994	mm	1.0 (-5 %)
lowest individual for 8 out of 10 values			-10%
lowest individual for an of the 10 values			-15%
Asperity Height (min. ave.)	GM 12	mm	0.25
Density (min.)	ASTM D 1505	g/cm <sup>3</sup>	0.94
Tensile Properties (min. ave.)	ASTM D 6693 typ IV		
Yield strength		kN/m	17
Break strength		kN/m	29
Yield elongation		%	12
Break elongation		%	750
Tear Resistance (min. ave.)	ASTM D 1004	N	130
Puncture Resistance (min. ave.)	ASTM D 4833	N	330
Stress Crack Resistance	ASTM D 5391	hr.	300
Carbon Black Content	ASTM D 1603	%	2 - 3
Carbon Black Dispersion	ASTM D 5596	Category	1 or 2
Oxidative Induction Time (OIT) (min. ave.) Standard OIT	ASTM D 3895	min.	100
Oven Aging at 85 °C Standard OIT (min. ave.) % retained after 90 days	ASTM D 5721 ASTM D 3895	%	55
UV Resistance High Pressure OIT (min. ave.) % retained after 1600 hrs	ASTM D 5885	%	-

Table A.3. Properties of the 1 mm Thick PTFE Geomembrane Sheet.

Properties	Unit	PTFE
General preoperties		
Density	g/cm <sup>3</sup>	2.18
Water Absorption	%	0
Mechanical properties		
Tensile Strength	MPa	20
Elongation at Yield	%	25 - 31
Tensile Strength at Break	MPa	9
Elongation at Break	%	> 200
Impact Strength	kJ/m <sup>2</sup>	15.5
Notch Impact Strength	kJ/m <sup>2</sup>	**
Ball indentation Hardness (Rockwell)	MPa	30
Shore Hardness	**	60 - 65
Flexural Strength ( $\sigma_{B3.5\%}$ )	MPa	550
Coefficient of Friction	**	0.06
Modulus of Elasticity	MPa	3000
Thermal properties		
Melting Temperature	C <sup>o</sup>	**
Permissible Service Temperatures		
Short Term Operating Temperature	C <sup>o</sup>	330
Long Term Operating Temperature	C <sup>o</sup>	260
Coefficient of Linear Thermal Expansion	K <sup>-1</sup> .10 <sup>-4</sup>	0.6
Thermal Conductivity at 20 C <sup>o</sup>	W/(m.K)	0.24
Electrical properties		
Volume Resistivity	$\Omega$ .cm	> 10 <sup>18</sup>
Surface Resistivity	$\Omega$	> 10 <sup>17</sup>
Dielectric Constant at 1 MHz		- / 2.1
Dielectric Strength	kV/mm	32

## REFERENCES

- Adir, K. 2013, *Mitigation of Earthquake Induced Geotechnical Hazards Using Tire Waste-Sand Mixtures*, MS. Thesis, Bogazici University, Istanbul.
- Arab, M.G., & Jr, E. Kavazanjian, 2010, "Time-Domain Analysis of Frictional Base Isolation Using Geosynthetics", *9th International Conference on Geosynthetics*, Vol. 2, pp. 695-698.
- Bhattacharya, S., D. Lombardi, L. Dighoru, M.S. Dietz, A.J. Crewe, & C.A. Taylor, 2012, "Model Container Design for Soil-Structure Interaction Studies", *Role of Seismic Testing Facilities in Performance- Based Earthquake Engineering*, Vol 5, pp. 135-158.
- Cagatay, A. 2008, *Investigation of the Effect of Tire Waste Inclusions on the Shear Strength Parameters of Sand*, MS. Thesis, Bogazici University, Istanbul.
- Chang, K.C., Y. B. Yang & J.D. Yau, 2002, "Base Isolation", *In Earthquake Engineering Handbook*.
- Ecemis, N., & I. Kahraman, 2012, "Design of Laminar Shear Box for One Dimensional Shaking Table Tests", *10th International Congress on Advances in Civil Engineering*.
- Edinçliler, A., G. Baykal & K. Dengili, 2004, "Determination of Static and Dynamic Behaviour of Recycled Materials for Highways", *Resources Conservation and Recycling*, Vol. 6, pp. 223-237.
- Georgarakos, P., M.K. Yegian & G. Gazetas, 2005, "In-Ground Isolation Using Geosynthetic Liners", *9th World Seminar on Seismic Isolation, Energy Dissipation and Active Vibration Control of Structures*. Kobe.

- Harris, H.G., & G.M. Sabnis, 1999, "Structural Modeling and Experimental Techniques", *Chemical Rubber Company*.
- Islam, S., M. Jameel & M.Z. Jumaat, 2011, "Seismic Isolation in Buildings to be a Practical Reality: Behavior of Structure and Installation Technique", *Journal of Engineering and Technology Research*, Vol. 8, pp. 99-117.
- Jafarzadeh, F., 2004, "Design and Evaluation Concepts of Laminar Shear Box for 1g Shaking Table Tests, *13th World Conference on Earthquake Engineering*.
- Kalpakci, V., 2013, *Seismic Isolation of Foundations by Composite Liners*, Ph.D. Thesis, Middle East Technical University, Ankara.
- Kavazanjian, E.J., B. Hushmand, & G.R. Martin, 1991, "Frictional Base Isolation Using a Layered Soil-Synthetic Liner System", *Proceedings of the Third U.S. Conference on Lifeline Earthquake Engineering*, Vol. 10, pp. 1139-1151.
- Lee, J.H., R. Salgado, A. Bernal, & C.W. Lovell, 1999, "Shredded Tires and Rubber-Sand as Lightweight Backfill", *Journal of Geotechnical and Geoenvironmental Engineering*, Vol. 4, pp. 132-141.
- Martelli, A., & M. Forni, 2010, "Seismic Isolation and Protection Systems", *The Journal of the Anti-Seismic Systems International Society*, Vol. 7, pp. 75-123.
- Monfared, H., A. Shirvani, & S. Nwaubani, 2013, "An Investigation into the Seismic Base Isolation from Practical Perspective", *International Journal of Civil and Structural Engineering*, Vol. 23, pp. 451-463.
- Patil, S.J., & R.G. Reddy, 2012, "State Of Art Review - Base Isolation Systems For Structures", *International Journal of Emerging Technology and Advanced Engineering*, Vol 78, pp. 438-453.
- Prasad, S.K., I. Towhata, G.P. Chandradhara, & P. Nanjundaswamy, 2004, "Shaking Table Tests in Earthquake Geotechnical Engineering", *Current Science*, Vol. 78,

- pp. 1398-1404.
- Tatlisoz, N., T.B. Edil, & C.H. Benson, 1998, "Interaction Between Reinforcing Geosynthetics and Soil-Tire Chip Mixtures", *Journal of Geotechnical and Geoenvironmental Engineering*, Vol 1, pp. 1109-1119.
- Tsang, H.H., 2008, "Seismic Isolation by Rubber-Soil Mixtures for Developing Countries", *Earthquake Engineering and Structural Dynamics*, Vol 6, pp. 283-303.
- Tsang, H.H., S.H. Lo, X. Xu, & M.N. Sheikh, 2012, "Seismic Isolation for Low-to-Medium-Rise Buildings using Granulated Rubber-Soil Mixtures: Numerical Study", *Earthquake Engineering & Structural Dynamics*, Vol 67, pp. 2009-2024.
- Tsang, H.H., X. Xu, & M.N. Sheikh, 2009, "Earthquake Protection by Tire-Soil Mixtures: Numerical Study", *New Zealand Society for Earthquake Engineering Conference*.
- Tsatsis, A.K., I.C. Anastasopoulos, F.L. Gelagoti, & R.S. Kourkoulis, 2013, "Effectiveness of In-soil Seismic Isolation Taking into Account of Soil-Structure Interaction", *18th International Conference on Soil Mechanics and Geotechnical Engineering*, Vol. 6, pp. 1635-1638.
- Whitman, R.V., & P.C. Lambe, 1986, "Effect of Boundary Conditions Upon Centrifuge Experiments Using Ground Motion Simulation", *The American Society for Testing and Materials*, Vol 90, pp. 61-71.
- Yegian, M.K., & M. Catan, 2004 "Soil Isolation for Seismic Protection Using a Smooth Synthetic Liner", *Journal of Geotechnical and Geoenvironmental Engineering*, Vol 65, pp. 1131-1139.
- Yegian, M.K., & U. Kadakal, 1998, "Seismic Response of Landfills with Geosynthetic Liners", *Journal of Geotechnical and Geoenvironmental Engineering*.
- Yegian, M.K., & U. Kadakal, 2004, November, "Foundation Isolation for Seismic Pro-

- tection Using a Smooth Synthetic Liner”, *Journal of Geotechnical and Geoenvironmental Engineering*, Vol 55, pp. 1121-1130.
- Yegian, M.K., & A.M. Lahlaf, 1992, “Dynamic Interface Shear Strength Properties of Geomembranes and Geotextiles”, *Journal of Geotechnical Engineering*, Vol. 22, pp. 760-779.
- Yegian, M.K., & A.M. Lahlaf, 1992, “Geomembranes as Base Isolation Station”, *Paul Geotechnical Fabrics Report*.
- Yegian, M.K., & Lahlaf, A.M., 1993, “Shaking Table Tests for Geosynthetic Interfaces”, *Proceedings of the Geosynthetics 93' Conference*. Vancouver, Canada.
- Yegian, M.K., U. Kadakal, & M. Catan, 1999, “Geosynthetics for Earthquake Hazard Mitigation”, *Geosynthetics '99: Specifying Geosynthetics and Developing Design Details*, Vol 77, pp. 87-100.
- Yegian, M., A.Y. Yee, & J.N. Harb, 1995, “Seismic Response of Geosynthetic/Soil Systems”, *Geoenvironment 2000*, Vol 1, pp. 1113-1125.
- Yegian, M., Z.Y. Yee, & J.N. Harb, 1995, “Response of Geosynthetics Under Earthquake Excitations”, *Geosynthetics '95 Conference*, Vol 2, pp. 677-689.